

Raman Spectroscopy in Identification and Assessment of Ovarian Cancer



Submitted by

Diana Frimpong

to the University of Exeter
as a thesis for the degree of

Doctor of Philosophy in Medical Sciences

In January 2024

This thesis is available for Library use on the understanding that it is copyright material and that no quotation from the thesis may be published without proper acknowledgement.

I certify that all material in this thesis which is not my own work has been identified and that no material has previously been submitted and approved for the award of a degree by this or any other University.

Academic Supervisors: Professor AC Shore, Professor N Stone

Clinical Supervisors: Miss C Newton, Mr J Frost

Abstract

Ovarian cancer is the leading cause of death in gynaecological cancers in the UK. Late presentation is associated with poor prognosis however attempts at a screening test have not demonstrated a mortality reduction. Complete cytoreduction has been proven to be pivotal in improving survival but there is no objective measure for residual disease. Advances in treatment are changing the landscape of ovarian cancer management however stage-based survival data suggests a continued need for highly impactful ways for improving early detection. This work assesses Raman spectroscopy as a diagnostic blood test for ovarian cancer and also explores its ability to separate cancer and non-cancer in tissue. Raman spectroscopy is a non-destructive diagnostic technique that has been explored, to various degrees, in breast, oesophageal, head and neck and bladder cancers, and yielded high accuracies for detection of cancer.

I have conducted a prospective observational cohort study evaluating Raman spectroscopy for:

- the identification of novel plasma markers diagnostic of ovarian cancer
- its diagnostic performance as an early detection blood test in women with symptoms of ovarian cancer
- its performance against histology for its ability to detect cancer in peritoneal and ovarian tissue
- the effect of chemotherapy on the ability of Raman spectroscopy to detect cancer in ovarian and peritoneal tissue

Biochemical changes in lipids, amino acids and carotenoids in plasma and, collagen in tissue, were found to characterize the difference between cancer and other tissue using Raman spectroscopy.

The technique was able to detect cancer in plasma with a sensitivity and specificity of 60% and 78% for all women presenting with ovarian cancer symptoms, and 90% and 94% when comparing only cancer and benign patients spectra using support vector machine classification modelling.

Raman spectroscopy was able to differentiate between cancer and benign spectra from ovarian tissue, with sensitivities and specificities of 94% and 98%, and cancer and benign peritoneal tissue, 86% and 98%. This model was also able to separate cancer and borderline ovarian tissue with a sensitivity of 98% and specificity of 89%.

In samples taken from patients after chemotherapy treatment, this technique was able to detect cancer in peritoneal tissue when compared to post chemotherapy benign tissue with an F1 score of 0.73 compared to 0.83 in samples taken at primary surgery, suggesting a possible effect of previous chemotherapy on the diagnostic ability of Raman spectroscopy. This difference needs to be explored further in future work with balanced group sizes.

Despite the limitations of sample size due to the constraints of a shortened recruitment time due to the COVID-19 pandemic, this work was successful in demonstrating the diagnostic potential of Raman spectroscopy in a range of clinical areas for ovarian cancer management.

Acknowledgements

I would like to thank University Hospitals Bristol and Weston NHS Foundation Trust for being the host site for this study, and for my research fellowship post without which this project would not have been possible.

I am extremely grateful to Dr Joya Pawade, consultant pathologist, Severn Pathology Services, for the time she dedicated to assessing the large volumes of slides for this study and continued support over the course of this project. I am forever indebted to Emmanuel Frimpong, biomedical scientist, Severn Pathology Services for his input into developing the sectioning protocols, completing all the tissue sectioning work for this study and his encouragement over the course of this project.

I want to thank Rachel Ndjendja and the clinical and nursing teams in St Michael's Hospital outpatients, for helping me keep up with potential participants and supporting sample collection.

I am grateful to the BioSpec team for their support and kindness in this journey. I have never met a more welcoming or warmer group of people and despite the difficult commute, my days in the lab always left me motivated and inspired to keep going because of them.

To my clinical supervisors Miss Claire Newton and Mr Jonathan Frost, thank you so much for your contribution to this project. I have really appreciated your time and encouragement, and your clinical expertise and insight have been invaluable for making this project a reality.

Professor Angela Shore, thank you for your attention to detail, patience and perseverance. There has been a lot to achieve in a short period of time in this work and without you keeping me on track I would not have been able to see it through.

Professor Nick Stone, your guidance and support have been invaluable. I am inspired and humbled by your kindness, experience, and knowledge. I have appreciated your time and patience, and I couldn't have dreamt up a better supervisor.

I would like to thank all the women who agreed to participate in this study and the women in my public involvement group who gave me feedback on my patient information documents.

I can never thank my parents enough for their prayers and everything they have sacrificed to give me the opportunities that I have had in life. I am grateful for my brother David and his wife Olivia, for their unwavering support, laughter and pep talks.

This thesis is dedicated to David,
I couldn't have asked for a better big brother.

List of Contents

ABSTRACT	3
ACKNOWLEDGEMENTS	5
LIST OF FIGURES	11
LIST OF TABLES	23
LIST OF ABBREVIATIONS	26
CHAPTER 1 - INTRODUCTION	28
1.1 ANATOMY AND PHYSIOLOGY	29
1.1.1 Embryology	29
1.1.2 The Mature Ovary.....	30
1.2 OVARIAN PATHOLOGY	32
1.2.1 Types of Ovarian Pathology.....	32
1.2.1.1 Benign pathology	32
Functional Cysts.....	32
Mature Cystic teratoma (Dermoid Cysts).....	32
Endometrioma.....	32
Benign Epithelial tumours	32
1.2.1.2 Borderline Tumours.....	33
1.2.1.3 Malignant neoplasm	33
1.3 OVARIAN CANCER.....	33
1.3.1 Background	33
1.3.2 Screening and early detection	34
1.3.3 Histological subtypes of Ovarian Cancer.....	38
Germ cell ovarian Tumours.....	38
Ovarian sex cord stromal tumours.....	38
Epithelial Ovarian Cancers (EOC).....	39
1.4 ASSESSMENT AND MANAGEMENT OF OVARIAN PATHOLOGY	40
1.4.1 Assessment of ovarian pathology.....	40
Laboratory tests	40
Ultrasound scan	41
Risk of Malignancy Estimation	41
1.4.2 Management of ovarian pathology	42
1.4.3 Investigations in secondary care and diagnosis.....	44
1.4.4 Management of ovarian cancer	44
Stage I and II	44
Stage II – IV.....	45
Targeted therapies	46
1.5 CONCLUSION.....	47
1.6 RAMAN SPECTROSCOPY.....	48
1.6.1 Relationship between light and molecules.....	48

1.6.2	Vibrational states of molecules	50
1.6.3	Measuring scattered photons	50
1.6.4	Biological applications of Raman spectroscopy	53
1.6.5	Application of Raman spectroscopy in Ovarian cancer	61
1.6.6	Conclusion	64
1.7	AIMS OF THIS THESIS	65
	Objectives	65
CHAPTER 2 – METHODS		67
2.1	ETHICAL APPROVAL AND CONSENT	68
2.2	STUDY POPULATION AND DESIGN	69
2.2.1	Population	69
2.2.2	Design	69
2.3	DATA COLLECTION	72
2.3.1	Sample collection and processing – Biofluids	72
2.3.2	Sample collection and processing – Tissue	72
2.4	SAMPLE SIZE CALCULATION	73
2.5	GENERAL RAMAN METHODS	74
2.5.1	Technical considerations	74
2.5.2	Analysis techniques	76
2.6	STUDY METHODS	78
2.6.1	Development of lab protocol - Biofluids	78
2.6.1.1	Refining the sample preparation	79
Blood component	79	
Collection medium	79	
Extraction and storage of plasma	79	
Does leaving the blood for prolonged periods of time at room temperature prior to centrifugation alter the assessment of plasma components by Raman Spectroscopy?	79	
2.6.1.2	Developing the biofluids Raman spectroscopy protocol	82
Assessing the effects of Backing Substrate	82	
Assessing the effect of drop size	84	
Optimum drying time prior to commencing Raman measurements	85	
2.6.1.3	Spectrometer considerations - Biofluids	87
System configuration	87	
Calibration	88	
2.6.1.4	Final lab protocol for plasma measurements	89
2.6.1.5	Spectral processing - Biofluids	90
2.6.2	Development of the lab protocol - Tissue	91
2.6.2.1	Preparation of tissue for clinical histopathology	91
2.6.2.2	Refining the tissue management plan	91
Preserving tissue	92	
Tissue sectioning	92	
2.6.2.3	Final lab protocol for tissue sectioning	96
2.6.2.4	Spectrometer considerations – tissue	97
Exposure time	97	

Number of accumulations	98
Size of area to be measured	99
2.6.2.5 Final lab protocol for tissue measurements	100
2.6.2.6 Spectral processing – Tissue.....	100
CHAPTER 3 – RAMAN SPECTROSCOPY OF PLASMA FOR OVARIAN CANCER	102
3.1 INTRODUCTION	103
3.2 AIMS	103
3.3 METHODS	103
3.4 OVERALL STUDY RECRUITMENT OUTCOMES	104
3.5 PLASMA RECRUITMENT OUTCOMES	108
Benign group	109
Borderline group.....	111
Cancer group.....	111
3.5 RAMAN RESULTS AND ANALYSIS.....	112
Measurements	112
Pre-processing.....	113
Peak positions and intensity	114
Multivariate analysis of the three-class group	119
Multivariate analysis of Cancer vs benign.....	120
Multivariate analysis of HGS cancer vs Benign.....	121
Multivariate analysis of Cancer vs Borderline	122
Multivariate analysis of Borderline vs Benign.....	122
Stage I and II disease.....	123
3.6 SUMMARY OF RESULTS.....	123
3.7 DISCUSSION.....	124
CHAPTER 4 – RAMAN SPECTROSCOPY OF OVARIAN AND PERITONEAL TISSUE.....	128
4.1 INTRODUCTION	129
4.2 AIMS	129
4.3 METHODS	129
4.4 RESULTS	130
4.5 TISSUE RECRUITMENT OUTCOMES	130
4.5.1 Benign group	131
4.5.2 Borderline group.....	131
4.5.3 Cancer group.....	131
4.5.4 Prior treatments, type of tissue available for analysis and point of collection.....	131
4.6 RAMAN SPECTROSCOPY TISSUE RESULTS AND ANALYSIS.....	133
Measurements	133
Pre-processing.....	134
4.6.1 Ovarian Tissue	135
Peak Positions and Intensity.....	135
Multivariate analysis of Cancer vs Benign pathology groups	143
Multivariate analysis of Cancer vs Borderline pathology groups	148
Multivariate analysis of Borderline vs Benign pathology groups.....	151

Multivariate analysis of IDS vs Primary - Cancer.....	154
4.6.2 Peritoneal tissue	157
Peak Positions and Intensity	157
Multivariate analysis of Cancer vs Benign (IDS)	162
Multivariate analysis of Cancer vs Benign (Primary Surgery).....	165
Multivariate analysis of IDS vs Primary surgery (Cancer)	167
4.6.3 Variations within the slides	168
Participant 007	169
Ovarian tissue (Primary surgery).....	169
Peritoneal tissue (IDS).....	171
4.7 SUMMARY OF RESULTS	172
4.8 DISCUSSION	172
CHAPTER 5 - CONCLUSIONS AND FURTHER WORK.....	176
5.1 STUDY LIMITATIONS	177
5.2 FUTURE WORK.....	182
5.3 CONCLUSION.....	184
APPENDICES	185
Appendix A: HRA approval	185
Appendix B: Research Ethics Committee	187
Appendix C: Participant Information Sheet A	192
Appendix D: Participant Information Sheet B	198
Appendix E: Participant Consent Form.....	202
Appendix F: Participant Background Information Collection Tool.....	203
Appendix G: Participant Diagnostic Information Collection Tool.....	205
Appendix H: Tentative peak assignment reference table - Tissue.....	206
Appendix I: Tentative peak assignments reference table - Plasma	208
Appendix J: Copyright for image from other source.....	209
BIBLIOGRAPHY	210

List of Figures

Figure 1 - The structure of the uterus, ovary and fallopian tubes including the oocyte at various stages of development. Image reprinted from Guyton and Hall Textbook of Physiology (Hall, 2021), with permission from Elsevier.	31
Figure 2 - International Federation of Gynaecology and Obstetrics criteria for staging ovarian cancer. Reproduced from (Prat, 2015).....	35
Figure 3 - Management of ovarian cysts of low malignancy risk. This figure summarises conservative and surgical management parameters for ovarian cysts with RMI <200 in both pre- and post-menopausal women (Kaloo PD. et al., 2011, MehasebSiddiqui and Bryden, 2016).....	43
Figure 4 - The electromagnetic spectrum. This image displays the spectrum of electromagnetic waves, and their wavenumbers. It illustrates increasing energy with decreasing wavelength and the position of visible light in this spectrum. This image is reprinted from (Cyberphysics, 2009) with permission. Original source unknown.....	48
Figure 5 - Raman Scattering. This figure illustrates the shift in energy levels (Raman shift) that can occur when a photon interacts with a molecule. If the molecule was at ground state (v_0), this interaction results in a higher vibrational state due to the scattered photon losing energy to molecular vibrations (stokes scattering). If the molecule was at an excited vibrational state (v_1), this interaction results in a lower energy state due to energy being transferred to the scattered photon from the molecule (anti stokes scattering). Adapted from (Smith and Dent, 2004a)	50
Figure 6 - Study flow chart for sample collection. This figure illustrates the protocol for tissue and blood sampling. Participant treatment plans were followed, and samples collected at the appropriate stages.	71
Figure 7 - Principal component scores distribution of plasma samples extracted and frozen without delay, 6, 12 and 24 hours after storage at either room temperature or in a fridge. This is a plot of two statistically significant principal	

components ($p=0.001$), where PC 1 is displayed on the x-axis and PC 8 is displayed on the y-axis. The circles represent the scores, and the colours represent the time delay prior to plasma extraction with 0hr being no delay prior to extraction. Samples kept in the fridge are labelled F in the legend and samples kept at room temperature are labelled R. 81

Figure 8 - White light image of 1.5 μ l of undiluted plasma on calcium fluoride (left) and stainless steel (right). The sample on calcium fluoride is more symmetrical and smaller (diameter 2250 vs 3800 microns) than the sample on stainless steel. 83

Figure 9 - Mean spectra of 1.5 μ l of undiluted plasma, taken from drops dried on glass, stainless steel and calcium fluoride substrates. A minimum of 60 spectra were collected from measurements of the protein ring on each substrate in triplicates. The number of spectra varied slightly due to the differences in the size of the dried drop depending on the substrate as discussed in figure 8. The glass spectrum in blue does not demonstrate any of the spectral features expected in plasma. The calcium fluoride (orange) and stainless steel (yellow) spectra are seen clearly on the plot on the right side of the figure. The stainless steel spectrum has a higher signal intensity and more prominent spectral features. 83

Figure 10 - Assessing plasma drop size for Raman spectroscopy. In this figure, the mean of the triplicate measurements for each drop size has been plotted with Raman intensity on the y-axis and wavenumber of the x-axis. Signal intensity increases with increasing drop size with 0.5 microlitre drop (blue) demonstrating the lowest signal intensity and the 2.5 microlitre drop (green) demonstrating the highest signal intensity. Spectra features such as peak position and shape are unchanged across the drops. 84

Figure 11 - Signal intensity of varying drop sizes of undiluted plasma. Intensity measurement taken of phenylalanine protein peak. 85

Figure 12 - Minimum drying time per drop volume. The minimum amount of time required for the protein ring to be visible under the microscope has been plotted in this figure with error bars. The blue bars represent the mean minimum time to dry of three repeats of this exercise, per drop of undiluted plasma. 85

Figure 13 - Drying time of 1.5 microlitre plasma. This is a figure of spectra taken every 2 minutes of freshly dropped plasma. Features expected for plasma become identifiable from 12 minutes onwards as seen with the orange, purple and green spectra. 86

Figure 14 – Raman spectral signal intensity of 1.5 microlitre drop of undiluted plasma on stainless steel over time, up to 40 minutes, being held at room temperature. The peak height of the amide II protein peak is plotted over time to demonstrate the changes in signal intensity as the sample dries. 87

Figure 15 – Renishaw inVia Raman system. This image was created by adapting the image from (Renishaw, 2021) brochure and the schematic from (BunaciuHoang and Aboul-Enein, 2017). 87

Figure 16 - Silicon spectrum. The silicon spectrum had only one peak at 520cm⁻¹. The position on this peak is used in calibration of the Raman spectrometer. 88

Figure 17 - PTFE spectrum. The PTFE spectrum has multiple peaks that are stable. The position of these peaks is checked when calibrating the Raman spectrometer. 89

Figure 18 - OCT compound spectrum. The optimum cooling temperature (OCT) compound spectrum is demonstrated in this figure. The spectrum was acquired by measuring OCT compound on a stainless steel slide using the Renishaw InVia spectrometer coupled with an 830 nm laser. Three accumulations of a five second exposure time on 100% laser was used. 93

Figure - 19 Leica systems cryostat microtome at Southmead hospital, North Bristol Trust, used for tissue sectioning in this project. This is an image of the freezing chamber of the cryostat. The panel labelled 1 is a panel field that contains control and the temperature display. The area labelled 2 is next to the Peltier element with two stations. In this image there is a chuck, 3, placed in the middle of the element across the two stations. The microtome labelled 4 is best appreciated in the zoomed in image to the right of the figure. There is a sample on acetate sheet loaded onto the chuck with water, sitting in the specimen holder, 5, ready for sectioning. The area labelled 6 is the blade holder. 94

Figure 20 - Signal to noise ratio of benign ovarian tissue of varying thickness. This signal to noise ratio figure is generated from one spectral measurement and shows increasing signal to noise ratio with tissue thickness..... 95

Figure 21 - Signal to noise ratio of benign peritoneal tissue. This signal to noise ratio figure is generated from one spectral measurement and shows increasing signal to noise ratio with tissue thickness. The higher 20 microns result was consistent in all three measurements of this tissue. 95

Figure 22 - Laser exposure time comparison. The orange spectrum represents a single accumulation of 15 seconds exposure time, and the blue spectrum represents a single accumulation of 10 seconds exposure time, plotted with wavenumber on the x-axis and Raman intensity on the y-axis. Spectral features are clearer with the longer exposure time however there is a contribution from cosmic rays as displayed in the smaller plot in the top right-hand corner of the figure. 98

Figure 23 – Number of accumulations per measurement comparison. The orange spectrum represents a single accumulation of 15 seconds exposure time, and the blue spectrum represents three accumulations of 5 seconds exposure time, plotted with wavenumber on the x-axis and Raman intensity on the y-axis. Whilst the single accumulation of prolonged exposure time spectrum appears to be slightly smoother or less noisy, there is no loss or change in spectral features and cosmic rays were not detected during this measurement. Three accumulations of five seconds exposure time was non-inferior to a single accumulation of 15 seconds exposure. 99

Figure 24 - Flow chart of overall recruitment outcome. Reasons for excluding participants are explained in the blue callout boxes. 104

Figure 25 - Age of participants. The box plots demonstrate the range of ages of the participants in the benign, borderline and cancer groups. The mean age, marked x, is 62 in the benign group (blue), 55 in the borderline (orange) and 64 in the cancer (grey) group. 108

Figure 26 - Menopausal status of participants. This figure illustrates the proportion of women in study group who were premenopausal, perimenopausal and

postmenopausal. Most of the women in the benign (blue), borderline (orange) and cancer (grey) groups were postmenopausal. 108

Figure 27 - Number of comorbidities per participant. This figure illustrates the distribution of medical comorbidities in benign (blue), borderline (orange) and cancer (grey) groups. Most participants had two or fewer comorbidities across all groups. 109

Figure 28 – CA-125 levels of benign and borderline participants. This figure illustrates the range of CA-125 levels in this group. Levels were lower in the benign group (blue) compared to the borderline group (orange). Normal CA-125 is less than 35 units/ml. 110

Figure 29 - CA-125 levels of cancer participants. This plot is presented separately to the benign and borderline values due to the large difference in range of results. Normal CA-125 is less than 35 units/ml..... 110

Figure 30 - Benign ovarian pathology. This figure illustrates the range of diagnosis of the participants in the benign group. Mucinous and serous cystadenomas accounted for over a third of benign ovarian pathology requiring surgery. 111

Figure 31 – Stage at diagnosis. The figure illustrates the distribution of stage of disease at diagnosis in the cancer group. 112

Figure 32 - White light image of dried plasma drops. This is an image of one of the slides of dried 1.5 microlitre drops of plasma measured in this study. Sample numbers are across the top in blue. The samples were measured in triplicates, A, B and C. 113

Figure 33 – Baseline subtraction. This figure is an image of the graphic user interface used to subtract the background signal and change the baseline of the plasma data. Each spectrum has its baseline subtracted separately however the same variables are used for all spectra in the data. The blue line represents the spectrum and the red line represents the baseline generated by least squares fit. 113

Figure 34 - Mean spectra of plasma for all pathology groups. In this figure, the benign spectrum (green), borderline spectrum (blue) and cancer spectrum (red)

are plotted together with wavenumber cm^{-1} in the x-axis and intensity on the y-axis..... 114

Figure 35 - Subtraction spectrum obtained from subtracting benign group from cancer group. Positive intensity values suggest increased concentration in the cancer group. Negative intensity values suggest increased concentration in the benign group. The broken line represents an arbitrary cut off and the dotted line represents two standard deviations above and below the mean. Peaks above these lines have been tentatively assigned. There are higher concentrations of tryptophan, lipids, amide III, amide I and CH rocking in the cancer group than in the benign group. There is a higher concentration of carotenoids in the benign group than in the cancer group..... 115

Figure 36 - Subtraction spectrum obtained from subtracting borderline group from cancer group. Positive intensity values suggest increased concentration in the cancer group. Negative intensity values suggest increased concentration in the borderline group. The broken line represents an arbitrary cut off and the dotted line represents two standard deviations above and below the mean. Peaks above these lines have been tentatively assigned. There are higher concentrations of phenylalanine, tryptophan, amide III, amide I and lipids in the cancer group than in the borderline group. There is a higher concentration of carotenoids in the borderline group compared to the cancer group..... 117

Figure 37 - Subtraction spectrum obtained from subtracting benign group from borderline group. Positive intensity values suggest increased concentration in the cancer group. Negative intensity values suggest increased concentration in the benign group. The broken line represents an arbitrary cut off and the dotted line represents two standard deviations above and below the mean. Peaks above these lines have been tentatively assigned. There are higher concentrations of C-S stretch and lipids in the borderline group than in the benign group. There is a higher concentration of phenylalanine, amide III, and amide I in the benign group..... 117

Figure 38 – Twenty-five principal components generated from benign, borderline and cancer spectra. The first principal component is in the top left corner, they continue consecutively to the right on each new line. Each PC is plotted with

wavenumber cm^{-1} on the x-axis and intensity on the y-axis. PC 21 and 24 do not meet the confidence level of 99% on analysis of variance. 119

Figure 39 – Histogram plot of linear discriminant scores classifying benign and cancer with sensitivity of 69% and specificity of 78%. The green histogram represents the scores of the benign group and the red histogram represents the scores of the cancer group. 121

Figure 40 - Histogram plot of linear discriminant scores classifying borderline and cancer with sensitivity of 80% and specificity of 77%. The blue histogram represents the scores of the borderline group and the red histogram represents the scores of the cancer group. 122

Figure 41 - Number of comorbidities. This figure illustrates the distribution of comorbidities within the benign (blue), borderline (orange) and cancer (grey) groups. The majority of the groups had more than two comorbidities and the cancer group had the highest disease burden..... 131

Figure 42 - White light map image of fresh frozen ovarian tissue. This figure demonstrates the relative appearances of the Raman map of ovarian tissue (left) and the H&E appearance of the same tissue (right)..... 133

Figure 43 - Baseline subtraction. This figure is an image of the graphical user interface used to change the baseline of the data. Each spectrum has its baseline subtracted separately however the same variables are used for all spectra in the data. In this figure, the spectrum (blue) can be seen with a red line (Baseline) underneath it. 134

Figure 44 - Mean spectra of benign ovarian pathology. In this figure, the mean of benign ovarian pathology spectra, generated from all 18 participants in the benign group, has been plotted and annotated with the wavenumber of the prominent peaks seen in this spectrum. Tentative assignments of these peaks are seen in Appendix H: Tentative peak assignment reference table. 136

Figure 45 – Mean spectrum of ovarian cancer. In this figure, the mean of ovarian cancer spectra, generated from the 11 participants in the upfront surgery cancer group, has been plotted and annotated with the wavenumber of the prominent

peaks seen in this spectrum. Tentative assignments of these peaks are seen in Appendix H: Tentative peak assignment reference table. 136

Figure 46 - Mean spectrum of borderline tumours. In this figure, the mean of borderline tumour spectra, generated from all 8 participants in the borderline group, has been plotted and annotated with the wavenumber of the prominent peaks seen in this spectrum. Tentative assignments of these peaks are seen in Appendix H: Tentative peak assignment reference table. 137

Figure 47 - Mean spectra of ovarian tissue of all pathology groups. In this figure, the green spectrum represents benign ovarian pathology, the blue spectrum represents borderline ovarian pathology, and the red spectrum represents cancer taken at upfront surgery. There are wavenumber regions with obvious differences in the groups such as seen at 851 cm^{-1} , 931 cm^{-1} , 1247 cm^{-1} and 1336 cm^{-1} and some more subtle areas with changes seen in only or two of the groups..... 137

Figure 48 – Subtraction spectrum obtained from subtracting benign from cancer. Positive intensity values suggest increased concentration in the cancer group. Negative intensity values suggest increased concentrations in the benign group. There is increased glycogen, lipids, amino acids, nucleotides, and amide I groups in cancer compared benign. There are lower concentrations of phosphate minerals, collagen, carotenoids, amide III, CH_3 modes in proteins and deoxyribose in the cancer group compared to the benign group..... 138

Figure 49 – Subtraction spectrum obtained from subtracting borderline from cancer. Positive intensity values suggest increased concentration in the cancer group. Negative values suggest higher concentrations in the borderline group. There is increased glycogen, phosphates, collagen, ribose, amino acids, lipids, cytosine, nucleic acids, CH_3 bending modes and amide I in the cancer group compared to the benign. There are lower levels of thymine, guanine, DNA, amino acids, collagen, carotenoids, deoxyribose, and amide I group in the cancer group compared to the borderline group. 139

Figure 50 – Subtraction spectrum obtained by subtracting benign from borderline. Positive intensity values suggest increased concentration in the borderline group. Negative values suggest higher concentrations in the benign group. There is increased glycogen, amino acids, lipids, DNA, nucleotides, and amide I in the

borderline group compared to the benign. There are lower levels of disulphide stretch in proteins, amino acids, collagen, amide III, CH3 deformation and amide I group in the borderline group compared to the benign group. 140

Figure 51 - Percentage contribution of principal components. This figure displays the percentage contributions of the first 10 PCs. They explain 90% of the data. The right hand axis showing the cumulative variance described. 143

Figure 52 – Twenty-five principal components generated from cancer and benign spectra. The first principal component is in the top left corner, they continue consecutively to the right on each new line. Each PC is plotted with wavenumber cm^{-1} on the x-axis and intensity on the y-axis. 144

Figure 53 – Histogram plot of linear discriminant scores classifying benign and cancer with a sensitivity of 98% and a specificity of 100%. The red histogram represents the scores of the cancer group and the green histogram represented the scores for the benign group. 145

Figure 54 – Mean ROC curve (black) following two-fold cross validation for cancer group in cancer and benign data. The upper (blue) and lower (orange) lines show each iteration. 147

Figure 55 - Twenty-five principal components generated from cancer and borderline spectra. Each principal component is plotted with wavenumber cm^{-1} on the x-axis and intensity on the y-axis. 148

Figure 56 - Histogram plot of linear discriminant scores classifying borderline and cancer with sensitivity of 99% and specificity of 99%. The blue histogram represents the scores of the borderline group and the red histogram represents the scores of the cancer group. 149

Figure 57 - Mean receiver operating characteristic curve (black) following two-fold cross validation for cancer group in cancer and borderline data. The upper (blue) and lower (orange) lines show each iteration. 150

Figure 58 – Twenty-five principal components generated from borderline and benign spectra. Each PC is plotted with wavenumber cm^{-1} on the x-axis and intensity on the y-axis. 151

Figure 59 - Histogram plot of linear discriminant analysis scores classifying benign and cancer with a sensitivity of 90% and specificity of 95%. 152

Figure 60 - Mean receiver operating characteristic curve (black) following two-fold cross validation. for borderline group in borderline and benign data. The upper (blue) and lower (orange) lines show each iteration. 153

Figure 61 - Mean spectra of ovarian tissue taken from participants at primary surgery (red) and interval debulking surgery (purple). 155

Figure 62 - Scores plot for PC1. This figure displays a scatter plot of PC1 against PC2 with data from primary cancer in red stars and data from IDS in purple filled circles. 155

Figure 63 - Principal component 1 for IDS vs primary. This was the only PC of significance for describing variance in this data. The main variables seen are lipids, glycogen, amide III beta sheet, adenine and nucleic acid base and ring activity. 156

Figure 64 - Mean spectrum of cancer. In this figure the mean of the spectra of (primary surgery) cancer peritoneal samples have been plotted and annotated with the wavenumber of the prominent peaks seen in this spectrum. Tentative assignments of these peaks are seen in Appendix H. 157

Figure 65 - Mean spectrum of benign peritoneal pathology. In this figure the mean of the spectra of benign peritoneal samples has been plotted and annotated with the wavenumber of the prominent peaks seen in this spectrum. Tentative assignments of these peaks are seen in Appendix H. 158

Figure 66 - Mean spectrum of IDS cancer group. In this figure the mean of the spectra of (cancer) IDS peritoneal samples have been plotted and annotated with the wavenumber of the prominent peaks seen in this spectrum. Tentative assignments of these peaks are seen in Appendix H. 158

Figure 67 - Mean spectrum of bIDS. In this figure the mean of the spectra of benign IDS peritoneal samples has been plotted and annotated with the wavenumber of the prominent peaks seen in this spectrum. Tentative assignments of these peaks are seen in Appendix H. 159

Figure 68 – Subtraction spectrum obtained from subtracting benign from benign IDS. Positive intensity values suggest increased concentration in the bIDS group. Negative intensity values suggest increased concentration in the benign group compared to bIDS. There are lower concentrations of thymine, tryptophan and collagen and higher levels of lipids, amino acids, amide I group, nucleic ring activity and carotenoids in the bIDS group compared to the benign group..... 160

Figure 69 - Subtraction spectrum obtained by subtracting cancer samples taken at primary surgery from those taken at IDS. Positive intensity values suggest increased concentration in the IDS group. Negative intensity values suggest increased concentrations in the primary surgery group. There are higher concentrations of tyrosine, collagen, phenylalanine, carotenoids, deoxyribose, and amide I and lower concentrations of nucleotides and lipids in the IDS group compared to the cancer group..... 161

Figure 70 – Twenty-five principal components generated from cancer and benign IDS spectra. The first principal component is the left top corner, they continue consecutively to the right on each new line. Each PC is plotted with wavenumber cm-1 In the x-axis and intensity on the y-axis..... 163

Figure 71 - Mean receiver operating characteristic curve (black) following two-fold cross validation for cancer group in the IDS cancer and bIDS data. The upper (blue) and lower (orange) lines show each iteration. The IDS group here are participants that ha samples taken at interval debulking surgery, and the resulting slide had cancer on it and the bIDS group represent similar patients background but their slides did not have cancer. 164

Figure 72 – Histogram plot of linear discriminant scores classifying IDS cancer and benign IDS with sensitivity of 81% and specificity of 91%. The green histogram represents the scores of the benign IDS group and the red histogram represents the cancer IDS group..... 165

Figure 73 – Principal component loadings for cancer vs benign (primary surgery) group. The pc loading on the left is PC3 and the loading on the right is PC4. 166

Figure 74 - Scores plot for principal component 4 and principal component 3. This figure displays a scatter plot of PC4 against PC3 scores when comparing cancer

and benign with data from cancer in red stars and data from benign in green filled circles. 166

Figure 75 - Twenty-five principal components generated from primary surgery and interval debulking surgery spectra (cancer). Each principal component is plotted with wavenumber cm^{-1} on the x-axis and intensity on the y-axis. 168

Figure 76 – Histogram plot of linear discriminant analysis scores classifying cancer and near cancer in the same participant with sensitivity of 98% and specificity of 98%. The blue histogram represents the linear discriminant scores for near cancer and the red histogram, the scores for cancer. 170

Figure 77 – H&E slide of fresh frozen peritoneal tissue. This sample was taken at interval debulking surgery. The green box at the top of the specimen is from an area with cancer and the green box near the middle of the specimen is from an area of fibrosis. The area with cancer is enlarged to demonstrate the areas of fibrosis interspersed within the cancer..... 171

List of Tables

Table 1 - U score allocation for Risk of Malignancy Index (RMI) score calculation. This table describes the score given depending on the number of characteristics displayed by the ovarian mass on ultrasound. This score is then multiplied by the menopausal status score and CA125 level to give the RMI score.....	41
Table 2 - 10 Simple Rules for identifying benign and malignant ovarian masses (Timmerman et al., 2008). This table describes the rules for predicting benign and malignant ovarian tumours based on the presence or absence of these morphological features on ultrasound scan, without the need for a CA125 test.	42
Table 3 - Summary of chemicals used in production of H&E slides. These can create contributions to the Raman spectrum are thus considered contaminants. In this table, alternatives being considered have been listed.....	92
Table 4 - Other cancer diagnosis. This table details the final diagnosis for participants excluded from the study for not having ovarian cancer.	105
Table 5 – Clinical characteristics of remaining 135 participants in this study summarised by pathology group. Included in this table are age, menopausal status, ethnicity, BMI, smoking status, comorbidities, diagnosis and stage of cancer at diagnosis.	107
Table 6 - Summary of tentative assignments of prominent peak positions in subtraction spectra of comparison groups. These peaks are deemed prominent using the arbitrary cut off of 0.01 intensity/arb.Units on the subtraction spectra.	118
Table 7 - Linear discriminant analysis and leave one sample out cross validation results for correct classification of cancer, borderline and benign in a three-class data set.....	120
Table 8 - Summary of tentative assignments of prominent peak positions in subtraction spectra of comparison groups. For the purposes of this comparison table, assignments that appear in varying modes in both positive (increased	

concentration) and negative (decreased concentration) intensities have been excluded.....	142
Table 9 - Displays the principal components with statistical significance in order of F value.....	145
Table 10 - Leave one out cross validation results for cancer classification in cancer and benign data. Included in this table is the linear discriminant analysis model performance and the F1 score.....	146
Table 11 - Displays the principal components with statistical significance in order of F value.....	148
Table 12 - Leave one out cross validation results for cancer classification in cancer and borderline data. Included in this table is the linear discriminant analysis model performance and the F1 score.....	150
Table 13 - Principal components with F_{ratio} greater than F_{crit} . This table displays the PCs of significance in the borderline/benign spectra.....	152
Table 14 – Leave one out cross validation results for borderline tumour classification in borderline and cancer data. Included in this table is the linear discriminant analysis model performance and the F1 score.....	153
Table 15 - Summary of tentative assignments of prominent peak positions in subtraction spectra of the groups. Tyrosine, phenylalanine, amide I, carotenoids and unassigned $1408-1410\text{cm}^{-1}$ appear to be higher in the IDS group of both tissue types.	162
Table 16 – Principal components with statistical significance in order of F value.	163
Table 17 - Leave one out cross validation results for IDS cancer vs benign of peritoneal tissue. Included in this table is the linear discriminant analysis model performance and the F1 score.	164
Table 18 – Principal components with statistical significance in order of F value for interval debulking surgery vs primary surgery (cancer).....	167

Table 19 - Performance scores of three class linear discriminant model for variation within the same participant. Included in this table is the linear discriminant analysis model performance and the F1 score..... 169

List of Abbreviations

α-FP	Alpha Fetoprotein
ANOVA	Analysis of Variance
AUC	Area Under the Curve
BGCS	British Gynaecological Cancer Society
CA-125	Cancer Antigen 125
CCD	Charge-Coupled Device
CI	Confidence Interval
CIN	Cervical Intraepithelial Neoplasia
CT	Computed Tomography
CTNNB1	Catenin Beta 1 (gene)
DCDRS	Drop Coating Deposition Raman Spectroscopy
DNA	Deoxyribonucleic Acid
EDTA	Ethylenediaminetetraacetic Acid
EM	Electromagnetic
EOC	Epithelial Ovarian Cancer
ER	Oestrogen Receptor
FIGO	International Federation of Gynaecology and Obstetrics
HE4	Human Epididymis 4
HCG	Human Chorionic Gonadotropin
HGS	High Grade Serous
H&E	Hematoxylin and Eosin
HRD	Homologous Recombination Deficiency
IDS	Interval Debulking Surgery
bIDS	Benign Interval Debulking Group (term used in this thesis for tissue with no evidence of cancer, taken from participants at post chemotherapy surgery for ovarian cancer)
LDA	Linear Discriminant Analysis
MCED	Multi-Cancer Early Detection
NCIC	National Cancer Institute of Canada (clinical trials group)
NCT	National Clinical Trials
NICE	National Institute for health and Care Excellence
PARP	Poly ADP Ribose Polymerase

PC	Principal Component
PCA	Principal Component Analysis
PLCO	Prostate, Lung, Colorectal and Ovarian (trial)
PLS	Partial Least Squares
PR	Progesterone Receptor
PS	Performance Status
PTFE	Polytetrafluoroethylene
REC	Regional Ethics Committee
RMI	Risk of Malignancy Index
ROC	Receiver Operating Characteristic (curve)
ROCA	Risk Of Ovarian Cancer Algorithm
SERS	Surface Enhanced Raman Spectroscopy
SNR	Signal to Noise Ratio
STDEV	Standard Deviation
STIC	Serous Tubal Intraepithelial Carcinoma
SVM	Support Vector Machine

Chapter 1 - Introduction

Ovarian cancer accounts for 2% of all new cancers and incidence is projected to rise in the UK by 5% in the next 15 years. Overall prognosis is poor, with a 10-year survival of 35% (Cancer Research UK) and it remains the leading cause of death in gynaecological cancers in the UK (NICE Guideline., 2011). No screening test exists and over half of diagnoses are made in advanced disease. The burden on the healthcare system is further compounded by a third of patients presenting as emergencies (NICE Guideline., 2011).

Whilst the treatment of ovarian cancer has improved significantly over the last decade, there remains opportunities to make strides in the detection and assessment of this disease. This thesis will explore the use of Raman spectroscopy as an early detection test for ovarian cancer, and in the classification of tissue into cancer and non-cancer groups. The ability of this technique to correctly classify ovarian and peritoneal tissue, even after chemotherapy treatment, would be extremely promising for the consideration of an objective assessment tool for residual disease.

This chapter will describe the ovary and its basic function, pathology seen in the ovary, and ovarian cancer assessment, management, and diagnosis. I will then go onto to review Raman spectroscopy and findings to date in relation to its biological applications.

1.1 Anatomy and Physiology

1.1.1 Embryology

Development of the female reproductive tract is closely associated with urinary tract development. The gonads develop from the intermediate mesoderm, which becomes the pronephros, mesonephros and metanephros. At 6 weeks gestation, the mesonephros, mesonephric duct, and mesonephric tubule are already formed as part of the development of the urinary system. An area of thickening and proliferation develops on the mesonephros known as the gonadal ridge.

Primitive germ cells from the yolk sac (epiblast germ line) migrate via the hind gut to invade the gonadal ridge. Clusters of germ cells form within the proliferative connective tissue of the mesenchyme, creating the primitive sex cords.

In the absence of testis-determining factor, a protein encoded by the SRY gene of the Y chromosome, the primitive sex cords extend into the medulla and degenerate to form a vascular stroma, with the surface epithelium becoming second generation cortical cords which later form ovarian follicles.

In the absence of anti-Mullerian hormone and testosterone, longitudinal invaginations in the coelomic epithelium overlying the urogenital ridges form the paramesonephric duct which enter the peritoneal cavity to become the fimbriae of the uterine tubes at the cranial end and fuses to form the uterus and upper vagina at the caudal end. The broad ligament is formed from the folds of peritoneum brought centrally by the fusion of the paramesonephric ducts.

The primitive cloaca is the end opening of the hind gut which is later divided to form the urogenital sinus anteriorly and rectum posteriorly. The lower half of the vagina is formed from the urogenital sinus and the external genitalia, from the cloacal folds. (Mitchell, 2009)

1.1.2 The Mature Ovary

The ovaries are on average $4 \times 3 \times 2 \text{cm}^3$ and suspended on either side of the uterus against the pelvic side wall, with fimbria of the fallopian tubes as borders superiorly (Figure 1).

Blood supply and innervation pass through the mesovarium, a peritoneal fold which supports the ovary along with the suspensory and proper ovarian ligaments. Innervation of the upper part of the ovary is derived from the renal and aortic plexuses and lower part from superior and inferior hypogastric plexuses.

The ovarian artery (branch of the abdominal aorta) and ovarian vein form the main vascular supply.

The surface of the ovary is covered by a thin layer of epithelium, beneath which is a thick collagenous coat (tunica albuginea). This coat covers the cortex and medulla. (Standring, 2021)

The ovary is responsible for the maturation and release of the oocyte, and production of sex hormones. At different stages of oocyte development, oestrogen and progesterone are produced by the granulosa and theca cells of the ovum as a result of positive and negative feedback from the gonadotrophins follicle-stimulating hormone (FSH) and luteinizing hormone (LH). This results in the rhythmic changes of the female monthly sexual cycle. (Hall, 2021)

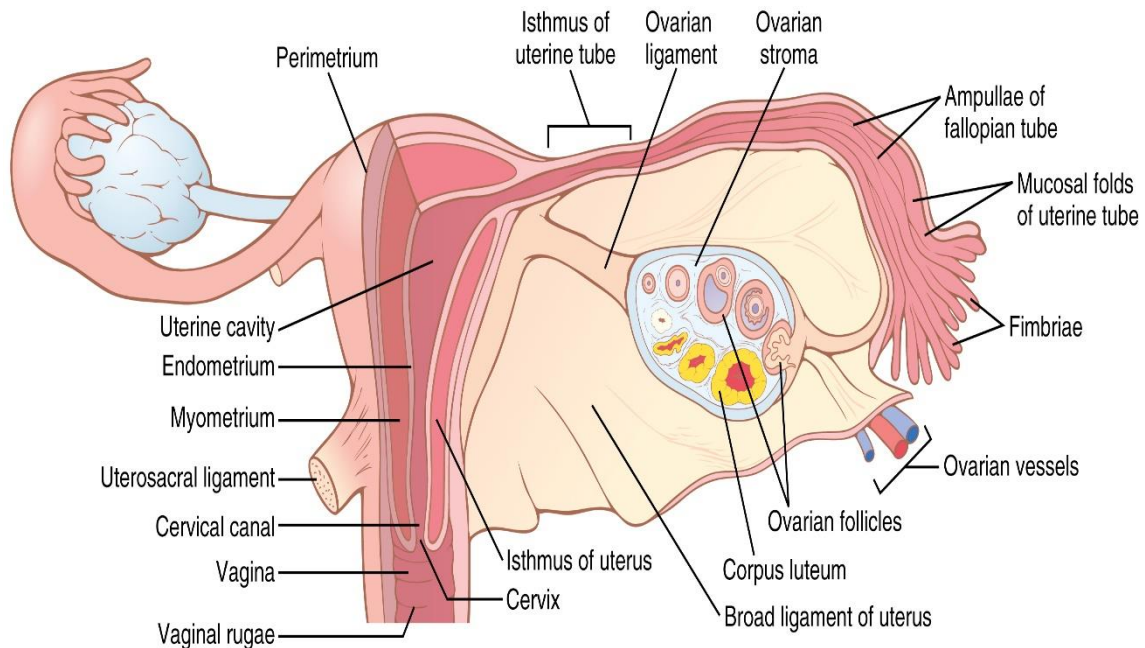


Figure 1 - The structure of the uterus, ovary and fallopian tubes including the oocyte at various stages of development. Image reprinted from Guyton and Hall Textbook of Physiology (Hall, 2021), with permission from Elsevier.

Oocyte maturation results in the development of a dominant follicle, which grows to up to 1.5 centimetres prior to rupture and release of the ovum (ovulation). The remaining granulosa and theca cells involute and go through a process of luteinization to form a mass, the corpus luteum. Over the following 12 days, this structure produces oestrogen, inhibin and progesterone and progressively involutes. Complete absorption of the corpus luteum results in a withdrawal of the negative feedback effect of these hormones thus triggering the release of the pituitary hormones which initiate a new ovarian cycle (Hall, 2021).

1.2 Ovarian Pathology

1.2.1 Types of Ovarian Pathology

1.2.1.1 Benign pathology

Functional Cysts

Following ovulation, bleeding can occur in the follicle filling the corpus luteal cyst with blood and forming a haemorrhagic cyst.

Primary follicles that begin to grow within a cycle but do not result in ovulation can occasionally form fluid filled cysts, follicular cysts, that persist on the ovary for a two to three menstrual cycles. These cysts can become as large as four to five centimetres.

Functional cysts tend to be self-remitting but can require intervention if rupture results in intra-abdominal bleeding. (KumarAbbas and Aster, 2017)

Mature Cystic teratoma (Dermoid Cysts)

These are slow growing tumours containing mature tissue (bone, hair etc) from at least two embryonic cell lines that occur in women of reproductive age. (Welter SM. and Khalifa MA.) They often require planned surgical intervention due the risk of pain and cyst accidents (rupture, haemorrhage or torsion) (Kaloo PD. et al., 2011).

Endometrioma

Endometriosis is a condition where endometrial-like tissue is found outside the uterus (Kennedy et al., 2005). The ovary is a common site for these deposits, which can result in blood filled masses called endometriomas. These can have fertility implications and consequently often result in surgical intervention (NICE Guideline., 2017).

Benign Epithelial tumours

These tumours arise from displaced surface epithelium and are either cystic (cystadenoma) or cystic with a stromal component (cystadenofibroma). They can further be divided depending on the type of epithelial cells, with mucin-secreting cells forming mucinous tumours and serous epithelial cells forming serous tumours. They both tend to be large, multicystic tumours (KumarAbbas and Aster, 2017).

1.2.1.2 Borderline Tumours

Borderline tumours are epithelial tumours that demonstrate some nuclear atypia without stromal invasion. As with other ovarian pathology, their epithelial cell type determines the subtype with serous and mucinous tumours accounting for 95% of borderline ovarian tumours (Hauptmann et al., 2017). They tend to present in premenopausal women and have a good prognosis, with a 5-year survival of 50-86% in advanced disease. Surgical management is required for staging and treatment of these tumours (BagadeEdmondson and Nayar, 2012).

1.2.1.3 Malignant neoplasm

Malignant neoplasms of the ovary encompass epithelial ovarian cancers, sex cord tumour and germ cell tumours. Primary peritoneal and fallopian tube cancers are grouped with epithelial ovarian cancer as they are treated in the same way (Cancer Research UK) and some epithelial ovarian cancers are thought to originate from the fallopian tube (Meyn and Lim, 2017). Management involves a combination of surgery and chemotherapy (BGCS, 2017). I will discuss ovarian cancer in further detail in section 1.3.

1.3 Ovarian Cancer

1.3.1 Background

Ovarian cancer is the sixth most common cancer with 20 new diagnoses daily in the UK. The risk of ovarian cancer increases with age, with a peak incidence at age 75-79 (Cancer Research UK). Ten-year survival rate is only 35% (Cancer Research UK).

Whilst it is considered to be a silent disease, some women experience the sensation of bloating, loss of appetite, early satiety, abdominal distension, abdominal pain, increase in girth, pelvic pressure, weight loss, fatigue, change in bowel habit and urinary frequency (NICE Guideline., 2011). Due to their non-specific nature, most women who have these symptoms will not have ovarian cancer. This is evident in investigations not being recommended unless women report persistent symptoms (NICE Guideline., 2011).

Advancing age, previous cancer, nulliparity and inherited genetic susceptibilities are risk factors for ovarian cancer. The use of the combined oral contraceptive pill is a protective factor (SundarNeal and Kehoe, 2015).

BRCA1, *BRCA2* and mismatch repair genes are the germline genetic susceptibilities seen in ovarian cancer. *BRCA 1 & 2* mutations are seen in 22% of high grade serous cancers (Crosbie et al., 2021) and confers a lifetime risk of 63% and 27%, respectively, for ovarian cancer (SundarNeal and Kehoe, 2015). Loss of function of these genes is associated with homologous recombination dysfunction (HRD) and subsequent loss of p53 (tumour suppressor gene) regulation (Kohn and Ivy, 2017). The four mismatch repair (MMR) genes are involved in DNA repair and mutations in these genes results in MMR deficiency (Lynch syndrome), which carries a 3-17% lifetime risk of ovarian cancer (Crosbie et al., 2021).

The International Federation of Gynaecology and Obstetrics (FIGO) classification is the consensus descriptor for the extent of disease in ovarian cancer. The criteria are listed in Figure 2.

1.3.2 Screening and early detection

Over half of ovarian cancers are diagnosed at advanced disease (stage III & IV) (Cancer Intelligence Team). Five year survival based on stage at diagnosis are 32% and 16% respectively, compared to 96% for stage I (Cancer Intelligence Team). This suggests a need for early detection for ovarian cancer however no reliable screening tool or early detection test exists. National engagement programmes such as Cancer Research UK Early Detection and Diagnosis of Cancer Roadmap highlight the need for novel approaches to early diagnosis for cancers such as ovarian cancer where no screening programme exists, and encourages and supports research and innovation in this area (Cancer Research UK). In addition to work being done for specific cancer types, there is interest in multicancer early detection (MCED) tests. A large-scale observational cohort study by Nicholson *et al*/analysed circulating tumour DNA in symptomatic patients referred to primary care. Overall the MCED test had a lower sensitivity for early stage cancers and the sensitivity for ovarian cancer (64.3%) was lower than published performance of CA-125 (Nicholson et al., 2023).

FIGO staging ovarian cancer 2014

STAGE I: Tumour confined to ovaries.

IA	Tumour limited to one ovary (capsule intact) or fallopian tube, no tumour on surface, negative washings
IB	Tumour involves both ovaries but otherwise description the same as stage IA
IC	Tumour limited to one or both ovaries with:
IC1	Surgical spill
IC2	Capsule rupture before surgery or tumour on ovarian or fallopian tube surface
IC3	Malignant cells in the ascites or peritoneal washings

STAGE II: Tumour involves one or both ovaries or fallopian tubes with pelvic extension (below the pelvic brim) or primary peritoneal cancer

IIA	Extension and/or implant on uterus and/or fallopian tubes and/or ovaries
IIB	Extension to other pelvic intraperitoneal tissues

STAGE III: Tumour involves one or both ovaries or fallopian tubes or primary peritoneal cancer, with cytologically or histologically confirmed spread to the peritoneum outside the pelvis and/or metastasis to the retroperitoneal lymph nodes

IIIA1	Positive retroperitoneal lymph nodes only:
IIIA1(i)	Metastasis <10 mm
IIIA1 (ii)	Metastasis >10 mm
IIIA2	Microscopic, extrapelvic (above the pelvic brim) peritoneal involvement with or without positive retroperitoneal lymph nodes
IIIB	Macroscopic, extrapelvic. peritoneal metastasis <2 cm with or without positive retroperitoneal lymph nodes
IIIC	Macroscopic, extrapelvic. peritoneal metastasis >2 cm with or without positive retroperitoneal lymph nodes. Includes extension to capsule of liver/spleen

STAGE IV: Distant metastasis excluding peritoneal metastasis

IVA	Pleural effusion with positive cytology
IVB	Parenchymal metastases and metastases to extra-abdominal organs

Figure 2 - International Federation of Gynaecology and Obstetrics criteria for staging ovarian cancer. Reproduced from (Prat, 2015).

Cancer Antigen (CA-125)

CA-125 is a glycoprotein found on the surface of epithelial cells derived from the coelomic epithelium (Charkhchi et al., 2020) and as such are found in the reproductive tract, gastrointestinal tract and respiratory tract, where it has a role in hydration, lubrication and barrier formation (Perez and Gipson, 2008, Streppel et al., 2012). CA-125 level has been found to be higher in premenopausal women, women with endometriosis, conditions that cause irritation or inflammation of the pelvic or abdominal cavities, pregnant women and women with a previous history of cancer as well as active non-ovarian cancers (Funston et al., 2020). Conversely, lower CA-125 levels are seen in women with African and Asian backgrounds, women who are postmenopausal, post hysterectomy and smokers (Charkhchi et al., 2020). The pathophysiology of CA-125 rise in ovarian cancer remains unclear, however (GandhiZubair and Bhatt) describe a serological rise in CA-125 as a result of the antigens being shed during disruption of the epithelial membrane barrier by pathological processes such as malignant transformation. This process might explain why, as the currently used tumour marker for risk assessment of ovarian cancer, CA-125 is positive in only 50% of clinically detectable stage I disease (Scholler and Urban, 2007). With a cut off of 35 units/ml, CA-125 has a sensitivity of 79% (95% CI 75.3 – 81.7%) and specificity of 78% (95% CI 73.2 – 82%) for ovarian cancer detection (Dodge et al., 2012); where sensitivity is the true positive rate (probability of a positive result if you have cancer) and specificity is the true negative rate (probability of a negative result in the absence of cancer).

Human Epididymis 4 (HE4)

HE4 is another secretory glycoprotein expressed by the ovary. On its own it is not helpful in the diagnosis of ovarian cancer in the post-menopausal woman as HE4 level increases with age. Whilst this can be overcome with age adjusted threshold levels, HE4 is also 20-30% higher in smokers (Urban et al., 2012, Bolstad et al., 2012) It was however demonstrated to be more accurate for the diagnosis of early ovarian cancers when compared to CA-125 alone in the primary care setting. When used together, CA-125 plus HE4 outperformed CA-125 alone and HE4 alone but was not as accurate as the use of both in Risk of Ovarian Malignancy Algorithm (ROMA) (Barr et al., 2022).

Risk of Ovarian malignancy Algorithm (ROMA)

ROMA score is calculated using menopausal status, HE4 and CA-125 levels in equation to determine the predictive index which is subsequently used to calculate the predicted probability of cancer as a percentage. This classifies women into a low risk or high-risk category. A meta-analysis of 32 studies demonstrated that ROMA outperforms HE4 and CA-125 in the prediction of epithelial ovarian cancers (Wang et al., 2014). Another meta-analysis in 2021 by Suri and colleagues echoed these results (Suri et al., 2021). There is ongoing work assessing the cost effectiveness of ROMA compared to CA-125 in the primary care setting (NCT06129968).

Randomised Control Trials

The aim of a screening test is to reduce morbidity and mortality (Fields and Chevlen, 2006) and unfortunately efforts to evaluate potential screening tests have failed to demonstrate a mortality reduction.

The first of the two largest randomised control trials on this topic, Prostate, Lung, Colorectal and Ovarian (PLCO) cancer screening randomised control trial, was conducted in the United States between 1993 and 2001 to evaluate the effect of screening for ovarian cancer on mortality. 78,216 women were randomised to yearly CA125 for 6 years and transvaginal scans for 4 years, or routine care. Participants were followed up for a maximum of 13 years. This study did not demonstrate a reduction in cancer mortality however there was lower than expected overall adherence with screening (79% and 78% by year four). Also, there was no change in the number of late-stage diagnosis in the intervention group suggesting that the two screening modalities used, CA-125 and transvaginal ultrasound, were not effective at detecting ovarian cancers early enough. The type of surgeon and type of systemic treatment used was not documented, both of which are important variables in cancer survival. Also noteworthy were the associated complications incurred in investigating false-positive screening (Buys et al., 2011). Extended follow, 15 years median, did not demonstrate a mortality benefit (Pinsky et al., 2016).

The second and more recent was the UK Collaborative Trial of Ovarian Cancer Screening (UKCTOCS) trial. This was a randomised controlled trial in the United Kingdom assigning 202,562 women aged 50-74 years to annual multimodal

screening (Risk of Ovarian Cancer Algorithm (ROCA) calculation of CA125 changes +/- ultrasound), annual transvaginal ultrasound alone or no screening. Participants were followed up for a median of 16 years. Unlike the PLCO trial, this study did manage to demonstrate a stage shift with a 47.2% higher incidence of stage I disease and 24.5% lower incidence in stage IV cancer in the multimodal screening group suggesting longitudinal CA-125 to be advantageous over single cut off CA-125. There was an increase in stage I mortality in the multimodal screening group which might account for the loss of impact of the stage shift of incidence of ovarian cancer, on mortality reduction. This might be inherent in the nature of this lethal disease or reflective of the limitations of ovarian cancer care during the screening and treatment period. There was a long follow up period in this study, during which the landscape of ovarian cancer treatment has changed significantly. This study concluded that population screening cannot be recommended as a reduction in mortality cannot be demonstrated (Menon et al., 2021).

1.3.3 Histological subtypes of Ovarian Cancer

Germ cell ovarian Tumours

Malignant ovarian germ cell tumours account for up to 5% of ovarian cancers and include, dependent on the germ cell line, dysgerminomas, immature teratomas, yolk sac tumours and embryonal tumours. They commonly occur in younger women, with the majority occurring between the ages of 14 and 54 years (Tidy et al., 2016). Raised α -FP and HCG correlates with stage and survival. Appropriate management is associated with a cure rate of 85.6% however women who relapse have poor outcomes (10% long term survival) (Murugaesu et al., 2006). Treatment tends to combination of chemotherapy and surgery with an aim of fertility preserving (Bailey and Church, 2005).

Ovarian sex cord stromal tumours

Ovarian sex cord tumours arise from ovarian follicles or their precursor cells and form 7% of ovarian cancers. They include granulosa cell tumours, theca-fibromas, Sertoli tumours and tumours of mixed or uncertain cell types, with granulosa cell tumours accounting for 90% of ovarian sex cord tumours. The subgroup, adult granulosa cell tumour, accounts for 95% of granulosa cell tumours making it the predominant ovarian sex cord stromal tumour. Peak incidence is age 50-55 years, whilst other ovarian sex cord tumours tend to occur

up to the early 30's. Adult granulosa cell tumours tend to carry a somatic mutation in the FOXL2 gene with higher expression of the gene having a worse prognosis. Inhibin is the predominant tumour marker for granulosa cell tumours. Due to the age of onset of sex cord tumours, treatment tends to be fertility sparing, with a combination of surgery, chemotherapy, hormonal and targeted therapy. (HarbiMcNeish and El-Bahrawy, 2021)

Epithelial Ovarian Cancers (EOC)

Epithelial ovarian cancers form 90% of ovarian cancers. They can be further divided by their histological subtype into high grade serous cancer (70%), endometrioid cancer (10%), clear cell cancer (10%), mucinous cancer (3%) and low grade serous cancer (<5%) (Cass and Newton, 2020).

In keeping with their benign and borderline counterparts, these histological subgroups of epithelial tumours arise from different types of epithelial cells. Clear cell and endometrioid ovarian cancers are both associated with endometriosis and are considered in the absence of expression of mismatch repair proteins (*MLH1*, *PMS2*, *MSH2* OR *MSH6*) in the immunohistochemistry of ovarian tumours. They both also share wild type p53 pattern and negative WT1 expression. However, endometrioid carcinomas show an adenofibromatous pattern with squamous metaplasia on microscopy, with patchy p16 immunostaining and oestrogen (ER) and progesterone (PR) receptor positivity whilst clear cell carcinoma is composed of clear cells arranged in papillary, glandular or solid patterns and is ER negative but positive for napsin A (BGCS, 2017), (WilkinsonVroobel and McCluggage, 2019).

Mucinous tumours tend to be confined to the ovary, with peritoneal involvement being an indication for ruling out metastasis from the gastro-intestinal tract (BGCS, 2017). They display CK7 positivity and CK20 negativity on immunohistochemistry (WilkinsonVroobel and McCluggage, 2019).

Low grade serous cancer is characterised by uniform cells with low mitotic activity, often with psammoma bodies, which can demonstrate invasive or non-invasive architectural patterns (Forgo and Longacre). As they are less chemo-sensitive, surgery is the mainstay of treatment (Grabowski et al., 2016). They are WT1 positive and display low proliferation of Ki67 on immunohistochemistry (WilkinsonVroobel and McCluggage, 2019).

High grade serous tumours differ from other epithelial tumours by their lack of architecture and abundance of enlarged malignant cells with dysmorphic nuclei. Serous tubal in situ carcinoma lesions (STIC) are thought to be precursors to this form of epithelial ovarian cancer. High grade serous tumours show genomic instability in DNA repair gene, *p53*, and are associated with mutations in *BRCA1* or *BRCA2* gene (Kohn and Ivy, 2017). Immunohistochemical features include mutant p53 staining (in 95% of cases), diffusely positive WT1 and p16 and moderate to high Ki67 staining.

These distinct morphological and immunohistochemistry profiles offer a simplified option of grouping EOC. Type 1 cancers (endometrioid, clear cell, mucinous and low grade serous) and type 2 cancers (high grade serous cancers, incorporating fallopian tube cancers) (SundarNeal and Kehoe, 2015). Type 1 tumours are associated with mutations, in varying incidence, in *KRAS*, *BRAF*, *PTEN*, *CTNNB1*, *ARID1A* and *PP2R1A*. They display significantly less genomic instability and are considered to be less aggressive tumours (Kurman, 2013). Type 2 tumours are associated with tumour p53 overexpression and, germline and somatic *BRCA 1* and 2 mutations (Levine et al., 2015).

1.4 Assessment and management of ovarian pathology

1.4.1 Assessment of ovarian pathology

History and careful examination are critical for discerning risk factors and clinical signs that might suggest the aetiology of ovarian pathology.

Laboratory tests

As discussed in section 1.3.2, CA-125 is the blood marker used in the assessment of complex ovarian pathology with the addition of Human Chorionic Gonadotrophin (HCG), alpha-feta protein (α -FP) and lactate dehydrogenase in women under the age of 40 years. In women, under the age of 40 years, false positive rates for CA-125 are higher due to this marker being elevated in some non-ovarian benign gynaecological pathology (Kalloo PD. et al., 2011). A level of

35 units/ml is considered a positive test and warrants an ultrasound scan of the abdomen and pelvis (NICE Guideline., 2011).

Ultrasound scan

A transvaginal ultrasound scan is the most effective way of assessing pelvic masses in both premenopausal (Kaloo PD. et al., 2011) and post-menopausal (MehassebSiddiqui and Bryden, 2016) women. A combination of both transabdominal and transvaginal scanning is occasionally required for larger masses. Ultrasound description of the features of the pelvic mass is used in risk calculation and subsequent decisions about further management.

Risk of Malignancy Estimation

The Risk of Malignancy Index (RMI) is the most widely accepted tool for the assessment of ovarian masses. A single score is calculated, and should the outcome be above the threshold of 200 (MehassebSiddiqui and Bryden, 2016), referral onto the gynaecological oncology team for further assessment is required. The score is calculated using the CA-125 value (IU/ml), menopausal status (M) and ultrasound description (U) of the mass (NICE Guideline., 2011).

$$RMI = U \times M \times CA125$$

Menopausal status is scored 1 for pre-menopausal and 3 for post-menopausal. Ultrasound is scored based on characteristics of the mass with each of the 5 characteristics, multilocular cysts, solid areas, metastases, ascites and bilateral lesions, scoring a point each. Table 1 displays the score given per number of characteristics displayed by the mass on ultrasound.

U score	Number of characteristics
0	0
1	1
3	2-5

Table 1 - U score allocation for Risk of Malignancy Index (RMI) score calculation. This table describes the score given depending on the number of characteristics displayed by the ovarian mass on ultrasound. This score is then multiplied by the menopausal status score and CA125 level to give the RMI score.

At the threshold of 200, RMI has sensitivity 78% (95% CI 71-85%), specificity 87% (95% CI 83-91%) (Kaloo PD. et al., 2011) for ovarian cancer prediction.

In premenopausal women, IOTA rules can be used to assess risk of malignancy without a CA125 test. These rules have reported sensitivities and specificities of 95% and 91% in this patient population. All women with a mass with any of the M rules ultrasound findings (Table 2) should be referred to the gynaecological oncology team for further assessment (Kaloo PD. et al., 2011).

B-Rules (predicting benign tumour)	M-rules (predicting malignant tumour)
Unilocular	Irregular solid tumour
Presence of solid components where the largest solid component has a largest diameter <7mm	Presence of ascites
Presence of acoustic shadows	At least four papillary structured
Smooth multilocular tumour with largest diameter (100mm	Irregular multilocular solid tumour with largest diameter \geq 100mm
No blood flow	Very strong blood flow

Table 2 - 10 Simple Rules for identifying benign and malignant ovarian masses (Timmerman et al., 2008). This table describes the rules for predicting benign and malignant ovarian tumours based on the presence or absence of these morphological features on ultrasound scan, without the need for a CA125 test.

1.4.2 Management of ovarian pathology

As discussed, women with an RMI score of \geq 200 are referred to the gynaecology oncology team for further assessment. The management of women with ovarian masses with lower RMI scores, in non-emergency situations depends on the wishes of the woman, her menopausal status, the size of the mass and her symptoms. In Figure 3, I attempt to summarise the management of these cysts with low malignancy risk based on the Royal College of Obstetricians and Gynaecologists guidelines for pelvic masses in premenopausal and postmenopausal women. The preferred surgical intervention is laparoscopy in both groups, due to faster postoperative recovery (Alessandri et al., 2006), with a recommendation of bilateral salpingo-oophorectomy in postmenopausal women as opposed to cystectomy (MehassebSiddiqui and Bryden, 2016). Where it is anticipated that the mass might have solid components, laparotomy should be considered to avoid complications with specimen retrieval (Kaloo PD. et al., 2011).

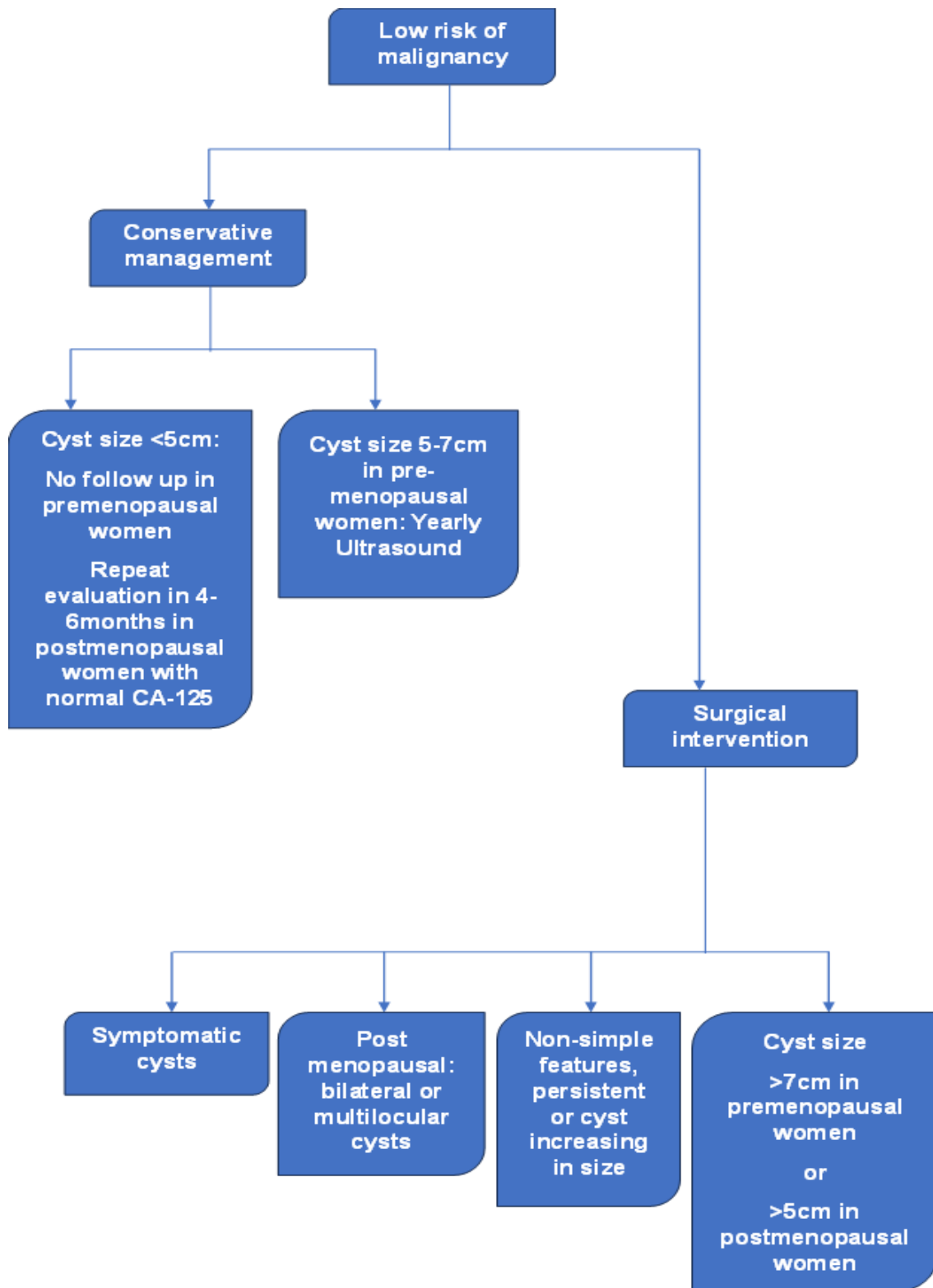


Figure 3 - Management of ovarian cysts of low malignancy risk. This figure summarises conservative and surgical management parameters for ovarian cysts with RMI <200 in both pre- and post-menopausal women (Kalloo PD. et al., 2011, MehasebSiddiqui and Bryden, 2016).

1.4.3 Investigations in secondary care and diagnosis

As discussed in section 1.4.1, women with any of the M-rules ultrasound findings and or women with an RMI score ≥ 200 are referred to the gynaecological oncology team for further assessment as they are high risk for or presumed to have ovarian cancer. Their presentation, examination findings, medical history and imaging are discussed at the multidisciplinary team meeting and options regarding further investigations and management plans are documented. The British Gynaecological Cancer Society (BGCS, 2017) recommends radiological staging of the disease using computer tomography (CT) imaging of the chest, abdomen and pelvis however the only way to make a diagnosis of ovarian cancer is tissue histology. Stage I disease refers to disease confined to the ovary, stage II is disease confined to the pelvis, stage III denotes involvement of the peritoneum and lymph nodes and stage IV indicates distant metastases (Berek et al., 2018). Disease stage influences management as a formal diagnosis of ovarian cancer must be made prior to administration of any cytotoxic medication thus prompting whether patients have a biopsy of extra ovarian disease or primary surgery to get tissue for their diagnosis.

1.4.4 Management of ovarian cancer

Treatment aims to prolong overall survival, and complete removal of all macroscopic disease, complete cytoreduction, has been demonstrated to be the most important independent factor (Vergote et al., 2010b).

Stage I and II

In patients where complete cytoreduction appears achievable on radiological staging (stage I and some stage II), primary surgery consisting of peritoneal washings, ascites sampling, total hysterectomy, bilateral salpingo-oophorectomy, peritoneal biopsies, omentectomy and pelvic and para aortic lymph node assessment is the standard of care (BGCS, 2017). This enables final diagnosis and staging of the ovarian cancer.

These patients are then offered systemic cytotoxic treatment (adjuvant chemotherapy). In the Cochrane meta-analysis (Lawrie et al., 2015) of five randomised control trials looking at adjuvant chemotherapy versus no chemotherapy or placebo in women with stage I or IIA epithelial ovarian cancers, high quality evidence demonstrated better five and ten year overall survival in the chemotherapy group. The data is incomplete for the subgroup analysis of women

with optimally staged low risk (stage IA) disease and individual factors should be taken into account in the decision for adjuvant chemotherapy in this group. This meta-analysis included the ICON1 (Collaborators, 2003) and ACTION (Trimbos et al., 2003) trials.

Stage II – IV

Where it is uncertain or unlikely that complete cytoreduction can be achieved, systemic treatment with platinum-based chemotherapy +/- paclitaxel is offered, followed by interval debulking surgery (IDS) and then adjuvant chemotherapy to complete six cycles of chemotherapy in total. This is the standard of care for patients with advanced disease (BGCS, 2017). Two randomised control trials demonstrated reduced morbidity, equal or better quality of life and similar survival in patients with primary chemotherapy compared to patients who had primary surgery.

The first trial, Neoadjuvant chemotherapy or primary surgery in stage IIIC or IV ovarian cancer, was undertaken by a collaborative group from the European Organization for Research and Treatment of Cancer, Gynaecological Cancer Group and the NCIC Clinical Trials Group. This study randomised 632 women to with stage IIIC and IV ovarian cancer to primary surgery or neoadjuvant chemotherapy. The median overall survival was 29 months and survival, as well as progression free survival, was non-inferior in the neoadjuvant chemotherapy group. One of the recruitment centres for this study was excluded, along with all data collected from the centre. It is unclear the number of participants and the impact on overall recruitment this had on the study (Vergote et al., 2010b).

The second trial, CHORUS trial, took place in hospitals across the UK and New Zealand. This study randomised 550 women with stage III and stage IV ovarian cancer to primary surgery and primary chemotherapy. Survival with primary chemotherapy was non-inferior to primary surgery (HR 0.87, upper bound of 90% CI 0.98). This trial had a higher median participant age (65 years) and associated lower performance status (68% PS1 and 2) compared other trials looking at advanced ovarian cancer, making it less comparable and possibly explaining the lower than expected overall survival (median 22-24 months). Nevertheless, there were better post operative adverse events and shorter inpatient stays in the primary chemotherapy group (Kehoe et al., 2015).

The surgical plan in the interval debulking surgery group is similar to the primary surgery group, plus removal of bulky lymph nodes and resection of disease from any viscera affected; maximum effort surgery (BGCS, 2017). Cochrane meta-analysis of 11 studies reporting analyses of residual disease demonstrated that where complete macroscopic resection is not achievable, achieving less than 1cm residual disease still confers benefit for overall survival. The quality of this evidence is however impacted by the high risk of bias in the studies included, lack of an objective assessment or documentation for the surgical effort or reasons for the levels of residual disease (Elattar et al., 2011).

Achieving complete resection can be complicated by the fibrotic changes that occur as a result of primary chemotherapy (Vergote et al., 2010b). Elattar et al also highlighted the need for a formal classification system for completeness of cytoreduction. There also remains no objective tool for assessing residual disease volume.

Targeted therapies

Advances in our understanding of the molecular changes in epithelial ovarian cancers has led to the development of targeted therapies that take advantage of these pathways. Some monoclonal antibodies and other antiangiogenics have been demonstrated to improve disease free survival when given as maintenance therapy. (Perren et al., 2011) demonstrated an increased progression free survival in high risk patients by 3.6 months with bevacizumab given with platinum-based chemotherapy than without it. (Burger et al., 2011) also demonstrated increased progression free survival, four months, with bevacizumab and chemotherapy compared to chemotherapy and placebo. Whilst (du Bois et al., 2016) also demonstrated increased survival with nintedanib, gastrointestinal adverse effects make this treatment not tolerable. Nevertheless, this study however reinforces these targeted therapies at increasing disease-free survival in ovarian cancer.

Poly-ADP ribose polymerase (PARP) inhibitors cause selective cell death by disrupting the repair pathway in cells that have homologous recombinant repair deficiencies (NeffSenter and Salani, 2017). This takes advantage of the *BRCA* mutation mediated genomic instability seen in some high grade serous ovarian cancers. In the double blind, phase 3 randomised control trial looking at niraparib in patients with newly diagnosed advanced ovarian cancer, 733 participants were

randomised to niraparib or placebo. 50% of the study population had homologous recombination deficiency. Niraparib increased the overall progression free survival for the study population by 5.6 months. In the group with homologous recombination deficiency, progression free survival was doubled (21.9 months niraparib compared to 10.4 months with placebo (González-Martín et al., 2019).

1.5 Conclusion

We continue to make advances in the treatment of ovarian cancer such as with the advent of targeted therapies however, we still appear to be fighting the clock on highly impactful ways of reducing mortality.

The stage-based mortality data, 32% and 16% five year survival at stage III and IV, makes a strong case for early detection being a key approach to tackling this issue. To achieve early detection, a biomarker able to detect early disease is required. Attempts at a screening test to date have used CA-125, a biomarker known to lack sensitivity in early disease. Both these significant attempts, PLCO and UKCTOCs trials, did not yield a mortality reduction and demonstrate our current inability to reach this goal. One potential novel method to provide an early biomarker is Raman spectroscopy which has shown potential in this role in other cancers (see section 1.6.4 below).

Another highly impactful way of reducing mortality from ovarian cancer would be to provide assurance of complete cytoreduction during surgery which has been shown to be pivotal in improving survival however currently this remains a subjective assessment. An objective tool of assessing residual disease burden would aid intraoperative decision making around maximum effort surgery. Raman spectroscopy has shown promise in this regard during surgery for the removal of other cancers (see section 1.6.4 below).

In the next section, Raman spectroscopy, I shall describe the technique and its use to date in the field of cancer detection.

1.6 Raman Spectroscopy

Raman spectroscopy is a phenomenon, observed by Raman and Krishnan in 1928, of the inelastic scattering of light from a sample (Smith and Dent, 2004a).

1.6.1 Relationship between light and molecules

Light is an electromagnetic (EM) wave with inherent energy. The electric and magnetic components vary in time, which creates different types of electromagnetic waves recognised by their differing frequency and wavelength; where frequency represents the number of waves over time and wavelength, the distance between peaks of two consecutive waves.

Due to the relationship between energy and frequency:

$$E = h\nu$$

where h is Planck's constant and ν is frequency, the long wavelength low frequency EM waves on the right of the spectrum have lower energy whilst the short wavelength high frequency EM waves on the left have higher energy (Figure 4).

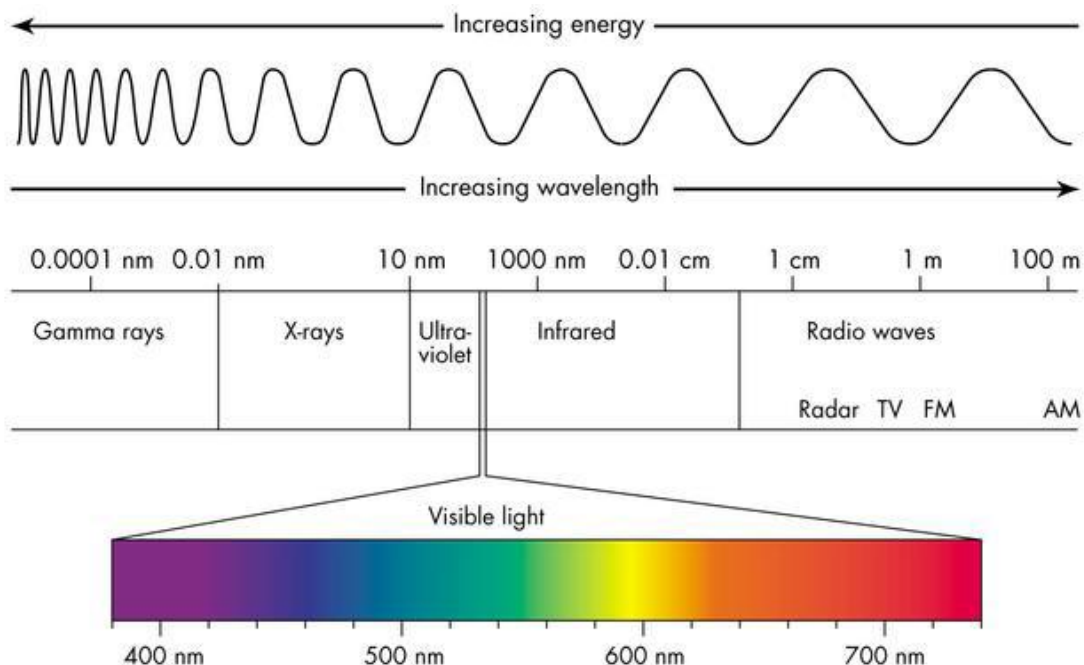


Figure 4 - The electromagnetic spectrum. This image displays the spectrum of electromagnetic waves, and their wavenumbers. It illustrates increasing energy with decreasing wavelength and the position of visible light in this spectrum. This image is reprinted from (Cyberphysics, 2009) with permission. Original source unknown.

When light interacts with matter, the photons of the electric field can –

- 1) have no interaction and pass through the molecule.
- 2) be absorbed and increase the energy state of the molecule if the energy sufficiently fits the gap between the ground and excited state of the molecule.
- 3) be scattered by the molecule.

When the photon is scattered from the molecule, the interaction can either occur efficiently with no change in energy (Rayleigh or elastic scattering) or with a change in the energy of the photon (Raman or inelastic scattering). (Tu, 1982)

Inelastic scattering

The difference in the energy of the scattered photon from its incident energy is called the Raman shift. This change in energy occurs if there is a change in the polarizability of the electron cloud around the molecule when it is in a vibrational mode.

The Raman shift can be to a higher or lower energy state level depending on the vibrational state of the molecule at the time of scattering (Figure 5). Molecules in the ground vibrational state will enter a temporary higher energy state (virtual vibrational state) during scattering and then rapidly de-excite to either the original energy state (Rayleigh scattering), a higher vibrational energy state due to the scattered photon losing energy to molecular vibrations (Stokes scattering), or molecules that were in a vibrationally excited state can revert to a lower energy state due energy being transferred to the scattered photon from molecule (Anti Stokes scattering).

Stokes scattering is more likely, i.e. more intense than anti-Stokes scattering. This is a result of most molecules existing at ground state at room temperature. This relationship between energy states of molecules and temperature is described by the Boltzmann distribution whereby, the proportion of molecules with higher energy increases as temperature increases. Thus the intensity of stokes and anti-stokes scattering varies depending on temperature. (Tu, 1982)

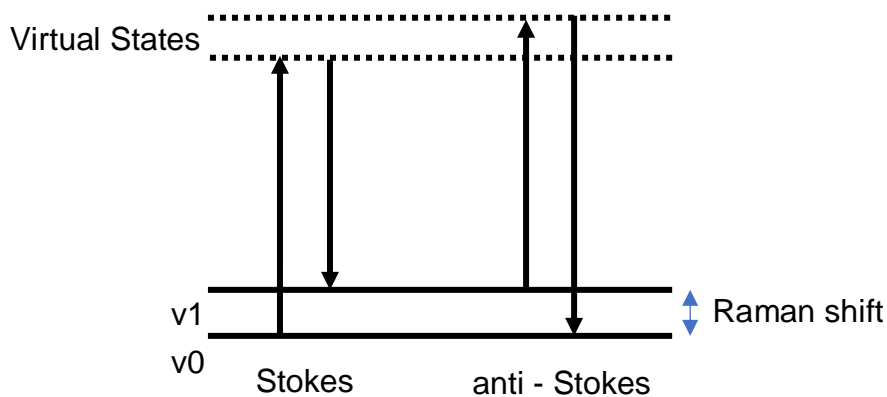


Figure 5 - Raman Scattering. This figure illustrates the shift in energy levels (Raman shift) that can occur when a photon interacts with a molecule. If the molecule was at ground state (v_0), this interaction results in a higher vibrational state due to the scattered photon losing energy to molecular vibrations (Stokes scattering). If the molecule was at an excited vibrational state (v_1), this interaction results in a lower energy state due to energy being transferred to the scattered photon from the molecule (anti Stokes scattering). Adapted from (Smith and Dent, 2004a)

1.6.2 Vibrational states of molecules

The Raman shift depends on the natural frequency of the molecule. Hooke's law described the relationship between frequency, bond strength and the mass of atoms where essentially the lighter the atom, the higher the frequency:

$$v = \frac{1}{2\pi c} \sqrt{\frac{K}{\mu}}$$

Where c is the velocity of light, K is the force constant of the bond and μ is the reduced mass of the atoms. The more complex the molecule the more vibrational modes it has, with each having its own natural frequencies. Measuring the frequencies of these modes by measuring the inelastic scattering of light, provides a spectroscopic fingerprint for the molecule. This forms the basis of peak assignments in Raman spectroscopy where the molecular composition of the molecule can be deduced by assigning the Raman shift (peaks) at different frequencies to reference vibrational groups (Smith and Dent, 2004c).

1.6.3 Measuring scattered photons

There are now many commercially produced machines available for Raman systems but in its basic form, the main components required to measure Raman spectra are an excitation source, a filter, grating and charge-coupled device (CCD). In this simple model, the photons are generated by the excitation source, the Rayleigh scattered photons are filtered out and Raman photons are dispersed

by a diffraction grating according to their wavelength thus appearing on the CCD in distinct positions. The image is captured by the CCD as the Raman spectrum.

Excitation Source

Diode lasers are commonly used with Raman systems for biological spectroscopy due to their energy efficiency, and high spectral resolution associated with their narrow laser bandwidths. Choosing laser wavelengths in the near infra-red or ultraviolet regions avoids contributions from fluorescence in the fingerprint region of the spectrum however this needs to be balanced with the effects on the biological sample. High frequency wavelengths such as ultraviolet region can be destructive to the sample thus having implications for both study design and translational prospects of Raman spectroscopy. Generally, near infra-red wavelengths between 785 and 830 nanometres (nm) are common place in biological studies with the 830 nm being preferable (Butler et al., 2016).

Filter and grating

Raman spectrometers have two key roles, one to remove the dominant elastically scattered light at the laser wavelength and two to separate the photons that are collected at shifted wavelengths to enable a spectrum to be measured. Historically this was achieved with a sequence of gratings, splitting the light into its component frequencies and over multiple steps, sufficient elastically scattered light would be rejected. This resulted in very few Raman scattered photons reaching the detector due to the relative inefficiency of the multiple gratings, thus requiring very long acquisition times. A major breakthrough occurred with the invention of notch filters, able to directly filter out the laser line by many orders of magnitude 10^6 to 10^7 (Carriere and Havermeier, 2012, Stone, 2001).

Notch filters which remove the laser frequency or more recently developed long pass edge filters are commonly used filters in Raman systems. They are coupled with one monochromator, functioning as a grating which sorts the Raman scattering according to wavelength. Notch/edge filters have the advantage of being small and efficient but, as they are specific to the excitation frequency, they cannot be tuned without being replaced which can be restrictive (Smith and Dent, 2004b).

Detector

Charge-coupled devices are used in Raman spectroscopy to convert Raman scattered photons into a read out, the Raman spectra. The CCD is a multichannel array, arranged in rows and columns, providing a measure of intensity at each wavelength. The collected Raman photons when incident on the CCD induce the production of photoelectrons in the detector. Each pixel in the CCD can be read out independently or summed together to provide all the photons at one wavelength for example. The more photons that arrive per wavelength, the higher the number of photoelectrons generated and therefore the higher the intensity of the readout signal at that point in the spectrum. For simplicity we convert the wavelength units into wavenumber ($\frac{1}{cm}$,) which is directly proportional to the energy of the Raman photon (and therefore molecular vibrational energy) and enables a spectrum to be equivalent / easily comparable, when measured at different laser wavelengths. (Stone, 2001)

Limitations of this technique

- 1) Weak process - Only a small number of photons are Raman scattered. This is reflected in higher power lasers typically used in Raman spectroscopy. It has implications on the sensitivity of the technique for detecting molecules present in low concentrations. (StoneKendall and Barr, 2001)
- 2) Fluorescence – This phenomenon involves the absorption of the incident photon and promotion of the molecule to a higher electronic energy state (as opposed to the almost instantaneous virtual state seen in the polarisation of molecules during scattering). Fluorescence emission occurs when the molecule returns to its ground state. Absorption and fluorescence can occur more easily than Raman scattering, if the laser photons are of sufficient energy to achieve electronic absorption. Therefore, fluorescence will be much more intense (more photons emitted) and it can have similar wavelengths, obscuring the Raman spectra. Fluorescence is wavelength dependent with the shorter wavelength region being more likely to create fluorescence contributions as higher frequency photons are more likely to induce electronic absorption. For this reason, lasers in the near infra-red region are preferred in Raman spectroscopy,

(StoneKendall and Barr, 2001, Smith and Dent, 2004b) as most molecules do not naturally absorb these photons.

- 3) Photodegradation – This is the degradation of molecules by photons through absorption. Consideration of the tissue type and laser spot profile when planning measurement protocols can mitigate this issue however there is a need to consider the trade-off between fluorescence and sample damage which can be limiting in what is inherently a low sensitivity test. (Butler et al., 2016)

Summary

Raman spectroscopy is a non-destructive technique that uses the inelastic scattering of light to determine the molecular composition of molecules. To maximise the potential for this technique, careful selection of the excitation source based on consideration of sample type and the risk of fluorescence contributions. This technique has great potential for application in biomedical science.

1.6.4 Biological applications of Raman spectroscopy

Since Raman scattering was observed in 1928, there have been significant advances in the quality, portability and complexity of equipment, and our understanding of Raman scattering and peak assignments. There are also areas with a clinical need where this technique could be useful, such as in the identification of tissue margins and/or in immediate or time sensitive diagnosis where traditional histology might not be appropriate or obtainable (StoneKendall and Barr, 2001). In this section, some of the work on biological applications, related to cancer, in Raman spectroscopy have been summarised.

Breast cancer

Since 2005, several groups have assessed the potential of Raman Spectroscopy for the diagnosis of breast cancer in *ex vivo* tissue. High sensitivity and specificity for the diagnosis of breast cancer was reported using 130 spectra from 58 patients (Haka et al., 2005), 94% and 96% respectively, although this work did not look at the biochemical changes and/or the performance of the model with different grades of breast cancer. These points were addressed by Rehman and colleagues (Rehman et al., 2007) who used Raman Spectroscopy to differentiate between grades of breast cancer and demonstrated significantly different relative and absolute peak intensities in the Raman spectra between the two grades but

did not then develop models to test the diagnostic performance. A later study, (Kong et al., 2014), used a cross validated model (that is, the prediction performance of their diagnostic model) which achieved 95.6% sensitivity and 96.2% specificity for the diagnosis of ductal carcinoma, however the spectral imaging technique used, raster-scanning, had high acquisition times making it unlikely that this system would translate to the *in vivo* clinical setting. It is notable that the sensitivity and specificity seen in both 2005 and 2014 studies (Kong et al., 2014, Haka et al., 2005) are similar despite different spectral imaging and analysis techniques.

A systematic review by Deng and colleagues (Deng et al., 2016) brought together all studies published until 2015 including the studies highlighted above. It demonstrated a sensitivity and specificity of 92 and 97% for the use of Raman spectroscopy to diagnose breast cancer. In this review, diagnostic accuracy for Raman was assessed using pooled data from the nine studies that had sufficient data to create a confusion matrix, meaning that potentially, good studies that did not present sufficient data to construct a table with true positives, false positives, true negatives, and false negatives were excluded. The studies included were small sample studies and there was insufficient data to review the effects of pathological subtypes. This does however reflect the large body of work that has been done on the application of this technique in breast cancer and there is ongoing work regarding its use for intraoperative margin assessment (HubbardShore and Stone, 2019).

I will discuss the use of this technique with lymph node assessment later in this section however, in relation to breast cancer, *ex vivo* Raman analysis of sentinel lymph nodes in breast cancer patients, measured using a Raman probe, achieved cross validation sensitivity of 92% and specificity of 100% in differentiating normal and affected lymph nodes. This result suggests that a probe could be used in the intra-operative setting to get immediate results on lymph node status (Horsnell et al., 2010).

Raman spectroscopy has also been used to try to establish cancer free margins in breast cancer. A pilot study by Haka and colleagues (Haka et al., 2006) using a Raman fibre probe achieved a sensitivity of 100% and specificity of 100% including the detection of a clinically missed positive margin that required a second procedure after histological confirmation. As expected for a pilot study,

participant numbers were small, nine participants, however this work suggested that margin analysis in breast cancer is feasible. Recently, Haskell and colleagues (Haskell et al., 2023) have progressed this work with Raman probe measurements of freshly excised breast tissue from 30 participants. Their prediction model was able to achieve a sensitivity of 77.1% and specificity of 90.8% for using high wave number Raman spectroscopy to predict normal versus benign tumour margins. Further research is required to facilitate translation of this work to clinical use.

Oesophageal cancer

There is a good body of working looking at the use of Raman spectroscopy to diagnose oesophageal cancer. Kendall and colleagues (Kendall et al., 2003) were able to predict cancer in patients undergoing surveillance for Barrett's oesophagus with sensitivities between 76 and 100% and specificities between 90 and 100%. The range in performance data in this model is due to lack of blinded consensus in the three histopathology opinions which were used as the gold standard in this work, further highlighting the need for an objective assessment of this very crucial pre-cancerous condition.

A systematic review of publications from 2007 to 2020 looking at Raman spectroscopy in the diagnosis of oesophageal cancer revealed 69 articles of which only 9 had enough data reported to be able to calculate pooled sensitivities and specificities. Seven studies measured tissue (four for *ex vivo* tissue and three for *in vivo*) and two studies measured urine and haemoglobin. Quality evaluation of the studies in this review showed low risk of bias and low applicability concerns. High quality evidence from this meta-analysis shows that Raman spectroscopy achieves a sensitivity of 91% and specificity of 92% for oesophageal cancer detection in tissue, compared to benign. This analysis did not include a subgroup analysis for different tumour types and thus, it is unclear whether the diagnostic performance achieved in this work is consistent across tumour types and stage of disease, both of which are important for consideration for clinical implementation. Most of the studies that were included were conducted in Asia which raises the question of possible selection bias and generalisability to all populations, although, in keeping with systematic reviewing guidelines two independent reviewers were used for the selection of studies to include in the systematic review (Hao et al., 2020).

In order to usefully progress work done to the *in vivo* clinical setting, the use of Raman spectroscopy through a fibre-optic probe would be essential. Barriers to consider would include size of the apparatus, i.e. making the system compact enough to work alongside other technologies in use in the clinical setting and developing a read-out method that does not require a spectroscopist to interpret the results. New medical devices require Medicines and Healthcare products Regulatory approval which can be a lengthy process. Day and colleagues (Day et al., 2009) designed and tested a miniature fibre optic probe, small enough to fit a medical endoscope channel with the view of *in vivo* diagnostics. The probe was tested on snap frozen tissue and demonstrated that spectra could be collected in a practical time frame. This endoscopic tool was used by Almond and colleagues (Almond et al., 2014) to measure 673 *ex vivo* samples from 62 patients undergoing surveillance for Barrett's oesophagus, or surgery for either high grade dysplasia or oesophageal adenocarcinoma. Participants having surgery for cancer had completed a course of neoadjuvant chemotherapy prior to their surgery. This technique was able to predict high grade dysplasia and adenocarcinoma with a sensitivity of 86% and specificity of 88%. It was also noted to be able to detect superficial disease but as noted in some of the earlier studies mentioned above, discordance in histological diagnosis between pathologists, who were acting as the gold standard for the study, had an impact on training classification models. Prior to this work, Bergholt and colleagues (Bergholt et al., 2011) had also successfully built a high accuracy, 96%, diagnostic model using measurements taken from a flexible fibre optic probe. For this work, 75 Raman spectra were generated from *in vivo* endoscopic measurements of the oesophagus taken from 27 patients using a flexible fibre probe. The pre-processed Raman spectra from these measurements were displayed in a graphical user interface however it is not clear whether analysis and assignment of spectra to pathology group was also performed in real time or separately later. The facility to analyse data and predict pathology in real time would be invaluable in the progress to translation of this technique to everyday clinical use.

Further work in this area is ongoing including a study looking at *in vivo* diagnostic testing with real time results (clinicaltrials.gov: NCT03468634).

Urological Cancer

Raman spectroscopy has been used to explore whether it is possible to differentiate between benign and malignant processes in the bladder and prostate, as well as understanding the biochemical changes associated with these pathologies. Stone and colleagues were able to identify and grade prostate adenocarcinoma from varying cell lines, representing varying biological aggressiveness with a sensitivity of 98% and spec 99% (Crow et al., 2005). This group then went on to achieve accuracies of 84% and 86% for the differentiation of snap frozen benign and malignant bladder and prostate samples using Raman spectra recorded with a fibreoptic probe. The sample size was too small for histological subgroup analysis however the results are promising for the use of Raman clinical systems (Crow et al., 2005b). They then went on to demonstrate the biochemical composition of bladder and prostate pathology. In this study, they described the relative concentrations of different constituents of normal, cystitis, carcinoma in situ and transitional cell carcinoma of the bladder and benign prostatic hypertrophy, prostatitis and prostate cancer (Stone et al., 2007). The work on fibre optic measurements was continued by Grimbergen and colleagues (Grimbergen et al., 2009) who used an endoscopic fibre based Raman probe to measure 107 bladder samples immediately after collection and achieved a cross validation sensitivity of 78.5% and specificity of 78.9% for differentiating normal and malignant bladder tissue. This study showed that small fibre probes were feasible for endoscopic measurements but highlighted the potential difficulties that can arise when there is more than one pathology type in the sample.

Colorectal Cancer

Raman spectroscopy has been used to explore colorectal cancer diagnosis using both tissue and biological fluids however the body of work is not as extensive as seen in oesophageal cancer. Molckovsky and colleagues differentiated adenomatous from hyperplastic polyps with a sensitivity of 91% and specificity of 95% with *ex vivo* samples. A separate diagnostic model was able to differentiate ten adenoma and nine hyperplastic polyps, using *in vivo* measurements, with a sensitivity of 100% and specificity of 89%. The measurements for both types of tissue were completed using a Raman fibreoptic probe. In this study, the model built using data from *ex vivo* samples did not perform well when tested on data collected from *in vivo* measurements suggesting different variables in Raman

classification of spectra taken *in vivo* and *ex vivo*. This has potential implications when considering translational research in Raman spectroscopy (Molckovsky et al., 2003). Work on serum diagnosis of colorectal cancer has also yielded high accuracies. LiYang and colleagues compared serum from 46 participants with colon cancer and 44 participants with rectal cancer against a control of 30 participants with no pathology. They demonstrated a diagnostic accuracy of 88% for colon cancer and 83% for rectal cancer using linear discriminant analysis suggesting that serum has the potential to be used to diagnose colorectal cancer. This result was not cross validated (LiYang and Li, 2012).

A systematic review and meta-analysis of thirteen studies assessing Raman spectroscopy in diagnosis of colorectal carcinoma by Zheng and colleagues demonstrated a pooled sensitivity and specificity of 94% and 94% for colorectal cancer detection. Whilst the selection criteria include use of histopathology as the standard, it does not specify whether these studies examined tissue or biological fluids. Unfortunately, this information is also omitted in the analysis and discussion sections of this systematic review (Zheng et al., 2019).

A large study looking at early detection of colorectal cancer using biological fluids is ongoing (REC: 14/WA/0028).

Head and Neck cancer

With the exception of lymph node work which has progressed extensively for other tumour types such as breast cancer, most of the work on head and neck cancers have been exploratory but demonstrated great potential for further feasibility or translational research.

Diagnosis of laryngeal cancer using Raman spectroscopy was explored in a small study by Stone and group, with 15 samples, seven normal, four with dysplasia and four with carcinoma. Samples were measured using a commercially available Raman spectrometer and demonstrated cross validation sensitivities and specificities of 83% and 94% for prediction of normal, 76% and 91% for prediction of dysplasia, and 92% and 90% for prediction of cancer. These results are limited by sample numbers but demonstrates promising diagnostic modelling for pharyngeal cancer using Raman spectroscopy (Stone et al., 2000).

An exploratory study of Raman application in thyroid cancers by using freshly excised tissue from 30 participants was able to identify the biochemical changes between carcinomas, adenomas and nodules or goitres, using principal component loads. They did not build models to explore diagnostic classification of these groups (Manfait et al., 2000).

For parathyroid cancer, a small study by Das and colleagues used Raman spectroscopy to compare nine parathyroid adenomas and six hyperplastic tissue using fresh frozen samples. This study achieved a cross validation sensitivity and specificity of 97% and 91% for detection of parathyroid adenomas, and 91% and 97% for parathyroid hyperplasia. Large numbers of spectra were taken from a small volume of samples, but this study demonstrated that Raman spectroscopy is a viable tool for parathyroid assessment as well as providing insight into the biochemical changes that occur in parathyroid adenomas and hyperplasia (Das et al., 2006).

As previously discussed, there has been more significant work done on lymph node assessment using Raman spectroscopy. One such study used the commercially available Raman system, Renishaw system 1000, to measure 103 lymph nodes from 23 patients with five pathologies. The pathologies were grouped into a benign group, a primary cancer group (Hodgkins lymphoma and non-Hodgkins lymphoma) and a secondary cancer groups (metastatic squamous cell carcinoma and metastatic adenocarcinoma). Using two different methods of diagnostic modelling, PCA-LDA and PLS-DA, they were able to demonstrate three class (benign, primary cancer and secondary cancer) sensitivities and specificities of 78% and 89%, and 81% and 89% respectively suggesting that Raman spectroscopy can detect cancer in lymph nodes and separate primary cancer from secondary or metastatic disease. Unfortunately, the groups were unbalanced and there were small numbers in the cancer groups, despite some participants providing both cancer and benign samples, with 18 of 23 belonging to the benign group and only 10/23 total across the cancer subgroups. Regardless of the small numbers, biochemical features representative of cancer in the lymph nodes have been highlighted by this work as well as the ability of Raman to discriminate between primary and metastatic disease (Lloyd et al., 2013). Following on, high accuracies were demonstrated by Fullwood in her PhD work using a Raman needle probe to assess head and neck lymph nodes. This

work achieved a cross validation sensitivity and specificity of 79% and 81% for identification of cancer from non- cancer. Whilst the sample size was small in the cancer group, 36 non-cancer samples and 14 cancer, there were clear spectral differences demonstrated between the two tissue types (Fullwood, 2017).

Brain

The body of work on brain tumours is limited. Earlier work explored classification of tumour and necrosis tissue in gliomas with a view of developing classification models that can be translated to aiding stereotactic surgery for glioblastoma. Koljenović and colleagues developed a classification model using fresh samples taken from 20 participants and tested this model on data from nine other participants, achieving an accuracy of 100% for tumour prediction. Despite the low numbers, high accuracy results on independent testing of this model suggests a robust model that needs to be tested further with to translation to *in vivo* measurements (Koljenović et al., 2002).

Biofluid diagnosis was explored by Mehta and colleagues, using serum samples collected from 35 healthy participants and 35 participants with meningioma to explore a diagnostic model for meningioma (Mehta et al., 2018). Cross validated PCA-LDA models demonstrated a classification accuracy of 92% for healthy and 80% meningioma. Subgroup analysis looking at specific grades of meningioma demonstrated an accuracy of 87% for grade I disease and 69% for grade II disease. This was an exploratory study and needs validation on a larger scale however the results are extremely promising for application to screening of high risk populations.

Gynaecological cancers (excluding ovarian cancer)

Raman spectroscopy has been explored using tissue and/or biological fluids for the detection of cervical and vulval cancers and pre cancers conditions.

The work in cervical cancer is complicated by factors such as cervical mucus, vascularity and contamination of samples with blood, and the variation in cell types (Lyng et al., 2015). Despite this, high accuracy for detection of cervical cancer, 85.7%, from samples of cervical inflammation and cervical intraepithelial (CIN) I, II, and III, has been demonstrated by Wang and colleagues using independent testing data. To achieve this, 210 dewaxed tissue sections were

measured using a commercially available Raman system coupled with a 532 nm laser source. This work also explored the biochemical changes that occur in the progression through the CIN stages to cancer (Wang et al., 2021).

Whilst the body of work for endometrial cancer is limited, one study looking at plasma diagnosis using attenuated total reflection-Fourier transform infrared spectroscopy was able to detect endometrial cancer and endometrial hyperplasia with high accuracy (Paraskevaidi et al., 2020). Another study looking at serum diagnosis of endometriosis, a benign condition that results from migration of endometrial cells outside of the uterus and increases the lifetime risk of ovarian cancer (KvaskoffHorne and Missmer, 2017), demonstrated a sensitivity and specificity of 100% with independent testing of a model on 15% of the original data, withheld from the training set (Parlatan et al., 2019). Due to overall low participant numbers, the test group was small, eight endometriosis and six control however this study provided novel insight into the subtle biochemical changes in sera of patients with endometriosis and suggested that beta carotene might have an influential role in endometriosis protection or prevention. This study was also limited by the availability of reference assignments and limited understanding of the correlative significance of some of the peak assignments generated from principal component loads in this study.

In the assessment of vulval cancer using Raman spectroscopy, a cross validation model for the differentiation of lichen sclerosus from other inflammatory vulval conditions using fresh vulval biopsies achieved a sensitivity of 91% and specificity of 80% (Frost et al., 2017). Similarly high accuracies were achieved by van Doorn and colleagues in a pilot study of operative margin assessment for vulval squamous cell cancer. They differentiated healthy tissue from carcinoma with an area under the ROC curve of 0.9, and cross validation sensitivity of 79% and specificity of 86% using Raman measurements of freshly resected vulval specimens. As is common with pilot and feasibility studies, sample numbers are small (van Doorn et al., 2021).

1.6.5 Application of Raman spectroscopy in Ovarian cancer

At the time of planning this work, December 2020, there were only a few studies assessing the application of Raman spectroscopy to ovarian cancer. Two studies were found in the literature looking at discrimination of ovarian tissue. Three

further studies, from the same group, evaluated biological fluids for ovarian cancer diagnosis. These five studies are discussed below.

The earliest work looking at Raman spectroscopy for its ability to discriminate between normal and cancer was completed by Krishna and colleagues. They measured washed specimens taken at routine biopsy using a commercially available Raman spectrometer. 24 samples were examined in total, 8 normal, 10 benign and 6 malignant. Unfortunately, neither patient demographics nor diagnosis are provided for their work, so it is uncertain what the difference between benign and normal is in this case. Their work was limited to the biochemical differences between the groups however they established that lipids and DNA vibrations were the main differentiating biochemical features in the spectra of malignant tissues using difference between the mean (Krishna et al., 2007). These biochemical changes are echoed by Maheedhar and colleagues who collected 72 spectra from eight normal and seven malignant fresh ovarian tissue samples using a 785 nm diode laser and a commercially available spectrometer. The mean spectra of the two pathology groups had clear differences in the spectra when plotted together with the malignant mean spectra exhibiting broad and stronger peaks at 834, 900, 1000 and 1165 cm^{-1} which were assigned to amide I and II proteins, lipids, shift in δCH_2 and DNA by the author. The normal spectra were noted to have stronger peaks at 855 and 940 cm^{-1} , however the author did not offer a suggestion for the molecular assignment of these peaks. Discriminating algorithms using principal component scores achieved a sensitivity and specificity of 88% and 84%. Half of the data set was randomly selected to build a training model which were tested on the remaining data. This model achieved 100% sensitivity and specificity suggesting that Raman spectroscopy is a viable option for discriminating cancer from normal in ovarian tissue. The sample numbers for this work as with all pilot studies was limited. Assignment and discussion of the biochemical changes responsible for the differences in the tissue is also incomplete, with the prominent peaks in normal tissue remaining unassigned in this work, likely consistent with the progress of peak assignments in biological tissues in Raman spectroscopy at the time. The author did not provide the data on characteristics of the cohort of participants in this work such as the type of ovarian cancer they had, stage of cancer or reasons for oophorectomy for the participants in the normal group; thus

appropriateness of the comparison groups cannot be commented on (Maheedhar et al., 2008).

The first of the three studies looking at biofluids assessed Raman spectroscopy for its ability to detect ovarian cancer in plasma. Owens and colleagues performed exploratory testing on 4 samples for ovarian cancer 4 samples for benign as part of a bigger study assessing attenuated total reflectance (ATR) Fourier transform infrared (FTIR) spectroscopy. They used a commercially available Raman spectrometer coupled with a 785 nm laser to collect 50 spectra from each sample and demonstrated classification accuracies of 74% for cancer detection using support vector machines. Other results for diagnostic modelling in this work are not provided and as expected for an exploratory study, the sample size was extremely small (Owens et al., 2014). This group went on to assess Raman spectroscopy in earnest, using two techniques, standard Raman spectroscopy and surface enhanced Raman spectroscopy (SERS) using silver nanoparticles, to measure plasma collected from 27 patients with ovarian cancer and 28 patients with benign conditions. The benign patients had benign gynaecological conditions or prolapse however the distribution of benign conditions is not provided by the author. For Raman spectroscopy, fresh frozen plasma was thawed and dried on aluminium foil, and subsequently measured using the commercially available InVia Renishaw spectrometer coupled with a 785 nm laser. Difference between the mean support vector machine (SVM) learning were used to analyse this data, followed by 5-fold cross validation. Peaks identified for discrimination of the pathology groups were assigned to amide I (1657cm^{-1}), CH_2 in lipids (1418 & 1301 cm^{-1}), amide III (1242 cm^{-1}) and amino acids/carbohydrates (916 cm^{-1}). Support vector machine classification achieved a sensitivity of 94% and specificity of 96%. The SERS data performed slightly worse, 87% and 89%. A subgroup analysis of the 17 early (stage I) cancers achieved a sensitivity of 93% and specificity of 97%. They demonstrated that CA-125 levels were not responsible for the separation seen in the data, confirming that separation in these groups is due to the presence of cancer and not an unintended use of Raman spectroscopy to measure CA-125. Whilst the author describes in detail the plan for building the SVM model for training the data set for classification of cancer and non-cancer, independent testing or prediction testing for this model is not discussed, thus the prediction performance of their

data set has not been tested. Nonetheless, the result of this work is highly encouraging for the use of Raman spectroscopy for plasma diagnosis of ovarian cancer. (Paraskevaïdi et al., 2018).

The third study, by the same group, compared different biofluids for ovarian cancer diagnosis using Raman spectroscopy. Blood plasma, blood serum, and ascitic fluid from 18 patients with epithelial ovarian cancer and 20 controls were assessed. Diagnoses in the control group were ovarian cyst (seven participants), leiomyomas +/-adenomyosis (seven participants), endometriosis (four) and normal (2). Fresh frozen plasma was thawed and dried on aluminium foil, and subsequently measured using the commercially available InVia Renishaw spectrometer coupled with a 785 nm laser. Following preprocessing steps, principal component analysis was used to explore the data and the results were further analysed using linear discriminant analysis, quadratic discriminant analysis and support vector machines. Ascitic fluid generated the lowest p-values and best discrimination performance with sensitivity and specificity performance above 80% compared to 60-73% for plasma and serum. It is however unclear how ascites for the benign group was collected. The author defines ascites collection for this study being sample aspiration at the time of surgery however does not account for the protocol when the patient has no ascites. In the discussion, the author acknowledges that ascites accumulation is uncommon within benign gynaecological conditions but participants in this study have some fluid to collect at the time of their surgery. This creates a problem when considering repeating this work on a larger scale to validate the role of Raman spectroscopy of ascites in cancer diagnosis and more importantly, considering translation research or clinical applications. The test loses its value if fluid volumes in the groups of interest are too low for safe collection of the sample (Giamougiannis et al., 2021a).

1.6.6 Conclusion

Stage-based survival data continues to support the need for early detection of ovarian cancer. For those unfortunately diagnosed in advanced disease, optimal cytoreduction remains the best surgical outcome for improving disease free survival. Raman spectroscopy has demonstrated high accuracies for detecting cancer in different biological tissues despite some studies having small numbers. It is not destructive and *in vivo* endoscopic probe work suggests it is easily

amenable to translation and thus it shows great promise. The results from the five highlighted studies from patients with ovarian cancer are very promising but require exploration in more clearly defined patient groups with larger numbers and with additional exploration of the effect that any prior cancer treatments may have on the ability of Raman Spectroscopy to discriminate between cancer and non-cancerous tissue. This thesis seeks to address these aspects.

1.7 Aims of this thesis

1. To evaluate Raman spectroscopy for the identification of novel plasma markers diagnostic of ovarian cancer and their diagnostic performance as an early detection test in women with symptoms of ovarian cancer.
2. To assess Raman Spectroscopy against histology for its ability to detect cancer in peritoneal and ovarian tissue from carefully characterised patients.
3. To evaluate the effect of chemotherapy on the ability of Raman spectroscopy to detect cancer in ovarian and peritoneal tissue.

Objectives

To realise these aims, the following objectives were set to guide experimentation and definition of laboratory protocols.

1. Study set up.
 - a. Define the study protocol.
 - b. Complete an ethics and human research authority application.
 - c. Recruit participants to the study.
 - d. Collect blood and tissue samples.
2. Plasma
 - e. Assess the discriminatory ability of Raman spectroscopy in assigning benign, borderline and cancer spectra taken from drop coating deposition Raman spectroscopy.
 - f. Build and test predictive models for the discrimination between cancer and benign.
3. Tissue

- g. Assess the discriminatory ability of Raman spectroscopy in assigning benign, borderline and cancer spectra taken from fresh frozen tissue.
- h. Build and test predictive models for the discrimination between cancer and benign.
- i. Test predictive ability against spectra taken from chemotherapy treated fresh frozen tissue.

Chapter 2 – Methods

Introduction

This chapter will describe the development of the methods by which Raman spectroscopy was used in this thesis to examine both biofluids (plasma) and tissue. I will first discuss the approvals sought to proceed with the study, the design of the study and the data collection plan used in sample collection for this work. I will then address the use of Raman spectroscopy and the analysis protocols, before then considering the development of a system to examine human biofluids and tissues. The challenges to be addressed are first described and then the approaches taken.

2.1 Ethical approval and consent

Health Research Authority (HRA) and research ethics committee approval was granted ([Appendix A](#)) for the collection, analysis and storage of blood samples, ovarian and peritoneal tissue after assessment by National Research Ethics Service Committee North West – Preston (REC reference – 21/NW/0092, [Appendix B](#)). The study was also registered on the publicly accessible database clinicaltrials.gov (identifier NCT04817449).

Potential participants were approached and given a full explanation of the study as well as written information via the appropriate information sheet ([Appendix C](#), [Appendix D](#)), and given time to consider whether or not to participate in the study. Written informed consent ([Appendix E](#)) was subsequently obtained from participants willing to participate in the study.

All samples were collected following the same consent procedure however the environment the potential participants were seen varied. Some participants received information in clinic but did not consent until the day of surgery, first treatment or intervention, to allow them the maximum amount of time to consider participation in the study.

2.2 Study population and design

2.2.1 Population

As discussed in chapter 1, ovarian cancer is a disease that predominantly affects adult women. With this in mind, and considering the aims set out in chapter 2.2, the inclusion and exclusion criteria were as below.

1. Inclusion criteria
 - Female
 - Symptoms of ovarian cancer.
 - Patients undergoing treatment for ovarian cancer.
2. Exclusion criteria
 - Age less than 18.
 - Women unable to consent due to communication difficulties.
 - Women unable to consent due to lack of capacity.

All patients presenting to gynaecology two week wait clinics and gynaecology oncology clinics with symptoms of ovarian cancer or undergoing treatment of ovarian cancer at either University Hospitals Bristol and Weston NHS Trust or Royal United Hospitals Bath NHS Trust were eligible to be considered for inclusion in the study. Translation services provided for clinical care was used where required for language barriers.

2.2.2 Design

To inform the study design, I conducted a survey of women attending gynaecology clinics regarding likelihood of agreeing to participate in a study that involves blood and tissue samples. Forty-eight women returned the survey. 94% felt that healthcare research was important with the remainder choosing “somewhat”. 62.5% were likely to participate in a study that involves blood samples however this increased to 83% with the option to have samples taken opportunistically. The main reason documented in the comments was a fear of blood or needles. Regarding tissue samples, 62.5% were likely to take part in a study involving tissue samples whilst the remainder were undecided. This work highlighted the importance of clear communication and explanation of the study as part of the recruitment process, particularly around ovarian and peritoneal tissue collection. A decision was made to create flexibility in timing of the

pretreatment blood sample; they were collected at the time clinically indicated routine venepuncture.

This is an observational cohort study. Figure 6 shows the proposed protocol of blood and tissue sampling.

Participants referred with suspicion of ovarian cancer were approached at their two week wait clinic appointments and given a written patient information sheet as well as a verbal explanation of the study. Some participants were happy to consent within the appointment for participation in the study and others provided consent, at follow up appointments or on the day of surgery regarding participation in the study after they had had time to reflect and discuss the study with others. All participants were assigned a study number and all data anonymised by use of the study number for identification going forward.

Those participants who were later confirmed to not have cancer were assigned to the comparator non-cancer groups. These groups allowed the assessment of whether Raman spectroscopy is altered in patients with cancer compared to those with benign or borderline ovarian disease.

Once written informed consent was given, participants entered the study. A blood sample was collected from participants prior to commencing any treatment. Tissue samples for research were collected for all participants that went on to have surgery for ovarian pathology regardless of their group.

At the completion of treatment, a further blood sample was collected from participants at their follow up appointment.

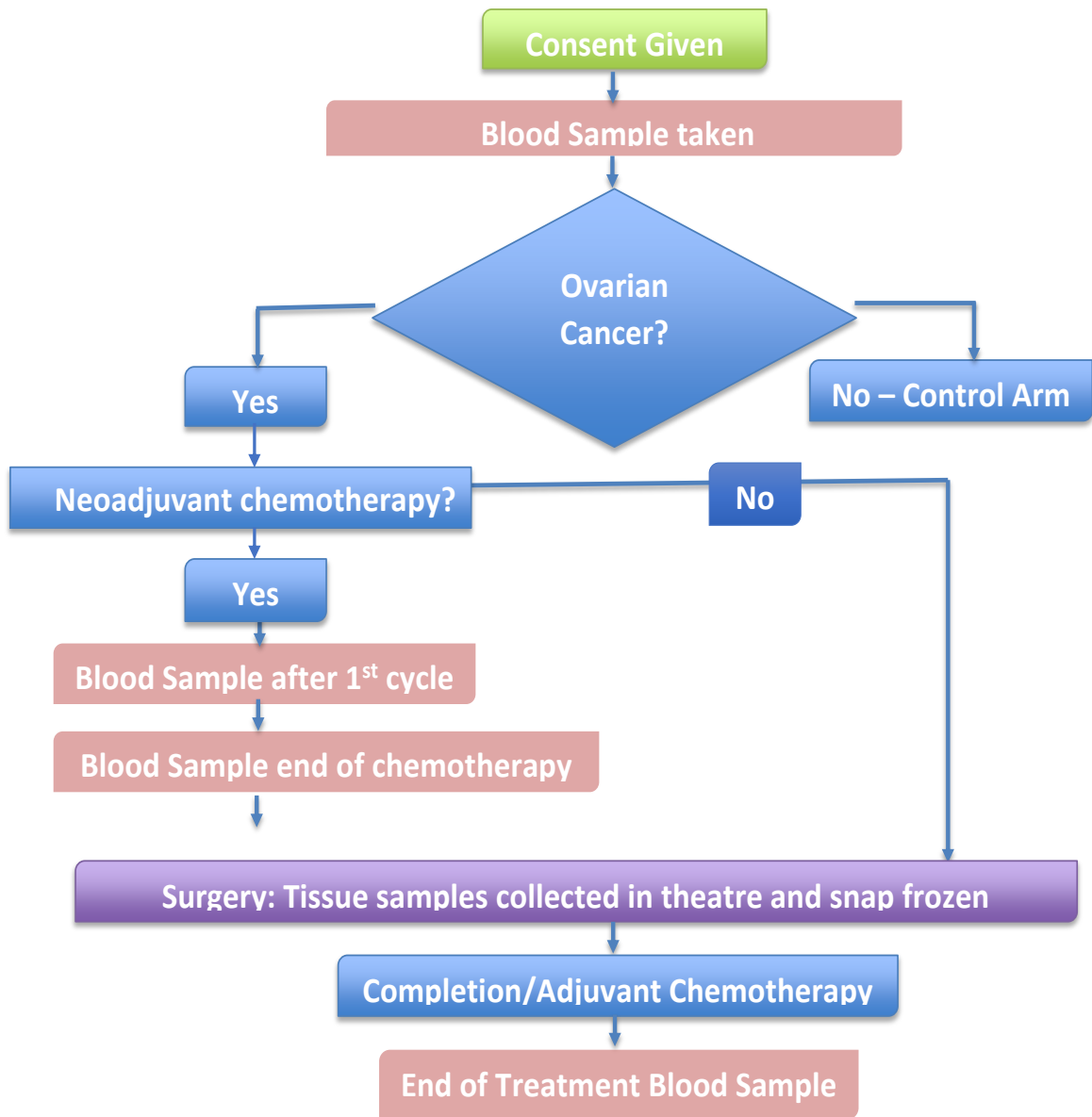


Figure 6 - Study flow chart for sample collection. This figure illustrates the protocol for tissue and blood sampling. Participant treatment plans were followed, and samples collected at the appropriate stages.

2.3 Data Collection

Participant information and medical history were collected using the background information sheet ([Appendix F](#)). This data was linked only to study ID and was updated over the course of the study to ensure any changes were captured. These were then collated into a spreadsheet.

A second collection tool, Diagnostic Information Sheet ([Appendix G](#)) was used for prospective documentation of investigation results, diagnosis, treatment, and outcomes. These were then collated into a spreadsheet.

2.3.1 Sample collection and processing – Biofluids

Following informed consent, wherever possible, samples were collected at the same time as routine venepuncture requested by their healthcare professional. On occasions where this opportunity was missed, sample collection was postponed till the next planned opportunity or participants were verbally consented for venepuncture purposefully to collect the study sample. Aseptic non-touch technique and Trust guidelines were followed in the collection of the samples in one 4ml EDTA vacutainer tubes labelled with the study number of the participant. Samples were left at room temperature and transported to the laboratory at the earliest opportunity but within six hours of collection. This allowed completion of participant recruitment from a clinic before plasma separation from the samples.

Samples were centrifuged at 2000g for 15 minutes and the plasma carefully pipetted into 1.5 ml Eppendorf tubes to give four aliquots of 110 µl of plasma. The remaining sediment (red and white cells, platelets and plasma) formed a fifth aliquot. All Eppendorf tubes were pre labelled with the study number and sample aliquot number and then submerged in liquid nitrogen till the samples were frozen. They were then retrieved and transferred to a -80°C freezer.

2.3.2 Sample collection and processing – Tissue

On the day of surgery, participants were highlighted to the surgeon and the consent form reviewed. The surgeon identified and removed 1cm biopsies of areas they identified to be normal, suspicious (surgeon unsure if normal or cancer), and obvious cancer. Depending on the extent of disease, representative samples of all these groups were not always obtained. For participants that had

already received chemotherapy, a sample of representative fibrosis was also biopsied.

All samples were placed on the acetate sheet on their side so that the superficial and deep surfaces faced out laterally, and then carefully placed inside previously labelled cryovials. The vials were labelled with study number, the surgeon's prediction of specimen type (normal, suspicious or cancer) and sample number. Samples were then submerged in liquid nitrogen and left in the dewar for transport from the operating theatre to the -80°C freezer.

2.4 Sample size calculation

To be able to proceed with the design of this feasibility study, power and sample size calculations were considered. Previous work looking at vibrational spectroscopy as a test for ovarian cancer, where it exists, is limited. As discussed in chapter 1, the few published studies have demonstrated very high sensitivities and specificities using small sample sizes. Consequently, the size of effect of the ability of Raman spectroscopy to identify ovarian cancer is not known. This was a barrier to attempts to perform a meaningful power calculation. Without this, a true sample size calculation for the number of participants required to adequately power this study was unattainable. Furthermore, for the same reasons, the number of independent spectral variables expected from this type of work is unknown.

As a result, we reviewed previously unpublished Raman Spectroscopy work within the department, the diagnostic performance of the current biomarker, Ca125, and the sensitivity of two week wait referrals for ovarian cancer. Previous work with a small number of participants (n=30) suggested 7-8 independent spectral variables. With an aim to measure 10 events per variable for this feasibility work, at least 80 cases are needed in the cancer group. The host site, University Hospitals Bristol and Weston NHS trust, sees on average 90 new cases of ovarian cancer a year, thus it is feasible to achieve this number across the two recruitment sites within the planned study recruitment period.

The interrogation of the effects of chemotherapy on the ability of Raman spectroscopy is novel. There is no pilot data to estimate spectral effect size of

ovarian cancer after chemotherapy treatment. This being the case, a pragmatic approach to selecting the number of participants has been taken based on expert opinion, taking into consideration the application of the technique at other tumour sites and incidence of ovarian cancer in this geographic area. It is anticipated that the number of participants for tissue spectral analysis of 30 for upfront surgery and 60 for interval debulking (30 good response, 30 poor response) will be realistic and achievable and should allow us to observe the spectral effect of ovarian cancer in tissue.

2.5 General Raman Methods

This section outlines the technical considerations to be factored in when applying Raman spectroscopy and analysis techniques used for the classification of vibrational spectra.

2.5.1 Technical considerations

Drop coating deposition Raman (DCDR)

DCDR is a technique for measuring molecules in a weak solution (Filik and Stone, 2007). When samples are deposited on hydrophobic surfaces, evaporation results in a change in concentrations of components which form into small rings known as the “coffee ring” effect. In essence, this is a highly reproducible technique that results in high concentrations of the protein and other molecules in a localised area, facilitating small volume measurements and resulting in dramatically increased signal to noise ratio (Zhang et al., 2003).

This approach achieved comparable diagnostic performance compared to surface enhanced Raman spectroscopy, a technique used to increase signal to noise ratio in plasma measurements, in a study of colorectal cancer detection in plasma (Li et al., 2015).

Signal to noise ratio (SNR)

There are unwanted contributions to the Raman spectrum (noise) that need to be accounted for when planning Raman spectral measurements as they can affect our ability to detect the Raman signal. The relationship between noise and signal, signal to noise ratio, is defined by the mean value of the spectral peak divided by

the standard deviation of the peak. Five sources of noise are described in the literature and summarised, from Raman spectroscopy for Chemical analysis (McCreery, 2000), in this section. These factors were considered when creating the protocol for Raman measurements described later in this chapter.

Shot noise is noise arising from the variance in the nature with which photons arrive at the detector. The relative variance with which photons arrive at the detector decreases with longer integration time thus the effect of shot noise on signal to noise ratio can be influenced by acquisition time; longer integration times result in decreased relative contributions from shot noise, in the absence of other noise sources, due to the increased signal in proportion to time.

Background noise is another source of noise which in this context refers to any photons detected from unintended sources such as stray laser light not removed by the filters and luminescence from the sample (fluorescence).

The CCD generates electrons in the detector which results in a thermally dependent signal, dark noise, independent of the laser or sample type. Detector cooling reduces dark noise.

In Raman spectroscopy, flicker noise is seen in scanning systems where variations in laser intensity can cause variations in Raman scattering. This is more likely to be observed in single channel spectrometers and is almost negligible with modern spectrometer configurations.

As discussed in section 1.6.3, scattered photons are converted to electrical charges at the CCD. Inaccuracies in the conversion of these electrical charges into a signal result in read out noise.

Cosmic rays

Cosmic rays are contaminants to the Raman spectrum generated by the release of electrons at the detector as a result interaction with high energy particles. These electrons are indistinguishable from photoelectrons and are read out as thin spikes in the spectrum. As they are not Raman peaks, these artefacts ought to be filtered out of the spectrum prior to analysis (Barton and Hennelly, 2019).

2.5.2 Analysis techniques

Peak assignment

As discussed in section 1.6.2, the spectral fingerprint of a molecule is determined by the natural frequencies of the vibrational modes within the molecule. Raman reference sheets of the characteristic Raman shifts seen in various tissues and substances have been compiled over time using de novo measurements of specific substances, and assignments from previously published work. Computer aided spectrum interpretation exists however, this technique tends to over or underfit with nearest assignment to the peak in question thus, has to be cross checked to ensure that assignments make sense for the substance measured (Smith and Dent, 2004b). Computer aided interpretation has not been used in this work.

Principal components

Raman data have multiple variables, not all of which explain the data. Principal component analysis is a multivariate analysis technique used to assess the main features or variables that explain the most variance in the data. In this technique, variables that explain the variance in the data are grouped together to form new variables, principal components (PC), which are linear combinations of the original variables. The first principal component accounts for most of the variance in the data set, centred around the mean. At right angles to the first PC is the second PC which accounts for the next largest variation after the influence of PC1 has been removed, and so on. When calculating principal components, values that describe the amount of variance in the data set, eigenvalue, is reported as the PC scores. These can be plotted to visualise the data within PCs. In Raman spectroscopy, the PCs can be inspected to understand the spectral features responsible for the variance in the data (Miller and Miller, 2010).

Analysis of Variance (ANOVA)

To determine the diagnostic significance of the PCs for the difference between pathology groups, ANOVA is employed. This technique assigns a value, F value, to the ratio between the variance between the sample means and the variation within the sample. The larger the F value, the greater the differences between the group means and thus the performance of the variable. A cut-off value, F_{crit} , is determined for the desired significance level using the F-distribution table.

Where the F value is greater than the F_{crit} , the PCs reach the significance level for differences between the pathology groups. (Miller and Miller, 2010).

Linear Discriminant Analysis (LDA)

This supervised technique models the differences between classes of data to create a rule, linear discriminant function, for the maximum separation of the data into groups. The output of this model can be summarised in a table, confusion matrix, where the classification performance of the model can be calculated.

Cross Validation

The training classification performance of the LDA model is considered optimistic as the data to be classified is included in generating the linear discriminant function. One way to address this is the use of cross-validation methods such as 'leave one out'. In this method, the linear discriminant function is found with one sample left out of the group and then used to assign the omitted sample. This is repeated in turn for every sample in the group and the collective predictive classification performance of the data set is reported (Miller and Miller, 2010).

In this thesis, leave one mean sample out performance is reported for some the analysis of tissue measurements. This refers to leave one out cross validation outcomes obtained by performing the analysis with the mean spectral data for each sample. The contribution of one sample is still left out however the data being used to find the linear discriminant function does not include all the individual spectra and hence the same variation as is seen with leave one sample out models containing all the data. In essence, the veracity of the prediction performance is tested by reducing the differences between the samples.

Performance measures

As this work relates to diagnostic testing, the ability of the model to correctly predict whether a sample belongs to the 'disease' or control group is calculated from the confusion matrix where sensitivity is the proportion of people with the disease that are correctly predicted to be in the disease group and specificity is the proportion of people without the disease who are correctly assigned to the benign group (Crandon, 2019).

The receiver operative characteristics curve is a graphical plot of the discriminatory ability of the diagnostic model. It is a powerful tool for factoring in

the cut-off value for the diagnostic test. The area under the curve represents the overall accuracy of the test (Lalkhen and McCluskey, 2008).

F1 score

Accuracy is the measure of correctly classified outcomes. When assessing the diagnostic ability of a test for cancer, such as is seen in some biological applications of Raman spectroscopy, the false negative rate is extremely important however this is not reflected in the accuracy of a test.

To account for this, the F1 score is reported in this thesis. The F1 score is the mean of precision and recall where:

$$F1\ score = 2x \frac{(precision \times recall)}{(precision + recall)}$$

Precision is the correct positive predictions (true positive) relative to the total positive predictions (true positive plus false positive) and recall is the sensitivity performance of the data. A score of 1 is the best possible outcome, with anything above 0.7 being acceptable (Ferguson et al., 2022, Zach, 2021).

2.6 Study methods

2.6.1 Development of lab protocol - Biofluids

Vibrational spectroscopy measurements are non-discriminatory and will generate output for all the molecular compounds in the fluid. Collection and storage methods, substrates used, set up on the spectrometer and measurement settings all affect, not just the reproducibility, but also the quality of the results. There are no internationally agreed or standardised protocols for drop coat deposition Raman spectroscopy (DCDRS), with most laboratories having varying availability and preference of laser wavelengths. This section looks at decisions made regarding the protocol for collection, preparation, and measurement of the samples in this study. Early experimental work was completed using previously stored plasma from previous work including samples from male participants.

2.6.1.1 Refining the sample preparation

Blood component

Whole blood contains red blood cells, white blood cells and platelets, in a liquid medium, plasma. When blood is allowed to clot, this liquid medium is referred to as serum. The clotting process binds some of the proteins in blood, thus plasma is the preferred fraction of whole blood for protein assessment including DNA (Vaught JB 2011). As this study is still exploratory with regards to the changes that separate cancer from non-cancer, exclusion of proteins through the clotting process would not be ideal, thus plasma was chosen for this study.

Collection medium

The tubes to collect blood from patients are available with different additives. The options available include, but are not limited to, non-additive clotting tubes and tubes with either citrate, ethylenediaminetetraacetic acid (EDTA), heparin, gel barriers and sodium fluoride with potassium oxalate. To stop blood clotting and be able to extract plasma, an anticoagulant additive is required in the collection tube. Of the options available, citrate has an unacceptable dilutional effect on plasma, and heparin binds some proteins besides antithrombin (Banfi Salvagno and Lippi, 2007) making EDTA the best anticoagulant for this investigation.

Extraction and storage of plasma

As previously mentioned, plasma is the remaining liquid after cells are removed from whole blood. EDTA blood was centrifuged at 2000g for 15 minutes, the recommended practice for depleting platelets and cells from plasma (Scientific, 2007). Plasma was carefully pipetted into aliquots of <110µl taking care not to disturb the layer of platelets and the heavier cells below, and it was snap frozen in liquid nitrogen before being stored at -80 degrees Celsius. The choice of temperature is due to demonstrated stability of the plasma metabolome at -80 degrees Celsius compared to higher temperatures (Wagner-Golbs et al., 2019).

Does leaving the blood for prolonged periods of time at room temperature prior to centrifugation alter the assessment of plasma components by Raman Spectroscopy?

In the proposed clinical investigation, the time from whole blood collection to separation of plasma may vary, depending on the location and duration of the clinic, time of participant recruitment and availability of equipment for centrifugation. Whether this variability influences the results of the Raman

spectroscopy was unknown. In order to assess the significance of this potential variability, a series of experiments were designed to explore the effect of changes in the duration of time whole blood remained uncentrifuged.

During the clinical study, blood samples would most likely be left in the clinic rooms, or be in transport, prior to centrifugation, it was therefore decided to leave samples at room temperature and to compare the results to samples stored at fridge temperature prior to centrifugation. If samples could be left for a considerable time before centrifugation, even if refrigeration was required, this would make the logistics of blood collection from patients at the more distant sites more feasible and thus a time interval of up to 24 hours was chosen for the experiments.

Twenty eight mls of whole blood were collected from a healthy female volunteer in seven (4ml) EDTA tubes. One aliquot was spun immediately at 2000g for 15 minutes and plasma snap frozen, this being the protocol expected to cause least change to the plasma constituents. Three samples were left at room temperature (18-20 degrees Celsius) and three samples were kept in the fridge (3-4 degrees Celsius). At 6, 12 and 24 hours from the time of collection, one sample from each temperature group was spun at 2000g for 15 minutes and the separated plasma snap frozen.

Raman spectroscopy measurement: All aliquots were measured together to avoid any differences that can be attributed to the measurement methodology. The samples were defrosted at room temperature for 30 minutes. The aliquots were mixed on a vibrating plate to ensure even distribution of proteins, then 1.5 μ l of plasma was pipetted from each aliquot in turn onto a single labelled stainless-steel slide. The samples were allowed to dry for a minimum of 40 minutes. A white light map image of the slide was taken using the 5x objective and measurements were taken around the dried ring using the 50x objective. The measurements were taken using the 830 nm laser with 1 accumulation of 1 second exposure at 100% laser power (around 130 mW). 64 spectra were collected per sample and the data transferred to MATLAB software for pre-processing and analysis. Pre-processing steps included filtering for cosmic rays (with a median filter) and normalising the data.

Results: When plotted together, there was no loss of spectral features across the groups and overall good signal to noise ratio, the lowest being 400. Figure 7 shows the mean-centred principal component scores of all the samples. The sample that was centrifuged without delay and flash frozen is shown in red on the right-hand side of the graph and is called 0hr. The samples which were stored for six hours are both seen grouping to the right-hand side of the graph along with the 0hr sample. The circles in each of the six hours groups are also tightly grouped when compared to twelve and twenty-four hour samples. The sample in the fridge for six hours (blue) sits more to the right, and is seen overlapping the red samples, than its room temperature counterpart (green).

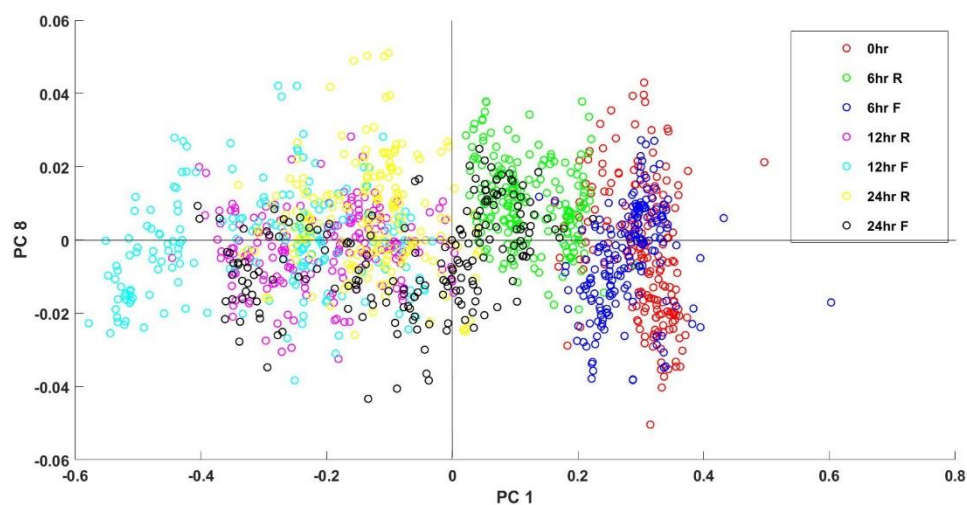


Figure 7 - Principal component scores distribution of plasma samples extracted and frozen without delay, 6, 12 and 24 hours after storage at either room temperature or in a fridge. This is a plot of two statistically significant principal components ($p=0.001$), where PC 1 is displayed on the x-axis and PC 8 is displayed on the y-axis. The circles represent the scores, and the colours represent the time delay prior to plasma extraction with 0hr being no delay prior to extraction. Samples kept in the fridge are labelled F in the legend and samples kept at room temperature are labelled R.

Discussion and conclusion: This study suggested that plasma constituents which are being assessed by Raman spectroscopy are altered if plasma is not separated from other blood constituents in a timely manner. The exact changes that are caused are not determinable by this experiment but given the aim is to identify native molecules which might provide a diagnostic marker for cancer every attempt should be made to maintain their integrity. However, the biofluids study design also needs to be pragmatic and enable patient recruitment across multiple sites. Given that, compared to blood centrifuged immediately and the separated plasma snap frozen, only small changes in metabolome were apparent when blood was stored in the fridge, or at room temperature, for 6 hours, it was

decided to adopt this time frame in the clinical study. The lack of easy access to refrigeration across all clinical sites, led to the decision to store at room temperature. Samples which were held at more than 6 hours at room temperature were discarded. The advantage of this being a single participant study is that the only changing variables are time and temperature as planned. This has the disadvantage of missing any variations in the rate of change of the samples between participants however I would expect any such changes to occur across all the time and temperature groups and there not impact the results.

2.6.1.2 Developing the biofluids Raman spectroscopy protocol

Assessing the effects of Backing Substrate

The choice of backing substrate (slide) on which the sample is deposited for positioning within the spectroscope can either optimise measurements and enhance spectral signal intensity or create spectral contributions and noise. Good spectral quality is beneficial because it reduces the extent of preprocessing required of the spectral data. There are also pragmatic factors such as the cost of substrates which must be weighed against the potential relative increase in signal intensity when choosing a substrate.

To assess the effect of the composition of the background slide on the Raman spectra from plasma in this study, 1.5 µl drops of previously frozen and thawed, stored plasma taken from healthy individuals, were measured on each of glass, polished stainless steel and calcium fluoride substrates. There was only one drop per substrate required. The samples were dried in an air conditioned lab for 40 minutes and then measured using the same Raman spectroscopy protocol described in the section – “Does leaving the blood for prolonged periods of time at room temperature prior to centrifugation alter the assessment of plasma components by Raman Spectroscopy?” on page 79.

Results: Sample viability and shape: Samples dried on calcium fluoride were smaller and perfectly symmetrical (Figure 8) but prone to cracking with occasional loss of part of the sample was observed when slides were not handled extremely cautiously. This would be a significant issue as the plasma aliquot would have to go through another freeze thaw cycle to enable a repeat of the lost dried drop and the effect of the freeze/thaw cycles on the Raman spectra of plasma is not known.

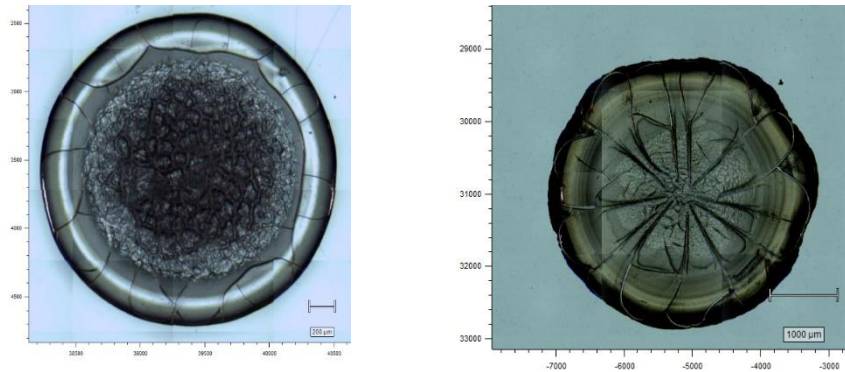


Figure 8 - White light image of 1.5 μ l of undiluted plasma on calcium fluoride (left) and stainless steel (right). The sample on calcium fluoride is more symmetrical and smaller (diameter 2250 vs 3800 microns) than the sample on stainless steel.

Spectral features and signal intensity: It was very clear that the glass substrate was unsuitable as only an objective signal was returned (Figure 9). Signal intensity of the measured sample was higher on polished stainless steel than calcium fluoride (phenylalanine peak at 1000 cm^{-1} of 186 on stainless steel vs 105 on calcium fluoride) and the larger size of the stainless slide allows for multiple drops to be dried at the same time. This offers a practical advantage when planning measuring large numbers of samples. There was no loss or change of spectral features between the two substrates (Figure 9).

Cost: Calcium fluoride slides retail at £25 per slide compared to £0.65 per slide for polished stainless steel. Summary and final protocol: Overall, polished stainless-steel slides offered equivalent quality of spectra with higher signal

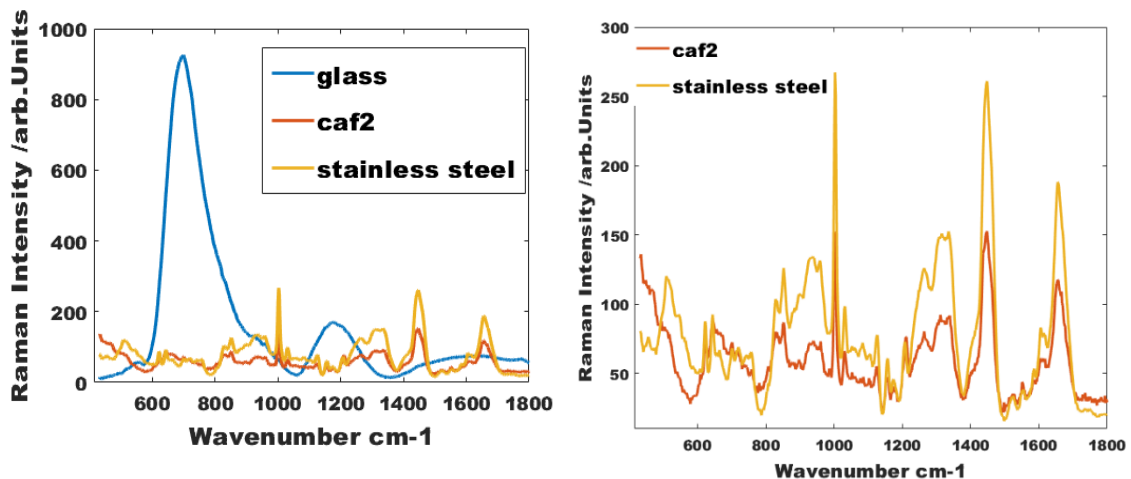


Figure 9 - Mean spectra of 1.5 μ l of undiluted plasma, taken from drops dried on glass, stainless steel and calcium fluoride substrates. A minimum of 60 spectra were collected from measurements of the protein ring on each substrate in triplicates. The number of spectra varied slightly due to the differences in the size of the dried drop depending on the substrate as discussed in figure 8. The glass spectrum in blue does not demonstrate any of the spectral features expected in plasma. The calcium fluoride (orange) and stainless steel (yellow) spectra are seen clearly on the plot on the right side of the figure. The stainless steel spectrum has a higher signal intensity and more prominent spectral features.

intensity at significantly lower cost and as a result was chosen as the substrate for this study.

Assessing the effect of drop size

As previously discussed, drop coated deposition Raman spectroscopy, is the measurement of the residual polymer ring from biofluids dried on hydrophobic surfaces. The volume of the drop affects drying time and size of the ring however it is unclear if the volume related protein load affects the spectral features or signal quality. Drops of varying volumes were measured to determine the appropriate drop size for the samples in this study. On a polished stainless-steel slide, drops of 0.5, 1, 1.5, 2 and 2.5 μl were deposited in turn in triplicates and allowed to dry at room temperature. Measurements were taken when all the drops had dried. Following a baseline subtraction step, the height of the phenylalanine 1000 cm^{-1} peak was measured.

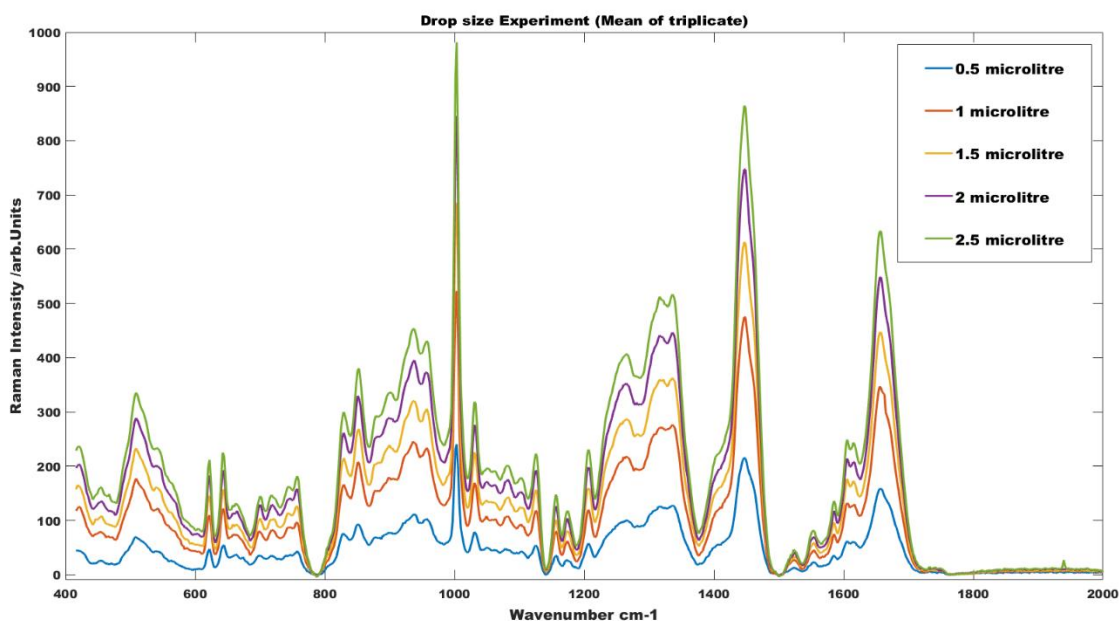


Figure 10 - Assessing plasma drop size for Raman spectroscopy. In this figure, the mean of the triplicate measurements for each drop size has been plotted with Raman intensity on the y-axis and wavenumber of the x-axis. Signal intensity increases with increasing drop size with 0.5 microlitre drop (blue) demonstrating the lowest signal intensity and the 2.5 microlitre drop (green) demonstrating the highest signal intensity. Spectra features such as peak position and shape are unchanged across the drops.

Results: The phenylalanine peak height increased with increasing drop volume (Figure 10, Figure 11). Spectral features were consistent across all the volumes (Figure 10) with no change in peak shape or position. Volume related drying time increased with increasing drop size as demonstrated in Figure 12. The 1.5 μl drop size was chosen as a compromise between signal intensity and drying time, whilst still ensuring clear spectral data.

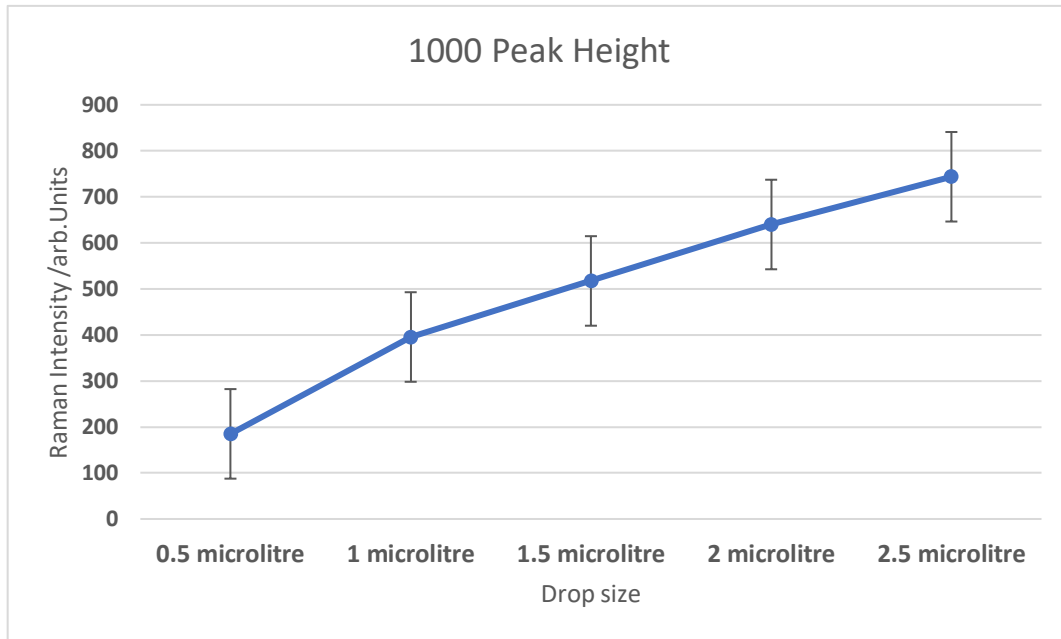


Figure 11 - Signal intensity of varying drop sizes of undiluted plasma. Intensity measurement taken of phenylalanine protein peak.

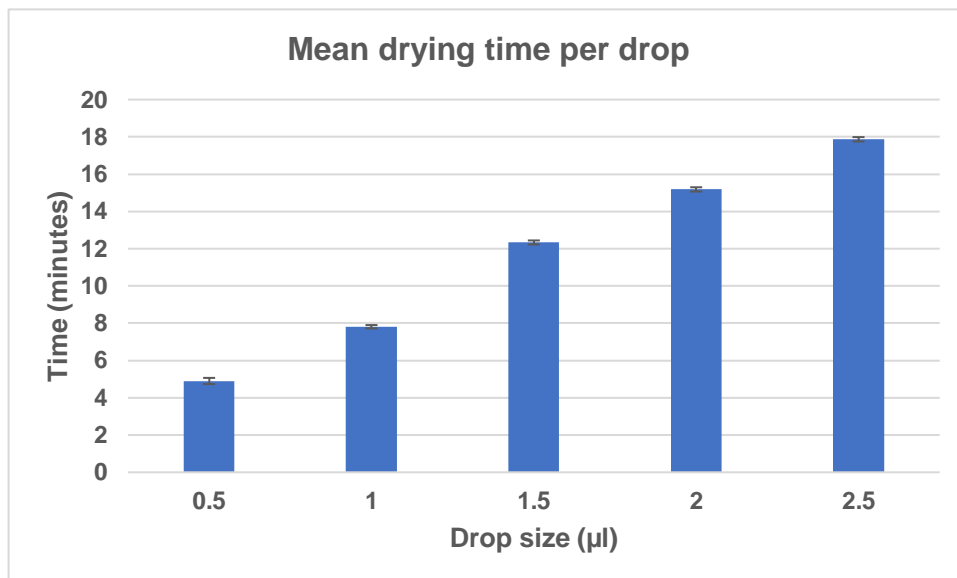


Figure 12 - Minimum drying time per drop volume. The minimum amount of time required for the protein ring to be visible under the microscope has been plotted in this figure with error bars. The blue bars represent the mean minimum time to dry of three repeats of this exercise, per drop of undiluted plasma.

Optimum drying time prior to commencing Raman measurements

When observed under the microscope during drying, the protein ring forms gradually as water evaporates from the sample. Measurements completed prior to completion of this process are uninterpretable due to the low sensitivity of the Raman scattering to the biomolecular concentrations in the biofluid, leading to a

low signal to noise ratio. The minimum drying time, to pre-concentrate the biomolecules of interest required prior to measuring the samples on the Raman spectrometer, was evaluated by taking single spectral measurements at regular intervals, of a 1.5 μl drop of undiluted plasma on polished stainless steel. The freshly dropped sample was mounted onto the spectrometer and single acquisitions of 100% power for one second exposure of the 830 nm laser were taken every 2 minutes from the fluid, or protein ring as it became visible, until 40 minutes. This experiment was repeated on three separate occasions.

Results: Prior to 12 minutes, Raman spectral features were not discernible (Figure 13).

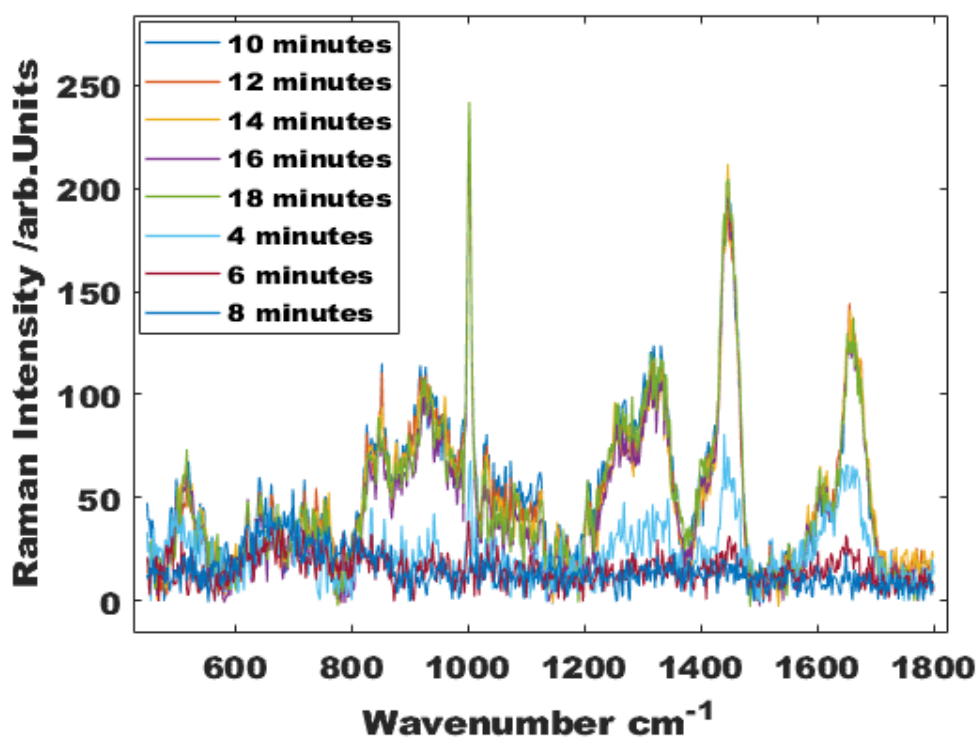


Figure 13 - Drying time of 1.5 microlitre plasma. This is a figure of spectra taken every 2 minutes of freshly dropped plasma. Features expected for plasma become identifiable from 12 minutes onwards as seen with the orange, purple and green spectra.

Signal intensity increased gradually up to 22 minutes where it plateaus (Figure 14). Measurements taken from 22 minutes to 40 minutes did not demonstrate any benefit to prolonged drying time. The minimum drying time changes with increasing drop volume, as discussed in the previous section on assessing drop size.

Summary: For a 1.5 μ l drop size, a minimum drying time of 30 minutes ensures that the sample will have dried even if there are mild variations in room conditions.

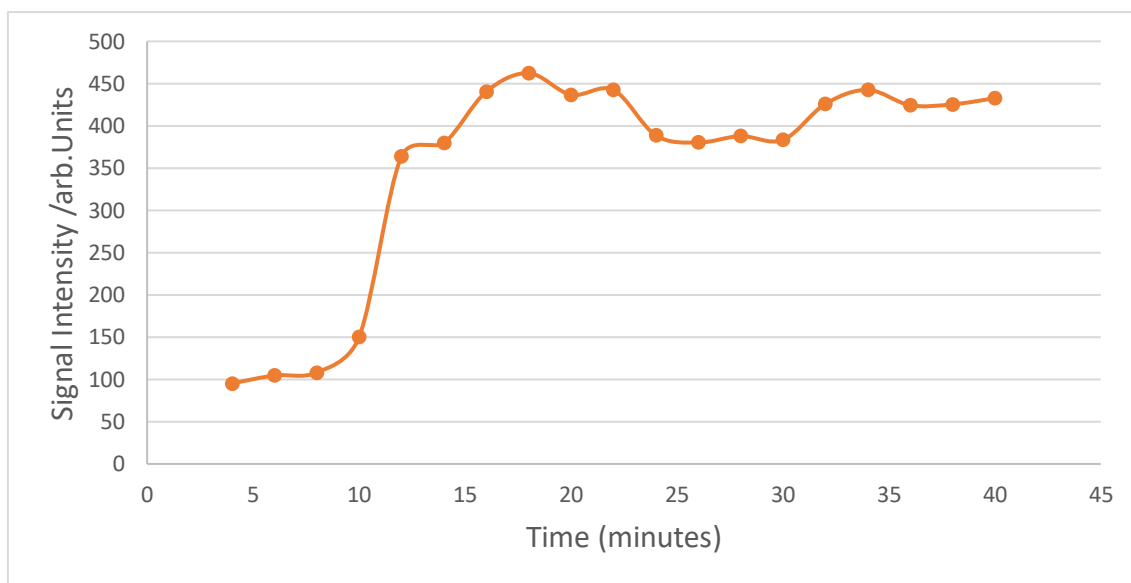


Figure 14 – Raman spectral signal intensity of 1.5 microlitre drop of undiluted plasma on stainless steel over time, up to 40 minutes, being held at room temperature. The peak height of the amide II protein peak is plotted over time to demonstrate the changes in signal intensity as the sample dries.

2.6.1.3 Spectrometer considerations - Biofluids

System configuration

A commercially available Raman spectrometer (Renishaw InVia Raman Microscope) was used for the biofluids experiments described in this thesis, coupled with a tuneable laser source and Leica microscope. Generally, wavelengths between 785 and 830 nm are required to achieve excitation. The 600 lines/mm grating was chosen of those available with this spectrometer to provide a fair compromise between good resolution and a spectral range that

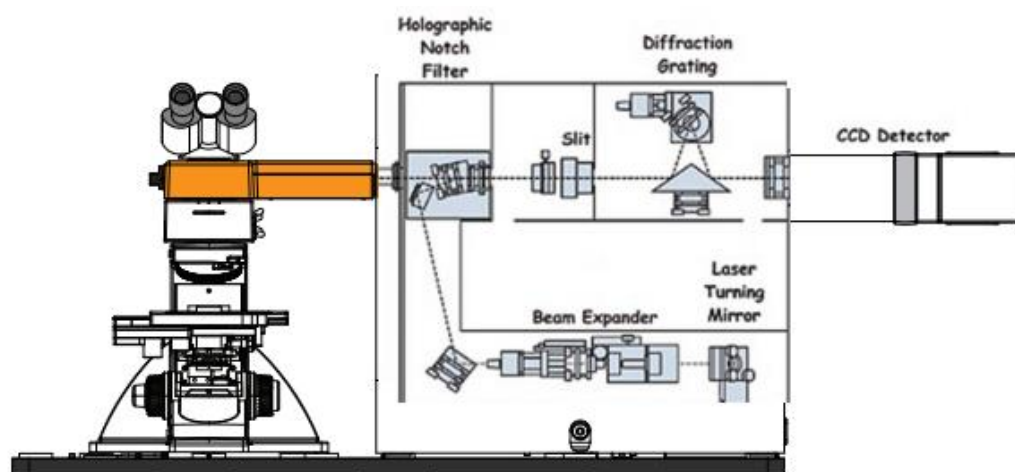


Figure 15 – Renishaw inVia Raman system. This image was created by adapting the image from (Renishaw, 2021) brochure and the schematic from (BunaciuHoang and Aboul-Enein, 2017).

covers the entire fingerprint region of the Raman spectra in a single acquisition. Figure 15 displays the schematic of the inVia system.

Calibration

The shared use of the spectrometer, changing lasers and inherent variations in equipment response create an obstacle for comparing Raman spectra taken at different times and locations. The use of samples with clear, highly reproducible Raman features to create calibration standards is one of the ways to manage this problem. Prior to commencing daily sample measurements, calibration tests were undertaken using an 830 nm laser with a grating position of 600 lines/mm. A spectral acquisition at 5% laser power was used to measure a silicon sample. The single significant peak (Figure 16) was checked for position, and an offset was applied if the wavenumber was greater than ± 0.5 off the recognised position of 520.5 cm^{-1} . A repeat of the measurement was carried out until the peak position was within range. The peak height was recorded as a marker of the signal intensity. Silicon also acts as an excellent reflective surface for checking the alignment of the laser beam. To check that peak positions remain stable when

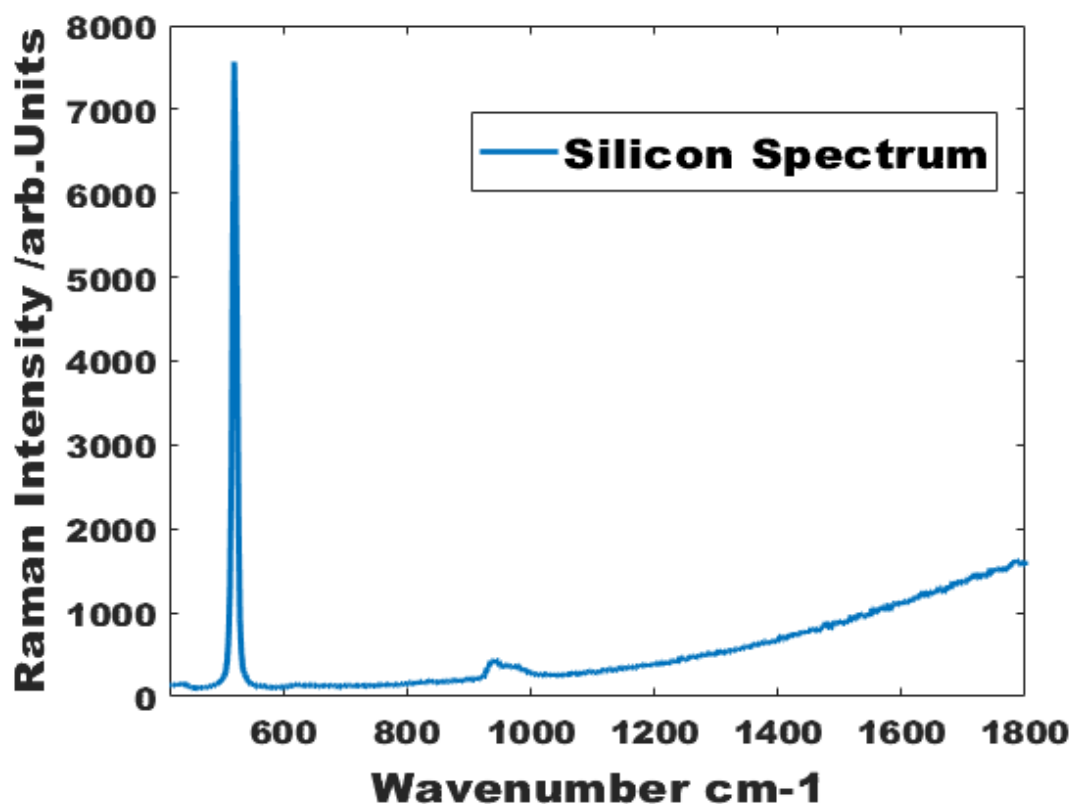


Figure 16 - Silicon spectrum. The silicon spectrum had only one peak at 520 cm^{-1} . The position on this peak is used in calibration of the Raman spectrometer.

there are multiple peaks, after any offset has been carried out using the silicon peak, a polytetrafluoroethylene (PTFE) sample was measured using 100% laser power (Figure 17).

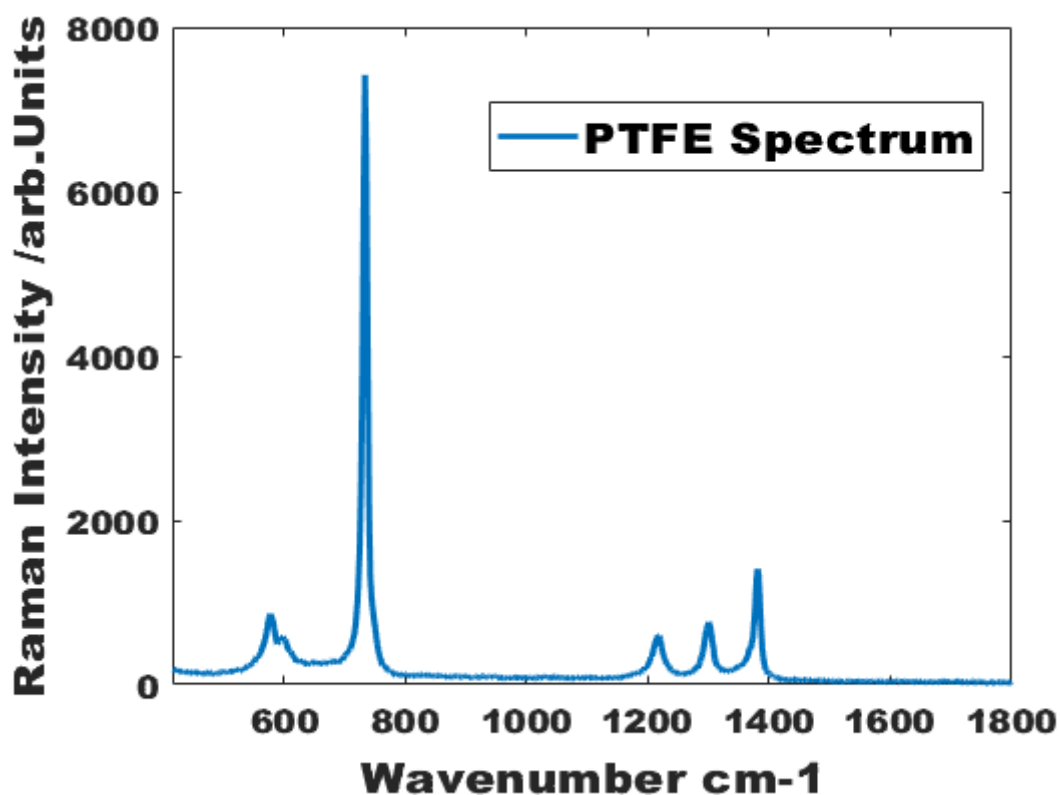


Figure 17 - PTFE spectrum. The PTFE spectrum has multiple peaks that are stable. The position of these peaks is checked when calibrating the Raman spectrometer.

Inter-spectrometer variances also pose a problem with collaboration and translation of Raman-related work. The green glass test is the locally used calibration test that measures green glass for its non-degradable fluorescence and uses the outcome after white light subtraction as a standard for calibrating independent spectrometers. A green glass calibration test was not performed in this work as the same spectrometer was used for all measurements.

2.6.1.4 Final lab protocol for plasma measurements

- 1) Equipment – Renishaw InVia Raman Microscope with 830nm edge laser, 600l/mm grating. Every day calibration tests were performed on the InVia using silicon, green glass and PTFE following the BioSpec group protocol (Gardner, 2021).

2) Defrosting samples – Samples to be measured were removed from the freezer. Samples were not defrosted unless it was clear they could be measured that day. A minimum time of 30 minutes passive defrost at room temperature was used. Plasma was checked to ensure plasma it was flowing freely in tube and there was no visible ice.

3) Even sample – Samples were mixed using a vibrating plate for 10 seconds prior to pipetting to ensure any proteins that have settled during defrosting are evenly distributed through the sample.

4) Pipetting – A volume of 1.5 μ l of plasma was pipetted unto stainless steel slides, three drops per sample. There were 9-10 samples per slide.

5) Drying – Samples were allowed to air dry at room temperature for 30-60 minutes and were not disturbed in this time to avoid disrupting the ring shape.

6) Imaging – A white light map of the slide using the 5x objective was captured and saved. The objective was then changed to 50x, without disturbing the stage and refocussed.

7) Measurements – The dried drop to be measured was selected and zoomed into. The map image acquisition function in MATLAB was used to trace out a circle outline over the protein ring in the active window. The measurement step distance was adjusted to get 64 spectra per ring. The measurement parameters were inserted; spectral range centre to 1500 cm^{-1} , laser exposure time to 1 second, power to 100% and accumulations to 2. The measurement was pre-saved to reduce active memory load on the Wire Software.

2.6.1.5 Spectral processing - Biofluids

Using the final protocol above, 64 spectra were acquired per drop achieving 192 spectra per participant (64 spectra for each of three drops per participant). All spectral measurements were viewed in the InVia Wire software to ensure there were no failed measurements prior to importing into the software MATLAB R2020b for processing. Both custom and new scripts, written by Professor Stone, for the purpose of this study were used. Spectral data were pre-processed to remove cosmic rays, baseline subtracted, and vector normalised. Visual

inspection was performed after each step. Obvious outliers were removed and replaced with the next spectra, being cautious not to take spectra from another drop or participant. Peak position and tentative assignment, and multivariate analysis of the data are discussed in chapter 3.

2.6.2 Development of the lab protocol - Tissue

2.6.2.1 Preparation of tissue for clinical histopathology

With the exception of samples taken intraoperatively for rapid histopathological assessment, frozen sections, biopsies and specimens taken for investigation and treatment of ovarian cancer are generally sent in formalin to the laboratory. The role of formalin is to preserve the tissue specimens. The standard pathway for tissue assessment is the production of hematoxylin and eosin (H&E) stained tissue slides for microscopic examination by the histopathologist and the issue of a formal report with a diagnosis. To achieve this, the formalin fixed specimens are examined, and macroscopic assessment is completed and documented. The specimen, depending on its size, is then dissected with representative sections of tissue sent for further processing. The tissue section is dehydrated using ethanol, and then xylene is used to replace the alcohol in a process called clearing, to facilitate the next step, impregnation with paraffin wax. The timing of this process varies depending on tissue size and fat content. The tissue sections are placed in moulds which are then filled with paraffin wax and rapidly cooled. The resultant wax block containing the tissue section can then be mounted onto a microtome to cut thin wax sections of 3-4 microns which are then transferred onto a glass slide.

To be able to appreciate the structures within the tissue, the staining process is required. The wax is removed using xylene, tissue rehydrated with ethanol and then dipped in hematoxylin dye. The slide is rinsed with alkaline water and then dipped in eosin dye. Hematoxylin highlights the nucleus and its contents whilst eosin highlights proteins and the cytoplasm. After a further alcohol wash to remove any remaining water, a further clearing with xylene is performed and then a glass cover slip is mounted (Dey, 2022).

2.6.2.2 Refining the tissue management plan

Whilst this process is not destructive to the tissue, it is evident that the specimen is exposed to a lot of different chemicals to produce a representative H&E slide for histopathological assessment. All of these chemicals give a Raman signal and

will create unwanted contributions to Raman assessment of the tissue. Consequently, a different approach is required to create slides for Raman assessment that does not include any of these chemicals. Each chemical used in the production of H&E slides has a purpose, as summarised below, and alternatives that fulfil the same aim have been considered in the planning of tissue management for Raman spectroscopy Table 3.

Chemical	Purpose	Alternative
Formalin	Preserve tissue	Snap Freeze
Ethanol	Create a wax block that facilitates mounting and sectioning of tissue	OCT block sectioning
Xylene		
Paraffin wax		
Hematoxylin	Staining Slide to allow differentiation of structures within the tissue	Unstained tissue
Scotts tap water		
Eosin		
Ethanol		
Xylene		

Table 3 - Summary of chemicals used in production of H&E slides. These can create contributions to the Raman spectrum are thus considered contaminants. In this table, alternatives being considered have been listed.

Preserving tissue

The only option for preserving tissue that does not involve the use of chemicals or reagents is freezing fresh tissue. The main variable to be considered is the freezing time. Slow freezing increases the risk of water expansion and the formation of water crystals, which can cause cracks and damage the tissue (Cunningham). As an alternative, liquid nitrogen immersion allows samples to achieve low temperatures quickly, reducing the risk of ice crystal formation. Other options such as isopentane with dry ice or nitrogen, dry ice with ethanol, etc were not considered due to their slower freezing times when compared to liquid nitrogen and safety around transport and use in the operating theatre environment (UAB Research).

Tissue sectioning

In clinical care, when frozen sections are required for intraoperative rapid workflow, the frozen samples are mounted unto the chuck using optimum cutting temperature (OCT) compound as the embedding matrix. This compound

(supplied by Fisher Scientific as Scigen Tissue-Plus™ OCT compound) consists of ethanol, glycols, and non-reactive agents (Fisher Scientific). Unfortunately, this compound generates a Raman signal (Figure 18) which will likely interfere with tissue assessment.

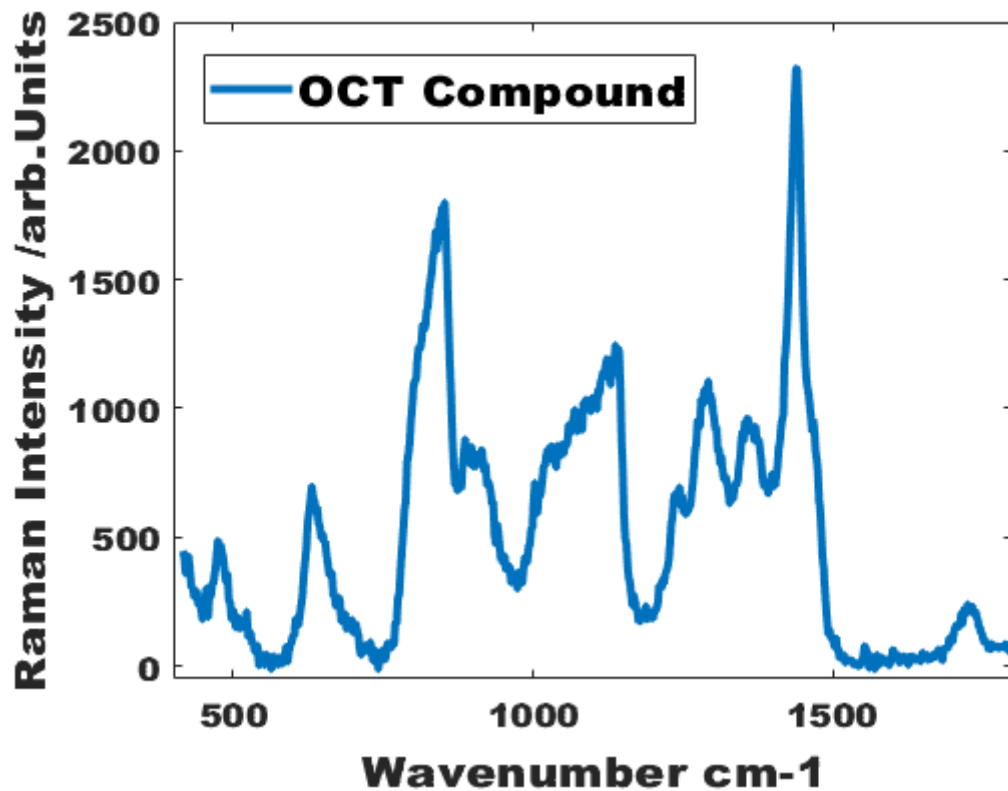


Figure 18 - OCT compound spectrum. The optimum cooling temperature (OCT) compound spectrum is demonstrated in this figure. The spectrum was acquired by measuring OCT compound on a stainless steel slide using the Renishaw InVia spectrometer coupled with an 830 nm laser. Three accumulations of a five second exposure time on 100% laser was used.

As such, an alternative approach is necessary. Previously, water has been used within the Stone group to mount the sample on the chuck. This approach was tested together with the biomedical scientist performing the frozen sections for this study to ensure confirm its suitability for ovarian and peritoneal tissue. This approach has been used for tissue sectioning in this work.

Striking the balance between enough water to keep the sample on the chuck and not so much as to create ice around the tissue was difficult. Samples were consequently placed on thin strips of cellulose acetate sheets, as described in section 2.3.2 sample collection and processing, prior to placing in a 1.5 ml cryovial and snap freezing in liquid nitrogen. This allowed a smaller amount of

water to be required to fix the fresh frozen sample and acetate complex to the chuck for sectioning (Figure - 19) in a cryostat microtome.

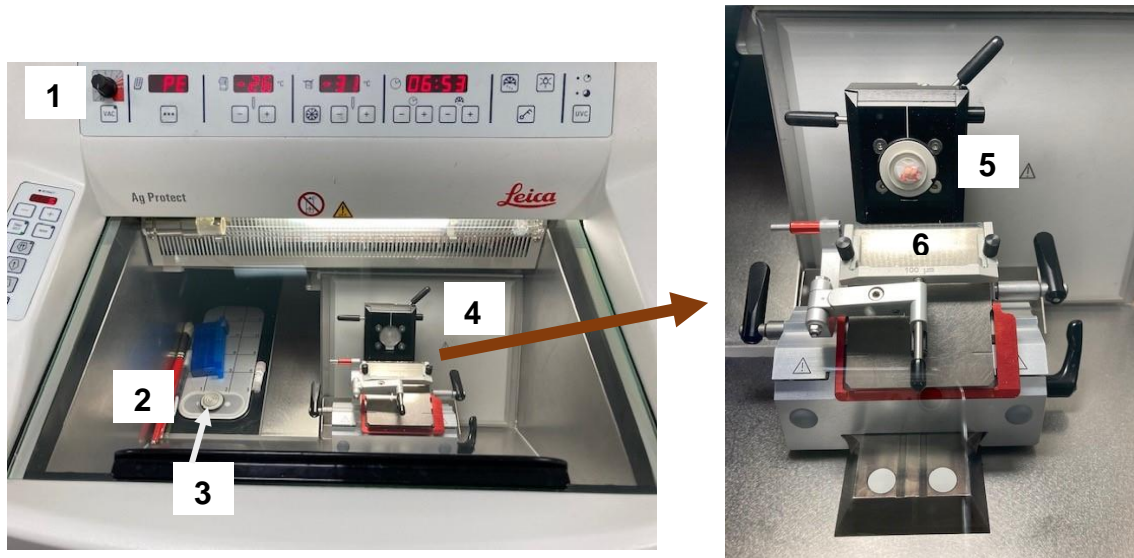


Figure - 19 Leica systems cryostat microtome at Southmead hospital, North Bristol Trust, used for tissue sectioning in this project. This is an image of the freezing chamber of the cryostat. The panel labelled 1 is a panel field that contains control and the temperature display. The area labelled 2 is next to the Peltier element with two stations. In this image there is a chuck, 3, placed in the middle of the element across the two stations. The microtome labelled 4 is best appreciated in the zoomed in image to the right of the figure. There is a sample on acetate sheet loaded onto the chuck with water, sitting in the specimen holder, 5, ready for sectioning. The area labelled 6 is the blade holder.

The fresh tissue sections were then transferred onto both stainless steel slides and glass slides. The first and last of three consecutive sections was transferred onto a glass slide and manually stained with hematoxylin and eosin. The middle fresh frozen section was transferred onto stainless steel and returned to the freezer for transport to University Exeter for Raman measurements.

Tissue thickness affects the ability of light to penetrate through for effective microscopic assessment, which is why traditionally tissue for H&E slides are 3-4 microns thin. Signal to noise ratio (SNR) in Raman spectroscopy is affected by tissue thickness with a correlative increase in signal to noise ratio as tissue thickness increases (Frost, 2019). To ascertain where the balance lies for ovarian and peritoneal tissue, single sections of 5 to 25 microns of both ovarian and peritoneal tissue were taken in pairs at five micron intervals. One of the pair was stained with haematoxylin and eosin and the other was kept frozen for fresh tissue Raman spectroscopy measurements. All H&E slides were reviewed by one consultant histopathologist to determine their suitability for microscopy and all five thicknesses were deemed interpretable for both tissue types.

The Raman slides were defrosted and measured on the Renishaw InVia Raman spectrometer (Renishaw, Wotton-Under-Edge, United Kingdom) coupled with an 830 nm laser using a 600 lines/mm grating. A single spectral acquisition was obtained using, 100% power for 1 accumulation of 5 seconds exposure. Two further spectral measurements were taken on separate occasions.

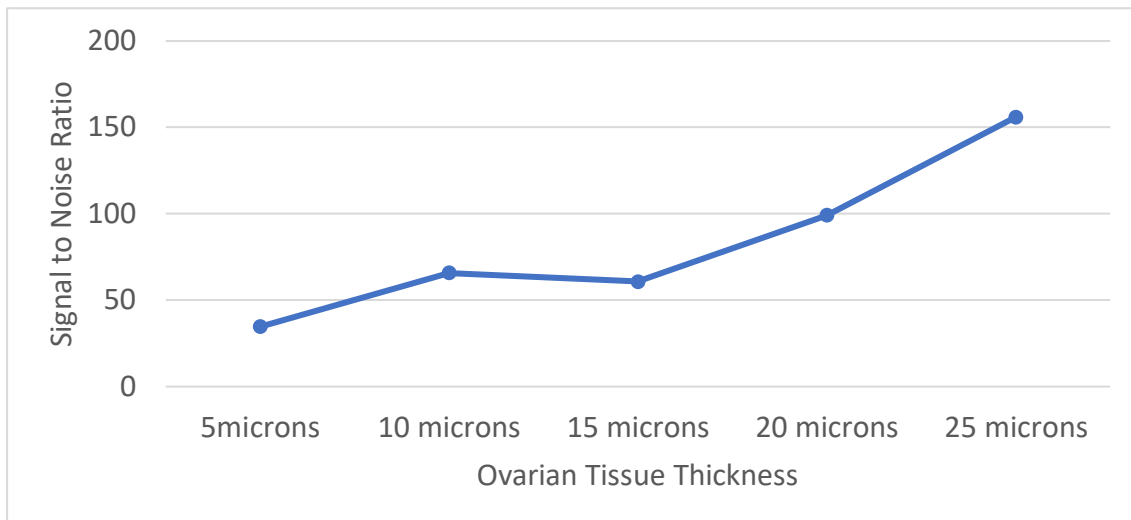


Figure 20 - Signal to noise ratio of benign ovarian tissue of varying thickness. This signal to noise ratio figure is generated from one spectral measurement and shows increasing signal to noise ratio with tissue thickness.

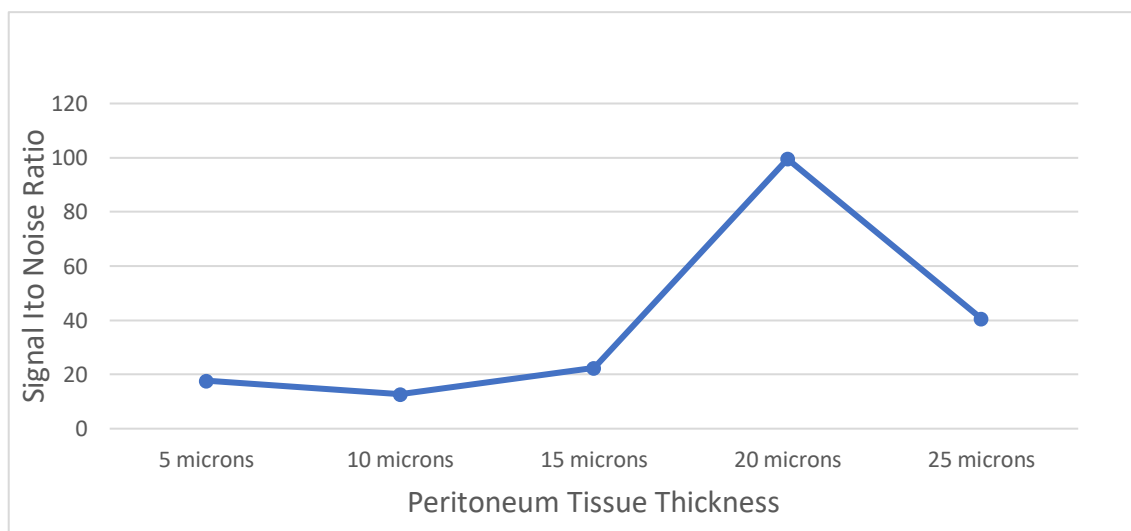


Figure 21 - Signal to noise ratio of benign peritoneal tissue. This signal to noise ratio figure is generated from one spectral measurement and shows increasing signal to noise ratio with tissue thickness. The higher 20 microns result was consistent in all three measurements of this tissue.

When considering the Raman spectra, there was a notably poor signal to noise ratio on the thinner sections of peritoneum. The 20 microns section of peritoneum had a consistently higher signal to noise ratio than the 25 microns sections (Figure 20, Figure 21). This was consistent with the repeat measurements of the same tissue. The experiment was not repeated on new tissue sections due to

limited availability of ovarian and peritoneal tissue. There was consistently good SNR with the 20 microns sections of both tissue types, thus it was chosen as tissue thickness for this work.

2.6.2.3 Final lab protocol for tissue sectioning

This protocol was developed with the support of a biomedical scientist who subsequently followed the protocol to complete the tissue sections required for this work.

1. The cryostat, mounting block, chucks and sectioning brush were washed with detergent and rinsed with water, and the microtome blade was replaced with a new one, to reduce the risk of contamination from previous work.
2. The clean chuck was placed in the cryostat and allowed the cryostat to reach ambient temperature (-23 to -27 degrees Celsius)
3. A drop of water was used to wet the chuck and the acetate covered surface of tissue block was placed onto the wet chuck.
4. The chuck was placed onto the Peltier freezing stage to allow the water to freeze and the sample to embed. This happened within a few seconds to up to a minute depending on the amount of water used.
5. The chuck was then mounted onto the mounting block and the microtome set for 20 microns tissue sections.
6. The first of three consecutive sections of tissue was transferred onto a glass slide, the second onto stainless steel and third onto another glass slide. Where there was an issue with any of the slides, the sections were discarded, and a fresh set cut to maintain three consecutive sections.
7. The section on the stainless steel slide was returned to a -80°C freezer in a slide mailer for Raman spectroscopy measurements to be carried out at a later date.
8. The tissue block to the -80°C freezer in its cryovial.
9. A manual staining process for haematoxylin and eosin was completed for the glass slides.

2.6.2.4 Spectrometer considerations – tissue

The same considerations for system configuration and calibration were used for tissue measurements as discussed for biofluids in chapter 2.2.1.

The settings for tissue measurements however required refining due to the change in sample type. Whilst the area of interest was marked on the H&E slides, the appearance of equivalent area on the Raman slides was unknown until samples were defrosted and white light mapped for measuring. One tissue block from this work was defrosted and measured to determine appropriate laser exposure time, number of accumulations of the measurement, and size of area to be measured. The details and findings of these experiments are described in this section. To preserve the limited number of samples available, this investigation was not repeated. However, prior to commencing formal measurements of the samples in this study, the slide used for these investigations was remeasured to ensure the findings held true.

Exposure time

As with all measurements of biological samples, the risk of sample damage or burning and photobleaching were considered when determining the appropriate laser exposure time for the tissue samples in this work. The aim of this experiment was to look at the minimum exposure time required to give clear spectral features without damaging the sample. Using the 830nm laser and a laser power of 100%, the sample was measured within the area marked on the H&E slide with an exposure time of two seconds. This yielded a very poor spectrum with spectral features that weren't discernible. The measurement was repeated with an exposure time of 10 seconds. A clear spectrum for tissue could be appreciated however some of the features were muted. At 15 seconds exposure time, these features were a lot clearer and there were peaks that were not visible with 10 seconds exposure time. A complication of the prolonged continuous exposure time is the increased risk of contributions of cosmic rays which was noted in this experiment (Figure 22). Due to these contributions and the risk of burning the tissue, higher exposure times were thus not tested.

Results: 15 seconds exposure time was chosen for this work; however, the issue of cosmic ray contributions has been factored into the planning of the number accumulations of measurements

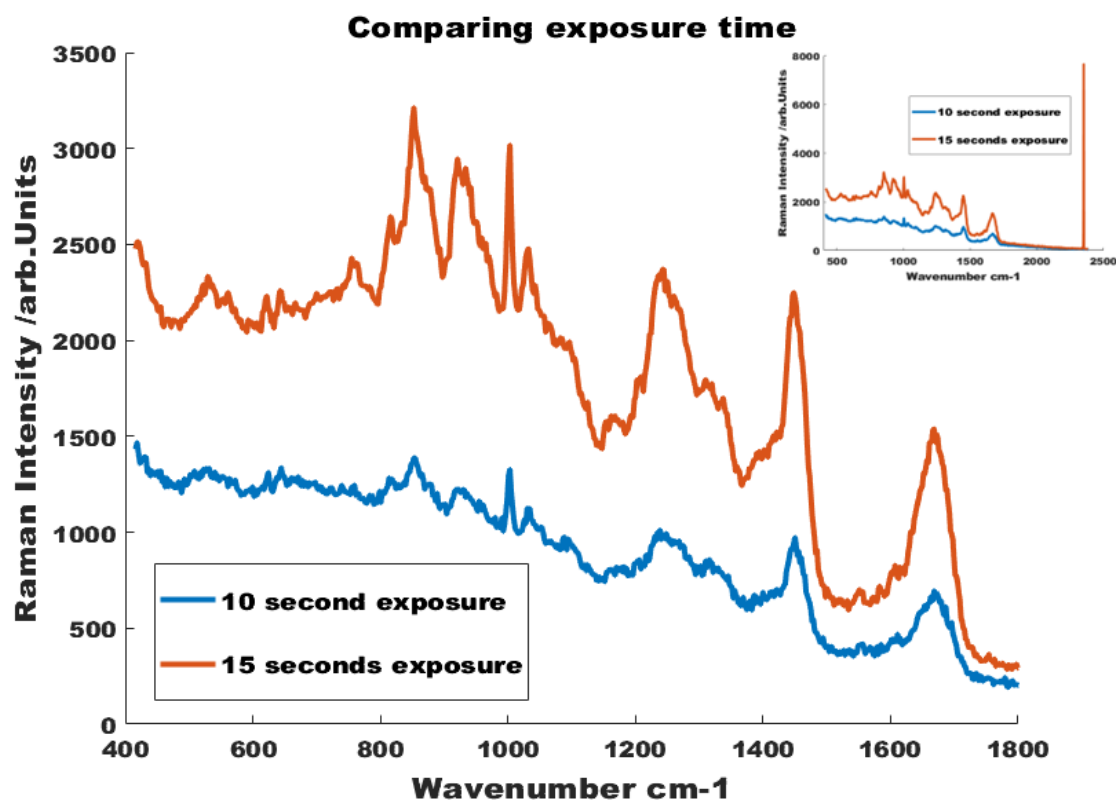


Figure 22 - Laser exposure time comparison. The orange spectrum represents a single accumulation of 15 seconds exposure time, and the blue spectrum represents a single accumulation of 10 seconds exposure time, plotted with wavenumber on the x-axis and Raman intensity on the y-axis. Spectral features are clearer with the longer exposure time however there is a contribution from cosmic rays as displayed in the smaller plot in the top right-hand corner of the figure.

Number of accumulations

As discussed above, a single accumulation of 15 seconds exposure resulted in cosmic ray contributions. Multiple accumulations of shorter measurements totalling 15 seconds exposure were considered. Three accumulations of five seconds exposure time provided similar signal but subtly worse (Figure 23) signal-to-noise ratio, due to the readout noise that accompanies each accumulation. As the total exposure time is still prolonged, on its own, multiple accumulations of shorter measurements does not eliminate the possibility of cosmic contaminants but it does allow the selection of automated removal of cosmic rays with a median filter during the measurement.

Results: Three accumulations of five seconds exposure time, with selection of the cosmic ray filter option, was chosen for this work.

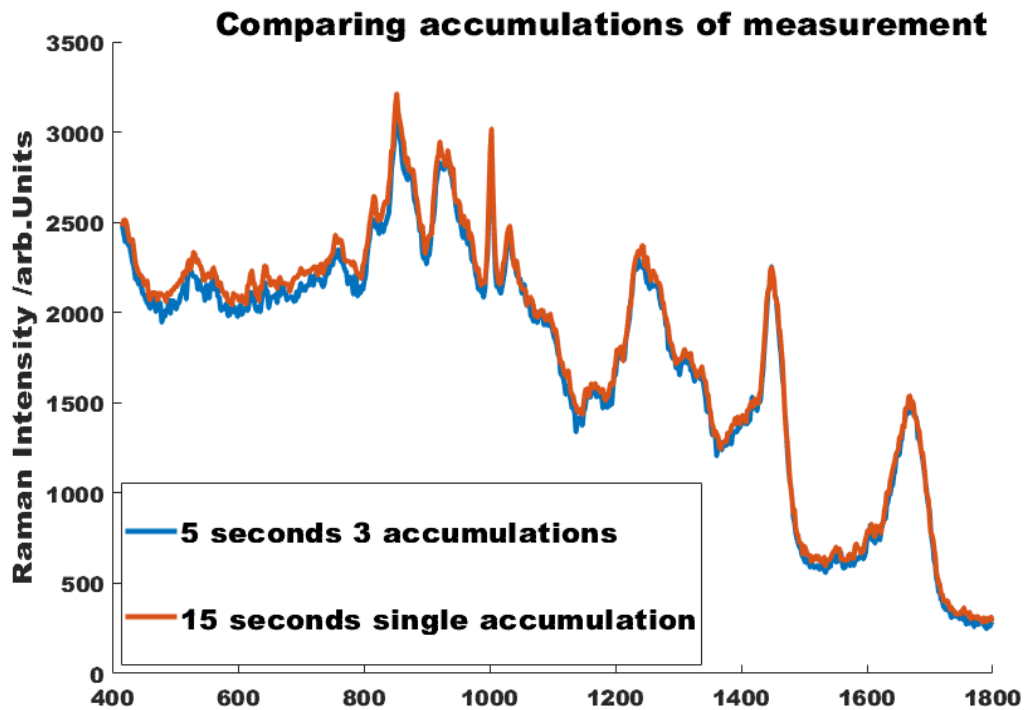


Figure 23 – Number of accumulations per measurement comparison. The orange spectrum represents a single accumulation of 15 seconds exposure time, and the blue spectrum represents three accumulations of 5 seconds exposure time, plotted with wavenumber on the x-axis and Raman intensity on the y-axis. Whilst the single accumulation of prolonged exposure time spectrum appears to be slightly smoother or less noisy, there is no loss or change in spectral features and cosmic rays were not detected during this measurement. Three accumulations of five seconds exposure time was non-inferior to a single accumulation of 15 seconds exposure.

Size of area to be measured

The factors considered in deciding the area to be measured were variation within the sample and duration of measurements.

Variation within the sample

It was considered that even within a small area of cancer, it is expected that there would be some variation within the tissue. In view of the exploratory nature of this work, it was important that any such subtle changes were not missed. This was a determining factor in the choice between single point measurements and map measurements. In exploring map measurement protocols for this work, it became evident that the spectral quality was impacted by drifts in focus over the course of the measurement and large numbers of spectra were generated from very small areas, which was excessive for capturing variation within the tissue.

Grid point measurements chosen as a compromise between the two; the advantage of which was multiple measurements in a given area to capture variation in the tissue but reduced measurement time and risk of losing spectral

quality. Given the volume of slides to be measured and time restriction on this work, a 300 by 300 microns square grid with 50 microns steps was chosen for this work. This resulted in 49 spectra per measurement and the measurements took 26 minutes per grid.

2.6.2.5 Final lab protocol for tissue measurements

- 1) Equipment – Renishaw InVia Raman Microscope with 830 nm edge laser, 600 l/mm grating. Every day calibration tests were performed on the InVia using silicon, green glass and PTFE following the BioSpec group protocol (Gardner, 2021).
- 2) Defrosting – Samples were removed from the freezer at least 10 minutes before they were to be measured. They were deemed to be completely defrosted when any water spots had dried out.
- 3) Imaging – A white light map image of the slide was completed using the 5x objective. The objective was then changed to 50x without disturbing the stage, and the focus was adjusted.
- 4) Where to measure – The map image of the Raman slide was compared to the marked H&E slide. The corresponding area of interest on the Raman slide was then selected and a square map image acquisition grid of 300 by 300 microns was placed on this area.
- 5) Measurement – The measurement settings were adjusted to 50 microns steps, which predicted 49 spectra. The spectral range centre was set to 1500 cm^{-1} , laser exposure time to five seconds, power to 100%, accumulations to three and automated cosmic ray removal option chosen. Each measurement was pre-saved as part of the set up to reduce active memory burden on the software.

2.6.2.6 Spectral processing – Tissue

Using the protocol above, 49 spectra were acquired per slide of tissue. All spectra were viewed in the InVia Wire software to ensure there were no failed measurements prior to exporting into the MATLAB R2020b software for processing. The data arrives in a three-dimensional cube which is then reshaped to two dimensions. Both custom, and new scripts written by Professor Stone for the purpose of this work were used. Spectral data were pre-processed with

saturation spectra replaced and baseline subtraction and data normalisation steps completed.

Testing the protocols

Ideally, the final protocols would have been tested on retrospective plasma and tissue samples from patients with benign, borderline and ovarian tumours prior to processing and measuring study samples to validate the approach. Unfortunately, this was not possible due to the availability of samples and time restraints.

Chapter 3 – Raman spectroscopy of plasma for ovarian cancer

3.1 Introduction

As discussed in chapter 1, Raman spectroscopy has shown great potential in cancer diagnostics and lends itself well as a potentially more specific test for ovarian cancer. Although limited, previous work has demonstrated high accuracies for cancer detection using small sample numbers. This chapter describes the overall study recruitment data, plasma specific results of study recruitment, Raman spectral measurements, analysis, and discussion.

3.2 Aims

This study aims to evaluate Raman spectroscopy for the identification of novel plasma markers diagnostic of ovarian cancer and their diagnostic performance as an early detection test in women with symptoms of ovarian cancer.

To do this, this work will assess:

- the discriminatory ability of Raman spectroscopy in assigning spectra taken from drop coating deposition Raman spectroscopy to benign, borderline and cancer pathology groups.
- build and test predictive models for the discrimination between cancer and benign, will be assessed.

3.3 Methods

The clinical protocol describing participant recruitment, inclusion and exclusion criteria, timings and method of blood collection are described in chapter 2 section 2.2 and 2.3 (page 63).

The preparation of the dried plasma drops, Raman spectroscopy instrumentation set up and measurement protocols are described in chapter 2 section 2.6 (page 71).

3.4 Overall study recruitment outcomes

Participants were recruited from two sites, University Hospitals Bristol and Weston (28th June 2021 to 30th September 2022) and Royal United Hospitals Bath (18th October 2021 to 30th September 2022) over an average of 12 months.

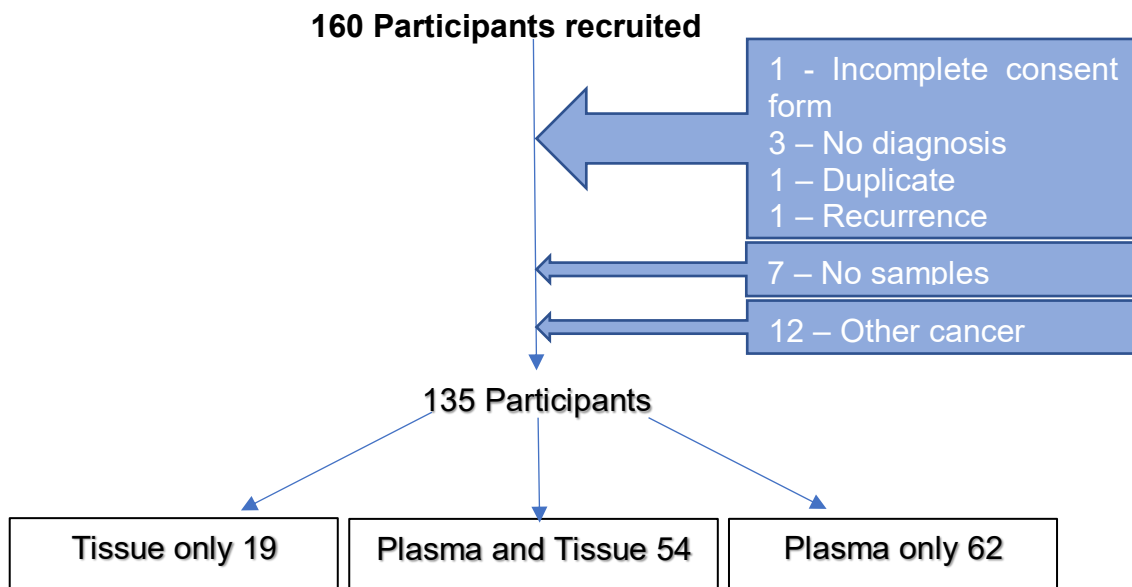


Figure 24 - Flow chart of overall recruitment outcome. Reasons for excluding participants are explained in the blue callout boxes.

160 participants were recruited all together however 13 participants were excluded for the following reasons: One participant had an incomplete consent form and started treatment before this could be remedied; three participants had no final diagnosis (because one declined surgery, one passed away prior to completing investigations and the third was unfit for surgery); One participant was recruited on two different occasions by different members of the research team thus one of her study numbers was excluded. One participant had a recurrence, not primary presentation with ovarian cancer, and samples could not be obtained from seven participants. Of the seven participants that did not have samples collected, one had planned blood collection with opportunistic samples requested by the clinician but unfortunately her research sample was not collected. She was unfit for surgery and thus had neither blood nor tissue samples in the study. The remaining six were recruited to have samples taken at interval debulking surgery however two had extremely good response to chemotherapy and there were no areas deemed appropriate for sampling, two had missed sampling opportunities

by the research team, one had surgery at a different site and the other had disease too extensive to be considered for surgery.

A further 12 participants were excluded as their final diagnosis was not ovarian cancer. All these participants were diagnosed with cancer of a different origin (Table 4).

Other Cancer Diagnosis	Number
Pancreatic Cancer	1
Endometrial Cancer	4
Leiomyosarcoma	1
Mesonephric-like adenocarcinoma	1
Malignant mesothelioma	1
Neuroendocrine tumour	3
Pseudomyxoma peritonei	1

Table 4 - Other cancer diagnosis. This table details the final diagnosis for participants excluded from the study for not having ovarian cancer.

In total 25 participants were excluded. The remaining 135 participants had either blood only (62), ovarian and or peritoneal tissue only (19) or both plasma and tissue (54) collected as part of the study, as summarised in Figure 24.

The demographic information for the 135 participants is summarised in Table 5 by pathology group and discussed further by sample type in this chapter and chapter 4. Of note, there is a lack of ethnic diversity in the study population. Diversity of participants is important to ensure generalisability of results and prevent worsening health inequalities however, the lack of diversity in this study is reflective of the lack ethnic diversity in Bath and Bristol and targeted recruitment is not likely to have made a significant difference.

Presenting complaint

Abdominal or pelvic pain, bloating, distension, and urinary symptoms accounted for half of the symptoms of women presenting with suspected ovarian cancer. For 11% of participants, ovarian pathology was an incidental finding following imaging for other reasons. Lower incidence presenting symptoms included unexplained weight loss, change in bowel habit, early satiety, pelvic pressure, postmenopausal bleeding, unscheduled bleeding, heartburn, back pain, prolapse, shortness of breath, nausea, and unilateral leg oedema.

Demographic information			
	Benign	Borderline	Cancer
	n=53	n=16	n=66
Age (years)			
<i>Mean (range)</i>	62 (24 – 87)	55 (29 – 85)	64 (36 – 88)
Parity			
0	8	4	11
1	10	2	9
2 or more	31	10	44
No data	4	-	2
Menopausal status			
Pre	9	4	5
Peri	2	2	1
Post	42	10	60
Smoking status			
Never smoked	35	10	42
Ex smoker	14	3	16
Smoker	4	3	8
Ethnicity			
White British	51	15	64
White European	1	0	0
Southeast Asian	1	0	1
South Asian	0	1	1
South American	0	0	1
BMI			
<i>Mean (range)</i>	27 (18-47)	32 (20-50)	27 (18-40)
CA-125			

	<i>Mean (range)</i>	55 (10-561)	90 (10-532)	1153 (10-15639)
No. of comorbidities				
	0-2	27	7	31
	3-5	17	6	28
	6-8	7	3	7
	9+	2	0	0
Diagnosis				
	Fibroma			
	Dermoid			
	Strum ovarii			High grade serous
	Endometriosis			Low grade serous
	Benign with small vessel vasculitis	Serous tumour		Clear cell
	Mucinous cystadenoma	Mucinous tumour		Mucinous
	Serous cystadenoma	Torsion/Necrosis		Endometrioid
	Simple Cyst	Endometrioid type		Adenocarcinoma NOS
	Fibrothecoma	Necrosis/Torsion		Granulosa cell
	Tubovarian Abscess			Sex Cord Stromal
	Brenner Tumour			
	Stage			
I		-	-	14
II		-	-	3
III		-	-	20
IV		-	-	29

Table 5 – Clinical characteristics of remaining 135 participants in this study summarised by pathology group. Included in this table are age, menopausal status, ethnicity, BMI, smoking status, comorbidities, diagnosis and stage of cancer at diagnosis.

3.5 Plasma recruitment outcomes

As described in detail in section 3.4, blood samples were collected from 116 participants. Of these, 46 had ovarian cancer, 16 borderline ovarian tumours and 54 benign ovarian pathology. The mean age for the study population was 62 years in the benign group, 55 years in the borderline group and 64 years in the cancer group (Figure 25). This is consistent with the age of incidence in the literature (BGCS, 2017).

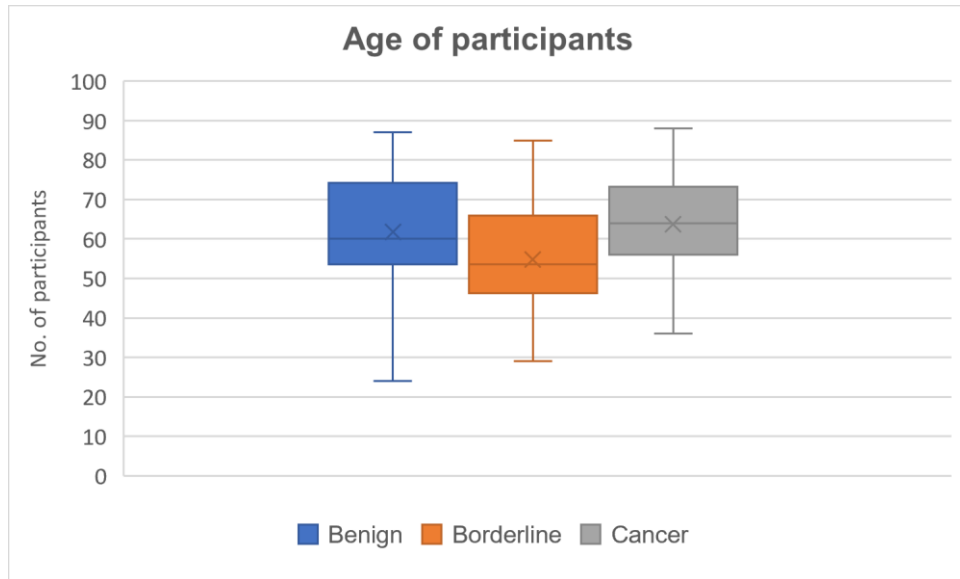


Figure 25 - Age of participants. The box plots demonstrate the range of ages of the participants in the benign, borderline and cancer groups. The mean age, marked x, is 62 in the benign group (blue), 55 in the borderline group (orange) and 64 in the cancer (grey) group.

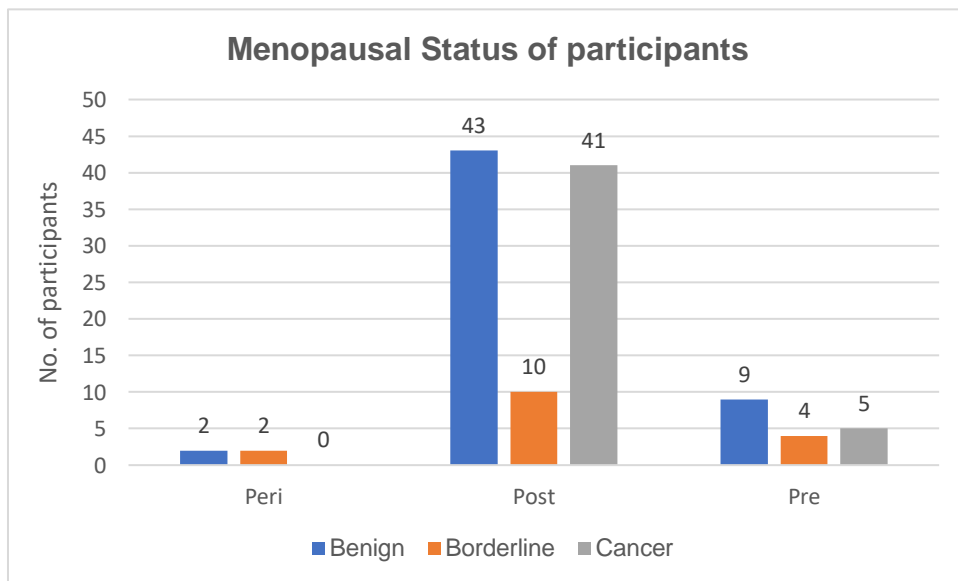


Figure 26 - Menopausal status of participants. This figure illustrates the proportion of women in study group who were premenopausal, perimenopausal and postmenopausal. Most of the women in the benign (blue), borderline (orange) and cancer (grey) groups were postmenopausal.

81% of the women in the study population were postmenopausal (Figure 26), consistent with what would be expected with the mean age of this population.

Across all three groups, most of the participants were non-smokers (never smoked or ex-smokers) and had fewer than 2 co-morbidities. Medical disease burden was highest in the benign group (Figure 27).

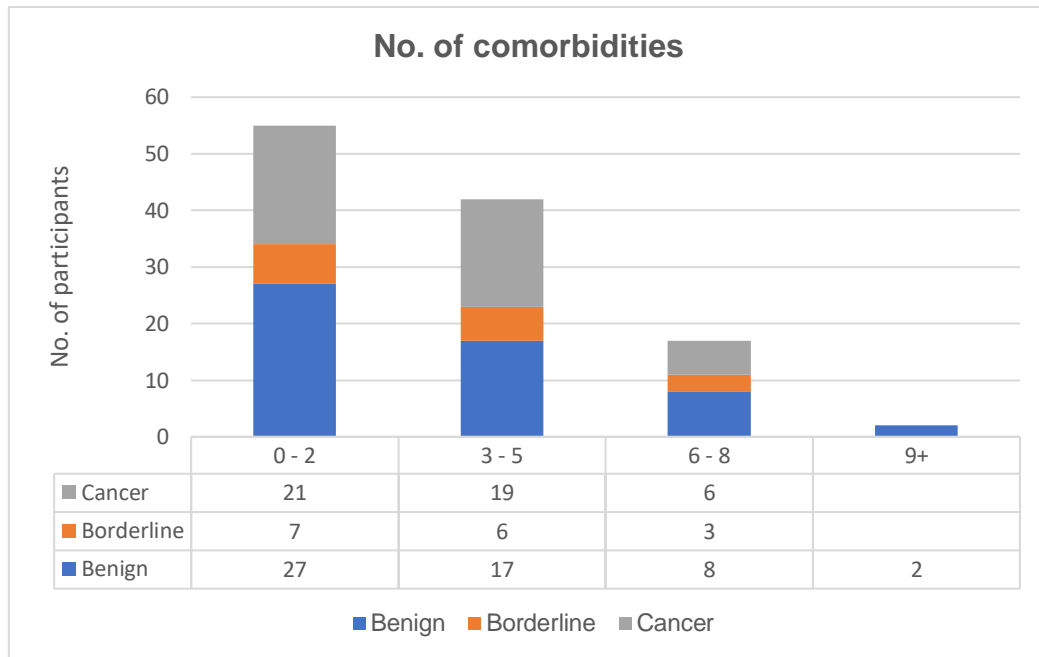


Figure 27 - Number of comorbidities per participant. This figure illustrates the distribution of medical comorbidities in benign (blue), borderline (orange) and cancer (grey) groups. Most participants had two or fewer comorbidities across all groups.

Benign group

Following discussion at the multidisciplinary team meeting, some participants in the benign group, 15 of 54 participants, were recommended surveillance or conservative management of their cysts as their pathology was deemed likely to be benign. This group is termed likely-benign in my thesis. As these participants did not have surgery, formal tissue diagnosis was never obtained. CA-125 levels were lower ($p < 0.001$) in the benign group compared to borderline and cancer (Figure 29) however the values ranged from 10 to 561 with the highest level seen in a patient with stage 4 endometriosis (Figure 28).

Mucinous and serous cystadenomas accounted for a third of the benign ovarian pathology. The remainder had a range of pathologies as illustrated in (Figure 30).

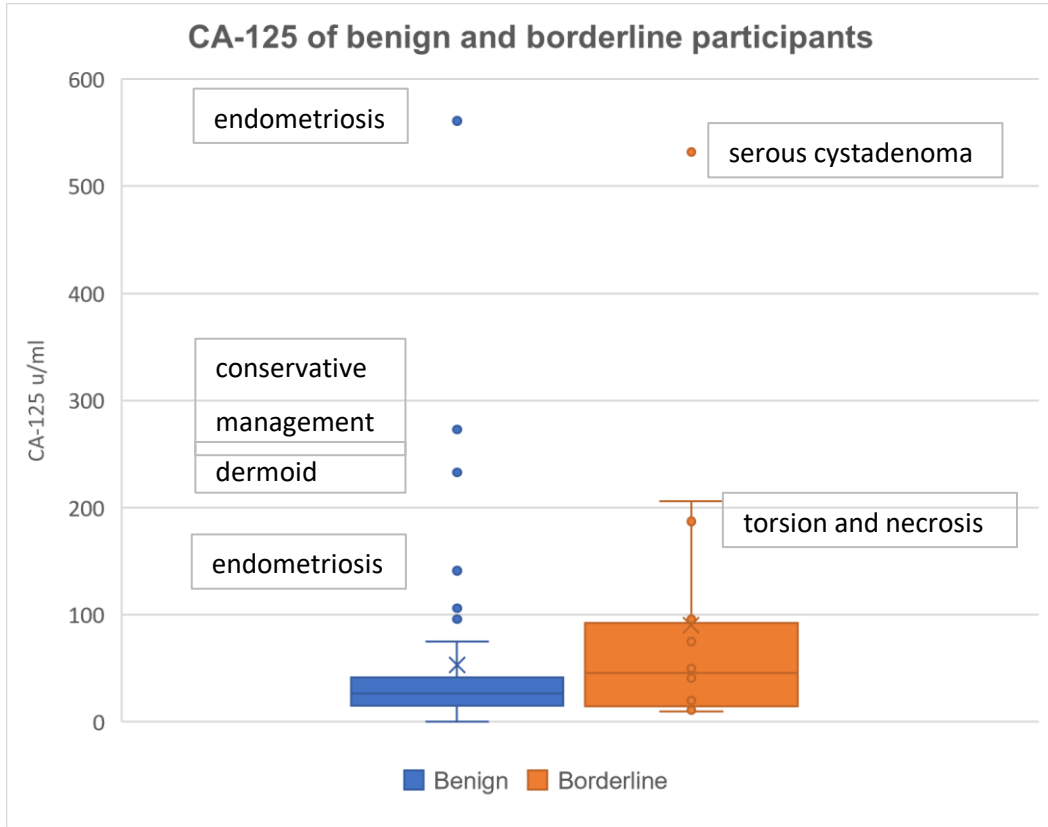


Figure 28 – CA-125 levels of benign and borderline participants. This figure illustrates the range of CA-125 levels in this group. Levels were lower in the benign group (blue) compared to the borderline group (orange). Normal CA-125 is less than 35 units/ml.

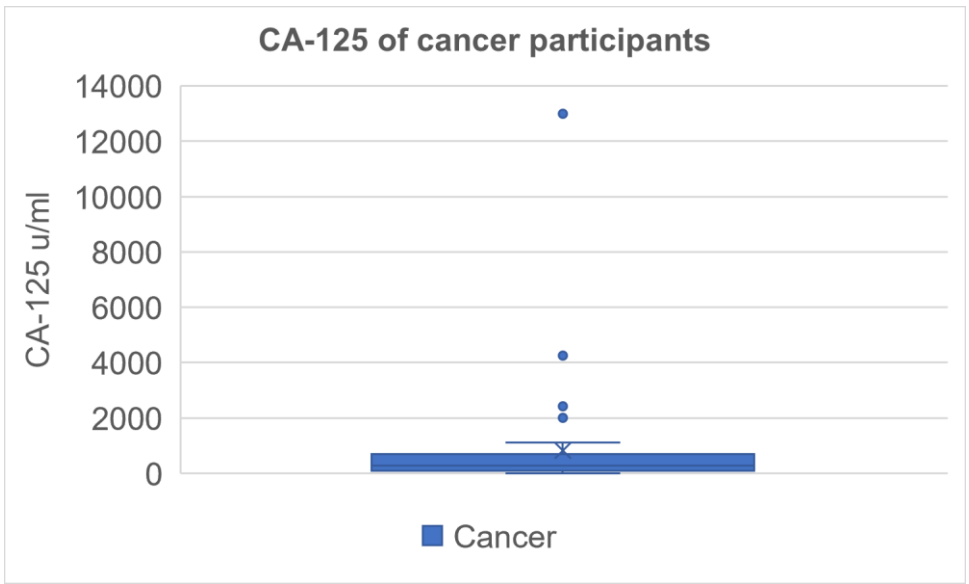


Figure 29 - CA-125 levels of cancer participants. This plot is presented separately to the benign and borderline values due to the large difference in range of results. Normal CA-125 is less than 35 units/ml.

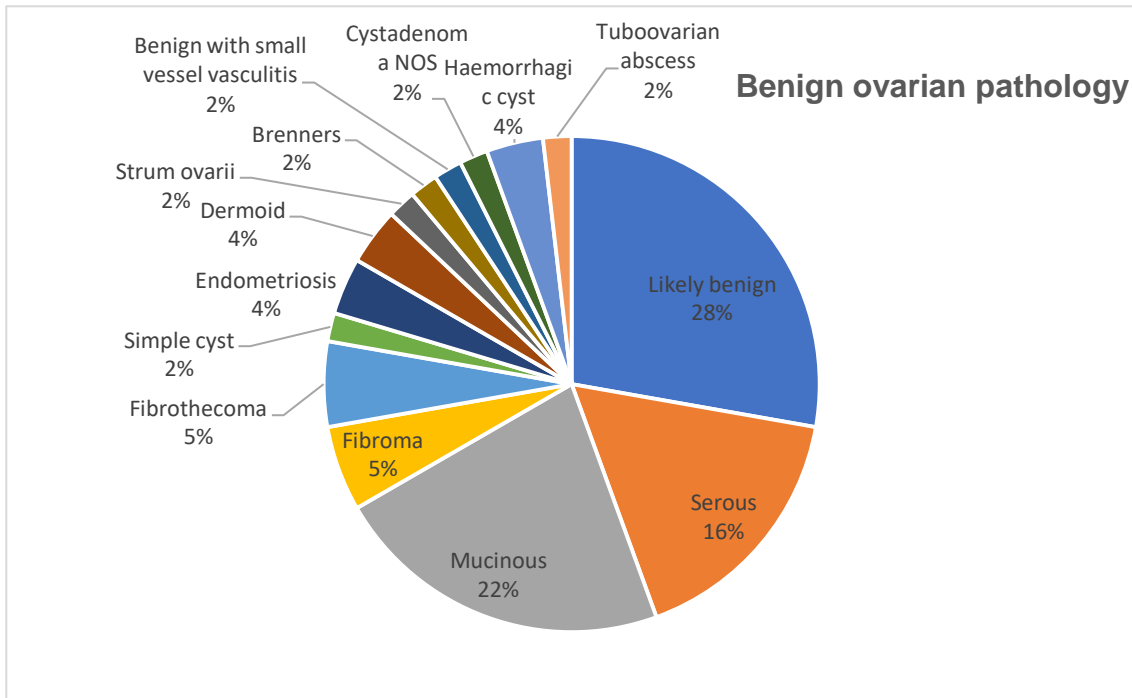


Figure 30 - Benign ovarian pathology. This figure illustrates the range of diagnosis of the participants in the benign group. Mucinous and serous cystadenomas accounted for over a third of benign ovarian pathology requiring surgery.

Borderline group

This group of 16 individuals was comprised of mostly serous (56%) and mucinous tumours (31%). There was one participant with an endometrial-type borderline tumour and a tortured borderline tumour with necrosis. Excluding the noted outliers (Figure 28), the majority of CA-125 levels were less than 100 U/ml in this group.

Cancer group

In this group of 46 individuals, 61% had high grade serous ovarian cancer, the remainder had low grade serous (13%), clear cell (9%), mucinous (7%), endometrioid (4%), granulosa cell (4%) and sex cord (2%) cancers. CA-125 levels were generally higher in this group and extremely broad, ranging from 10 to 15,639U/ml. The group had five (11%) participants with cancer (two low grade serous, one clear cell, one high grade serous and one granulosa cell ovarian cancer) with normal (<35 U/ml) CA-125 levels. All of these participants had stage I disease, except for one with low grade serous cancer who had stage III disease.

When looking at the high grade serous group only, 96% of participants had a positive CA-125.

Two thirds of participants were diagnosed in advanced disease (Figure 31), consistent with national data (Cancer Intelligence Team).

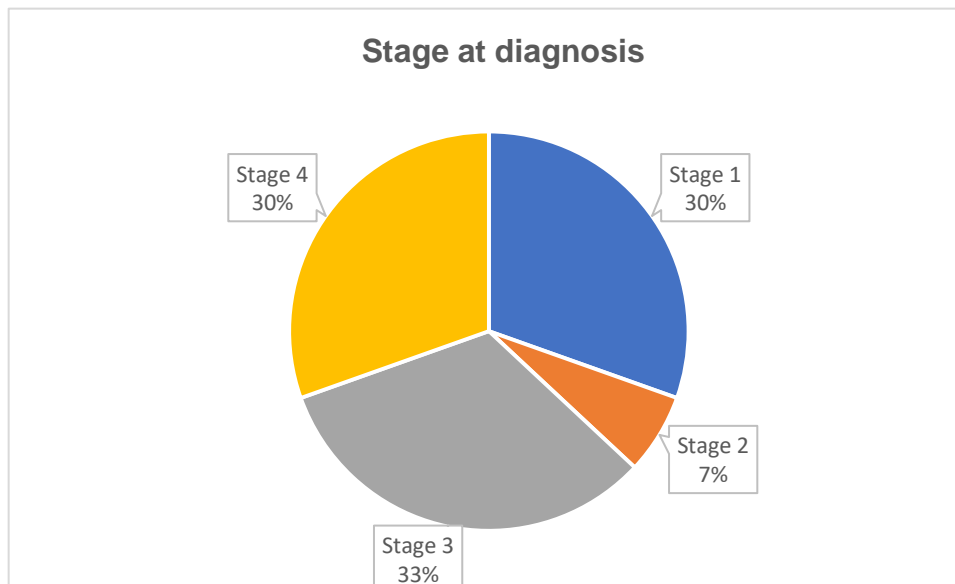


Figure 31 – Stage at diagnosis. The figure illustrates the distribution of stage of disease at diagnosis in the cancer group.

3.5 Raman results and analysis

The protocol for blood collection, centrifugation, and preparation of the plasma samples for Raman Spectroscopy is described in section 2.3.1. The Raman spectroscopy measurement protocols are described in section 2.6.1. Raman spectra were obtained using the Renishaw InVia spectrometer (Renishaw, Wotton-Under-Edge, United Kingdom) and 830nm laser using a 600lines/mm grating.

Measurements

The dried samples (one per participant) were exposed to the laser for an acquisition time of one second at 100% power which was adequate to improve signal to noise ratio with two accumulations of the measurement as described in chapter two. Samples were measured in triplicates (Figure 32), with 64 spectra collected per drop resulting in 192 spectra per participant. All 22,272 spectra were used in this assessment.

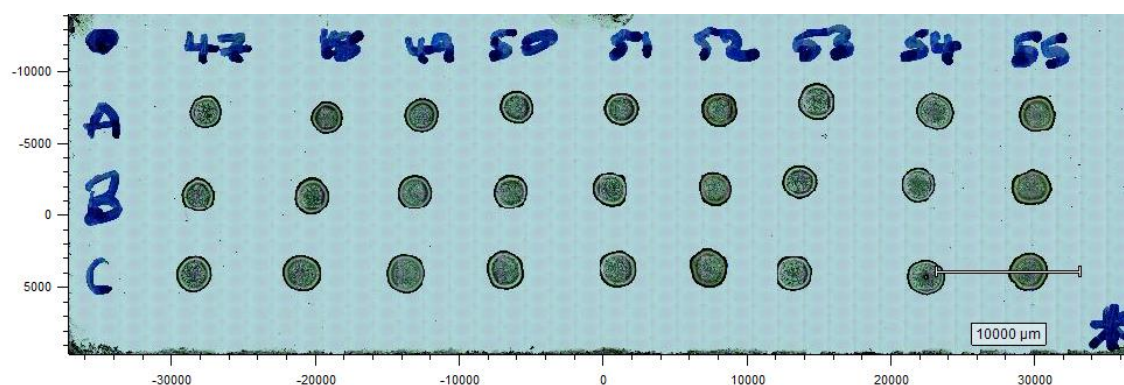


Figure 32 - White light image of dried plasma drops. This is an image of one of the slides of dried 1.5 microlitre drops of plasma measured in this study. Sample numbers are across the top in blue. The samples were measured in triplicates, A, B and C.

Pre-processing

Spectra outside of the fingerprint region were truncated leaving the wavenumber region of 450 to 1800 cm^{-1} . Cosmic ray contributions were then filtered out of data.

To reduce variations in intensity and background, a baseline subtraction step has been completed using a graphical user interface to visualise the data when changing the baseline variables. Figure 33 demonstrates the baseline subtraction used for this data.

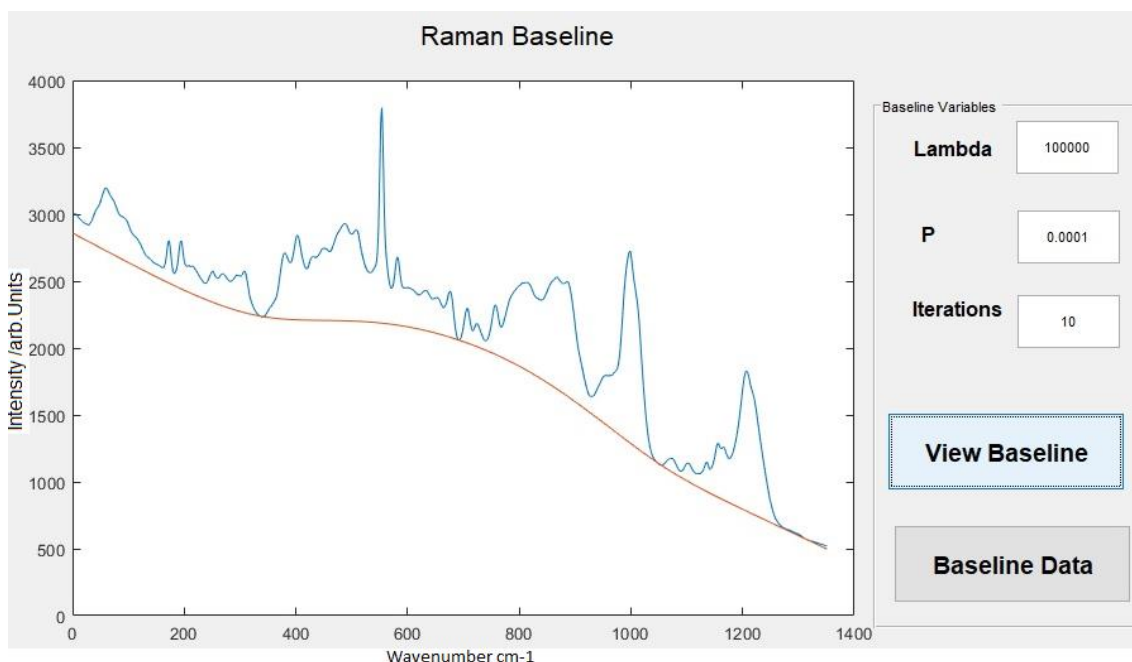


Figure 33 – Baseline subtraction. This figure is an image of the graphic user interface used to subtract the background signal and change the baseline of the plasma data. Each spectrum has its baseline subtracted separately however the same variables are used for all spectra in the data. The blue line represents the spectrum and the red line represents the baseline generated by least squares fit.

To avoid differences in pathology groups being falsely attributed to large signal intensity differences, a normalisation step has been completed to scale the values of the intensity of the collected signal to the range of zero to one across the whole spectrum, i.e., the highest was scaled to one and the lowest zero.

Peak positions and intensity

As discussed in the plasma recruitment results, there were 54 benign, 16 borderline and 46 cancer participants. One sample from each participant was measured. Following the pre-processing steps, the mean spectrum for benign, borderline and cancer have been plotted together in Figure 34. The differences between the groups are particularly subtle, as demonstrated by the small number of peak positions where the three colours can be delineated. To expose these subtle differences, each pathology group has been subtracted from the other, in turn, to generate subtraction spectra that highlight the variables that are responsible for differences in the groups. Tentative assignments of these peaks have been made for this work in Appendix I using reference tables (Stone, 2001, Kendall, 2002) (Talari et al., 2015) chosen after a search of the literature and previous work done on plasma.

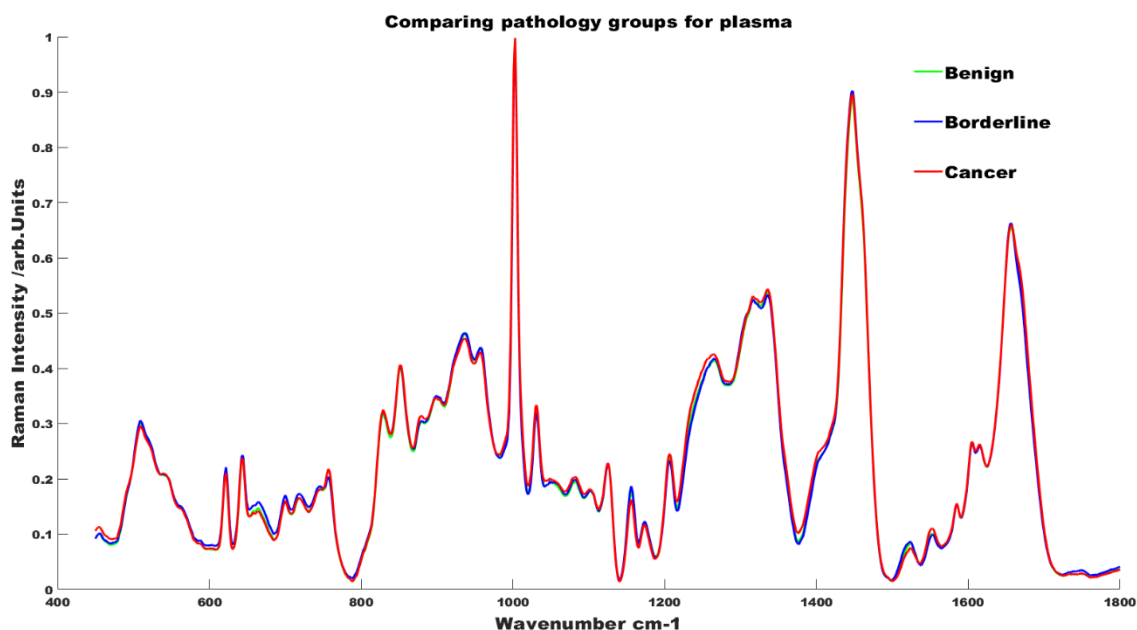


Figure 34 - Mean spectra of plasma for all pathology groups. In this figure, the benign spectrum (green), borderline spectrum (blue) and cancer spectrum (red) are plotted together with wavenumber cm^{-1} in the x-axis and intensity on the y-axis.

Cancer minus benign

The benign group was subtracted from the cancer group (Figure 35). The subtlety of the differences is reflected in the intensity scale seen in the y-axis. This goes from 0.03 to -0.03. To avoid overfitting of peaks that would not be noticeable if the spectrum were not zoomed in for display purposes, an arbitrary threshold of 0.01 arb.Units has been created, represented by the broken lines in Figure 35. Outside of this range, the subtraction spectrum reveals positive intensity values at 757, 876, 1012, 1073, 1232, 1360, 1379, 1392, 1435, 1548 and 1673 cm^{-1} suggesting a higher concentration of tryptophan (757, 1012, 1360 & 1548 cm^{-1}), $\nu(\text{C-C})$ stretch of hydroxyproline (876 cm^{-1}), lipids (1073, 1379 & 1435 cm^{-1}), amide III C-N stretch and N-H bonding (1232 cm^{-1}) group, CH rocking (1392 cm^{-1}) and amide I group (1673 cm^{-1}) in cancer group compared to the benign group. There is a negative intensity value at 1158 cm^{-1} suggesting lower concentration of carotenoids in the cancer group compared to the benign group.

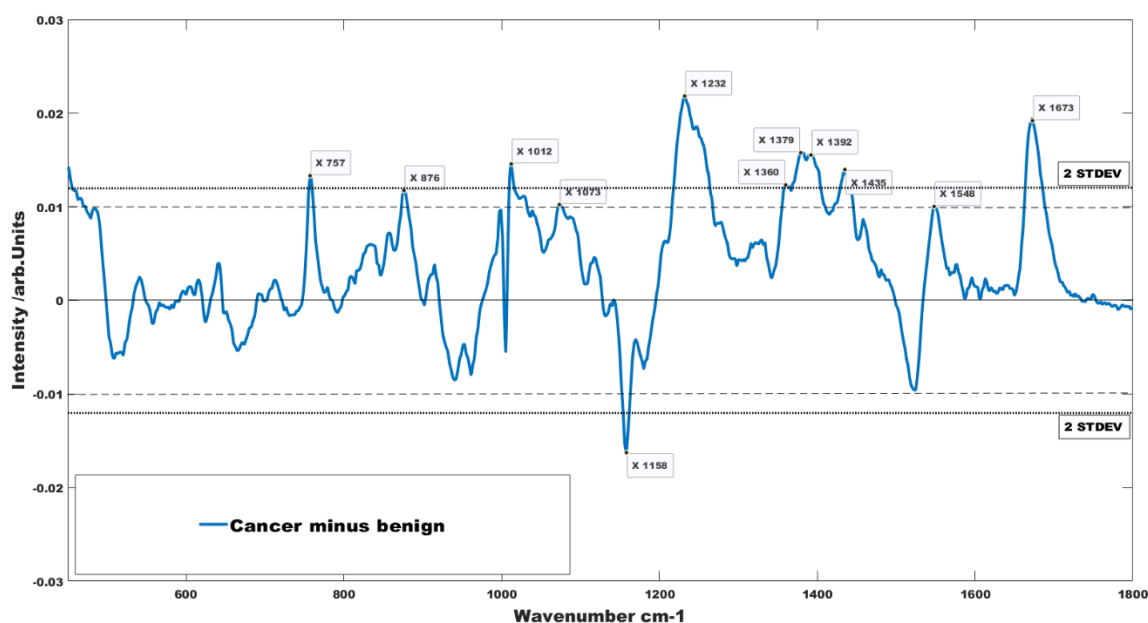


Figure 35 - Subtraction spectrum obtained from subtracting benign group from cancer group. Positive intensity values suggest increased concentration in the cancer group. Negative intensity values suggest increased concentration in the benign group. The broken like represents an arbitrary cut off and the dotted line represents two standard deviations above and below the mean. Peaks above these lines have been tentatively assigned. There are higher concentrations of tryptophan, lipids, amide III, amide I and CH rocking in the cancer group than in the benign group. There is a higher concentration of carotenoids in the benign group than in the cancer group.

A dotted line can be seen in Figure 35; this line, STDEV line, represents two standard deviations above the mean, to be used as an alternative approach to

deciding which peaks are relevant in this peak assignment exercise. On this occasion, the STDEV line excludes fatty acids of the lipids group (1073cm^{-1}) and one of the tryptophan assignments (1548cm^{-1}).

Cancer minus Borderline

The borderline group was subtracted from the cancer group (Figure 36). Using the arbitrary cut off, there is a positive intensity value at 758, 999, 1010, 1025, 1232, 1329, 1359, 1382, 1392, 1548 and 1672 cm^{-1} suggesting higher concentrations of tryptophan ($758, 1010, 1359$ & 1548 cm^{-1}), glycogen (1025cm^{-1}), phenylalanine (999 cm^{-1}), amide III C-N stretching and N-H bonding (1232 cm^{-1}), CH_3CH_2 wagging mode in purine bases of nucleic acids (1329 cm^{-1}), CH_3 in lipids (1382 cm^{-1}), CH rocking (1392 cm^{-1}) and amide I (1672 cm^{-1}) in the cancer group compared to the borderline group.

There is a negative intensity value at 625, 669, 944, 961, 1156 and 1517 cm^{-1} suggesting lower concentration of carotenoids (1156 & 1517 cm^{-1}), symmetric stretch of phosphate (961 cm^{-1}), C-C stretch of protein (944 cm^{-1}), C-S stretch mode (669 cm^{-1}) and phenylalanine (625 cm^{-1}) in the cancer group compared to the borderline group.

The STDEV line in Figure 36 reduces the number of peaks in the negative intensity peaks to just carotenoids (1156 cm^{-1}), and the positive intensity peaks to phenylalanine, tryptophan, amide III, amide I and lipids.

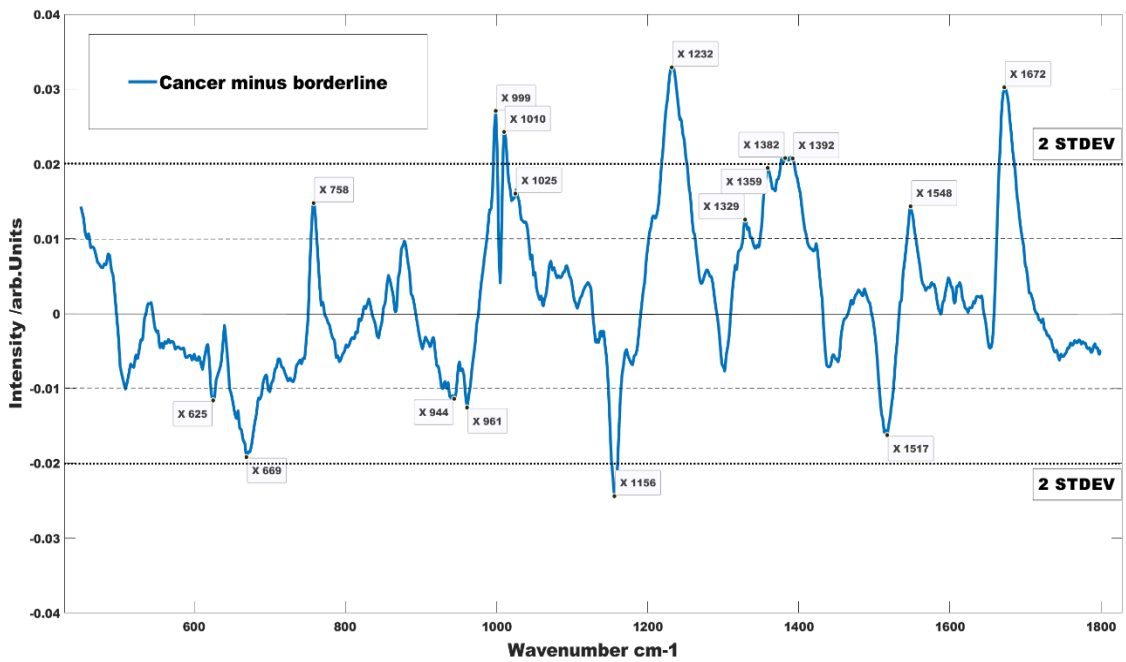


Figure 36 - Subtraction spectrum obtained from subtracting borderline group from cancer group. Positive intensity values suggest increased concentration in the cancer group. Negative intensity values suggest increased concentration in the borderline group. The broken like represents an arbitrary cut off and the dotted line represents two standard deviations above and below the mean. Peaks above these lines have been tentatively assigned. There are higher concentrations of phenylalanine, tryptophan, amide III, amide I and lipids in the cancer group than in the borderline group. There is a higher concentration of carotenoids in the borderline group compared to the cancer group.

Borderline minus benign

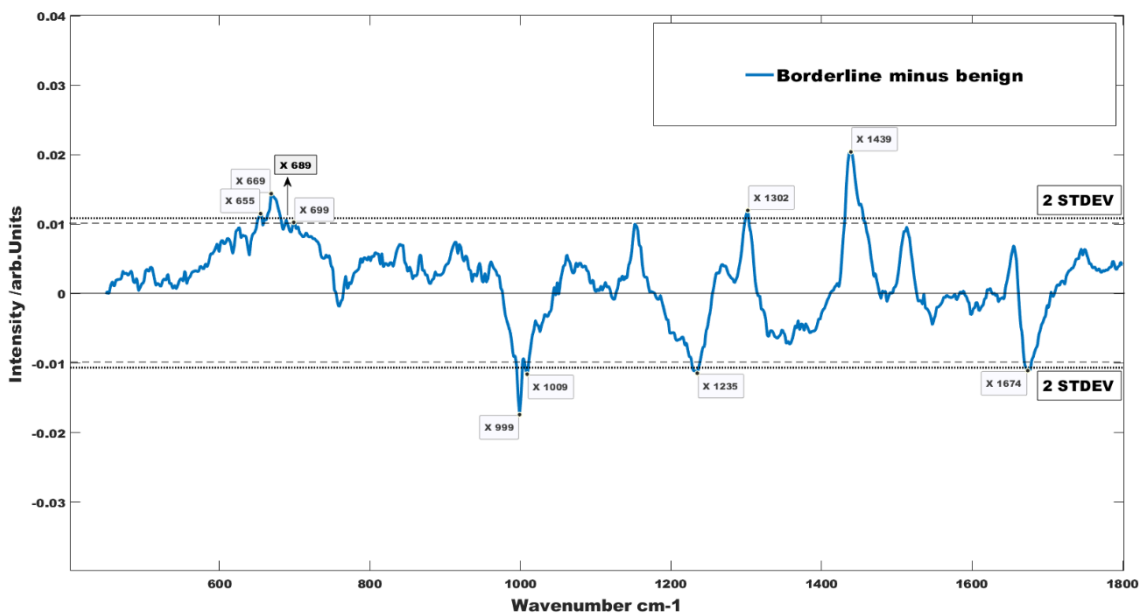


Figure 37 - Subtraction spectrum obtained from subtracting benign group from borderline group. Positive intensity values suggest increased concentration in the cancer group. Negative intensity values suggest increased concentration in the benign group. The broken like represents an arbitrary cut off and the dotted line represents two standard deviations above and below the mean. Peaks above these lines have been tentatively assigned. There are higher concentrations of C-S stretch and lipids in the borderline group than in the benign group. There is a higher concentration of phenylalanine, amide III, and amide I in the benign.

The benign group was subtracted from the borderline group (Figure 37). Using the arbitrary cut off, there is a positive intensity value at 655, 669, 689, 699, 1302 and 1439 cm^{-1} suggesting higher concentrations of unassigned (655, 689 & 699 cm^{-1}), C-S stretch mode (669 cm^{-1}) and lipids (1302 & 1439 cm^{-1}) in the borderline group compared to the benign group.

There is a negative intensity value at 999, 1009, 1235 and 1674 cm^{-1} suggesting lower concentration of phenylalanine (999 & 1009 cm^{-1}), amide III C-N stretching and N-H bonding and amide I in the borderline group compared to the benign group.

The STDEV line in Figure 37 reduces the number of peaks in the positive intensity peaks to C-S stretch and lipids.

	Cancer vs Benign	Cancer vs Borderline	Borderline vs Benign
Increased Concentration	<ul style="list-style-type: none"> - Lipids - Amide III C-N stretch and N-H bonding - CH rocking - Amide I - Tryptophan - $\nu(\text{C-C})$ stretch of hydroxyproline 	<ul style="list-style-type: none"> - Lipids - Amide III C-N stretch and N-H bonding - CH rocking - Amide I - Phenylalanine (999 cm^{-1}) - CH_3CH_2 wagging in purine bases of nucleic acids - Glycogen 	<ul style="list-style-type: none"> - Lipids - C-S stretch mode - Unassigned (655, 689, 699 cm^{-1})
Decreased Concentration	<ul style="list-style-type: none"> • Carotenoids 	<ul style="list-style-type: none"> • Carotenoids • Symmetric stretch of phosphate • C-C stretch of protein • C-S stretch mode • Phenylalanine (625 cm^{-1}) 	<ul style="list-style-type: none"> • Amide III C-N stretch and N-H bonding • Phenylalanine • Amide I

Table 6 - Summary of tentative assignments of prominent peak positions in subtraction spectra of comparison groups. These peaks are deemed prominent using the arbitrary cut off of 0.01 intensity/arb.Units on the subtraction spectra.

Table 6 summarises assignments that can be used to separate the comparison groups based on peak positions and intensities. Based on recurrence across the groups, it can be inferred that benign ovarian pathology can be characterised by higher concentration of carotenoids and cancer can be characterised by a higher concentration of lipids, amide III and I groups. Multivariate analysis has been performed to examine the perceived differences between these groups and their significance.

Multivariate analysis of the three-class group

All the data has been analysed together to look at whether Raman spectroscopy can separate the three classes when looking at all the features within this study population.

22,272 spectra (116 participants) were used for this analysis, 10,368 (54 participants) from the benign group, 3,072 (16 participants) borderline group and 8,832 (46 participants) from the cancer group. The spectra were pre-processed together as discussed earlier in this chapter. Mean centred principal component analysis was performed on this data using the statistics and machine learning toolbox of the MATLAB software. 25 principal components were generated (Figure 38) to describe the data.

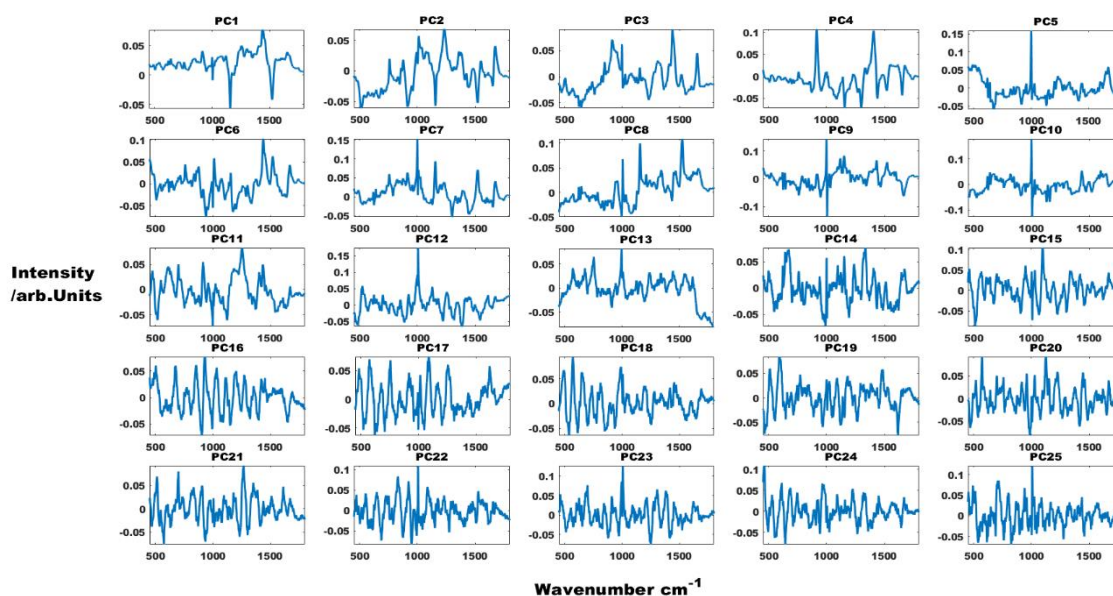


Figure 38 – Twenty-five principal components generated from benign, borderline and cancer spectra. The first principal component is in the top left corner, they continue consecutively to the right on each new line. Each PC is plotted with wavenumber cm^{-1} on the x-axis and intensity on the y-axis. PC 21 and 24 do not meet the confidence level of 99% on analysis of variance.

Analysis of Variance (ANOVA) was used to identify the most significant principal components for differentiating between the three groups. 23 of the 25 PCs achieved greater than 99% significance level of discrimination and were used to build further models. Presented in Table 7 are the results of the linear discriminant analysis (LDA) classification model with sensitivity and specificity as outputs, as well as the results of leave one sample out cross validation of this model for correct classification of each of the pathology groups.

	Sensitivity	Specificity
LDA		
Benign	62%	69%
Borderline	55%	92%
Cancer	67%	82%
Leave one sample out cross validation		
Benign	54%	67%
Borderline	41%	83%
Cancer	60%	78%

Table 7 - Linear discriminant analysis and leave one sample out cross validation results for correct classification of cancer, borderline and benign in a three-class data set.

The groups have been analysed against each other in turn to assess the performance data in two class analysis.

Multivariate analysis of Cancer vs benign

19,200 spectra (100 participants) were used for this analysis, 10,368 (54 participants) from the benign group and 8,832 (46 participants) from the cancer group. The spectra were pre-processed together and mean centred principal component analysis was performed. 25 principal components were generated to describe the data. Of these, 17 reached 99% confidence level on ANOVA for this data set. An LDA model built using these PCs achieved a sensitivity of 69% and specificity of 78% for the cancer group. Figure 39 displays a histogram of the LDA scores. The model was validated using leave one sample out cross validation,

which achieved a sensitivity of 63% and specificity of 72%. The F1 score for this model was 0.64.

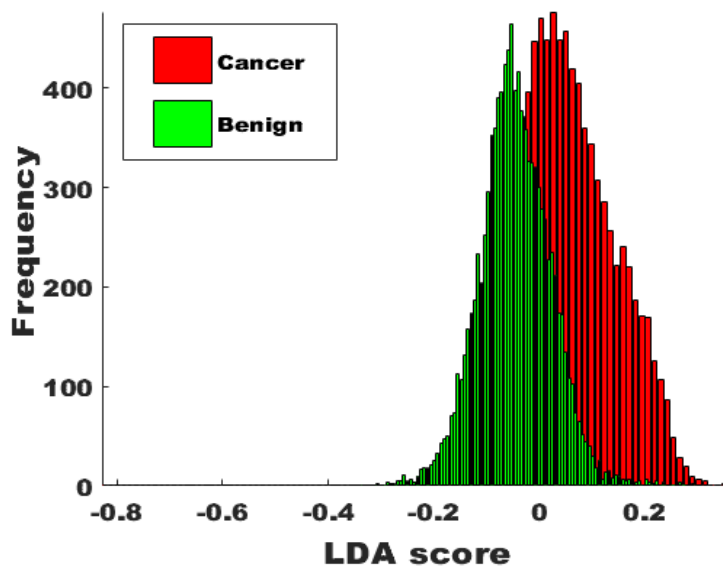


Figure 39 – Histogram plot of linear discriminant scores classifying benign and cancer with sensitivity of 69% and specificity of 78%. The green histogram represents the scores of the benign group and the red histogram represents the scores of the cancer group.

Multivariate analysis of HGS cancer vs Benign

As discussed in chapter 1, epithelial ovarian cancers account for 90% of ovarian cancers. High grade serous cancer (HGS) accounts for 70% of epithelial cancers making it the most common type of ovarian cancer. To explore their influence on the cancer group, spectra from participants with HGS cancer have been compared to the benign group.

15,744 spectra (82 participants) were used for this analysis, 10,368 (54 participants) from the benign group and 5,376 (28 participants) from the HGS cancer group. The spectra were pre-processed together and mean centred principal component analysis was performed. 20 of the 25 principal components generated reached 99% confidence level on ANOVA. They were used to build an LDA model which achieved a sensitivity of 70% and specificity of 85%. The analysis was repeated with leave one sample out cross validation, which achieved a sensitivity of 62% and a specificity of 79%. The F1 score for this model was 0.61.

Multivariate analysis of Cancer vs Borderline

11,904 spectra (62 participants) were used for this analysis, 3,072 (16 participants) from the borderline group and 8,832 (46 participants) from the cancer group. The spectra were pre-processed together and mean centred principal component analysis was performed. 25 principal components were generated to describe the data. Of these, 19 reached 99% confidence level on ANOVA for this data set. An LDA model built (Figure 40) using these PCs achieved a sensitivity of 80% and specificity of 77% for the cancer group. The analysis was repeated with leave one sample out cross validation, which achieved a sensitivity 73% and specificity of 66%. The F1 score for this model was 0.79.

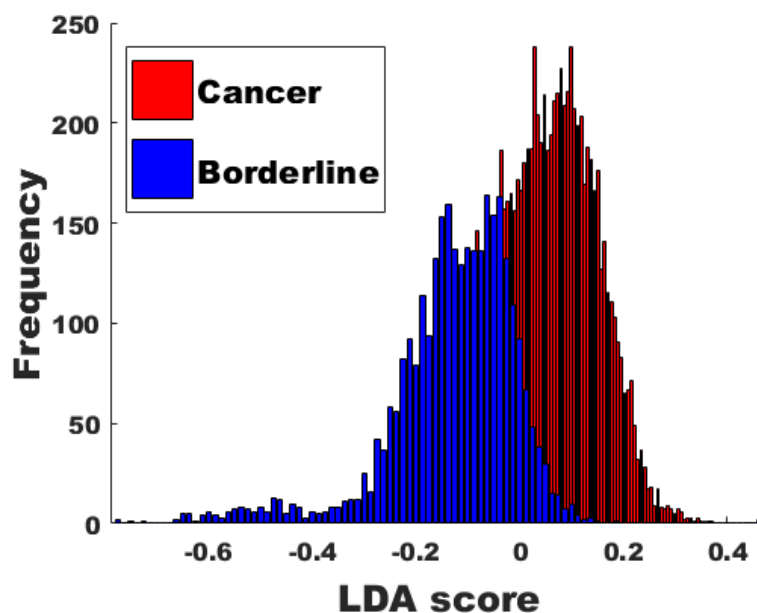


Figure 40 - Histogram plot of linear discriminant scores classifying borderline and cancer with sensitivity of 80% and specificity of 77%. The blue histogram represents the scores of the borderline group and the red histogram represents the scores of the cancer group.

Multivariate analysis of Borderline vs Benign

13,440 spectra (70 participants) were used for this analysis, 10,368 (54 participants) from the benign group and 3,072 (16 participants) from the borderline. The spectra were pre-processed together and mean centred principal component analysis was performed. 25 principal components were generated to describe the data. Of these, 18 reached 99% confidence level on ANOVA for this data set. An LDA model built using these PCs achieved a sensitivity of 68% and specificity of 78% for the cancer group. The analysis was repeated with leave one

sample out cross validation, which achieved a sensitivity of 45% and specificity of 72%. The F1 score was 0.38.

Stage I and II disease

As discussed in chapter 1, CA-125 is negative in half of clinically detectable stage one disease (Scholler and Urban, 2007). To assess the performance of Raman spectroscopy as an early detection tool, spectra from participants with stage I and II ovarian cancer were analysed separately. 6,528 spectra (34 participants) were used for this analysis, 3,264 (17 participants) from the benign group and 3,264 (17 participants) from the cancer group. The spectra were pre-processed together and mean centred principal component analysis was performed. 25 principal components were generated, of which 14 PCs reached 99% confidence level on ANOVA for this data set. An LDA model built using these PCs achieved a sensitivity of 71% and specificity of 70% for the cancer group. The analysis was repeated with leave one sample out cross validation, which achieved a sensitivity of 52%, specificity of 53% and accuracy 0.53. For this dataset, CA-125 alone achieved a sensitivity of 76%, specificity of 47% and accuracy of 0.62

Multivariate analysis of the borderline and cancer spectra from participants with early disease included 6,336 spectra (33 participants) of which 3,072 (16 participants) were from the borderline group and 3,264 (17 participants), the cancer group. After pre-processing and PCA analysis, 15 PCs reached 99% confidence level on ANOVA. An LDA model built using these PCs achieved a sensitivity of 77% and specificity of 74% for the cancer group. The analysis was repeated with leave one sample out cross validation, which achieved a sensitivity of 63%, specificity of 65% and accuracy 0.64. CA-125 achieved a sensitivity of 76%, specificity of 38% and accuracy of 0.58.

3.6 Summary of results

The biochemical composition of plasma changes with cancer, distinguishable by an increase in lipids and amino acids and a decrease in carotenoid concentrations. PCA-LDA model for the classification of ovarian cancer in all women who present with symptoms of ovarian cancer (study population)

achieved a sensitivity of 67% and specificity of 82%. Leave one sample out cross validation of this model achieved a sensitivity of 60% and specificity of 78%. Two class models for cancer classification achieved subtle changes in the PCA-LDA model sensitivities but did not have a notable impact on cross validation outcomes. In stage I and II disease, Raman spectroscopy had better accuracy for cancer detection in cancer and borderline datasets but did not achieve the comparable accuracy in cancer and benign datasets.

3.7 Discussion

This work set out to evaluate Raman spectroscopy for identification of novel plasma markers for ovarian cancer detection and to assess their diagnostic performance.

The results highlight a biochemical difference in plasma of patients with Ovarian cancer, identifiable by Raman spectroscopy, of the concentrations of amino acids, lipids and carotenoids. This upregulation of lipids and amino acids has been reported in other work looking at metabolic changes in other cancers, with increased plasma lipid reported in hepatocellular carcinoma, prostate cancer, lymphoma and lymphoblastic leukaemia (JeongLee and Chun, 2021). Amino acids have been reported to support cancer cell growth and protein synthesis (Li and Zhang, 2016), with some amino acids such as proline (noted to be increased in cancer in this work) associated with aggressive cancer phenotypes and poor prognosis due to the negative effects of increased proline concentrations on cell behaviour (Togashi et al., 2014, D'Aniello et al., 2020). Lower concentrations of carotenoids seen in the cancer group are consistent with literature which has suggested that higher exposure to carotenoids is associated with lower risk of ovarian cancer (Cramer et al., 2001), as well as higher plasma concentrations inferring some protection in ovarian cancer risk (Jeong et al., 2009). Similar observations were discussed in a recent review by Udensi and colleagues for breast, colorectal and oral cancers, including using Raman spectroscopy to measure carotenoids in these cancers, where carotenoids were described as a prominent feature amongst other biomolecular features and were not used on their own to predict cancer. Carotenoids have not been examined on their own as a plasma cancer biomarker (Udensi et al., 2022).

This study was able to demonstrate the ability of Raman spectroscopy to classify cancer in plasma with a cross validation F1 score of 0.62. When compared to the serum test currently used for cancer detection, CA-125, this technique was able to achieve the same specificity for cancer detection as is published for CA-125, 78% versus 77.9% (95% CI, 73.2–82.0%) however the sensitivity performance was lower for this work, 60% vs 78.7% (95% CI, 75.3–81.7%) (Dodge et al., 2012). When compared to the two previous studies on Raman spectroscopy in ovarian cancer with clear diagnostic modelling, the work by Giamougiannis and colleagues which used PCA-LDA models to achieve a sensitivity and specificity of 56% and 73%, was closer to the results seen in this work than 94% and 96% seen in the work by Paraskevaïdi and colleagues. There are some differences between this work and the latter that might account for the different accuracies (Giamougiannis et al., 2021a, Paraskevaïdi et al., 2018). Firstly, this work compared patients with ovarian pathology or symptoms suggestive of ovarian cancer, resulting in a more diverse benign group with more challenging biochemistry than would be seen with the women with prolapse that form the comparative group in the Paraskevaïdi study. Secondly, a different modelling technique, Gaussian kernel support vector machines was used by Paraskeveidi and colleagues. Applying the same technique as described in their work to my data, the model achieves a sensitivity and specificity of 90% and 94%, area under the curve of 0.98 and F1 score of 0.9 for detecting cancer. Whilst SVM is easy to use and can be effective with small sample sizes, it can be prone to overfitting when data cannot be easily separated by the line (hyperplane), thus requiring non-linear (Kernel trick) approaches. In clinical applications of Raman spectroscopy, it is expected that data will be complex due to the range of pathologies that come under the umbrellas of benign and cancer and in some cases, as seen in this work, multiclass analysis is required. This is the reason for the use of PCA-LDA modelling in this work. With that said, the performance of the SVM model with the data from this work is comparable to the work by Paraskevaïdi and colleagues and better than the published performance of CA-125 alone. CA-125 performance for patients participating in this study was sensitivity and specificity of 89% and 57% and F1 score of 0.7. Whilst the SVM model and specificity of the PCA-LDA model outperform this, the PCA-LDA model sensitivity does not quite reach this result (Raman Spectroscopy 60% vs CA-125 89%). The CA-125 performance in this work is also higher than previously

published meta-analysis for CA-125, 78.7% (95% CI, 75.3–81.7%) (Dodge et al., 2012) but this is expected as all the women participating in this study had been referred with suspected ovarian pathology and part of decision making model for the referral is a positive CA-125. This introduces an element of bias and would explain the higher than expected sensitivity of CA-125 in this group of carefully selected women. Isolation of the early cancers (stage I and II) saw a lower performance of CA-125 when comparing cancer to benign however this still outdid the cross-validation accuracy of Raman spectroscopy (0.62 vs 0.53). Whilst a mortality reduction was not demonstrated in the UKCTOCS study, an increase in the incidence of early cancers was seen (Menon et al., 2021). This suggests that a multimodal approach for early detection is the best way forward. Human epididymis 4 (HE4), a tumour marker that has been associated with ovarian cancer, did not demonstrate any added value when used alongside CA-125 and ultrasound characteristics in a multimodal approach for ovarian cancer diagnosis in a cohort of women from the UKCTOCS trial (Gentry-Maharaj et al., 2020). Whilst the accuracy of Raman spectroscopy is not as expected for cancer detection from benign, it is uncertain whether use in conjunction with age, CA-125 and ultrasound markers could augment care pathways and this an area of interest for further review. At this stage I would be cautious about considering Raman spectroscopy as a replacement for CA-125 in a multimodal test.

This is the first work to compare the plasma of patients with borderline ovarian tumours and ovarian cancer in this way. Despite the smaller participant numbers in the borderline group and some overlap in the biochemistry in these two groups as demonstrated in Table 6, the prediction model achieved an F1 score of 0.79 for cancer detection compared to borderline cancer. A more balanced comparison group of early cancers and borderline tumours achieved a cross-validation accuracy of 0.64 compared to 0.56 for CA-125. If successfully translated into clinical practice, there could be a role for this model in deciding mode of surgery for patients with complex pelvic masses of unknown malignant potential. Patients with potentially early stage borderline tumours by radiological description and low probability of cancer according to this test could potentially have laparoscopic surgery instead of a laparotomy. As discussed in chapter 1, investigations and extensive treatment for suspected ovarian cancer is associated with complications (Buys et al., 2011). Combined with ultrasound

description of the mass, there is potential for a powerful mode of surgery decision tool and further research is needed to develop this hypothesis.

Chapter 4 – Raman spectroscopy of ovarian and peritoneal tissue

4.1 Introduction

As discussed in chapter 1, optimal cytoreduction remains the best surgical outcome for improving disease free survival however the intraoperative assessment of residual disease remains subjective. Raman spectroscopy has been able to discriminate between cancer and benign tissue with high accuracies in breast and oesophageal cancer (Kallaway et al., 2013). The only study applying Raman spectroscopy to ovarian cancer also achieved high accuracies with a total sample number of 15 (Maheedhar et al., 2008). This chapter describes the tissue specific results of study recruitment, Raman spectral measurements, analysis, and discussion.

4.2 Aims

This study aims to assess Raman Spectroscopy against histology for its ability to detect cancer in peritoneal and ovarian tissue from carefully characterised patients and evaluate the effect of chemotherapy on the ability of Raman spectroscopy to detect cancer in this group.

To do this, this work will:

- assess the discriminatory ability of Raman spectroscopy in assigning benign, borderline and cancer spectra taken from fresh frozen tissue.
- build and test predictive models for the discrimination between cancer and benign.
- test predictive ability against spectra taken from chemotherapy treated fresh frozen tissue.

4.3 Methods

The clinical protocol describing participant recruitment, inclusion and exclusion criteria, timings and method of tissue collection are described in chapter 2 section 2.2 and 2.3 (page 63).

The processing of the tissue and preparation for Raman spectroscopy instrumentation, set up and measurement protocols are also described in section 2.6 (page 71).

4.4 Results

The overall study recruitment outcomes are detailed in chapter 3, section 3.4. This chapter describes the tissue specific results of study recruitment, Raman spectral measurements, analysis and discussion.

4.5 Tissue recruitment outcomes

As described in detail in section 3.4, ovarian and/or peritoneal samples were collected from 73 participants. 20 participants had benign ovarian pathology, 11 borderline tumours and 42 ovarian cancers. The mean age in this cohort was 57 years in the benign group, 55 years in the borderline and 62 years in the cancer group. Most of the participants were post-menopausal across all three groups, accounting for 83% of the participants and non-smokers (never smoked and ex-smokers) accounted for 90% of participants. Just over half of the participants had more than two comorbidities, with the highest medical disease burden seen in the cancer group (Figure 41).

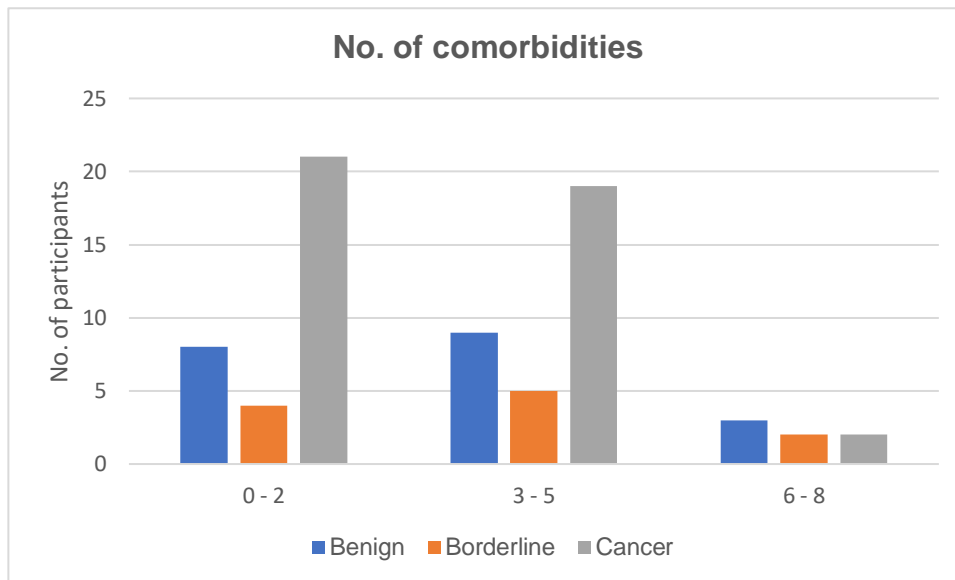


Figure 41 - Number of comorbidities. This figure illustrates the distribution of comorbidities within the benign (blue), borderline (orange) and cancer (grey) groups. The majority of the groups had more than two comorbidities and the cancer group had the highest disease burden.

4.5.1 Benign group

Mucinous and serous cysts accounted for two thirds of benign ovarian pathology in this cohort. The remaining benign ovarian pathology included three participants with fibromas and, one participant each with mature teratoma, endometriosis, strum ovarii and benign cyst demonstrating small vessel vasculitis.

4.5.2 Borderline group

Excluding the participant that had a torted borderline tumour, all participants of this group had stage 1 disease. 5/11 (45%) had mucinous borderline tumours and 5/11 (45%) had serous borderline tumours.

4.5.3 Cancer group

Ovarian cancer types in this group were predominantly high grade serous cancer which accounted for 73% cancers. The remaining 27% comprised of 4/42 low grade serous (10%), 2/42 mucinous (5%), 3/42 clear cell (7%), and 1/42 each of endometroid, sex cord and granulosa cell tumours (7%).

4.5.4 Prior treatments, type of tissue available for analysis and point of collection

27 participants (8 stage III and all stage IV) received neo-adjuvant chemotherapy. Ovarian and/or peritoneal samples were collected at interval debulking surgery depending on the surgeons assessment. The remaining 15 participants had upfront surgery, at which their ovary and peritoneal samples were collected.

Both peritoneal and ovarian samples were collected from 40 of the 73 participants, peritoneal samples only from 23 participants and ovarian samples only from 12 participants.

For the ovarian group, the only ovarian samples from 2/52 participant were excluded; one was damaged (part of tissue missing from the slide), and tissue morphology was obscured by blood in the other. There were a further 11/52 participants whose only ovarian tissue contribution could not be included as the sample was not representative of their diagnosis. Eight had ovarian cancer but their samples did not have cancer and three had borderline ovarian tumours but their samples did not have any tumour. Spectra from ovarian tissue were collected from the remaining 39 participants.

In the peritoneal group, the only peritoneal samples from 7/63 participants were excluded; five were too small to measure using the Raman measurement protocol, one had been through too many freeze thaw cycles in establishing the measurement protocol and one was damaged (part of tissue missing from slide). There were a further 24/63 participants whose only peritoneal tissue contribution was not representative of their diagnosis. 16 had cancer but their samples did not have cancer and eight had borderline tumours, but their samples did not. These samples were still measured, and some are used as a separate comparative group (bIDS) which will be discussed in section 4.6.2 however their absence from the main comparative groups is reflected in the small sample numbers. Spectra from peritoneal tissue were collected from the remaining 34 participants to form the main comparative groups.

Where there was more than one tissue block of the same tissue type, with the same pathology from one participant, only one slide was measured, meaning there was only one contribution per pathology type per tissue type per participant.

4.6 Raman spectroscopy tissue results and analysis

The protocol for tissue collection and sectioning for Raman spectroscopy is described in chapter 2.

Raman spectra were obtained using the Renishaw InVia spectrometer (Renishaw, Wotton-Under-Edge, United Kingdom) and 830nm laser, using a 600 lines/mm grating.

As discussed in chapter 2, the defrosted ovarian and peritoneal tissue samples were scanned using the white light map function of the Raman InVia spectrometer. This generated a rendering of the fresh frozen tissue, an example of which is demonstrated in Figure 42. All the corresponding H&E slides were assessed, with areas of significant pathology marked, by a consultant pathologist from Severn Pathology services, North Bristol NHS Trust. The Raman white light image was compared to the corresponding H&E slide and the marked area which represented the area of interest was then chosen to be measured by Raman spectroscopy.

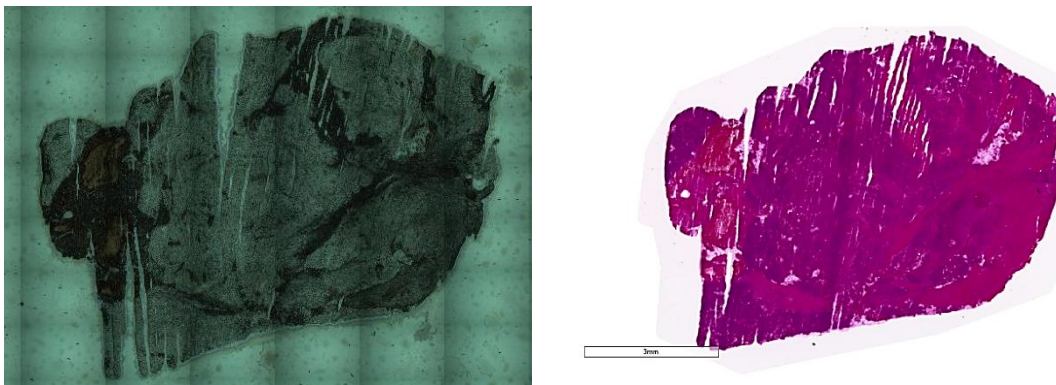


Figure 42 - White light map image of fresh frozen ovarian tissue. This figure demonstrates the relative appearances of the Raman map of ovarian tissue (left) and the H&E appearance of the same tissue (right).

Measurements

The tissue was exposed to the laser for a total acquisition time of 15 seconds, comprising of three accumulations of five seconds exposure to enable automated rejection of cosmic rays. Measurements were taken from a square grid of 300 microns per side, in 50-micron steps resulting in 49 spectra per measurement. The area of grid placement was determined using the shape and prominent architecture of areas of equivalence on comparison of the two images.

Pre-processing

As the area of interest in Raman spectroscopy is the fingerprint region, spectra were truncated, leaving the wavenumber region of 450 to 1800 cm^{-1} .

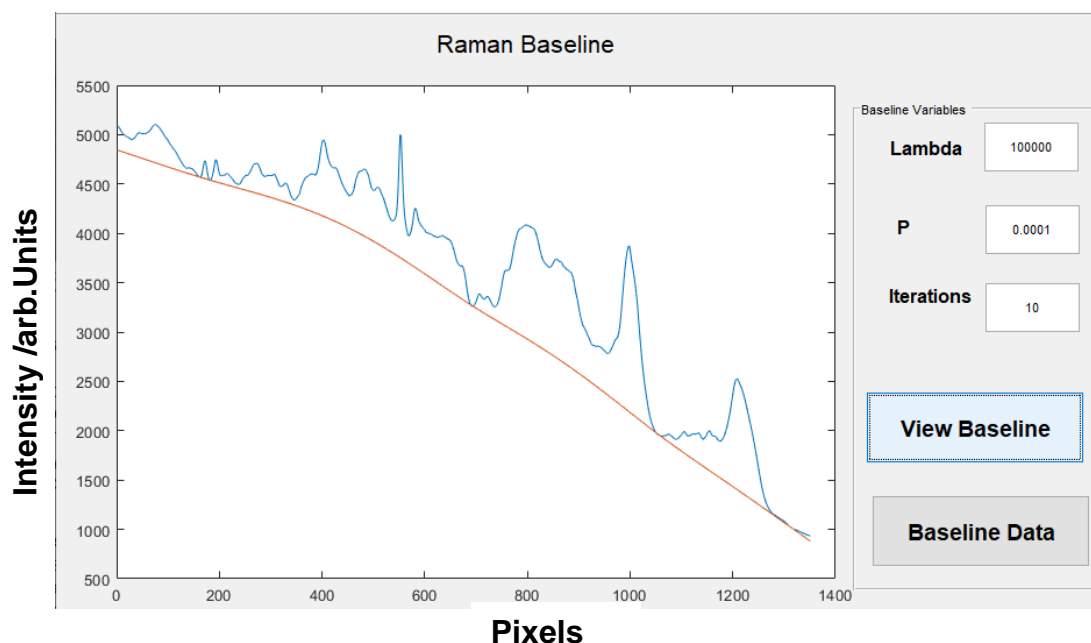


Figure 43 - Baseline subtraction. This figure is an image of the graphical user interface used to change the baseline of the data. Each spectrum has its baseline subtracted separately however the same variables are used for all spectra in the data. In this figure, the spectrum (blue) can be seen with a red line (Baseline, underneath it).

Due to the nature of the sample, fluorescence contributions and saturation of the CCD was noted on occasion. Fluorescence and saturation spectra were therefore replaced with the mean of the spectra before and after or two spectra before or two spectra after, being careful not to use spectra from a different sample or participant.

To reduce variations in intensity and background, a background subtraction step has been completed using a graphical user interface within MATLAB software to visualise data when changing the baseline variables. Figure 43 demonstrates the baseline subtraction used for this data.

Large differences in signal intensity, not inherent to the molecular differences in the tissue can occur such as variations in signal output of the apparatus on different measurement days and changes in objective focus between samples. To avoid differences in pathology groups being falsely attributed to these intensity differences, a normalisation step has been completed to scale the values of the intensity of each collected spectrum to the range of zero to one.

4.6.1 Ovarian Tissue

Peak Positions and Intensity

There was one tissue sample from each of the 18 participants in the benign group, 8 in the borderline group and 13 in the cancer group. Within the cancer subgroup, 2 samples were from interval debulking surgery (IDS) and 11 were from primary surgery. Following the preprocessing steps of baseline subtraction and normalisation, the mean spectrum of each pathology group was generated using all spectra collected for that pathology group (i.e., mean of 49 x number of participants in the group) to ensure that contributions from different subtypes within the groups are seen. The spectrum for benign ovarian pathology (Figure 44), ovarian cancer (Figure 45) and borderline ovarian tumours (Figure 46) have been plotted to determine the common prominent peaks seen in Raman spectroscopy of the ovary. The figure has been annotated with the wavenumbers of the prominent peak positions. Tentative assignments of these peaks have been made for this work (Appendix H: Tentative peak assignment reference table) using reference tables (Stone, 2001, Kendall, 2002) chosen after a search of the literature for previous work done on similar tissue types.

The three pathology groups are shown together in Figure 47. There are areas with very prominent differences in peak height such as seen at wavenumbers 851cm^{-1} , 931cm^{-1} , 1247cm^{-1} and 1336cm^{-1} . There are also some subtle changes which might be best demonstrated by looking at the image generated by subtracting one pathology group from the other.

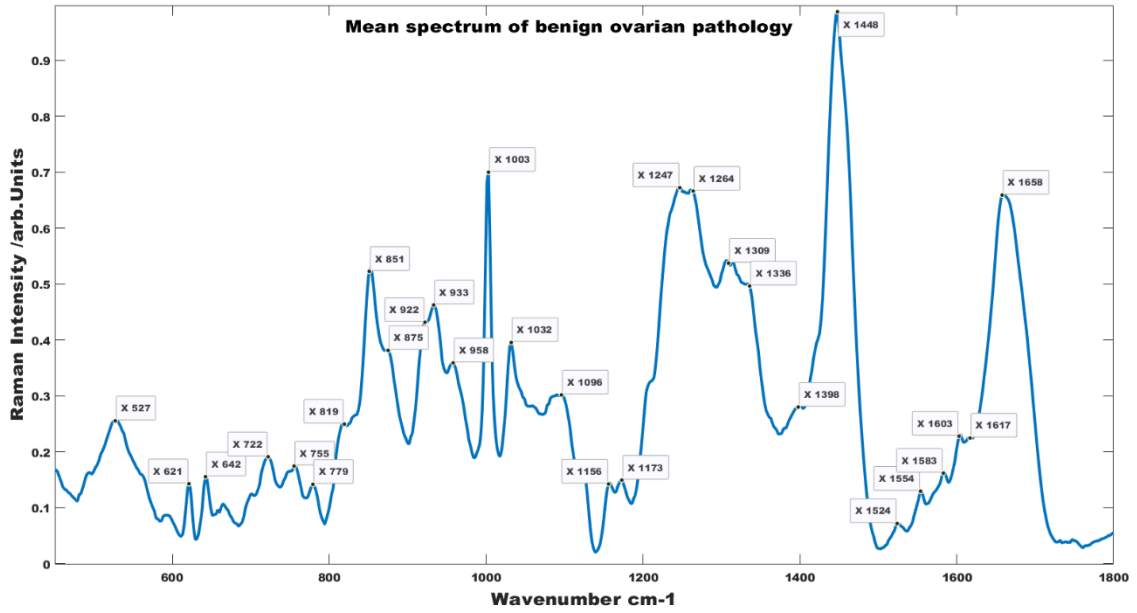


Figure 44 - Mean spectra of benign ovarian pathology. In this figure, the mean of benign ovarian pathology spectra, generated from all 18 participants in the benign group, has been plotted and annotated with the wavenumber of the prominent peaks seen in this spectrum. Tentative assignments of these peaks are seen in Appendix H: Tentative peak assignment reference table.

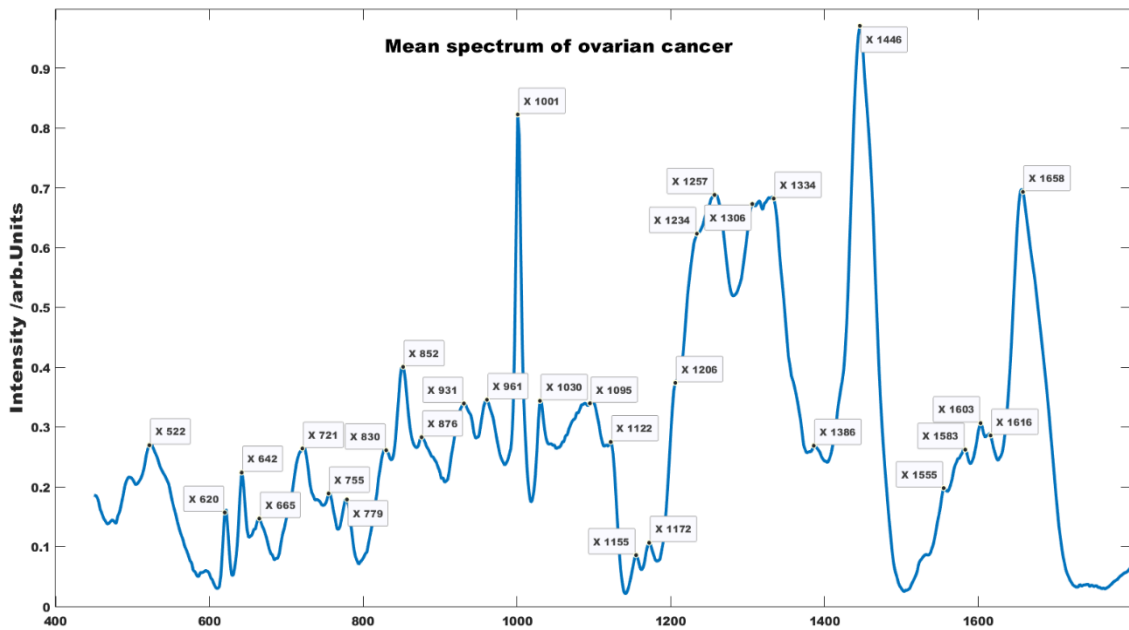


Figure 45 – Mean spectrum of ovarian cancer. In this figure, the mean of ovarian cancer spectra, generated from the 11 participants in the upfront surgery cancer group, has been plotted and annotated with the wavenumber of the prominent peaks seen in this spectrum. Tentative assignments of these peaks are seen in Appendix H: Tentative peak assignment reference table.

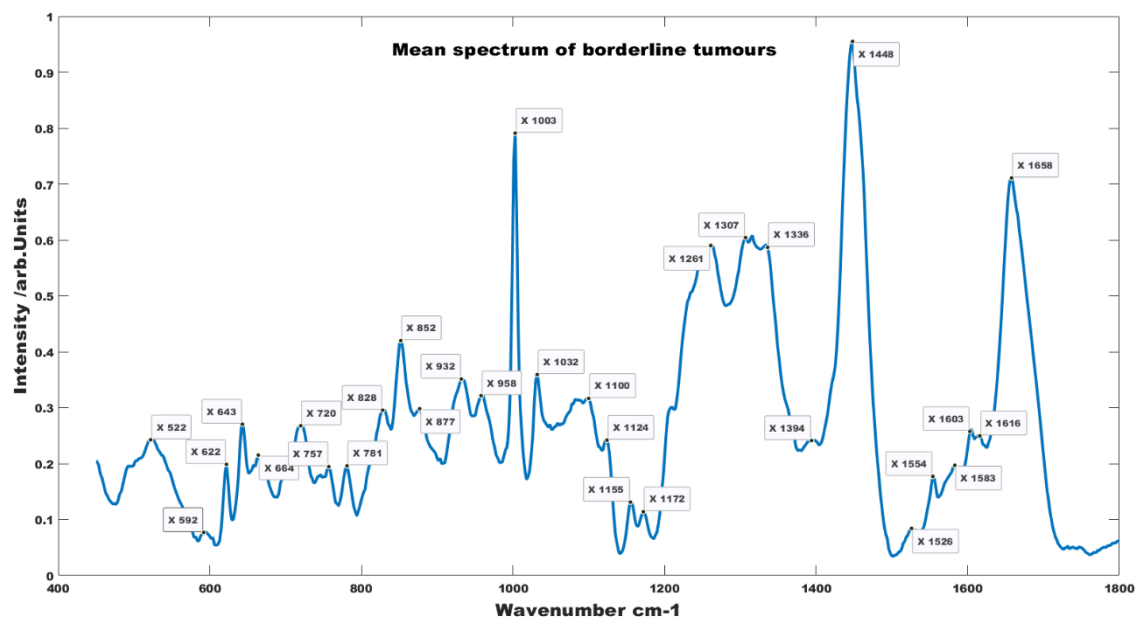


Figure 46 - Mean spectrum of borderline tumours. In this figure, the mean of borderline tumour spectra, generated from all 8 participants in the borderline group, has been plotted and annotated with the wavenumber of the prominent peaks seen in this spectrum. Tentative assignments of these peaks are seen in Appendix H: Tentative peak assignment reference table.

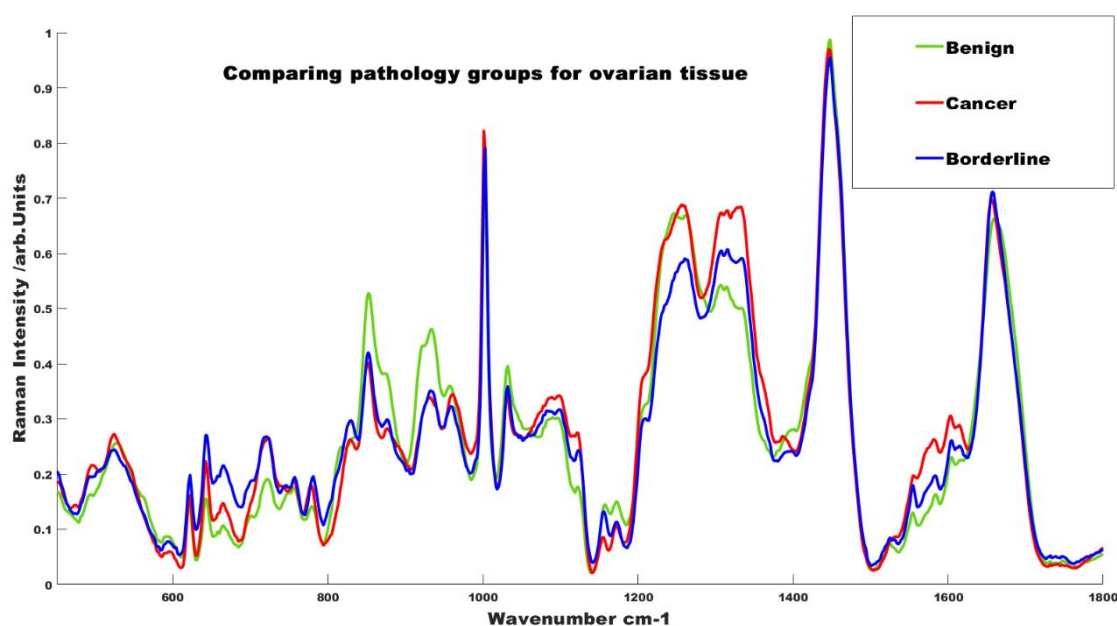


Figure 47 - Mean spectra of ovarian tissue of all pathology groups. In this figure, the green spectrum represents benign ovarian pathology, the blue spectrum represents borderline ovarian pathology, and the red spectrum represents cancer taken at upfront surgery. There are wavenumber regions with obvious differences in the groups such as seen at 851 cm^{-1} , 931 cm^{-1} , 1247 cm^{-1} and 1336 cm^{-1} and some more subtle areas with changes seen in only or two of the groups.

Difference between the mean

The benign group was subtracted from the cancer (upfront surgery) group to demonstrate the differences between the two groups (Figure 48). The subtraction spectrum reveals a positive intensity value at wavenumbers 497, 520, 545, 642, 663, 711, 724, 777, 1001, 1074, 1119, 1205, 1218, 1256, 1332, 1438, 1573 and 1652 cm^{-1} suggesting higher concentration in the cancer group of, glycogen and glucose (497 & 520 cm^{-1}), lipids (545, 1074, 1119 & 1438 cm^{-1}), amino acids (642, 1001 & 1205 cm^{-1}), nucleotides (663, 711, 724, 777, 1256, 1332 & 1573 cm^{-1}) and amide I groups (1652 cm^{-1}) compared to the benign group. There was a negative intensity value at wavenumbers 563, 591, 812, 856, 919, 935, 1035, 1159, 1176, 1240, 1276, 1400, 1415, 1465, 1635 and 1689 cm^{-1} suggesting lower concentrations in the cancer group of phosphate minerals (591 cm^{-1}), collagen (812, 856, 919 & 935 cm^{-1}), amino acids (1035 & 1176 cm^{-1}), carotenoids (1159 cm^{-1}), amide III groups (1240 & 1276 cm^{-1}), CH_3 modes in proteins (1400 & 1415 cm^{-1}) and deoxyribose (1465 cm^{-1}) compared to the benign group.

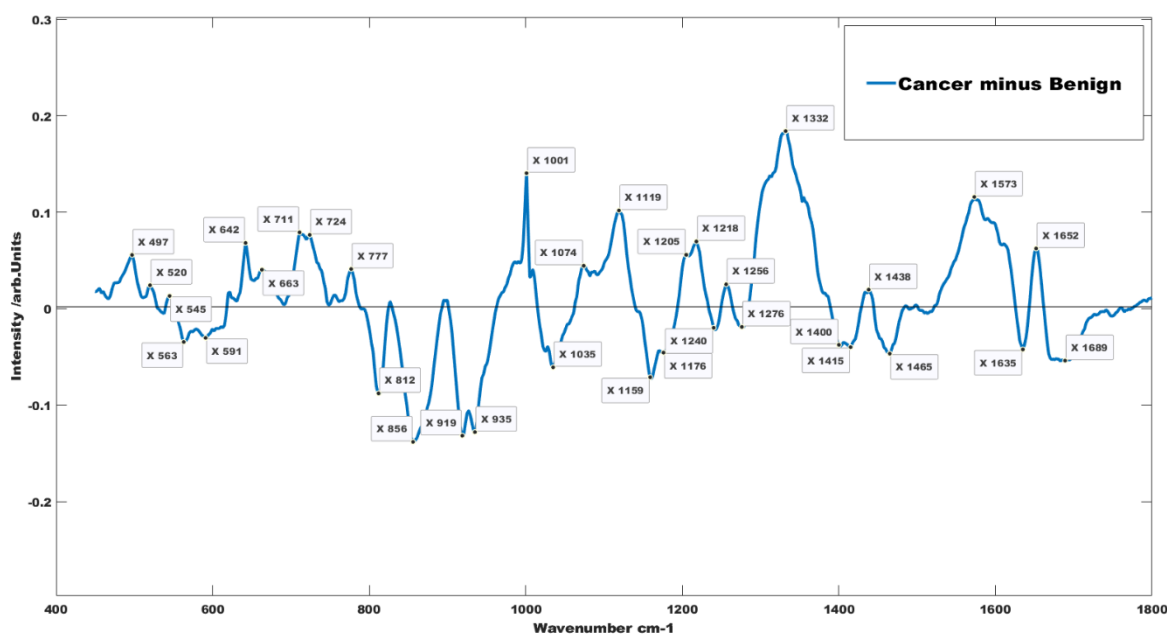


Figure 48 – Subtraction spectrum obtained from subtracting benign from cancer. Positive intensity values suggest increased concentration in the cancer group. Negative intensity values suggest increased concentrations in the benign group. There is increased glycogen, lipids, amino acids, nucleotides, and amide I groups in cancer compared benign. There are lower concentrations of phosphate minerals, collagen, carotenoids, amide III, CH_3 modes in proteins and deoxyribose in the cancer group compared to the benign group.

The borderline group was also subtracted from the cancer (upfront surgery) group (Figure 49). The subtraction spectrum reveals a positive intensity value at wavenumbers 496, 522, 892, 912, 972, 1000, 1069, 1095, 1118, 1220, 1255, 1327, 1360, 1386, 1442, 1573, 1597 and 1650 cm^{-1} suggesting higher concentration in the cancer group of glycogen and glucose (496 & 522 cm^{-1}), phosphates (1069 & 1095 cm^{-1}), collagen (892 cm^{-1}), ribose (912 cm^{-1}), amino acids (1000, 1360 & 1597 cm^{-1}), lipids (1118, 1442 cm^{-1}), cytosine (1255 cm^{-1}), nucleic acids (1327, & 1573 cm^{-1}), CH_3 bending mode (1386 cm^{-1}) and amide I (1650 cm^{-1}) compared to the borderline group. There was a negative intensity value at wavenumbers 647-690, 787, 807, 831, 861, 936, 1005, 1034, 1137, 1158, 1176, 1464, 1519, 1667 cm^{-1} suggesting lower concentrations in the cancer group of thymine and guanine (broad peak 647-690 cm^{-1}), DNA (807 & 831 cm^{-1}), amino acids (1005, 1034 & 1176 cm^{-1}), collagen (861 & 936 cm^{-1}), carotenoids (1519 & 1158 cm^{-1}), deoxy-ribose (1464 cm^{-1}) and amide I group (1667) compared to the borderline group.

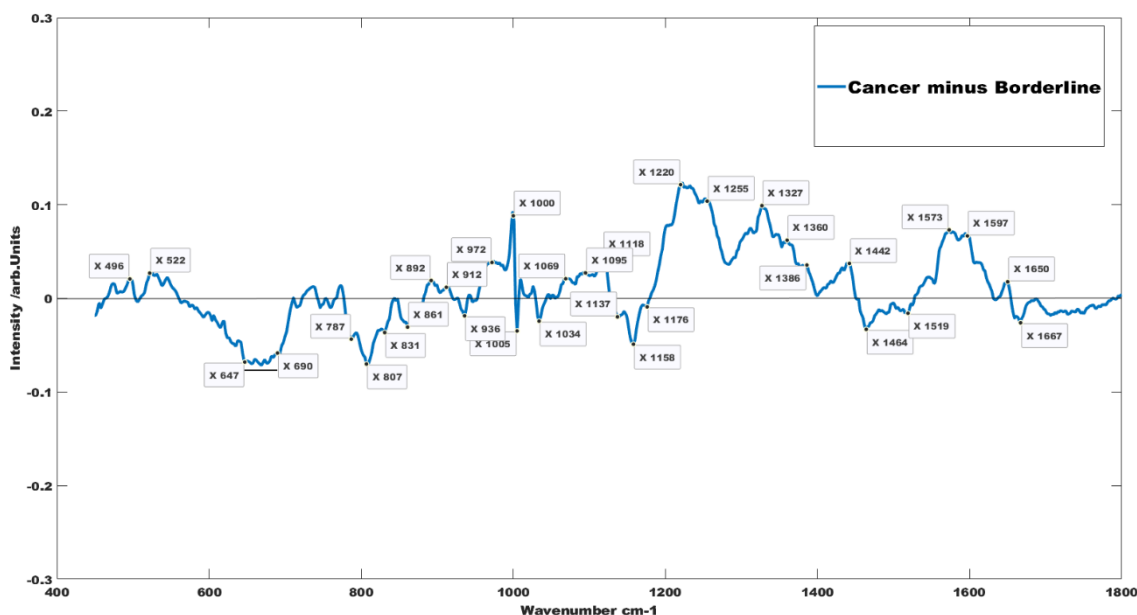


Figure 49 – Subtraction spectrum obtained from subtracting borderline from cancer. Positive intensity values suggest increased concentration in the cancer group. Negative values suggest higher concentrations in the borderline group. There is increased glycogen, phosphates, collagen, ribose, amino acids, lipids, cytosine, nucleic acids, CH_3 bending modes and amide I in the cancer group compared to the benign. There are lower levels of thymine, guanine, DNA, amino acids, collagen, carotenoids, deoxyribose, and amide I group in the cancer group compared to the borderline group.

To evaluate the differences in the two non-cancer groups, benign group was subtracted from the borderline group (Figure 50). The subtraction spectrum reveals a positive intensity value at wavenumbers 497, 643, 666, 716, 981, 827, 1003, 1074, 1127, 1336, 1555, 1576 & 1655 cm^{-1} suggesting higher concentration in the borderline group of glycogen (497 cm^{-1}), amino acids (643, 1003 & 1555 cm^{-1}), nucleotides (666, 716, 981, 1336 & 1576 cm^{-1}), DNA (827 cm^{-1}), lipids (1074 & 1127 cm^{-1}) and amide I (1655 cm^{-1}) compared to the benign group. There was a negative intensity value at wavenumbers 532, 565, 814, 855, 918, 935, 1026, 1040, 1242, 1415, 1635 and 1690 cm^{-1} suggesting lower concentrations of disulphide stretch in proteins (532 cm^{-1}), collagen (814, 855, 918 & 935 cm^{-1}), amino acids (1026 & 1040 cm^{-1}), amide III group (1242 cm^{-1}), CH₃ deformation (1415 cm^{-1}) and amide I group (1635 & 1690 cm^{-1}) compared to benign group.

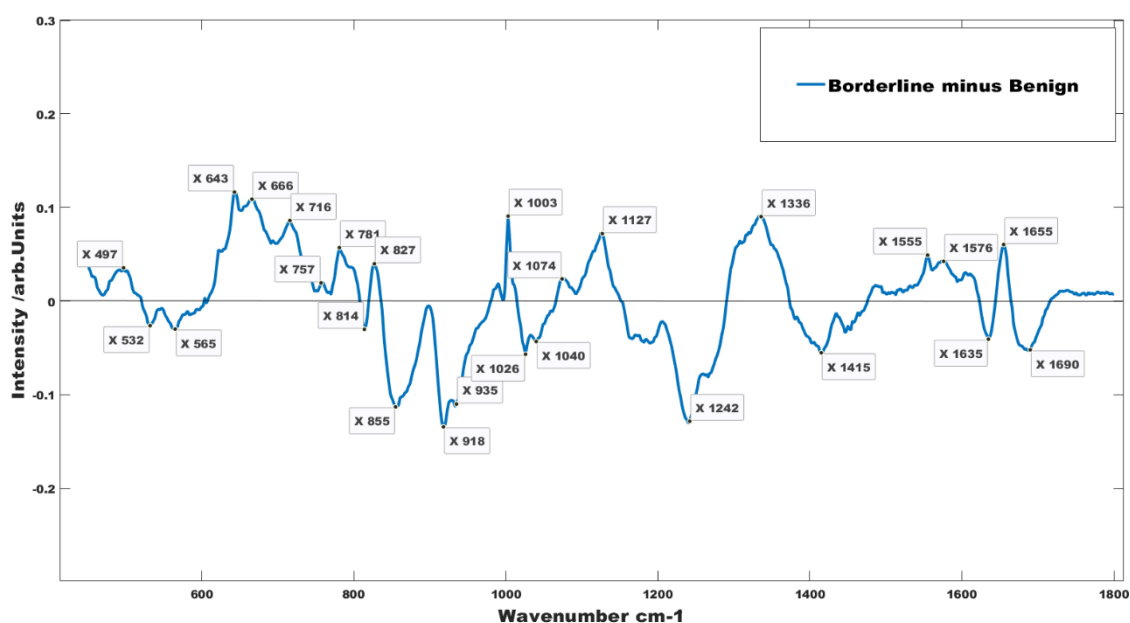


Figure 50 – Subtraction spectrum obtained by subtracting benign from borderline. Positive intensity values suggest increased concentration in the borderline group. Negative values suggest higher concentrations in the benign group. There is increased glycogen, amino acids, lipids, DNA, nucleotides, and amide I in the borderline group compared to the benign. There are lower levels of disulphide stretch in proteins, amino acids, collagen, amide III, CH₃ deformation and amide I group in the borderline group compared to the benign group.

The same intensity range has been used for all three subtraction spectra. It is noticeable that the intensity difference between the groups is less obvious in the cancer minus borderline group than the other two comparison groups. There are also more assignments in different forms and vibrational modes in this comparison group than there are in the cancer/benign and borderline/benign groups. Table 8 summarises assignments that can be used to separate the comparison groups based on peak intensities. For this purpose, assignments that appear on both sides in different modes have been excluded such as in the borderline vs benign group where phenylalanine appears in the positive influence at 1003 cm^{-1} (breathing mode) and in the negative influence at 1040 cm^{-1} .

Based on the distributions of assignments in Table 8 there is increased glycogen lipids and nucleotide bases in cancer and borderline ovarian tissue and increased collagen and carotenoids in benign tissue. This is consistent with the increased metabolic and nuclear activity and destruction of cellular architecture seen in varying amounts in cancer and borderline disease. Carotenoids are antioxidants and as such are an unsurprising feature to be seen alongside higher concentrations of collagen in benign ovarian tissue.

The remaining assignments in Table 8 do not appear as consistently in either group as the aforementioned assignments. It should be remembered that these changes represent differences in intensity at the same wavenumbers between the two groups. To explore this further, multivariate analysis techniques have been used to determine the statistically significant features of this data and whether they can be used to reliably classify the data into their pathology groups.

	Cancer vs Benign	Cancer vs Borderline	Borderline vs Benign
Increased Concentration	<ul style="list-style-type: none"> - Glycogen - Lipids - Nucleotide bases: <i>Thymine</i> <i>Adenine</i> <i>Cytosine</i> <i>Uracil</i> <i>Guanine</i> - Amide I 	<ul style="list-style-type: none"> - Glycogen - Lipids - Nucleotide bases: <i>Cytosine</i> <i>Adenine</i> - Nucleic acid ring vibrations - Amide I alpha helix - Amino acids: <i>Tryptophan</i> - Phosphates - Collagen - CH₂ rocking. - Ribose - CH₃ bending modes. 	<ul style="list-style-type: none"> - Glycogen - Lipids - Nucleotide bases: <i>Thymine</i> <i>Adenine</i> <i>Guanine</i> - DNA - Amino acids: <i>Tyrosine</i> <i>Tryptophan</i>
Decreased Concentration	<ul style="list-style-type: none"> • Collagen • Carotenoids • Phosphate minerals • Amide 3 beta-sheet and alpha helix secondary protein structures. • CH₃ modes in proteins. • Deoxyribose 	<ul style="list-style-type: none"> • Collagen: <i>hydroxyproline</i> • Carotenoids • Thymine • Amide I: <i>C=O stretch</i> • DNA • Deoxyribose 	<ul style="list-style-type: none"> • Collagen • Disulphide stretch in proteins. • Amide III beta-sheet protein secondary structure • CH₃ deformation

Table 8 - Summary of tentative assignments of prominent peak positions in subtraction spectra of comparison groups. For the purposes of this comparison table, assignments that appear in varying modes in both positive (increased concentration) and negative (decreased concentration) intensities have been excluded.

Multivariate analysis of Cancer vs Benign pathology groups

To assess the discriminatory ability of Raman spectroscopy in assigning cancer and benign, 1,421 spectra were used for analysed: 882 (18 participants) from benign ovarian pathology and 539 (11 participants) from ovarian cancer. One spectrum was replaced due to saturation and the combined data set of spectra were pre-processed together as discussed earlier in this chapter. Mean centred principal component analysis (PCA) was performed on this data set using the statistics and machine learning toolbox of the MATLAB software. 25 principal components (PC) were generated however 90% of the data can be described by the first 10 PCs (Figure 51). (Figure 52) displays all 25 PCs for this data set.

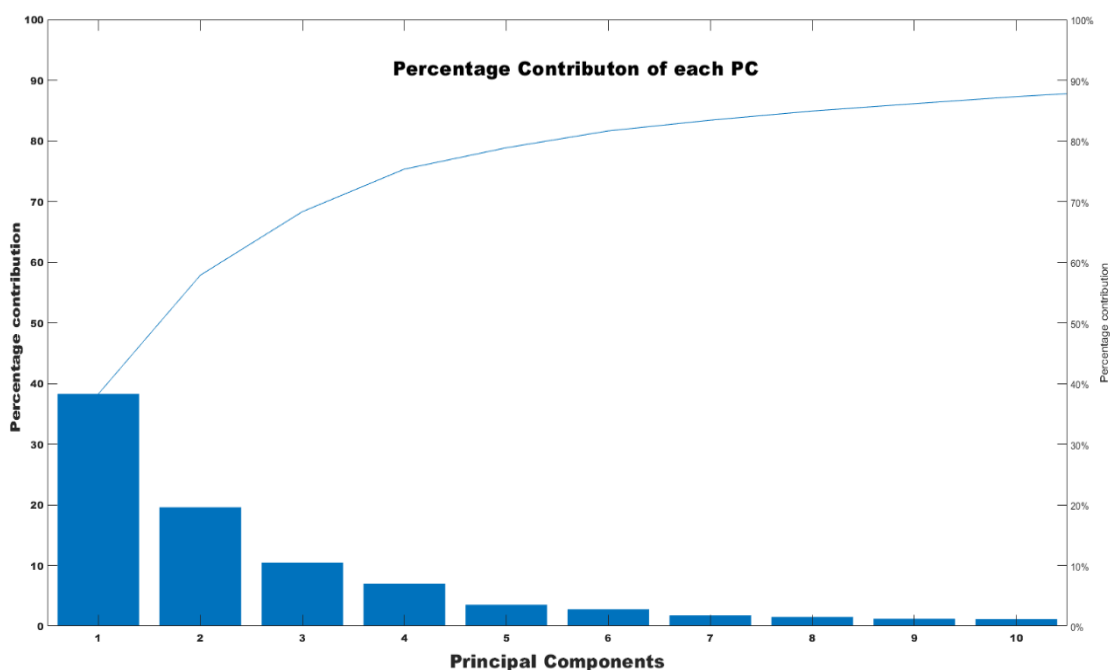


Figure 51 - Percentage contribution of principal components. This figure displays the percentage contributions of the first 10 PCs. They explain 90% of the data. The right hand axis showing the cumulative variance described.

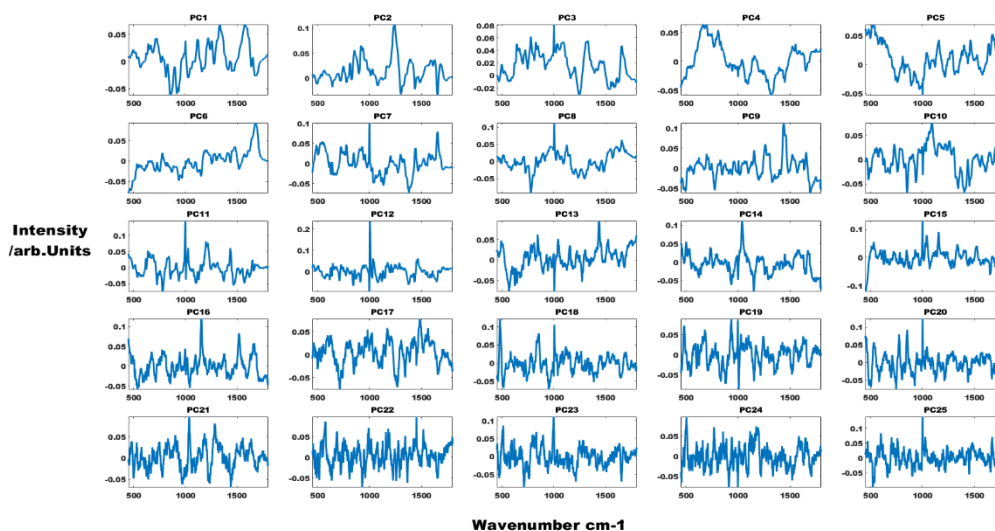


Figure 52 – Twenty-five principal components generated from cancer and benign spectra. The first principal component is in the top left corner, they continue consecutively to the right on each new line. Each PC is plotted with wavenumber cm^{-1} on the x-axis and intensity on the y-axis.

Analysis of variance (ANOVA) was used to identify the most significant principal components for differentiating between cancer and benign ovarian tissue, using a significance level of 99%. 13 of the 25 PCs had greater than 99% level of discrimination and were used to build further models (Table 9).

PC1 had a significantly higher F value compared to the other PCs of significance. Within the PC loadings, the variables furthest away from zero in either direction have the strongest influence. For PC1, these were nucleic acid pyrimidine ring and ring vibrations followed by cytosine, 1222 (unassigned), lipids, phenylalanine breathing mode, adenine, twisting mode of tyrosine and glycogen. The variables with the strongest negative influence were collagen, carotenoids and amide I.

There is a broad positive contribution for the nucleotide bases thymine, adenine, cytosine and uracil in PC4 and disulphide stretch of proteins in PC5.

Principal Component	F value ($F_{crit} 10.8, p=0.001$)
1	859
4	160
5	110
3	85
12	77
2	69
9	56
13	54
15	33
11	24
23	26
19	14
20	12

Table 9 - Displays the principal components with statistical significance in order of F value.

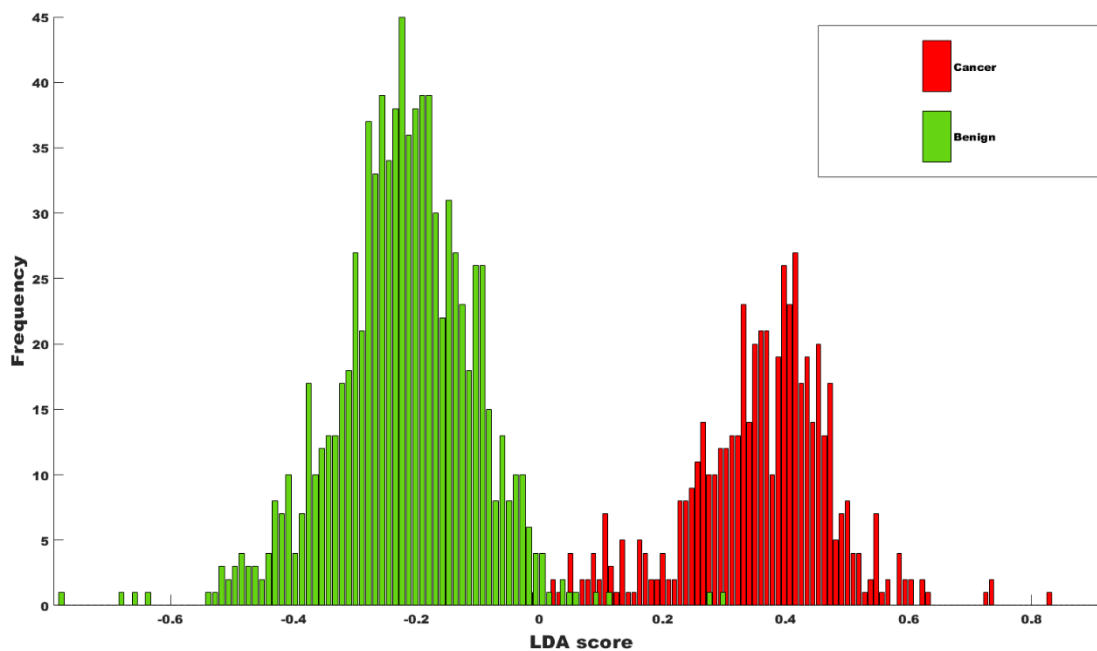


Figure 53 – Histogram plot of linear discriminant scores classifying benign and cancer with a sensitivity of 98% and a specificity of 100%. The red histogram represents the scores of the cancer group and the green histogram represented the scores for the benign group.

The principal components with statistical significance were used to generate a linear discriminant analysis (LDA) classification model as described in methods section 2.5.2, with sensitivity and specificity output documented for classifying cancer correctly. The LDA model achieved a sensitivity of 98% and specificity of 100%. The scores of this model are displayed in a histogram (Figure 53).

This analysis was repeated using leave one sample out cross validation, using either all the spectra per participant or the mean spectra per participant. The output of this analysis, sensitivity, specificity, and a mean receiver operating characteristic (ROC) curve with standard deviation are displayed in Table 10. The mean ROC curve (Figure 54) is generated using all the specificity and sensitivity data of each leave one sample out cross validation classification result. An F1 score has also been calculated to measure the accuracy of the cross-validation model.

	Sensitivity	Specificity	AUROC	F1 score
LDA	98%	100%	-	0.99
Leave one sample out cross validation	94%	98%	0.97	0.95
Leave one mean sample out	91%	83%	-	0.83

Table 10 - Leave one out cross validation results for cancer classification in cancer and benign data. Included in this table is the linear discriminant analysis model performance and the F1 score.

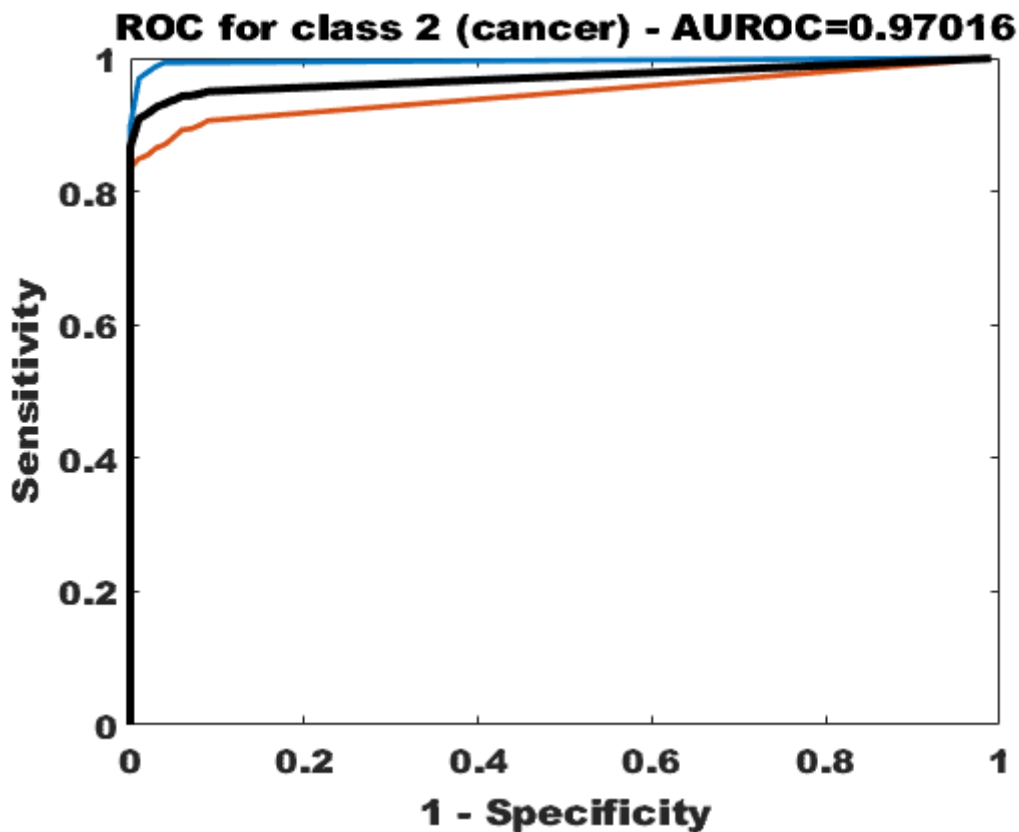


Figure 54 – Mean ROC curve (black) following two-fold cross validation for cancer group in cancer and benign data. The upper (blue) and lower (orange) lines show each iteration..

Summary

Thirteen of the twenty-five principal components created for this data can describe the spectral data with a confidence of 99% with prominent variables being glycogen, nucleotide base activity, collagen, lipids and carotenoids. This data has been used to build a model that has achieved 98% sensitivity and 100% specificity for discriminating between cancer and benign ovarian tissue. Cross validation of this result was successful with a leave one sample out sensitivity of 94%, sensitivity of 98% and F1 score 0.95 confirming the accuracy of the validation model.

Multivariate analysis of Cancer vs Borderline pathology groups

931 spectra were used for this analysis, 392 (8 participants) from borderline tumours and 539 (11 participants) from ovarian cancer. Two spectra were replaced, one from each pathology group, due to saturation. The spectra were then pre-processed together as discussed earlier in this chapter. Mean centred PCA was performed and 25 PCs (Figure 55) were generated. As seen with the cancer/benign group, 90% of the data can be described by the first 10 PCs.

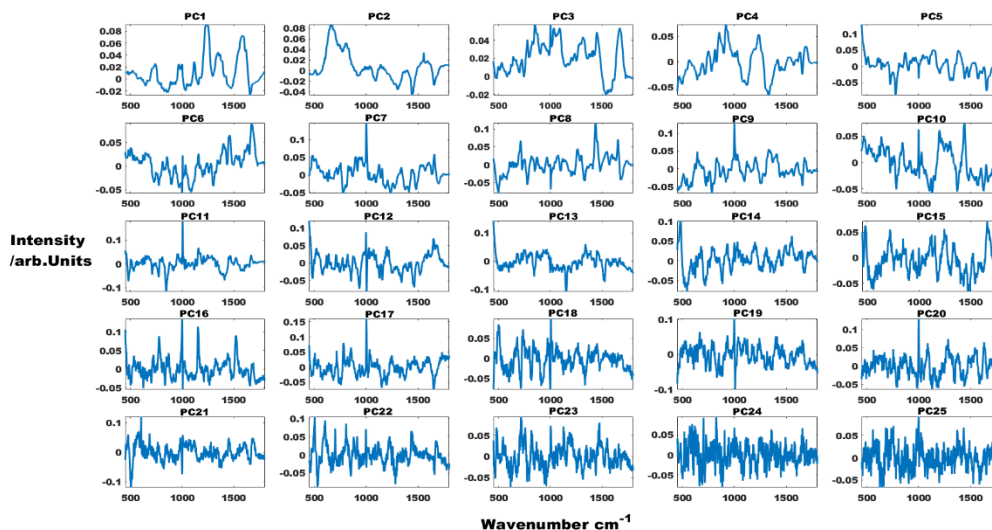


Figure 55 - Twenty-five principal components generated from cancer and borderline spectra. Each principal component is plotted with wavenumber cm^{-1} on the x-axis and intensity on the y-axis.

11 of the 25 PCs reached the threshold of greater than 99% significance (Table 11) for discrimination of cancer and borderline spectra using ANOVA.

Principal Component	F value ($F_{\text{crit}} 11, p=0.001$)
11	163
6	157
1	133
10	88
2	86
9	63
12	57
17	55
19	31
5	23
3	16

Table 11 - Displays the principal components with statistical significance in order of F value.

Examining the PCs with the highest F-values, the strongest influences in PC11 are a positive phenylalanine breathing mode and a negative collagen. There is a further negative contribution from CH3 deformation. PC1 has only positive influences, the strongest of which is seen with amide III beta sheet, then nucleic acids, tryptophan, lipids, phenylalanine, and phosphate ion stretching. PC6 has positive contributions from amide I, deoxyribose, uracil and adenine, and negative influences from amide III, collagen and symmetric phosphate ion stretching.

Using only the PCs with statistical significance linear discriminant analysis was performed. The model achieved a sensitivity of 99% and specificity of 99%. The scores of this model are displayed in a histogram (Figure 56).

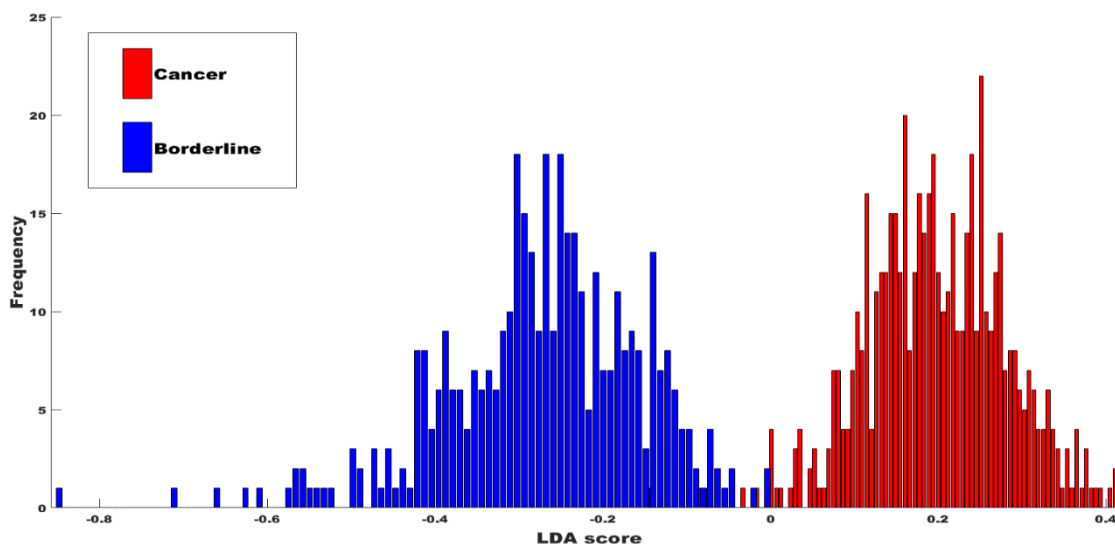


Figure 56 - Histogram plot of linear discriminant scores classifying borderline and cancer with sensitivity of 99% and specificity of 99%. The blue histogram represents the scores of the borderline group and the red histogram represents the scores of the cancer group.

This analysis was repeated using leave one sample out and leave one mean sample out cross validation, with sensitivity, specificity, prediction AUROC and F1 score highlighted in Table 12. The sample size was too small for accurate leave one mean sample out cross validation.

	Sensitivity	Specificity	AUROC	F1 score
LDA	99%	99%	-	-
Leave one sample out cross validation	98%	89%	0.99	0.94
Leave one mean sample out	-	-	-	-

Table 12 - Leave one out cross validation results for cancer classification in cancer and borderline data. Included in this table is the linear discriminant analysis model performance and the F1 score.

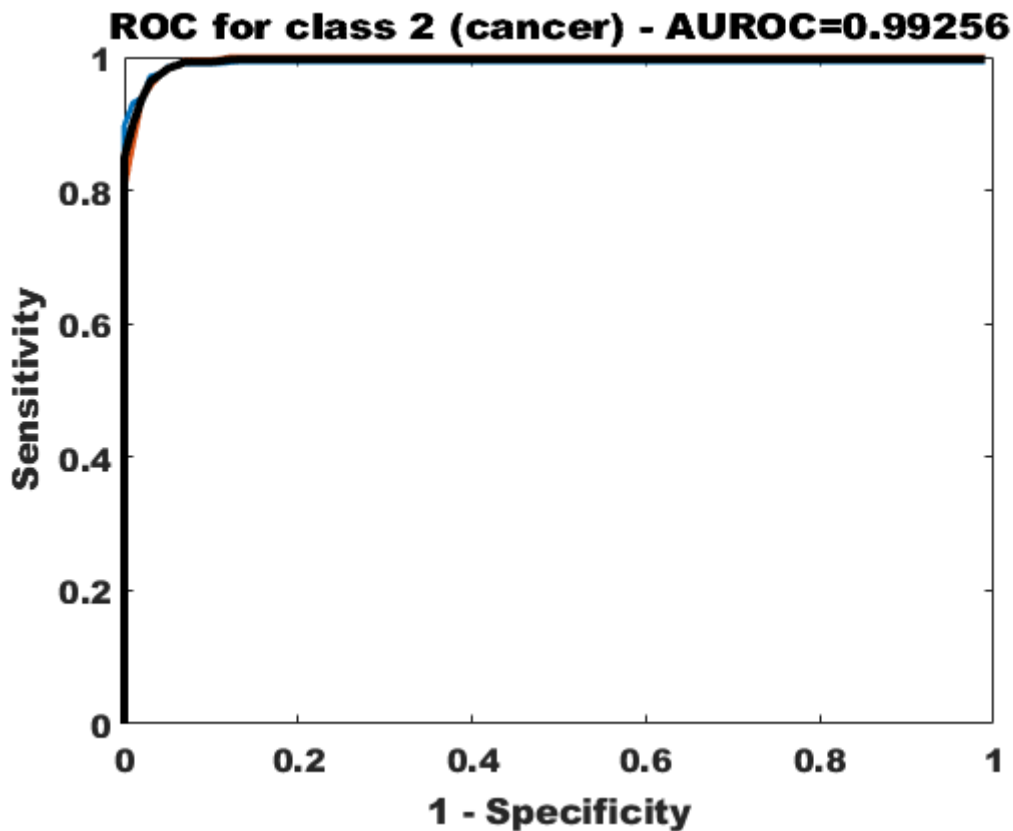


Figure 57 - Mean receiver operating characteristic curve (black) following two-fold cross validation for cancer group in cancer and borderline data. The upper (blue) and lower (orange) lines show each iteration.

Summary

11 of the 25 principal components created for this data can describe the data with a confidence of 99% with prominent variables being phenylalanine, collagen, amide III beta sheet, nucleic acids, phosphate ion stretching, tryptophan, lipids and phosphate ion stretching. This data has been used to build a model that has achieved 99% sensitivity and 99% specificity for discriminating between cancer and benign ovarian tissue. Cross validation of this result with leave one sample

out was successful with a sensitivity of 98%, sensitivity of 89% and F1 score 0.94 confirming the accuracy of the validation model.

Multivariate analysis of Borderline vs Benign pathology groups

1,274 spectra were used for this analysis, 882 (18 participants) from benign and 392 (8 participants) from borderline tumours. One spectrum was replaced due to saturation. The spectra were then pre-processed together as discussed earlier in this chapter. Mean centred PCA was performed, and 25 PCs (Figure 58) were generated. 9 of the 25 PCs reached the threshold of greater than 99% significance (Table 13) for discrimination of borderline and benign spectra using ANOVA.

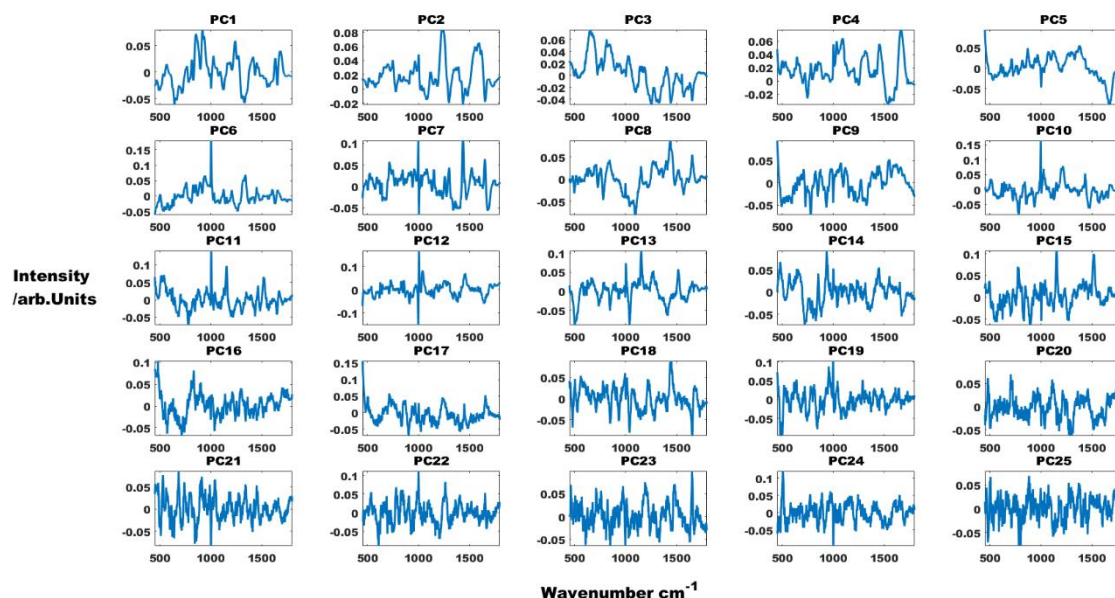


Figure 58 – Twenty-five principal components generated from borderline and benign spectra. Each PC is plotted with wavenumber cm^{-1} on the x-axis and intensity on the y-axis.

PC1 has a strikingly higher F value than the other significant PCs. The strongest positive influence is collagen followed closely by amide III beta sheet. Amide I and antisymmetric CH_3 deformation also offer a strong positive influence in this PC. The negative influences are tyrosine, nucleic acids, and adenine. Carotenoids offer a strong positive influence in PC 13 in two peak position, 1156 and 1519 cm^{-1} .

Including PCs with statistical significance, LDA achieved a sensitivity of 90% and specificity of 95%. The scores of this model are displayed in a histogram (Figure 59).

Principal Component	F value ($F_{crit} 11, p=0.001$)
1	751
13	133
12	93
7	57
6	56
14	33
24	23
23	17
15	13

Table 13 - Principal components with F_{ratio} greater than F_{crit} . This table displays the PCs of significance in the borderline/benign spectra.

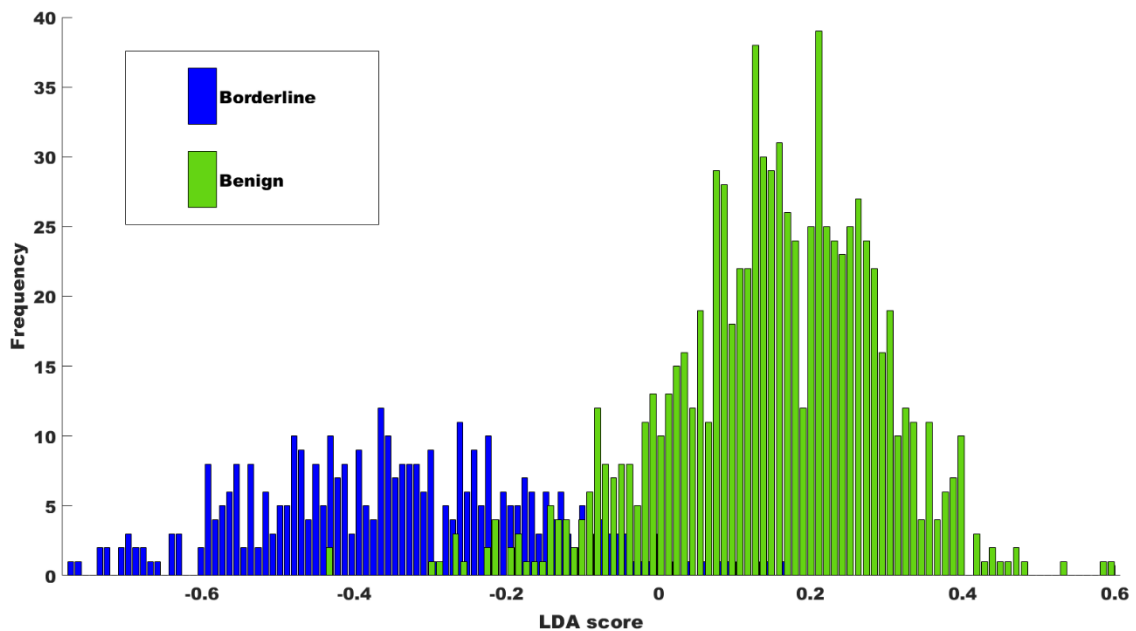


Figure 59 - Histogram plot of linear discriminant analysis scores classifying benign and cancer with a sensitivity of 90% and specificity of 95%.

This analysis was repeated using leave one sample out and leave one mean sample out cross validation, with sensitivity, specificity, prediction AUROC and F1 score highlighted in (Table 14).

	Sensitivity	Specificity	AUROC	F-score
LDA	90%	95%	-	-
Leave one sample out cross validation	72%	93%	0.88	0.77
Leave one mean sample out	88%	83%	-	0.78

Table 14– Leave one out cross validation results for borderline tumour classification in borderline and cancer data. Included in this table is the linear discriminant analysis model performance and the F1 score.

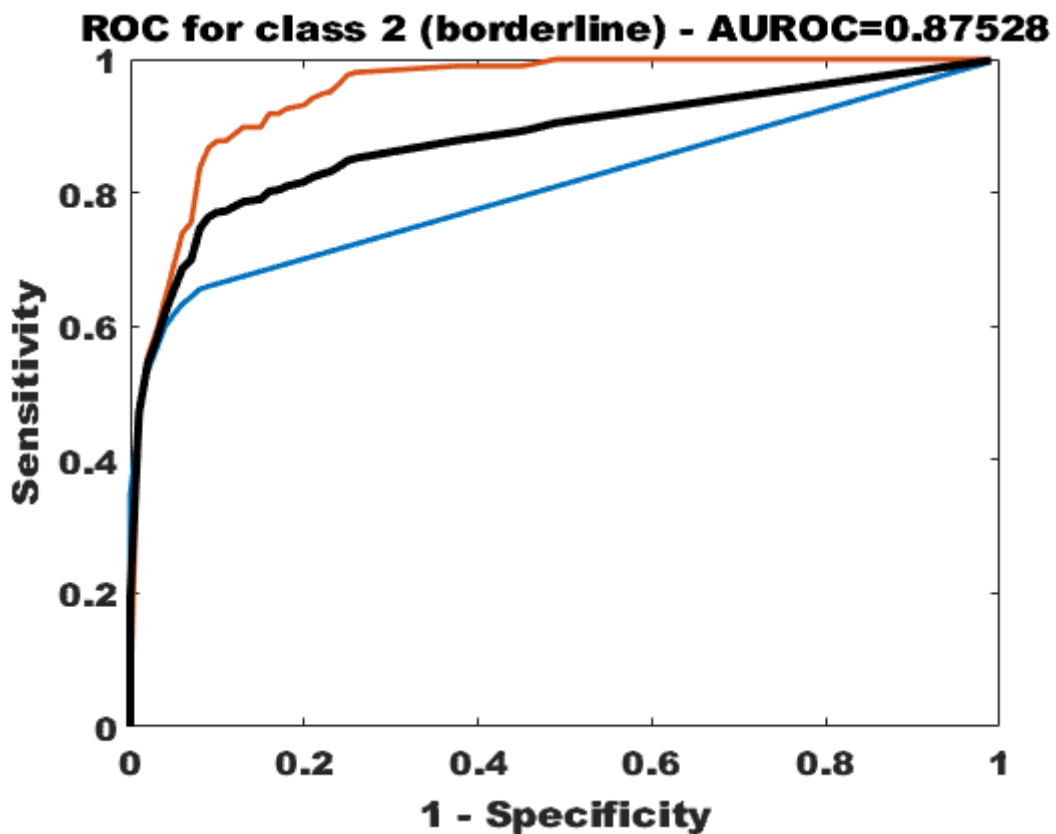


Figure 60 - Mean receiver operating characteristic curve (black) following two-fold cross validation. for borderline group in borderline and benign data. The upper (blue) and lower (orange) lines show each iteration.

Summary

9 of the 25 PCs created for this data can describe the data with a confidence of 99% with prominent variables being carotenoids, collagen, amide III beta sheet, tyrosine, adenine and nucleic acids. Whilst the supervised LDA achieved a sensitivity of 90% and specificity of 95%, this diagnostic model did not fare as well leave one sample out cross validation. This is reflected in the F1 score of 0.77.

Multivariate analysis of IDS vs Primary - Cancer

Unfortunately, this analysis is limited due to low numbers of participants, two, in the IDS group. As both IDS participants had high grade serous cancer, two participants with high grade serous cancer in the primary surgery group were chosen by study ID to create an appropriate control group. Whilst it is an incredibly small sample size, one of the aims of this project was to understand the effect of chemotherapy on the ability of Raman spectroscopy to detect cancer in tissue making this work worthwhile. Also, if clear variables are identified that separate these two groups, the results can contribute to a sample size calculation in future work.

196 spectra were used for this analysis, 98 each from IDS and upfront surgery groups. One spectrum was replaced due to saturation. The spectra were then pre-processed together as discussed earlier in this chapter. The mean spectra of the groups are plotted together in (Figure 61). Mean centred PCA was performed, and analysis of variance demonstrated only PC1 as significant. It has been noted that the F value for PC1 was 432 (F_{crit} 11.2). The variables in this PC were all in the positive direction with strong influence from amide III beta sheet, nucleic acids pyrimidine ring, nucleic acids purine bases, lipids and adenine (Figure 63). The scores for PC1 are displayed in figure (Figure 62), plotted against PC2 to facilitate displaying the data in this manner.

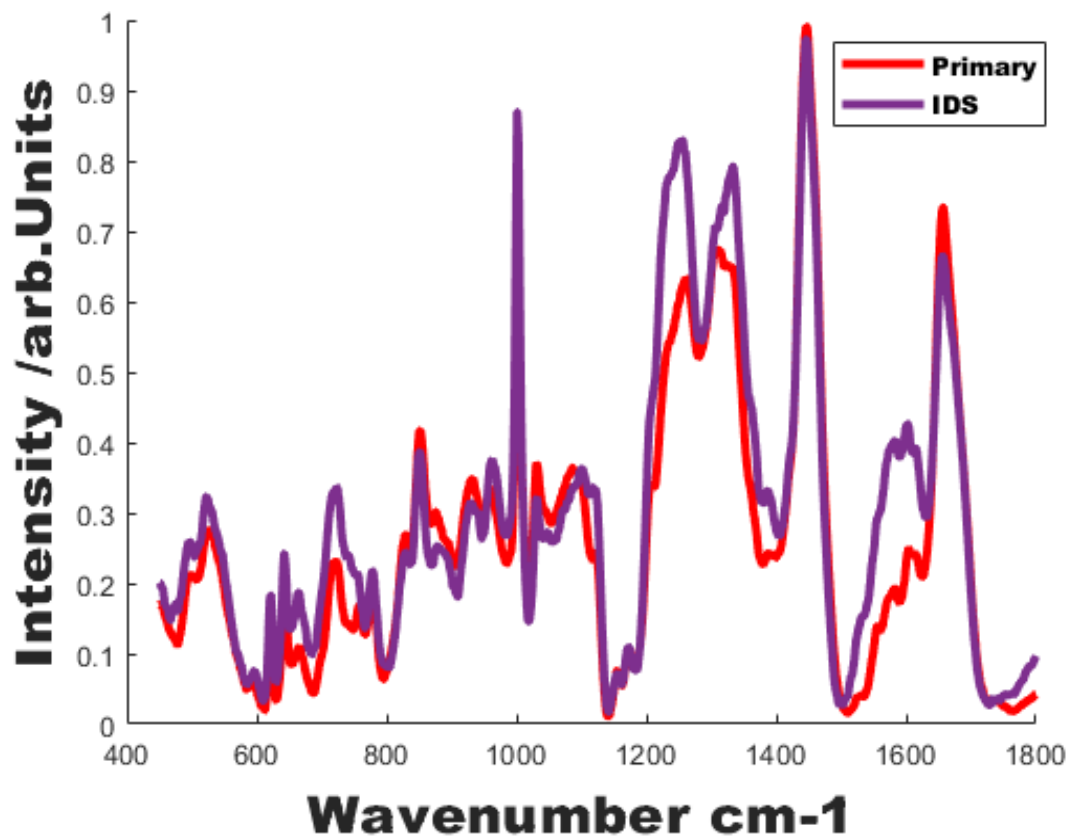


Figure 61 - Mean spectra of ovarian tissue taken from participants at primary surgery (red) and interval debulking surgery (purple).

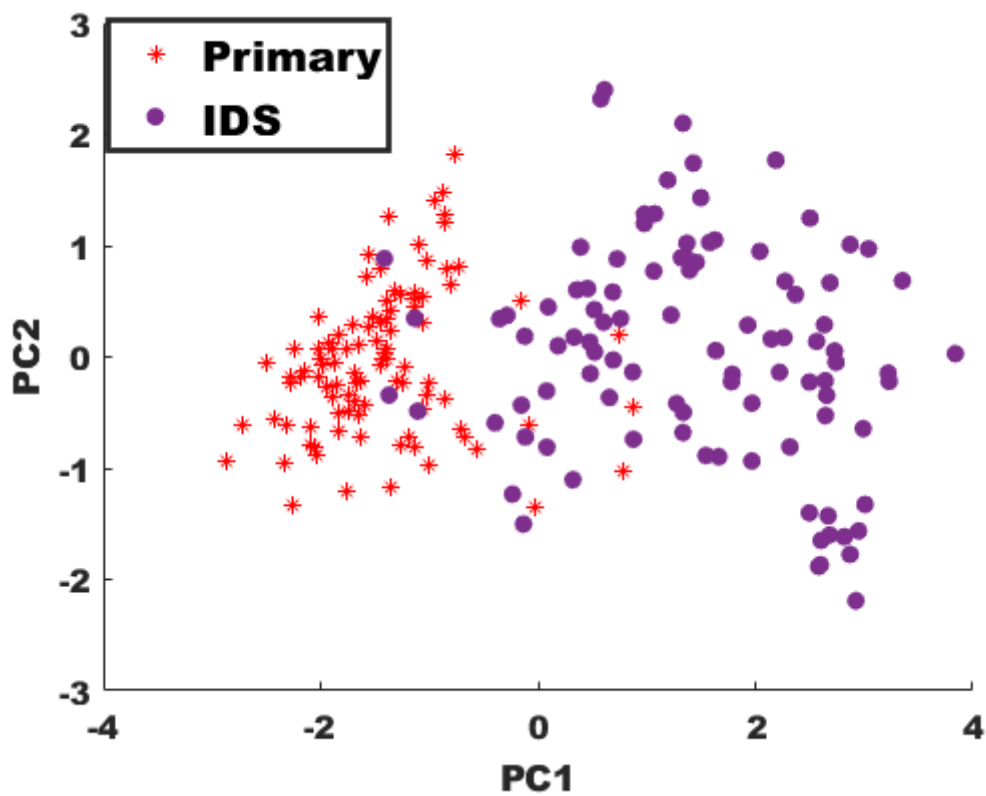


Figure 62 - Scores plot for PC1. This figure displays a scatter plot of PC1 against PC2 with data from primary cancer in red stars and data from IDS in purple filled circles.

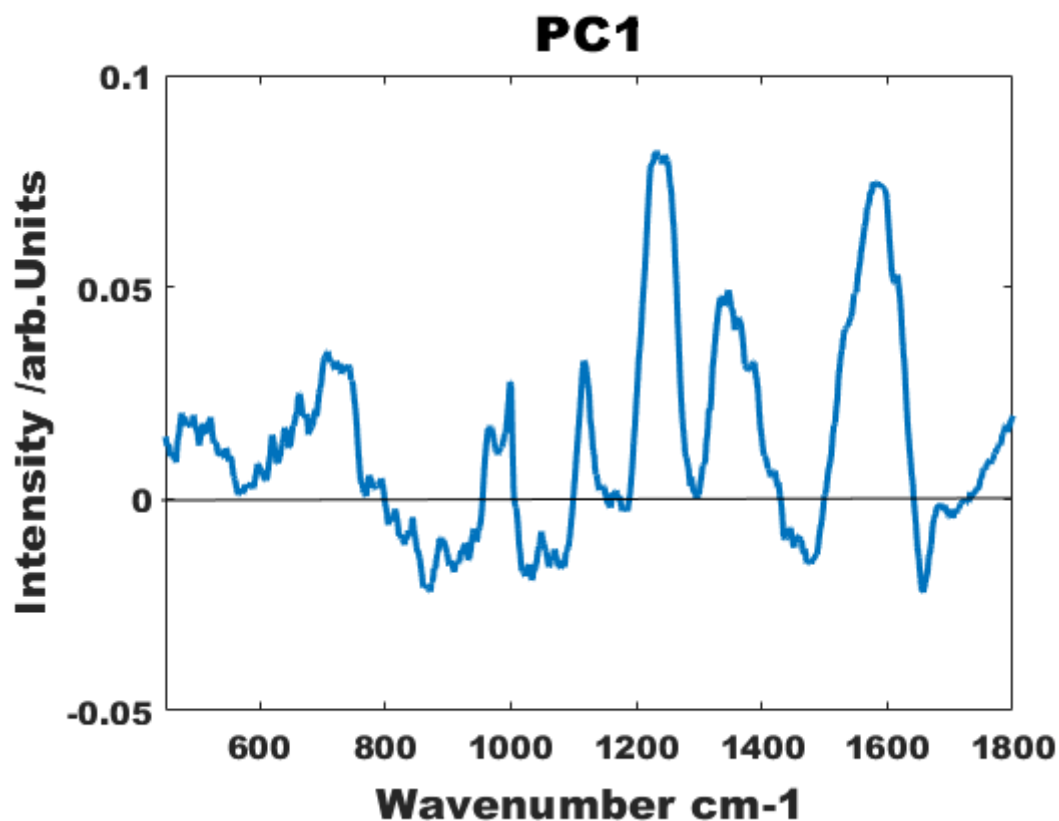


Figure 63 - Principal component 1 for IDS vs primary. This was the only PC of significance for describing variance in this data. The main variables seen are lipids, glycogen, amide III beta sheet, adenine and nucleic acid base and ring activity.

Linear discriminate analysis achieved a sensitivity of 97% and specificity of 97% and leave one sample out cross validation achieved sensitivity of 84% and specificity of 89%.

Summary

The data is limited by low sample numbers however there is one statistically significant principal component with 6 variables that can explain the variance in the data with a confidence of 99%. This is reflected in high LDA sensitivity and specificity and leave one sample out cross validation model achieving 84% sensitivity and 89% specificity.

4.6.2 Peritoneal tissue

Peak Positions and Intensity

There was one sample each from 9 participants of the benign group, 1 in borderline and 24 in cancer. Within the cancer subgroup, 19 samples were from interval debulking surgery (IDS) and 5 were from primary surgery. Two of the benign samples were too small to measure using the tissue measurement protocol and have been excluded from this analysis.

There was a second benign group, with 19 samples, which comprised of spectra taken from slides from IDS tissue blocks deemed to have no cancer present on histopathological assessment. This group will be termed group bIDS groups.

Following the preprocessing steps of baseline subtraction and normalisation, the mean spectrum for benign peritoneum (Figure 65), primary cancer (Figure 64), IDS cancer (Figure 66) and bIDS (Figure 67) have been plotted and annotated with the wavenumber of the prominent peaks. Tentative assignments for this work have been made using the reference table in Appendix H.

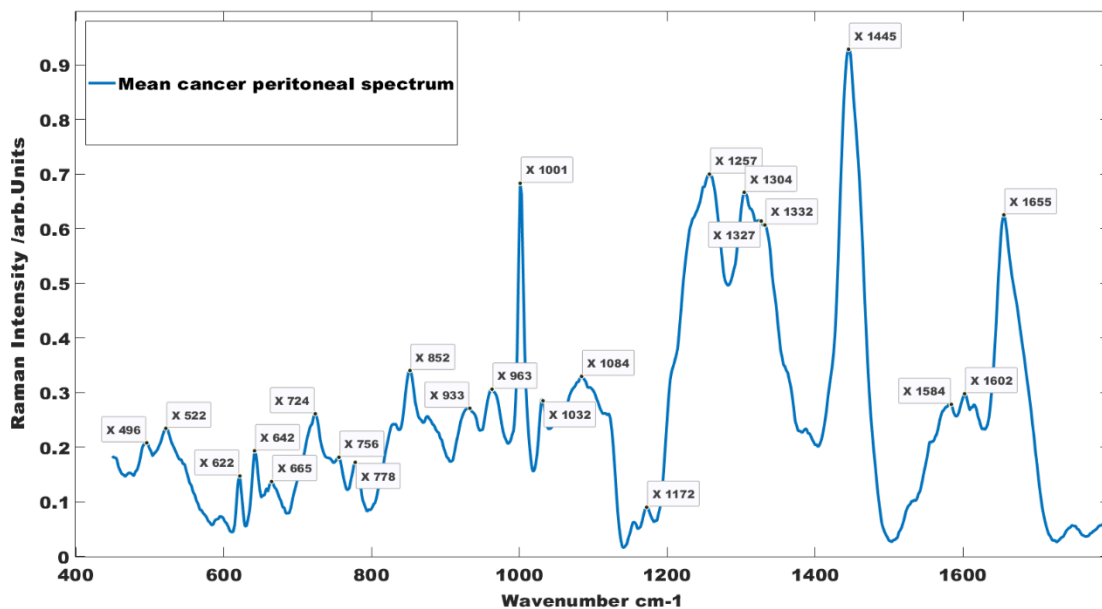


Figure 64 - Mean spectrum of cancer. In this figure the mean of the spectra of (primary surgery) cancer peritoneal samples have been plotted and annotated with the wavenumber of the prominent peaks seen in this spectrum. Tentative assignments of these peaks are seen in Appendix H.

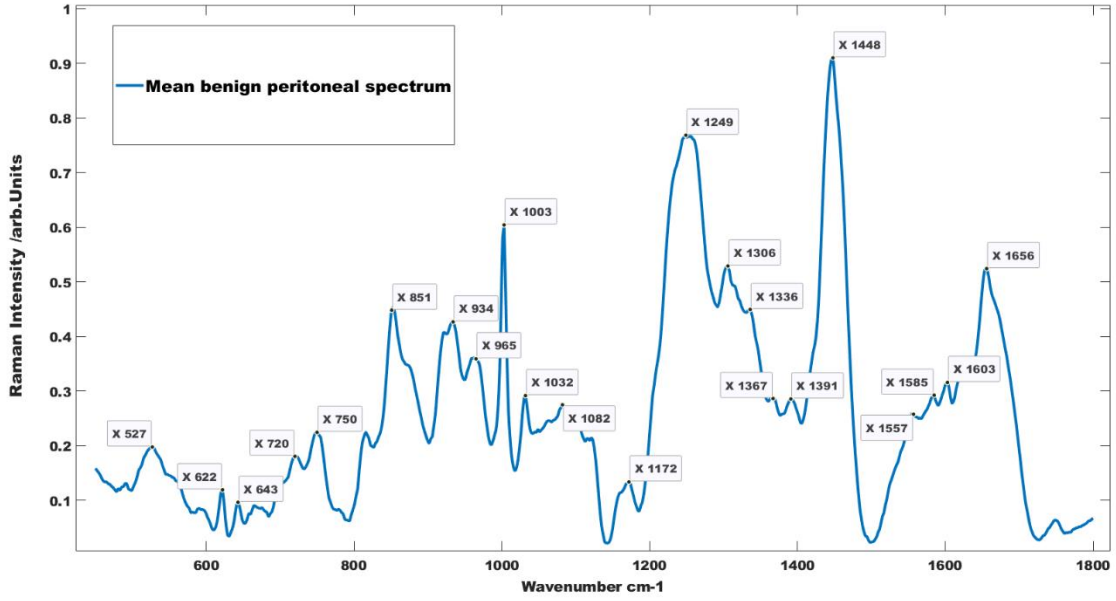


Figure 65 - Mean spectrum of benign peritoneal pathology. In this figure the mean of the spectra of benign peritoneal samples has been plotted and annotated with the wavenumber of the prominent peaks seen in this spectrum. Tentative assignments of these peaks are seen in Appendix H.

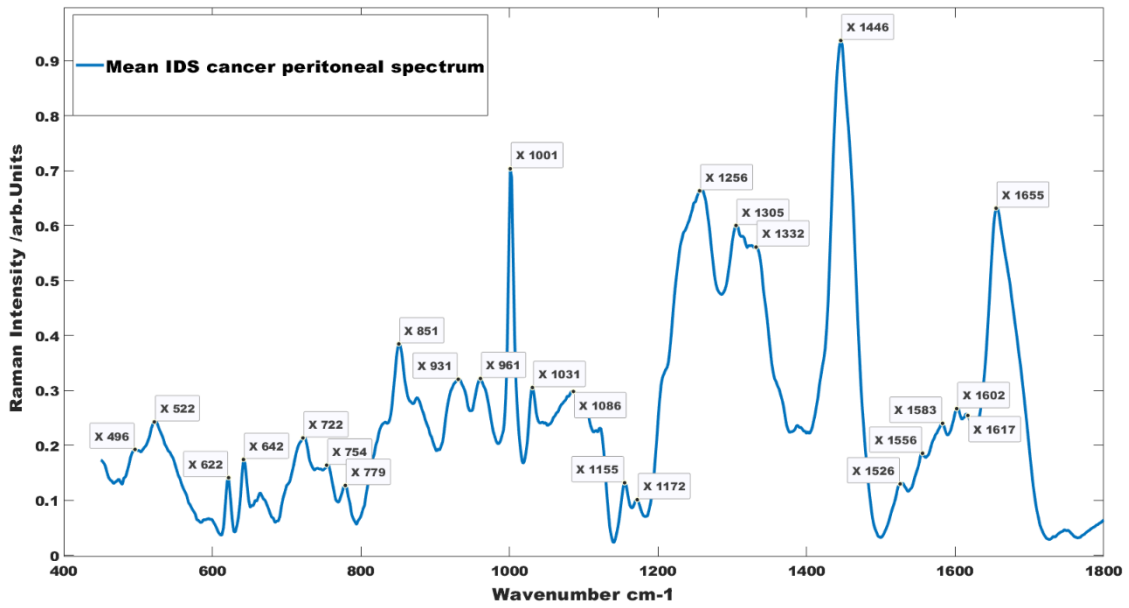


Figure 66 - Mean spectrum of IDS cancer group. In this figure the mean of the spectra of (cancer) IDS peritoneal samples have been plotted and annotated with the wavenumber of the prominent peaks seen in this spectrum. Tentative assignments of these peaks are seen in Appendix H.

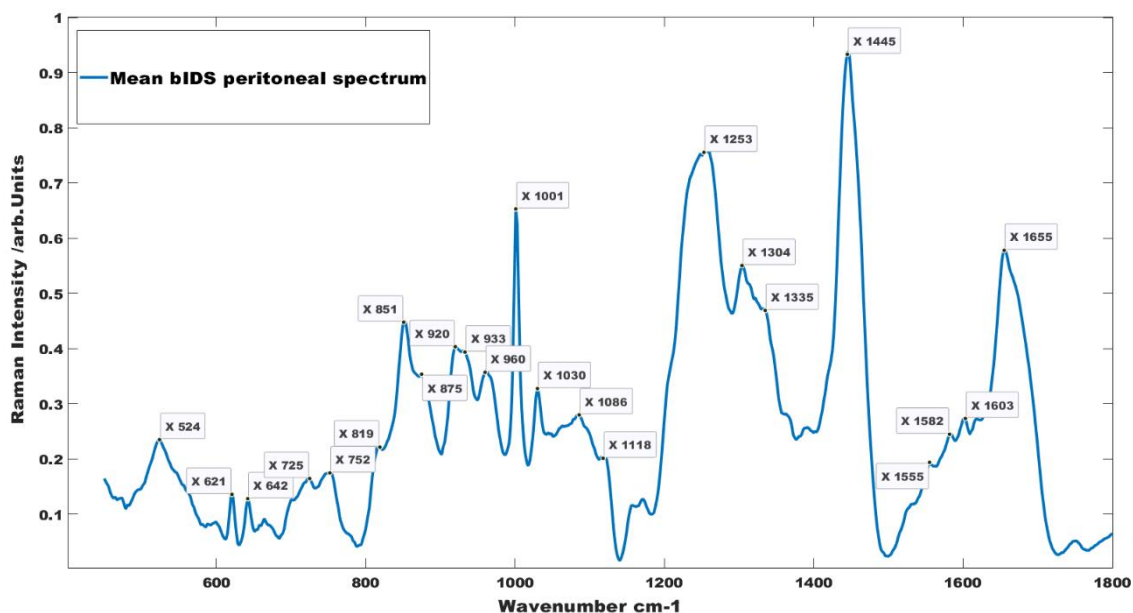


Figure 67 - Mean spectrum of bIDS. In this figure the mean of the spectra of benign IDS peritoneal samples has been plotted and annotated with the wavenumber of the prominent peaks seen in this spectrum. Tentative assignments of these peaks are seen in Appendix H.

Difference between the mean

To understand the changes that occur in benign peritoneal tissue after chemotherapy, the benign group was subtracted from the bIDS group. The differences in the group are subtle, which is reflected in the low intensity of the subtraction spectrum. There is a positive intensity value at 523, 641, 836, 914, 1001, 1028, 1150, 1198, 1327, 1408, 1440 and 1665 cm^{-1} suggesting a higher concentration in the bIDS group of disulphide stretch in proteins, amino acids (tyrosine and phenylalanine), ribose, nucleic acid ring vibrations, lipids, Amide I group carotenoids and one unassigned (1408 cm^{-1}) when compared to the benign group. There is a negative intensity value at 748, 935, 1556 & 1622 cm^{-1} suggesting a lower concentration of thymine, collagen and tryptophan when compared to the benign group (Figure 68).

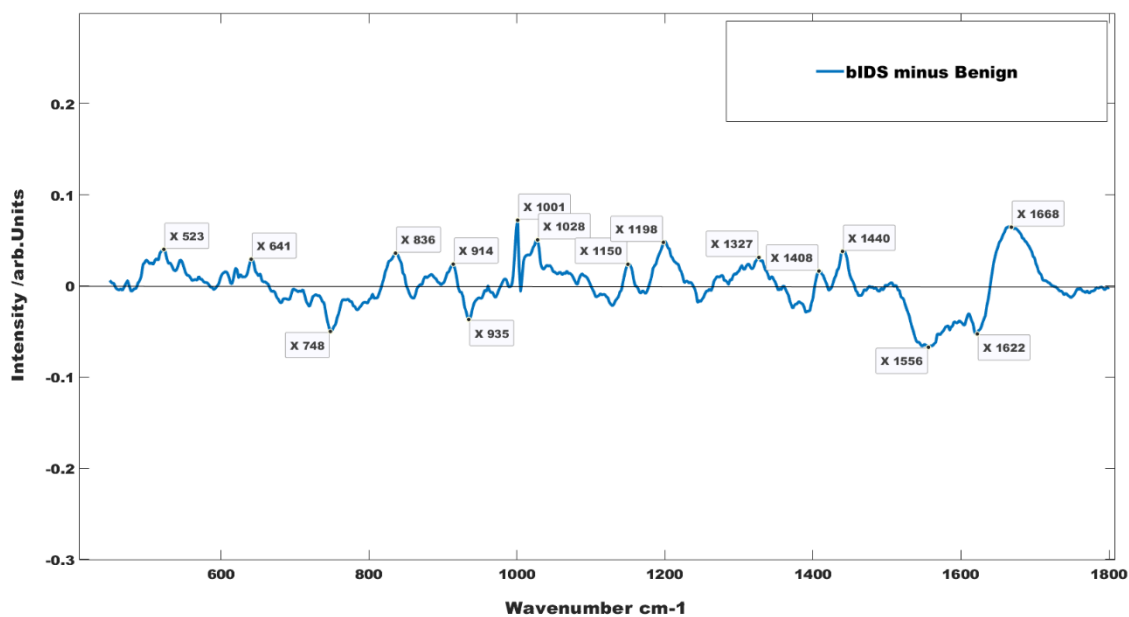


Figure 68 – Subtraction spectrum obtained from subtracting benign from benign IDS. Positive intensity values suggest increased concentration in the bIDS group. Negative intensity values suggest increased concentration in the benign group compared to bIDS. There are lower concentrations of thymine, tryptophan and collagen and higher levels of lipids, amino acids, amide I group, nucleic ring activity and carotenoids in the bIDS group compared to the benign group.

To investigate the effect of chemotherapy on peritoneal tissue with cancer, the primary surgery and IDS groups was also explored. The spectra were subtracted and again the changes were subtle however there were positive intensity peak values at 851, 917, 934, 1003, 1027, 1156, 1410, 1463, 1523, 1635 and 1666 cm^{-1} suggesting higher concentrations of tyrosine, collagen, phenylalanine, carotenoids, deoxyribose, Amide I group and one unassigned (1410 cm^{-1}) in the IDS group compared to the primary surgery cancer group. There were negative intensity values at 724, 778, 1116, 1302 and 1571 cm^{-1} suggesting lower concentrations of nucleotides (adenine, cytosine & uracil breathing ring, guanine) and lipids in the IDS group compared to the primary surgery group (Figure 69).

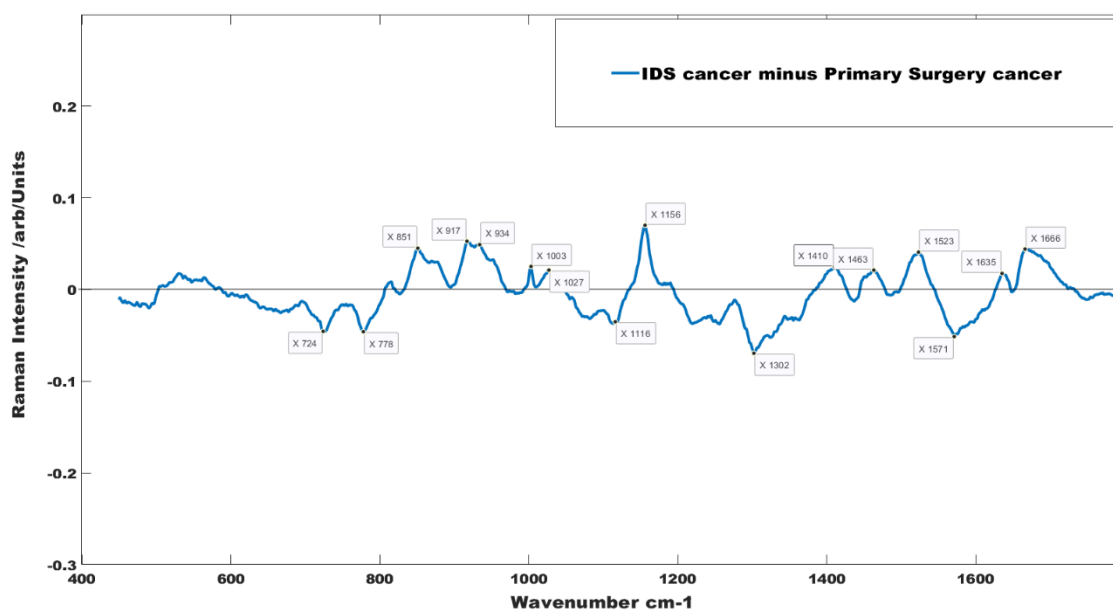


Figure 69 - Subtraction spectrum obtained by subtracting cancer samples taken at primary surgery from those taken at IDS. Positive intensity values suggest increased concentration in the IDS group. Negative intensity values suggest increased concentrations in the primary surgery group. There are higher concentrations of tyrosine, collagen, phenylalanine, carotenoids, deoxyribose, and amide I and lower concentrations of nucleotides and lipids in the IDS group compared to the cancer group.

For this study population, the effects of chemotherapy on both cancer and benign samples are summarised in Table 15. Despite the significant morphological differences between benign and cancer tissue, there appears to be consistent increase concentrations of tyrosine, phenylalanine, carotenoids, amide I and the unassigned 1408-1410 cm^{-1} after chemotherapy in both tissue types.

	Benign IDS vs Benign	Cancer IDS vs Cancer
Increased Concentration	<ul style="list-style-type: none"> - Disulphide stretch of protein - Amino acids <div style="margin-left: 20px;"><i>Tyrosine</i></div> <div style="margin-left: 20px;"><i>Phenylalanine</i></div> - Ribose - Carotenoids - Amide I - Unassigned 1408 cm⁻¹ - Nucleic ring vibrations - Lipids 	<ul style="list-style-type: none"> - Collagen - Amino acids: <div style="margin-left: 20px;"><i>Tyrosine</i></div> <div style="margin-left: 20px;"><i>Phenylalanine</i></div> - Deoxyribose - Carotenoids - Amide I - Unassigned 1410 cm⁻¹
Decreased Concentration	<ul style="list-style-type: none"> • Collagen • Thymine • Tryptophan 	<ul style="list-style-type: none"> • Lipids • Nucleotides: <div style="margin-left: 20px;"><i>Adenine</i></div> <div style="margin-left: 20px;"><i>Cytosine</i></div> <div style="margin-left: 20px;"><i>Uracil</i></div> <div style="margin-left: 20px;"><i>Guanine</i></div>

Table 15 - Summary of tentative assignments of prominent peak positions in subtraction spectra of the groups. Tyrosine, phenylalanine, amide I, carotenoids and unassigned 1408-1410cm⁻¹ appear to be higher in the IDS group of both tissue types.

Multivariate analysis of Cancer vs Benign (IDS)

To further explore the differences between the post chemotherapy cancer and benign group, multivariate analysis of IDS cancer and bIDS groups was performed. 1,862 spectra were used for this analysis, 931 (19 participants) from IDS cancer and 931 (19 participants) from bIDS. Six spectra were replaced due to saturation and the spectra were pre-processed together as discussed earlier in this chapter. Mean centred PCA was performed, and the PCs are displayed in (Figure 70). ANOVA has been used to identify the most significant PCs for differentiating between cancer and benign in IDS tissue using a confidence level of 99%. 11 of the 25 PCs met the threshold (Table 16) and were used to build further models.

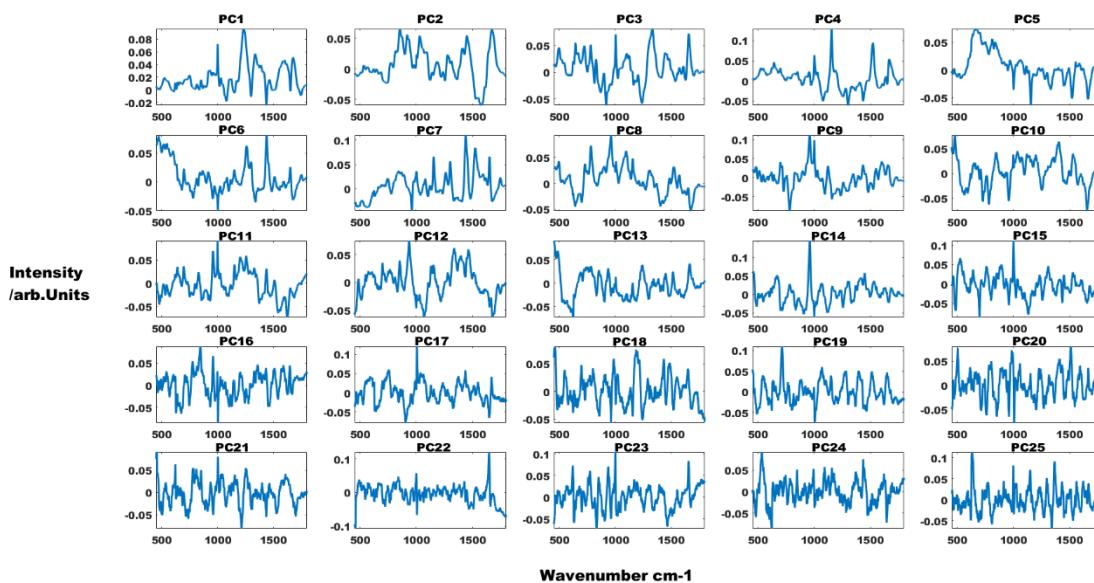


Figure 70 – Twenty-five principal components generated from cancer and benign IDS spectra. The first principal component is the left top corner, they continue consecutively to the right on each new line. Each PC is plotted with wavenumber cm-1 In the x-axis and intensity on the y-axis.

Principal Component	F Value ($F_{crit} 11, p=0.001$)
3	916
6	163
15	60
10	28
2	23
1	19
16	19
23	19
19	17
8	12
4	12

Table 16 – Principal components with statistical significance in order of F value.

PC3 had a significantly higher F value compared to the other PCs of significance. Within the PC loadings, the variables furthest away from zero in either direction have the strongest influence. For PC3, the variables with the strongest positive influence were nucleic acid ring vibrations, amide I group, phenylalanine, tyrosine, nucleotides (adenine, cytosine and uracil), glycogen, phosphate stretch of DNA and lipids. The strongest negative influences are amide III beta sheet, carotenoids and collagen.

The significant PCs were used to build an LDA model (Figure 72) which achieved 81% sensitivity and 91% specificity. The analysis was repeated using leave one sample out and leave one mean sample out cross validation, with sensitivity, specificity, prediction AUROC and F1 score highlighted in Table 17.

	Sensitivity	Specificity	AUROC	F1 score
LDA	81%	91%	-	-
Leave one sample out cross validation	68%	81%	0.79	0.73
Leave one mean sample out	68%	84%	-	0.74

Table 17 - Leave one out cross validation results for IDS cancer vs benign of peritoneal tissue. Included in this table is the linear discriminant analysis model performance and the F1 score.

ROC for class 2 (Cancer IDS) - AUROC=0.78613

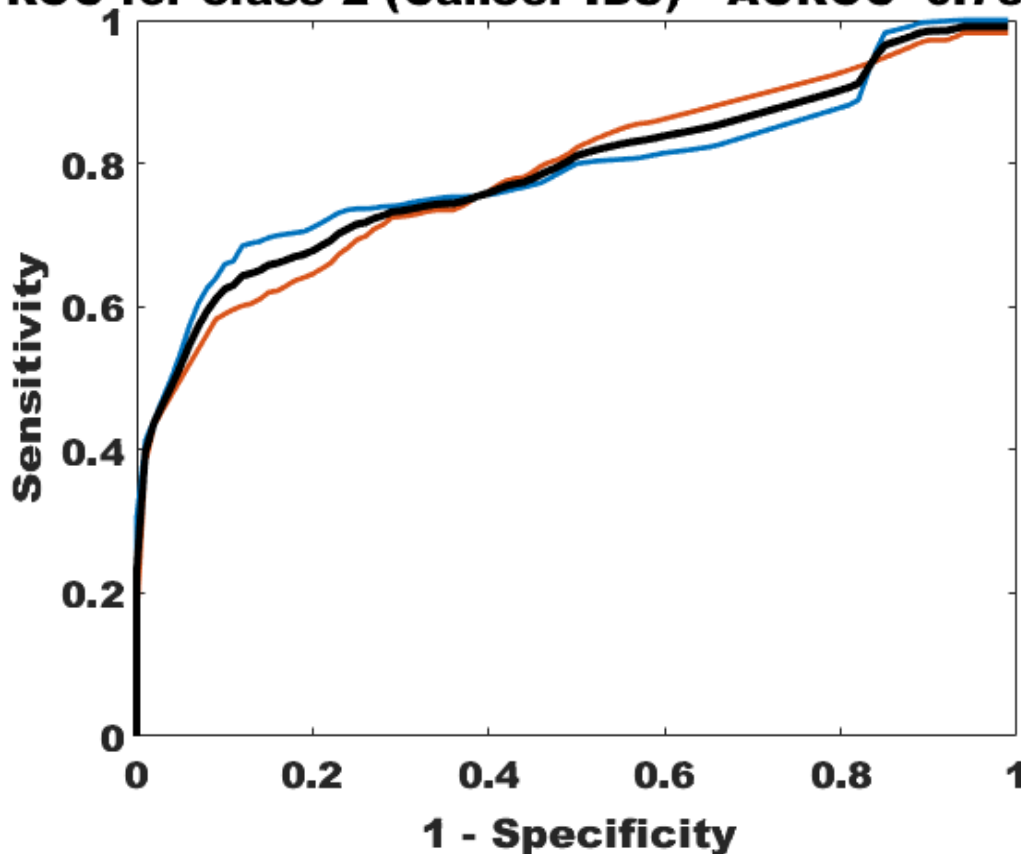


Figure 71 - Mean receiver operating characteristic curve (black) following two-fold cross validation for cancer group in the IDS cancer and bIDS data. The upper (blue) and lower (orange) lines show each iteration. The IDS group here are participants that ha samples taken at interval debulking surgery, and the resulting slide had cancer on it and the bIDS group represent similar patients background but their slides did not have cancer.

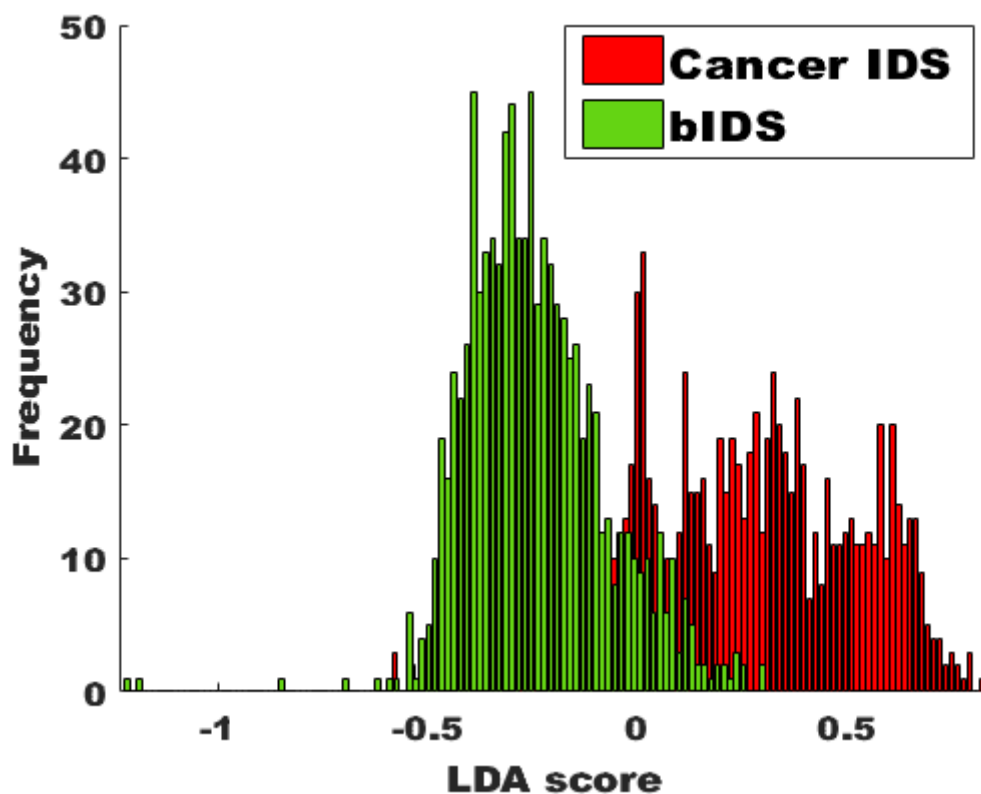


Figure 72 – Histogram plot of linear discriminant scores classifying IDS cancer and benign IDS with sensitivity of 81% and specificity of 91%. The green histogram represents the scores of the benign IDS group and the red histogram represents the cancer IDS group.

Summary

11 of the 25 PCs created for this data can describe the data with a confidence of 99% with prominent variables being nucleic acid ring vibrations, amide I group, phenylalanine, tyrosine, nucleotides (adenine, cytosine and uracil), glycogen, phosphate stretch of DNA, lipids, amide III beta sheet, carotenoids and collagen. The diagnostic model achieved a sensitivity of 68% and specificity of 81% on leave one out cross validation.

Multivariate analysis of Cancer vs Benign (Primary Surgery)

Unfortunately, this analysis is limited due to low numbers in each group. There are 5 participants in the cancer group (245 spectra) and 9 in the benign group (441 spectra). 8 spectra were replaced due to saturation. The spectra were then pre-processed together as discussed earlier in this chapter. Mean centred PCA was performed, and analysis of variance demonstrated two PCs of significance,

PC 3 and PC 4 (Figure 73). The strongest positive influences are amide III alpha helix, nucleic acid ring vibrations, lipids, amide I, tyrosine, nucleotides (adenine, cytosine and uracil), phenylalanine, triglycerides and disulphide stretch of proteins. The strongest negative influences are thymine, collagen, amide III beta helix, tyrosine and tryptophan. The PC scores are plotted in figure (Figure 74).

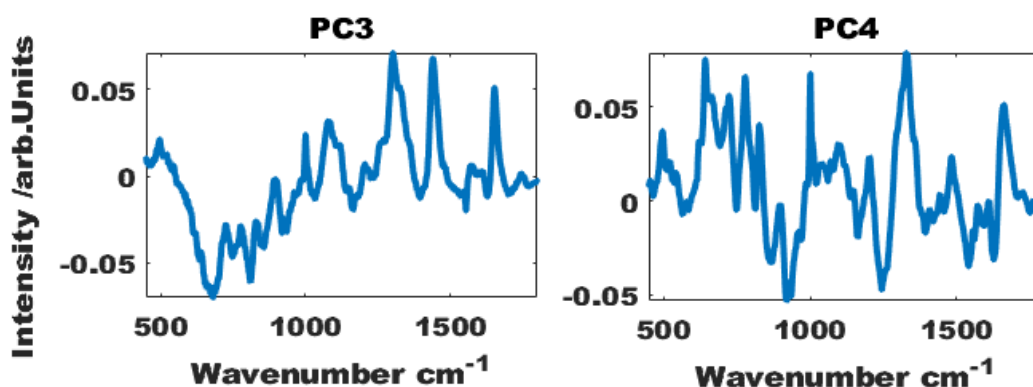


Figure 73 – Principal component loadings for cancer vs benign (primary surgery) group. The pc loading on the left is PC3 and the loading on the right is PC4.

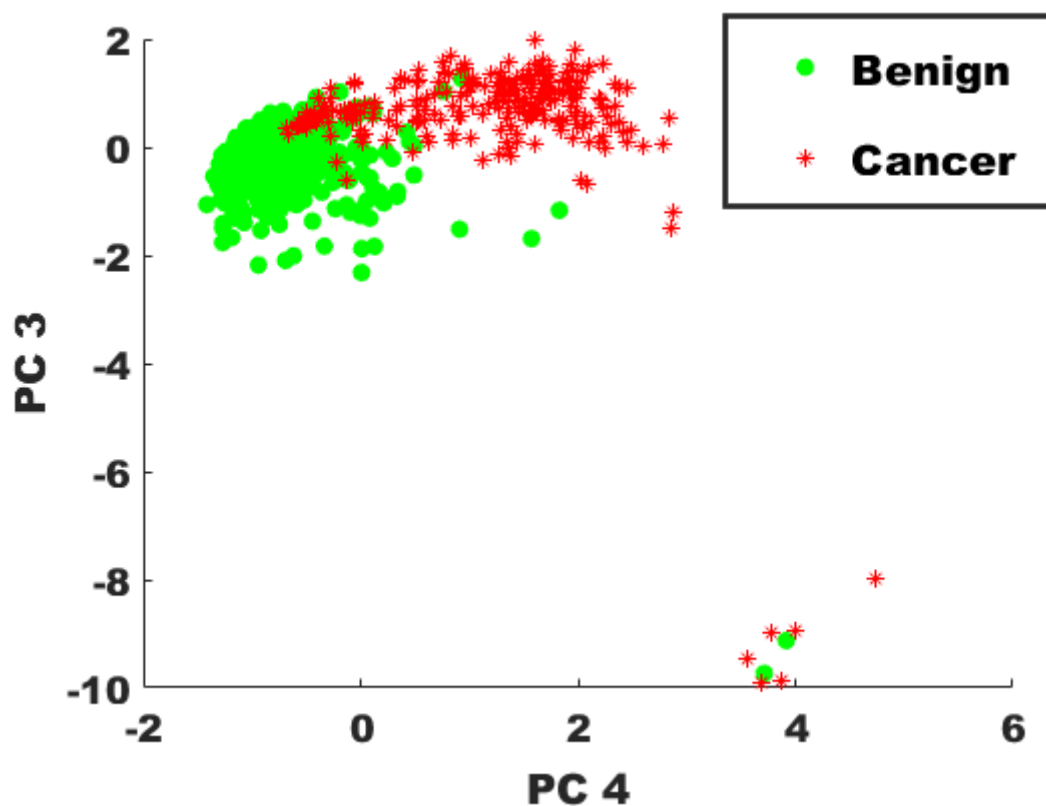


Figure 74 - Scores plot for principal component 4 and principal component 3. This figure displays a scatter plot of PC4 against PC3 scores when comparing cancer and benign with data from cancer in red stars and data from benign in green filled circles.

Linear discriminate analysis demonstrated a sensitivity of 86% and specificity of 98%. Leave one sample out cross validation achieved a sensitivity of 78% and specificity of 84% with an F1 score of 0.83.

Summary

Despite the lower sample numbers, there were two PCs with a minimum of six variables each that explain the variance in the data with a confidence of 99%. LDA achieved sensitivity of 86% and specificity of 98% and leave one sample out model achieved an F1 score 0.83.

Multivariate analysis of IDS vs Primary surgery (Cancer)

To explore the effect of chemotherapy on cancer in peritoneal tissue, analysis of cancer from primary surgery and IDS was performed. As there are only five samples of peritoneal tissue from participants who had primary surgery, this group is also limited. To explore differences between the groups, five IDS samples were picked at random. There were 490 spectra in this analysis, 245 from the primary surgery group and 245 from the IDS group. Two spectra were replaced due to saturation. The spectra were then pre-processed together. Mean centred PCA was performed, and analysis of variance demonstrated eight PCs that reached the threshold of 99% confidence. The PCs are listed in Table 18 and their loadings in Figure 75.

Principal Component	F value ($F_{crit} 11, p=0.001$)
10	119
18	49
4	41
12	18
7	17
2	17
6	17
20	15

Table 18 – Principal components with statistical significance in order of F value for interval debulking surgery vs primary surgery (cancer).

There is some repetition across the PCs, however overall, the variables with a positive influence are hydroxyapatite, phenylalanine, glycogen, disulphide stretch in protein, amino acids (tyrosine and phenylalanine), nucleotides (thymine, adenine, guanine, cytosine and uracil (ring)), lipids and amide I. The negative influence includes collagen, amide III beta sheets, carotenoids and 1408 cm^{-1} unassigned.

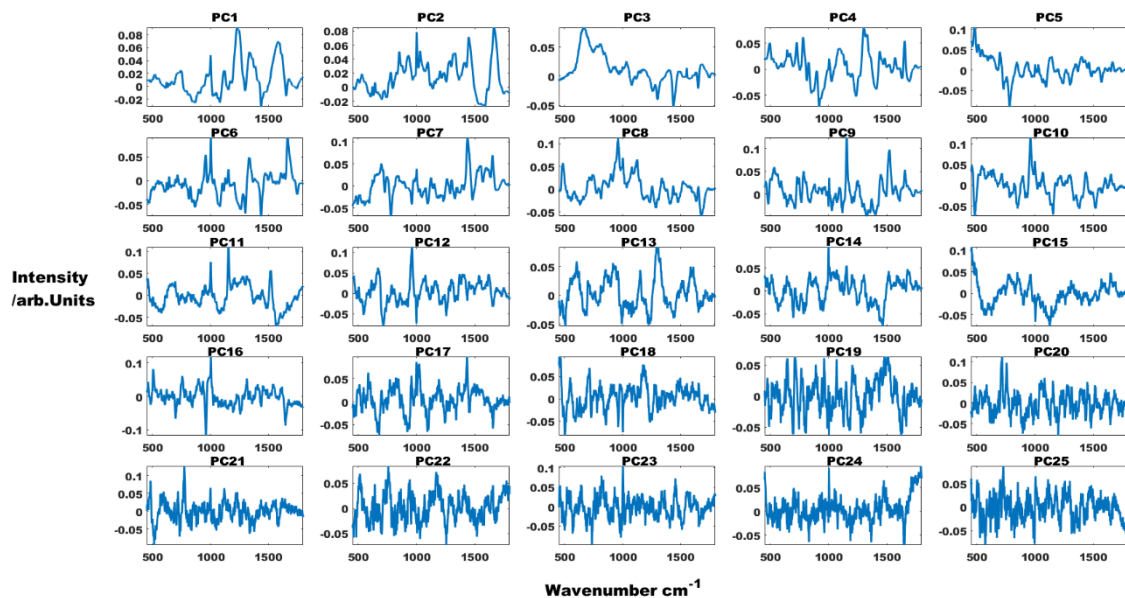


Figure 75 - Twenty-five principal components generated from primary surgery and interval debulking surgery spectra (cancer). Each principal component is plotted with wavenumber cm^{-1} on the x-axis and intensity on the y-axis.

LDA achieved a sensitivity of 92% and specificity of 86%. The cross-validation model for this group achieved a sensitivity of 25% and specificity of 31%.

4.6.3 Variations within the slides

The tumour burden of the slides used varied; some slides had tumour throughout, and others had areas of tumour as well as areas with no cancer. For the purposes of measurement of this tissue, the areas of tumour were identified and marked out by the consultant pathologist. To understand whether Raman spectroscopy can discern the changes between cancer and areas near the cancer, within the same 3 mm section, measurements were taken of these two areas in the small number of cases that had both representative areas and the results are outlined in this section.

Participant 007

This participant had ovarian tissue samples taken at interval debulking surgery. Raman spectral measurements were taken, using the tissue measurement protocol, from an area representing cancer and an area representing fibrosis and analysed together. PC3 and PC2 explained the data with a confidence of 99% on ANOVA and were used to create a linear discriminate model which achieved 90% sensitivity and 94% specificity.

To interrogate whether this area near cancer had different features on Raman spectroscopy when compared with benign tissue taken elsewhere from the same participant, a three-group model was assessed. The groups were cancer, near cancer (same slide as cancer) and benign (taken from a different tissue block from this participant). Four principal components explained the variance in this data with a confidence of 99% on ANOVA and were used to create a linear discriminate model, the results of which are detailed in Table 19.

	Sensitivity	Specificity	F1 score
Cancer	88%	97%	0.90
Near cancer	92%	98%	0.94
Benign	98%	94%	0.93

Table 19 - Performance scores of three class linear discriminant model for variation within the same participant. Included in this table is the linear discriminant analysis model performance and the F1 score.

Despite the small numbers, this supervised classification model has correctly classified the three tissue types with high accuracy.

Ovarian tissue (Primary surgery)

Six participants who had tissue samples collected at primary surgery had both areas of cancer and areas without cancer in their samples. One was excluded from this exploratory analysis due to poor sample quality. The remaining five participants had clear areas of cancer and a separate area near the cancer that was benign. Their data have been pooled to look at a two-class analysis of cancer and near cancer. All five near cancer areas represented stromal fibrosis.

490 spectra were used for this analysis, 245 from cancer and 245 from near cancer. Four principal components were demonstrated to be able to describe the

data with 99% confidence. Against an F_{crit} of 11, the significant PCs were PC2 (F value 400), PC3 (F value 205), PC4 and PC1 (F value 19 & 17). The variables with a positive influence were nucleic acid bases and ring vibrations, DNA phosphate stretch, amino acids (tyrosine and phenylalanine) and amide I C=O stretch. Collagen, carotenoids and amide III beta sheet were the variables of negative influence.

Linear discriminant model built using these PCs achieved a sensitivity of 98% and specificity of 98%. A histogram displaying the scores of this model is seen in Figure 76.

The analysis was repeated with leave one sample out cross validation and the model achieved a sensitivity of 95% and specificity of 96%. The F1 score for this model is 0.95.

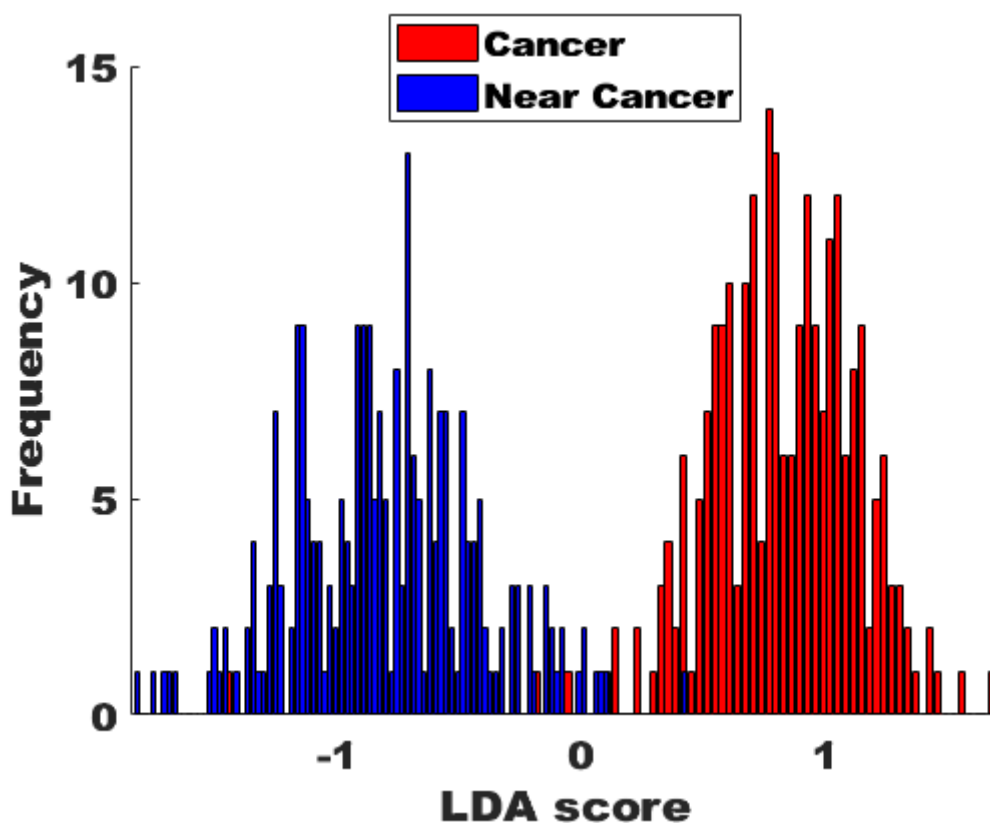


Figure 76 – Histogram plot of linear discriminant analysis scores classifying cancer and near cancer in the same participant with sensitivity of 98% and specificity of 98%. The blue histogram represents the linear discriminant scores for near cancer and the red histogram, the scores for cancer.

Peritoneal tissue (IDS)

18 participants had peritoneal samples collected at interval debulking surgery that had both areas with cancer and areas without cancer. Their data have been pooled to look at a two-class analysis of cancer and near cancer. The areas of near cancer had fibrosis.

1,764 spectra were used for this analysis, 882 from cancer and 882 from near cancer. Against an F_{crit} of 10.8, there were 11 principal components that reached the 99% significance level. PC3 had a distinctly high F value at 495 and the variables in this PC were a negative influence from collagen and amide III beta sheet and a positive influence from amino acids (tyrosine, phenylalanine), nucleotides (adenine, cytosine, uracil and guanine) and deoxyribose. PC1 demonstrates a strong positive influence for amide III beta sheet and then nucleic acid pyrimidine ring, guanine and phenylalanine. There is a negative influence for lipids in this PC.

A linear discriminant model was built using the principal components that reach significance. This model achieved a sensitivity of 77% and specificity of 87%. The analysis was repeated with leave one sample out cross validation which achieved a sensitivity of 61% and a specificity of 64%.

It is noted that the areas of cancer for peritoneal tissue, likely due to it being a site of metastases, were less condensed when compared to the ovarian samples.

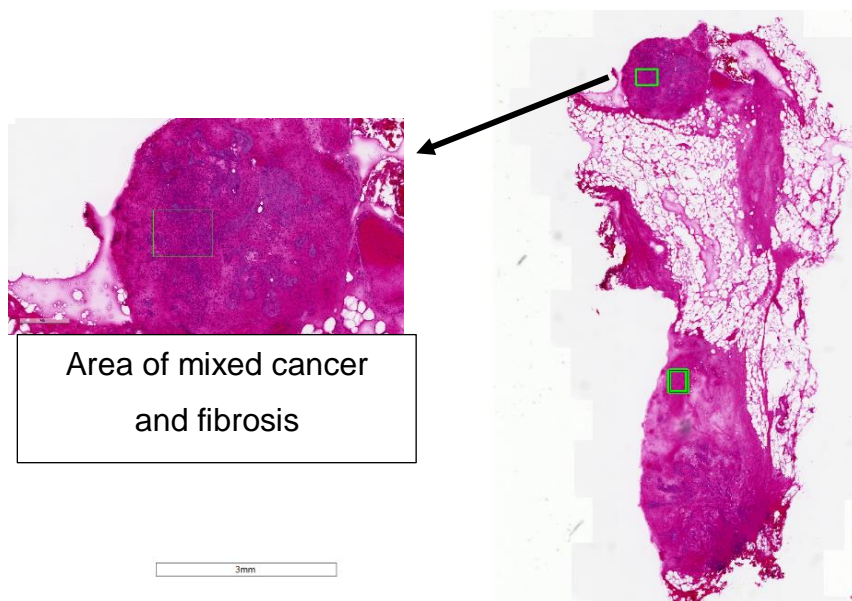


Figure 77 – H&E slide of fresh frozen peritoneal tissue. This sample was taken at interval debulking surgery. The green box at the top of the specimen is from an area with cancer and the green box near the middle of the specimen is from an area of fibrosis. The area with cancer is enlarged to demonstrate the areas of fibrosis interspersed within the cancer.

It is possible that not all of the 49 spectra from this area of measurement represent cancer. Figure 77 illustrates one of the samples used to build this model. To reduce the variation within the measurements, this analysis has been repeated using the mean of the spectra per participant. This achieved an LDA sensitivity of 94% and specificity of 94%. Leave one mean sample out cross validation achieved 67% and 72%. Whilst this is an improvement on the previous model, it does not explain the difference in performance between this group and the ovarian group.

4.7 Summary of results

The biochemical changes in ovarian and peritoneal tissue seen in cancer in this work are characterised by lower concentrations of carotenoids and collagen and higher concentrations of nucleic acid base activity, glycogen, lipids and amino acids. Interestingly, the inverse appears to be true after chemotherapy treatment. PCA-LDA models for the classification of cancer achieved cross validation sensitivities and specificities of 94% and 98% in ovarian tissue and 86% and 98% in peritoneal tissue when compared to benign, and 98 and 89% in ovarian tissue when compared to borderline.

In samples taken from patients after chemotherapy treatment, this technique was able to detect cancer in peritoneal tissue when compared to post chemotherapy benign tissue with a cross validation sensitivity and specificity of 68% and 81%.

Variation in tissue type within the same sample were correctly classified with accuracies greater than 0.9 in ovarian tissue. This was harder to demonstrate in peritoneal tissue, with a pooled sensitivity of 61% and specificity of 64%.

4.8 Discussion

This work set out to assess Raman spectroscopy against histology for its ability to detect cancer in peritoneal and ovarian tissue from carefully characterised patients and evaluate the effect of chemotherapy on the ability of Raman spectroscopy to detect cancer in this group.

Increased nucleic acid base activity, glycogen, lipids and amino acids, and decreased collagen and carotenoid concentrations were characteristic of cancer in ovarian tissue. With the exception of carotenoids which are not assigned in their work, these changes are consistent with the peak assignments in the previous pilot study by Maheedhar and colleagues, and add to the biochemical changes found by Krishna and colleagues (Krishna et al., 2007, Maheedhar et al., 2008). The previous pilot study achieved sensitivity and specificity of 100% with independent testing, whilst this work was able to achieve a sensitivity and specificity of 94% and 98% for cancer detection in ovarian tissue after leave one out cross validation when comparing cancer and benign ovarian tissue. This study had double the participant numbers and more variation in the benign comparison group than seen in the pilot study by Maheedhar et al but was still able to demonstrate the ability of Raman spectroscopy to detect cancer in ovarian and peritoneal tissue with high accuracies (Maheedhar et al., 2008).

As the body of work on Raman spectroscopy in ovarian cancer is limited, there is no previous work on borderline tumours, peritoneal disease or chemotherapy effects on ovarian and peritoneal tissue. The current work has demonstrated high diagnostic performance, sensitivity and specificity of 98% and 89%, for the detection of cancer from borderline ovarian cancer tissue for the first time. This finding is promising for the use of Raman spectroscopy for intraoperative assessment of pelvic masses. Currently, when the malignant potential of a mass is uncertain, an excision biopsy is taken intraoperatively and sent for fast histological turn around (frozen section), for a diagnosis to enable decision making regarding the extent of the surgery. Frozen sections have the limitation of poor sampling, inferior quality sections and in some areas increased anaesthetic time due to the location of the histopathology laboratory (Jaafar, 2006). Whilst further translational research is required, these results suggest that Raman spectroscopy has the potential to be used as an intraoperative test in place of frozen sections.

Due to the very small sample numbers in the ovarian tissues, the post chemotherapy performance is best explored with the peritoneal tissue. The prediction model for peritoneal cancer when compared to benign tissue for patients having undergone chemotherapy treatment prior to surgery and thus tissue sampling, achieved a sensitivity and specificity of 68% and 81% and F1

score of 0.73. Whilst this performance is fair, higher performance results were achieved with the same comparison (that is peritoneal cancer versus benign peritoneal tissue) in participants that had primary surgery and thus had not received chemotherapy, 78% and 84% respectively and F1 score 0.83. Excluding chemotherapy, the main difference between these groups was a smaller sample size in the primary surgery comparison groups, 17 vs 38 participants, however this does not account for the difference in sensitivity, as a smaller sample size is more likely to cause a type II error rather than improve diagnostic performance. One can infer then that chemotherapy use affects cancer detection in peritoneal tissue however, in a small two group comparison of peritoneal cancers, this assertion was not supported. In this analysis of 10 peritoneal cancer tissues, five of which had exposure to chemotherapy prior to Raman and five had not, the cross-validation model failed, sensitivity 25% and specificity 31%, to predict differences between the cancer in these two cancer groups suggesting that chemotherapy does not create a significant enough difference in residual cancer to be a detectable difference in the two groups. The LDA model for this comparison was able to detect differences between the peritoneal cancer pretreated with chemotherapy and the peritoneal cancer not previously exposed to chemotherapy with a sensitivity of 92% and specificity of 86%. This raises the possibility that the cross validation prediction model failed due to low sample numbers meaning that leaving one sample out did not leave enough features to correctly predict the groups. The impact of sample size and recruitment are further discussed in chapter 5 of this thesis.

Whilst variations within the samples was not planned within the scope of this work, it has resulted in impressive diagnostic performance which is promising for the use of Raman spectroscopy in the assessment of residual disease in ovarian cancer. Cancer within the same 3 mm slide as fibrosis and benign areas was correctly classified with high accuracies greater than 0.9. As discussed in chapter 1, complete cytoreduction is pivotal to increasing ovarian cancer survival but assessment of post chemotherapy tissue can be difficult due to fibrosis (Vergote et al., 2010a). This work demonstrates that Raman spectroscopy has the potential to be used as a tool to guide surgeons to cancer within fibrosis. The availability of such a tool would allow surgeons the option of intraoperative testing of areas of uncertainty at interval debulking surgery. In 2018 rapid evaporative

ionisation mass spectrometric technique (REIMS), 'iKnife', was demonstrated to be an accurate intraoperative tool for differentiating cancer from benign (cross validated accuracy 0.94) and cancer from borderline (cross validation accuracy 0.90) using snap frozen ovarian tissue. This represents a lower accuracy than achieved using Raman spectroscopy for this work. More importantly, the REIMS technique burns tissue in order to generate aerosol for mass spectroscopy (Phelps et al., 2018). This is a destructive technique ensuring that the area of testing cannot be reanalysed or used for other diagnostic, or adjuvant tests seen in cancer management. Whilst this may not be critical in patients having post chemotherapy surgery, it might pose a major problem in patients having primary surgery limiting its utility compared to a Raman spectroscopy probe. As an adjunct to the current care, a Raman spectroscopy probe could reduce the need for frozen sections and facilitate decisions regarding the extent of surgery thus enabling complete cytoreduction. Further translational research is required.

Chapter 5 - Conclusions and Further Work

This chapter will build on the discussions started in chapter 3 and chapter 4 of this thesis. I will first address the limitations of the study and then discuss the potential for future work based on the contributions of this study. I will then conclude this thesis.

5.1 Study Limitations

Sample size

A limiting factor in this study was sample size. Whilst participant numbers were higher than previously published work, they became diluted when divided into different groups for analysis making independent testing nonviable. Previous work has selected women with known cancer and women with known benign disease to compare cancer and benign. In designing this study for women presenting with symptoms of ovarian cancer, I inadvertently relinquished control over the case mix and subgroup numbers. With respect to the plasma study, this had the advantage of ensuring that the diagnostic model would be reflective of, and applicable to, the population of women it would be used for and in this case, has highlighted a difference in diagnostic performance compared to comparison of selected known cancer and benign controls. For ovarian and peritoneal tissue, it has also created an opportunity to assess borderline tumours for the first time.

Be that as it may, I must acknowledge that the main influence on sample size in this work was time. The planned recruitment period for this study was shortened due to the length of my research post and the impact of recruiting patients and collecting data, in most parts, alone, as well as delays at the start of the project due to the COVID-19 pandemic and associated restrictions on lab activity and clinical research. Furthermore, due to the nature of measurements and analysis used in this work, batch measurement of samples was required meaning that a dedicated measurement and analysis time had to be factored in, further reducing recruitment time. Whilst protocols developed to ensure the stability of plasma during prolonged periods at room temperature aided independent recruitment and safe transport of samples across sites, patient recruitment was time consuming which meant that attempts from clinical staff to help with recruitment and sample collection across both sites became unrealistic. The distance

between the sites and oncology clinics being held at the same time on both sites further restricted my ability to recruit efficiently. The original study plan included a blood sample after first cycle of chemotherapy and at the end of treatment however a pragmatic decision was made not to pursue these appointments as dividing my time further would have had a significant impact on overall recruitment.

Histopathology consensus

In previous work looking at Raman spectroscopy of biological samples, two or three pathologists were consulted due to a known lack of consensus between pathologists for cancer and pre-cancer (Stone et al., 2004). One potential limitation of this work was that only one pathologist was consulted for histopathological assessment of the tissue slides and thus identification of the site on the slide at which Raman Spectroscopy was undertaken. It is important to note though that all participants had a formal histological diagnosis as part of their clinical care by one of the gynaecology pathologists at their respective Trust, and there was no discrepancy between their clinical diagnosis and diagnosis given for their research samples.

Another limitation of this work is establishing a protocol that accounts for the unknowns. Whilst H&E slides were marked by a consultant pathologist to determine where to measure, the viability of these areas for measurements could not be determined until the Raman slides were defrosted and scanned. This meant that there was some decision making required on my part regarding the corresponding area on the Raman slide to measure, particularly in cases where the slide was slightly distorted from storage. This was deemed an acceptable complication to measurements as it avoided alternative techniques to tissue preparation that would introduce contaminants that create Raman contributions however, it creates some interobserver differences such that if the same samples were to be remeasured, outside of changes expected from another freeze thaw cycle, the same results might not be achieved. To mitigate this, the area measured was marked on the digital H&E slides to ensure the work is reproducible and I received training from the histopathologist and guidance on the features of cancer in the slides prepared for this work. In future work, should

time allow, measurement of the whole Raman slide would create an opportunity for retrospective review of the white light image by a histopathologist and only spectra in the identified region used for analysis. A better option should the technology become available, would be integration of artificial intelligence to overlay the marked H&E image and identify the relevant areas to be measured.

Previous studies

As discussed in section 1.6, previous work applying Raman spectroscopy to ovarian cancer is limited. In some of the earlier work using Raman spectroscopy to assess biological samples, not all the peaks were assigned by the authors to specific molecules. It is expected that as more work is done on Raman spectroscopy of epithelial cancers, the reference tables for peak assignments will become more extensive thus expanding our understanding of the biochemical differences that separate disease and non-disease states of biological samples. In this work, there were three peaks each from the plasma and tissue studies that I could not assign to molecules.

Since the initial literature search and commencement of this study, there has been further published work looking at Raman spectroscopy in ovarian cancer, including the use of surface enhanced Raman spectroscopy to predict chemotherapy responsiveness and/or resistance (Asare-Werehene et al., 2023, Tan et al., 2022, Honda et al., 2021). There are two studies of note assessing plasma; Giamougiannis and colleagues assessed Raman spectroscopy in ovarian cancer, using urine, serum and plasma. Participants were recruited consecutively which reduced patient selection bias and created a diverse group of benign pathologies within the benign group, more reflective of the population of women likely to require investigations for suspected ovarian cancer. This study also had a good sample size, 116 cancer and 307 benign. The plasma and serum groups were divided into patients that had not received treatment, 71, and patients that had received chemotherapy treatment, 45, compared to a control group, 307, with benign gynaecological conditions. Multiple models were used to explore separation within the groups and the plasma model was the best performing model. Using partial least square discriminant analysis and independent testing, the diagnostic model achieved a sensitivity of 59% and specificity of 90% for cancer detection in patients who have not received any treatment. This is comparable to the previous work by Giamougiannis and

colleagues and the results of cancer detection in this thesis using PCA based modelling. The model using urine measurements achieved a sensitivity of 45% and specificity of 85% (Giamougiannis et al., 2021b). The study was robust in its patient recruitment approach, sample size and use of different models to find the best diagnostic performance of this technique. It is somewhat disappointing that even with consecutive recruitment, none of the participants had borderline tumours however it is unclear at what stage in the clinical pathway patients were recruited as this may account for the exclusion of the patient group. Within the analysis of their work, Giamougiannis and colleagues suggest that some of the peaks seen in their cancer group, and to a lesser extent their neoadjuvant cancer group, are related to mucin which they attribute to CA-125 (mucin-16). This is contradictory to the findings of Paraskeveidi and colleagues who concluded that differences in CA-125 levels were not responsible for the separation seen in their cancer and benign groups (Paraskevaidei et al., 2018). With the exception of the phenylalanine peak traditionally seen at 1000 cm^{-1} , none of the remaining five peaks attributed to mucin by Giamougiannis and colleagues ($880, 950, 1380, 1600, 1680\text{ cm}^{-1}$) (Giamougiannis et al., 2021b) are seen in either my plasma measurements in this thesis or the other recent work on Raman spectroscopy in ovarian cancer by Chen and colleagues. In the study by Chen and colleagues, 79 healthy participants are compared to 95 symptomatic participants, of which 62 are diagnosed with ovarian cancer and 33 are diagnosed with a benign ovarian cyst. SelectKBest function in Python and chi-squared test were used select relevant spectral features and back-propagation neural network was used to train models, which achieved a sensitivity and specificity of 83% and 82% for cancer detection with independent testing. As is evident in their work, the separation of healthy or normal participants from participants with benign ovarian pathology highlights the differences in these groups, which are significant enough to be able to distinguish three separate states of ovarian health using Raman spectroscopy. Whilst the epidemiology of the participants and CA-125 levels is not included to allow for comparisons with other work, it is clear that this was a good study with groups that better reflected the patient population than previous work on this topic and had ample participant numbers, albeit unbalanced groups. The study explored another option of machine learning and validated their results with independent testing (Chen et al., 2022a).

The only relevant recent tissue study compared 4 ovarian cancer, 3 endometrial cancer and 1 benign mucinous cyst using a hand held probe. A total of 27 *ex vivo* specimens of ovarian tissue, uterine tissue, omentum and fallopian tube were taken from nine patients and an average of five spectral single point measurements were taken per specimen. Only 70 of the 125 spectra were used in the analysis, on account of omentum and low cancer burden specimens being excluded. Of the 70 spectra utilised 42 were benign and 28 were cancer. Patients who had received chemotherapy prior to surgery were not separated within the cancer group. It is unclear how many patients made up the 70 spectra used in analysis however support vector machine was used to create a diagnostic model and leave one patient out was used to assess the prediction performance of this model. The SVM model achieved a sensitivity of 93% and specificity of 88% but the cross validation results are not given. There is a lot of ambiguity around the study methods and analysis of this paper; a lot of spectra are collected from a very small number of specimens for example the benign group comprises of measurements from four ovarian samples taken from the same participant. After the exclusion of a large number of spectra, it is unclear what the make up of the remaining 28 cancer spectra are and how many participants they represent. Lastly, the mix of endometrial and ovarian cancers highlights the efficacy of Raman spectroscopy for cancer detection, but does not aid in the understanding of the biochemical changes underpinning ovarian cancer (David et al., 2022).

There is a growing body of work looking at haptoglobin measurement in ovarian cyst fluid using surface enhanced Raman spectroscopy for detection of ovarian cancer. This technique has achieved high accuracies greater than 90% and in all the published work it has been compared to the performance of CA-125 for ovarian cancer detection. This is an unfair comparison, and seems clinically irrelevant, as the role of CA-125 is risk assessment prior to surgery and to decide if surgery is necessary and haptoglobin measurements cannot be taken until cyst fluid is aspirated at the time of surgery (Perumal et al., 2019, Beffara et al., 2020, Moothanchery et al., 2022). One study compared haptoglobin performance with frozen sections and reported 100% accuracy for frozen sections and 90.8% accuracy for haptoglobin measurements within their work. This is promising for haptoglobin as a test to replace frozen sections due to the quicker turn around time with a hand held Raman device (Perumal et al., 2019) and overcoming some

of the limitations of frozen sections such as availability of a pathologist and freezing artefacts. Frozen sections have also been demonstrated to not perform well with borderline tumours with an accuracy rate of 78.6% (Jaafar, 2006). The non-cancer group in the work by Perumal and colleagues included borderline tumours. Cancer and borderline tumour detection in this thesis, using standard Raman spectroscopy, outperformed haptoglobin performance with SERS with sensitivities and specificities of, 94% and 98%, and 98% and 89%, versus 95% and 98% respectively.

5.2 Future work

Moving forward, this work could be advanced in terms of increasing sample size, reassessing the effect of chemotherapy on the detection of cancer, and considering Raman probe measurements for tissue.

Sample size

As discussed in limitations, whilst sample size was appropriate for the duration of recruitment and exceeded previous work on this topic (at the time of design of the study), subgroup analysis was difficult as sample sizes became too small for independent testing and for the results of the analysis to be confidently considered generalisable to the population. This was inevitable due to lack of extensive evidence to perform an effective sample size calculation at the beginning of the study and the real-life constraints of resources and time. More recent biofluid work has involved large sample sizes but more importantly, the growing trend of consecutive recruitment as seen in my study. For both tissue and plasma, future work will need to factor in subgroup analysis of other ovarian pathology such as borderline tumours when calculating total sample size for the study. In adopting the approach by Chen and colleagues, I would also recommend separating the healthy and benign controls (Chen et al., 2022b) in both tissue and biofluid work resulting in following four overall groups:

- normal or healthy
- benign ovarian pathology
- borderline ovarian pathology
- cancer

Development of *ex vivo* probe tissue measurements

This work has demonstrated the potential for Raman spectroscopy to differentiate between benign, borderline and cancer tissue with high accuracies. To consider this technique intraoperatively, and potentially replace the need for frozen sections, the next proposed step would be *ex vivo* measurements of snap frozen tissue blocks from the three groups with a Raman probe. Raman probes are portable devices that allow quick measurements to be taken and as discussed in chapter 1, have been adapted for the access needs of each tumour site. For example, fibreoptic probes that fit in endoscopic channels for use at endoscopy for cancer detection in the oesophagus. The performance of the model with this form of measurement needs to be assessed:

- 1) when areas of tissue are not carefully selected
- 2) when tissue contains more than one pathology i.e. cancer and benign or borderline and benign
- 3) for the suitability of the different types of Raman probes for ovarian cancer.

It would be expected that sufficient evidence from this would lead to *in vivo* measurements and large scale clinical trials.

Reassessing chemotherapy effect in peritoneal tissue

This was the first work looking at the effect of previous chemotherapy treatment on cancer detection within peritoneal tissue in ovarian cancer and as such, there is a lot of learning from this work. We have established that cancer and non-cancer within the same small sample can be differentiated with high accuracies even after chemotherapy however the overall accuracy for cancer detection in post chemotherapy tissue was not as good as seen in tissue taken at primary surgery (F1 score 0.73 vs 0.83). As detailed in the discussion in section 4.8, It is unclear from this work whether there is a true chemotherapy effect on cancer detection at interval debulking surgery using Raman spectroscopy. Further work is needed in a trial adequately powered to quantify the effect of previous chemotherapy on cancer detection. It is expected that sufficient evidence would lead to large *in vivo* trials to assess the potential of Raman probes to detect cancer at interval debulking surgery with an aim of solving the clinical need for an objective assessment of residual disease.

5.3 Conclusion

This work confirms that Raman spectroscopy has great potential as a diagnostic test for ovarian cancer by detecting biochemical changes that occur in cancer and classifying cancer and borderline ovarian pathology. Depending on the modelling technique, it performs better than the currently used test CA-125.

This work has contributed to the understanding of the biochemical changes in ovarian and peritoneal tissue in ovarian cancer and the effect of chemotherapy on the ability of the technique to detect those changes. Further study is required on the clinical applications of this technique for intraoperative residual disease assessment and risk stratification of ovarian masses.

Appendices

Appendix A: HRA approval



Dr Diana Frimpong
Senior Clinical Research Fellow UHBW, PhD Student
University of Exeter
University Hospitals Bristol and Weston NHS
Foundation Trust
St Michaels Hospital
Southwell Street
Bristol
BS2 8EG

Email: approvals@hra.nhs.uk
HCRW.approvals@wales.nhs.uk

07 May 2021

Dear Dr Frimpong

**HRA and Health and Care
Research Wales (HCRW)
Approval Letter**

Study title:	Molecular Spectroscopy in Identification and Assessment of Ovarian cancer
IRAS project ID:	288711
Protocol number:	2020-21-12
REC reference:	21/NW/0092
Sponsor	University of Exeter

I am pleased to confirm that [HRA and Health and Care Research Wales \(HCRW\) Approval](#) has been given for the above referenced study, on the basis described in the application form, protocol, supporting documentation and any clarifications received. You should not expect to receive anything further relating to this application.

Please now work with participating NHS organisations to confirm capacity and capability, [in line with the instructions provided in the "Information to support study set up" section towards the end of this letter.](#)

How should I work with participating NHS/HSC organisations in Northern Ireland and Scotland?

HRA and HCRW Approval does not apply to NHS/HSC organisations within Northern Ireland and Scotland.

If you indicated in your IRAS form that you do have participating organisations in either of these devolved administrations, the final document set and the study wide governance report

(including this letter) have been sent to the coordinating centre of each participating nation. The relevant national coordinating function/s will contact you as appropriate.

Please see [IRAS Help](#) for information on working with NHS/HSC organisations in Northern Ireland and Scotland.

How should I work with participating non-NHS organisations?

HRA and HCRW Approval does not apply to non-NHS organisations. You should work with your non-NHS organisations to [obtain local agreement](#) in accordance with their procedures.

What are my notification responsibilities during the study?

The standard conditions document "[After Ethical Review – guidance for sponsors and investigators](#)", issued with your REC favourable opinion, gives detailed guidance on reporting expectations for studies, including:

- Registration of research
- Notifying amendments
- Notifying the end of the study

The [HRA website](#) also provides guidance on these topics, and is updated in the light of changes in reporting expectations or procedures.

Who should I contact for further information?

Please do not hesitate to contact me for assistance with this application. My contact details are below.

Your IRAS project ID is **288711**. Please quote this on all correspondence.

Yours sincerely,



Natalie Marking
Approvals Specialist

Email: approvals@hra.nhs.uk

Copy to: *Ms Pam Baxter*

Appendix B: Research Ethics Committee



Health Research Authority

North West - Preston Research Ethics Committee

Barlow House
3rd Floor
4 Minshull Street
Manchester
M1 3DZ

Please note: This is the favourable opinion of the REC only and does not allow you to start your study at NHS sites in England until you receive HRA Approval

07 May 2021

Dr Diana Frimpong
Senior Clinical Research Fellow UHBW, PhD Student University of Exeter
University Hospitals Bristol and Weston NHS Foundation Trust
St Michaels Hospital
Southwell Street
Bristol
BS2 8EG

Dear Dr Frimpong

Study title:	Molecular Spectroscopy in Identification and Assessment of Ovarian cancer
REC reference:	21/NW/0092
Protocol number:	2020-21-12
IRAS project ID:	288711

Thank you for your letter of 28 April 2021, responding to the Research Ethics Committee's (REC) request for further information on the above research and submitting revised documentation.

The further information has been considered on behalf of the Committee by the Chair.

Confirmation of ethical opinion

On behalf of the Committee, I am pleased to confirm a favourable ethical opinion for the above research on the basis described in the application form, protocol and supporting documentation as revised, subject to the conditions specified below.

Good practice principles and responsibilities

The [UK Policy Framework for Health and Social Care Research](#) sets out principles of good practice in the management and conduct of health and social care research. It also outlines the responsibilities of individuals and organisations, including those related to the four elements of [research transparency](#):

1. [registering research studies](#)
2. [reporting results](#)
3. [informing participants](#)
4. [sharing study data and tissue](#)

Conditions of the favourable opinion

The REC favourable opinion is subject to the following conditions being met prior to the start of the study.

Confirmation of Capacity and Capability (in England, Northern Ireland and Wales) or NHS management permission (in Scotland) should be sought from all NHS organisations involved in the study in accordance with NHS research governance arrangements. Each NHS organisation must confirm through the signing of agreements and/or other documents that it has given permission for the research to proceed (except where explicitly specified otherwise).

Guidance on applying for HRA and HCRW Approval (England and Wales)/ NHS permission for research is available in the Integrated Research Application System.

For non-NHS sites, site management permission should be obtained in accordance with the procedures of the relevant host organisation.

Sponsors are not required to notify the Committee of management permissions from host organisations

Registration of Clinical Trials

All research should be registered in a publicly accessible database and we expect all researchers, research sponsors and others to meet this fundamental best practice standard.

It is a condition of the REC favourable opinion that **all clinical trials are registered** on a publicly accessible database within six weeks of recruiting the first research participant. For this purpose, 'clinical trials' are defined as the first four project categories in IRAS project filter question 2. Failure to register a clinical trial is a breach of these approval conditions, unless a

deferral has been agreed by or on behalf of the Research Ethics Committee (see here for more information on requesting a deferral:

<https://www.hra.nhs.uk/planning-and-improving-research/research-planning/research-registration-research-project-identifiers/>

If you have not already included registration details in your IRAS application form, you should notify the REC of the registration details as soon as possible.

Further guidance on registration is available at:

<https://www.hra.nhs.uk/planning-and-improving-research/research-planning/transparency-responsibilities/>

Publication of Your Research Summary

We will publish your research summary for the above study on the research summaries section of our website, together with your contact details, no earlier than three months from the date of this favourable opinion letter.

Should you wish to provide a substitute contact point, make a request to defer, or require further information, please visit:

<https://www.hra.nhs.uk/planning-and-improving-research/application-summaries/research-summaries/>

N.B. If your study is related to COVID-19 we will aim to publish your research summary within 3 days rather than three months.

During this public health emergency, it is vital that everyone can promptly identify all relevant research related to COVID-19 that is taking place globally. If you haven't already done so, please register your study on a public registry as soon as possible and provide the REC with the registration detail, which will be posted alongside other information relating to your project. We are also asking sponsors not to request deferral of publication of research summary for any projects relating to COVID-19. In addition, to facilitate finding and extracting studies related to COVID-19 from public databases, please enter the WHO official acronym for the coronavirus disease (COVID-19) in the full title of your study. Approved COVID-19 studies can be found at: <https://www.hra.nhs.uk/covid-19-research/approved-covid-19-research/>

It is the responsibility of the sponsor to ensure that all the conditions are complied with before the start of the study or its initiation at a particular site (as applicable).

After ethical review: Reporting requirements

The attached document "After ethical review – guidance for researchers" gives detailed guidance on reporting requirements for studies with a favourable opinion, including:

- Notifying substantial amendments
- Adding new sites and investigators
- Notification of serious breaches of the protocol
- Progress and safety reports

- Notifying the end of the study, including early termination of the study
- Final report
- Reporting results

The latest guidance on these topics can be found at <https://www.hra.nhs.uk/approvals-amendments/managing-your-approval/>.

Ethical review of research sites

NHS/HSC sites

The favourable opinion applies to all NHS/HSC sites taking part in the study, subject to confirmation of Capacity and Capability (in England, Northern Ireland and Wales) or management permission (in Scotland) being obtained from the NHS/HSC R&D office prior to the start of the study (see "Conditions of the favourable opinion" below).

Non-NHS/HSC sites

I am pleased to confirm that the favourable opinion applies to any non-NHS/HSC sites listed in the application, subject to site management permission being obtained prior to the start of the study at the site.

Approved documents

The final list of documents reviewed and approved by the Committee is as follows:

<i>Document</i>	<i>Version</i>	<i>Date</i>
Covering letter on headed paper [Cover Letter]		04 March 2021
IRAS Application Form [IRAS_Form_05032021]		05 March 2021
Other [Data Management Plan]	1.1	23 April 2021
Other [Provisional Opinion Response Letter]		28 April 2021
Participant consent form [Consent to Contact Form]	1	15 February 2021
Participant consent form [Consent Form]	1.1	26 April 2021
Participant information sheet (PIS) [Participant Information Sheet A]	1.1	26 April 2021
Participant information sheet (PIS) [Participant Information Sheet B]	1.1	26 April 2021
Research protocol or project proposal [Research Protocol]	1.1	16 April 2021
Sample diary card/patient card [Contact Card]	1	17 February 2021
Sample diary card/patient card [Participant Background Information Data Collection Tool]	1	17 February 2021
Sample diary card/patient card [Diagnostic Information Data Collection Tool]	1	15 February 2021
Summary CV for Chief Investigator (CI) [288711_CI CV HRA_Spectroscopy in Ovarian Cancer_V1.0]	1	
Summary CV for student [Curriculum Vitae]		
Summary CV for supervisor (student research)		
Summary, synopsis or diagram (flowchart) of protocol in non technical language [Study Flow Chart]	1	25 February 2021
Summary, synopsis or diagram (flowchart) of protocol in non technical language [Study Flow Chart 2]	1	03 March 2021

Statement of compliance

The Committee is constituted in accordance with the Governance Arrangements for Research Ethics Committees and complies fully with the Standard Operating Procedures for Research Ethics Committees in the UK.

User Feedback

The Health Research Authority is continually striving to provide a high quality service to all applicants and sponsors. You are invited to give your view of the service you have received and the application procedure. If you wish to make your views known please use the feedback form available on the HRA website:

<http://www.hra.nhs.uk/about-the-hra/governance/quality-assurance/>

HRA Learning

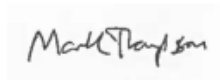
We are pleased to welcome researchers and research staff to our HRA Learning Events and online learning opportunities– see details at:

<https://www.hra.nhs.uk/planning-and-improving-research/learning/>

IRAS project ID: 288711 Please quote this number on all correspondence

With the Committee's best wishes for the success of this project.

Yours sincerely



**On behalf of Professor Karen Wright
Chair**

Email: preston.rec@hra.nhs.uk

Enclosures: "After ethical review – guidance for researchers" [\[SL-AR2\]](#)

Copy to: Ms Pam Baxter

Appendix C: Participant Information Sheet A



Placeholder for local NHS logo
(e.g Bristol or Bath)

Participant Information Sheet

Study Title: Molecular Spectroscopy in Possible Assessment and Detection of Ovarian Cancer

This study is being undertaken as part of a PhD project.

Chief Investigator: Dr Diana Frimpong (PhD student)

Clinical Lead: Miss Claire Newton (Consultant Gynaecological Oncologist)

Sponsor: University of Exeter

We would like to invite you to take part in our research study. Although the study is about cancer, we are also recruiting women who do not have cancer; please do not take this leaflet as an indication on a diagnosis.

Joining the study is entirely up to you. We would like you to understand why the study is being done and what it would involve for you. One of our team will go through this information sheet with you and answer any questions you may have. Please ask us if there is anything that is not clear to you or if you would like more information.

What is the purpose of the study?

We hope that this study will help towards improving the care of women by finding another way of diagnosing ovarian cancer.

To achieve this, we aim to use the results of this study to develop, in the future, a new blood test for diagnosis and an objective tool for assessing cancer removal during surgery.

Why have I been invited?

You have been invited to take part because either:

- your GP has referred you to the hospital to have further checks on your ovary or
- you have been found to have a change on your ovary during an emergency hospital admission.

What is the technique being tested?

The technique being tested for the research study is called Raman Spectroscopy. Raman Spectroscopy is a non-invasive technique that allows us to use light to determine what makes up the sample being tested. This technique has been successful in identifying cancer in breast, prostate and head and neck cancer cases. It has not been used to look for signs of ovarian cancer at surgery in this way before.

What would taking part involve?

It is your decision whether or not to take part in the study. If you choose to take part, you will be given this information sheet to keep and asked to sign a consent form. You are still free to withdraw consent at any time without giving a reason. Your decision whether or not to take part will not influence the care you receive or affect your legal rights.

If after reading the information you agree to take part in the study and provide your consent, the team will then need to collect some health information about you such as medication you take regularly and pre-existing health problems.

A small amount (equivalent to 1 teaspoon) of blood will then, with your consent, be taken for the study.

If your doctor does not give a diagnosis of cancer, we will not need any further samples from you. We will later check your records to find out your diagnosis.

If unfortunately, you are told you have ovarian cancer, we would be very grateful for your continued participation in the study. Depending on what treatment your doctors recommend, we might need a further 1 or 3 blood samples. These will be the same amount as the first sample.

Should you require an operation, we would need to collect 2 to 3 very small samples of tissue (less than the size of your smallest fingernail), from the surgery site where the cancer is to be removed, plus some small amounts of tissue from other areas next to where the cancer is to be removed. No extra tissue will be removed beyond that which the surgeon was planning to remove anyway.

During your follow up at the hospital if there are signs of cancer coming back, we would like as part of the study, to collect another blood sample (equivalent to 1 teaspoon amount), to see if we might have been able to pick up any earlier signs.

Please see the diagram on next page for a summary of the information above.

What are the possible benefits of taking part?

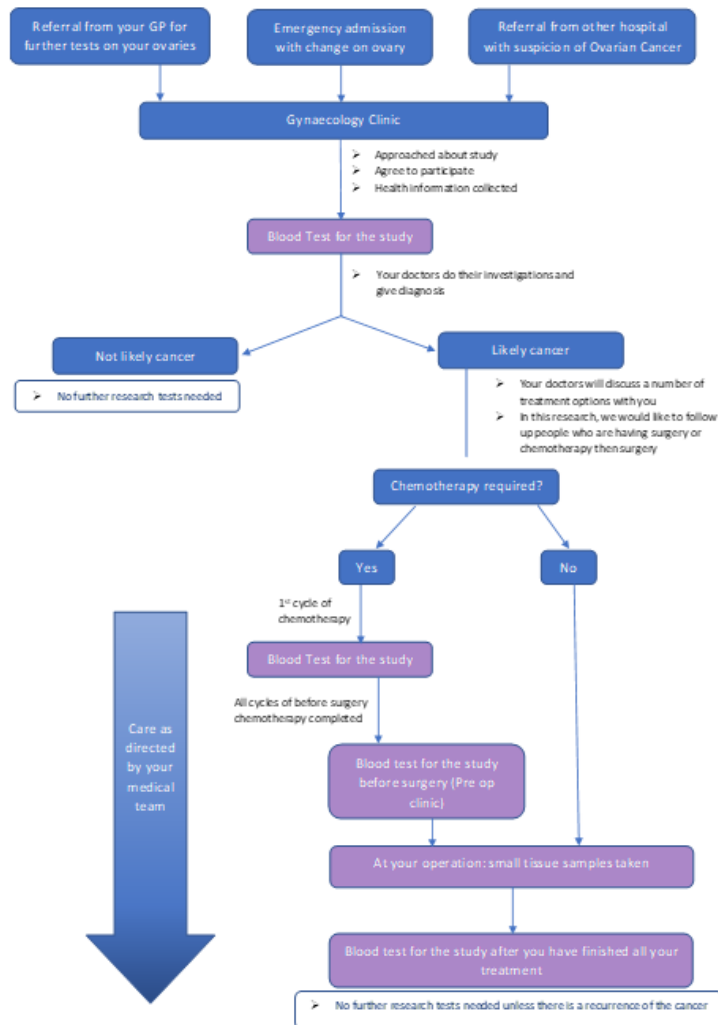
Your participation in this study may not have any direct benefit to you or your care, although it is hoped that the results of this study could make a difference in the early diagnosis and care of women in the future and we thank you for your interest.

What are the possible disadvantages of taking part?

We will make every effort to take the study blood samples at the same time as routine samples being requested by your doctor, to minimise visits. It will also help to reduce the chances of the researcher missing your routine appointments if we offer you a contact card. This will allow the hospital to let the research team know when you are due to visit. The card will have a named contact person, their mobile number and the date or timing of when your next research blood samples are due. Please show this card when you are about to have a blood test and they will contact the researcher.

On occasion, you might require an extra blood sample to be taken in order for the study sample to be obtained. Having any blood sample collected can cause some brief discomfort. When we collect the study sample please let us know if you would like a local anaesthetic cream to desensitise the area prior to the blood sample.

Summary of Participant Journey



Will my taking part in this study be kept confidential?

For the purposes of this study we will also use consent to protect your confidentiality and provide you with choice in your participation. All information collected in this study will be kept strictly confidential and stored either on an encrypted password protected computer, or in a locked cabinet at NHS sites which can only be accessed by the PhD researcher and research supervisors.

You will be allocated a unique participant number, which will ensure the information collected about you and from your blood and tissue samples will be protected and cannot be identified by anyone else.

Any personally identifiable information will be stored separately and securely from information obtained from the research and will be securely destroyed after 5 years. We keep your information for 5 years to allow the research team to check your health records to follow up any changes that have occurred since you finished treatment, such as recurrence of the cancer.

Your rights to access, change or move your information are limited, as we need to manage your information in specific ways in order for the research to be reliable and accurate. If you withdraw from the study, we will keep the samples and information about you that we have already obtained. To safeguard your rights, we will use the minimum personally-identifiable information possible.

Due to regulatory changes in the way that data is processed (General Data Protection Regulation 2018 and the Data Protection Act 2018) the University of Exeter's lawful basis to process personal data for the purposes of carrying out research is termed as a 'task in the public interest'. The University will endeavour to be transparent about its processing of your personal data and this information sheet should provide a clear explanation of this.

If you do have any queries about the University's processing of your personal data that cannot be resolved by the research team, further information may be obtained from the University's Data Protection Officer by emailing dataprotection@exeter.ac.uk or at www.exeter.ac.uk/dataprotection.

If you have any concerns about how the data is controlled and managed for this study then you can also contact the Sponsor Representative, Pam Baxter, Senior Research Governance Officer, whose details are at the end of the information sheet.

What will happen to my samples at the end of the study?

If you agree to participate in the study, you will have an opportunity to choose what happens at the end of the study to the anonymised samples and information collected from you. With your permission, samples and data may be transferred to the Peninsula Research Bank at the University of Exeter. They will be stored securely and used in future research if you provide consent. Alternatively, samples can be destroyed at the end of the study.

You will be able to indicate your choice on the consent form.

Will I be informed of the outcome of the study?

Any results shared from the study will be anonymised to protect your confidentiality.

Anonymised research data and supporting information may also be published openly on the University of Exeter's repository, Open Research Exeter ([ORE Home \(exeter.ac.uk\)](https://ore.exeter.ac.uk))

A plain language summary of the results will also be available on Open Research Exeter should you wish to access a copy of the study results, which can be found at <https://ore.exeter.ac.uk/repository/>

The results of the study will be submitted for publication in scientific journals and may be presented at scientific meetings.

The results will also be shared with cancer charities that have supported the study and social media might also be used to share outcomes from this study in an anonymised format.

Who has reviewed this study?

The study has been reviewed by the Preston Research Ethics Committee and the Health Research Authority (HRA) Assessment process to obtain HRA Approval.

Will the study be monitored?

The study will be monitored in accordance with the University standard audit and monitoring procedures as well as participating NHS Trust's Research and Innovation departments standard procedures.

What if something goes wrong?

If you have any concerns about how you have been approached, or treated during the research study, or experienced any harm as a result of taking part, please contact the lead researcher as below.

If you wish to make a formal complaint, please contact the hospital's Patient Advice and Liaison Service (PALS), or the Sponsor Representative from the **University of Exeter** (as below).

University Hospitals Bristol NHS Foundation Trust
Patient Support and Complaints Team
A201, Welcome Centre
Bristol Royal Infirmary
Upper Maudlin Street
Bristol. BS2 8HW
Tel: 01173421050
Email: PSCT@uhbw.nhs.uk

Head of PALS
RUH Bath NHS Trust
Coombe Park
Bath
BA1 3NG
Tel: 01225825656
Email: ruh-tr.PALS@nhs.net

Sponsor Representative contact details:

Ms Pam Baxter
Senior Research Governance Officer
University of Exeter
Research Ethics and Governance Office
Lafrowda House
St Germans Road
Exeter
EX4 6TL
Tel: 01392 723588
Email: p.r.baxter2@exeter.ac.uk

Thank you for taking the time to read this information sheet and for considering your participation in this research study.

Appendix D: Participant Information Sheet B



Placeholder for local NHS logo

(e.g Bristol or Bath)

Participant Information Sheet B

Study Title: Molecular Spectroscopy in Assessment and Detection of Ovarian Cancer

This study is being undertaken as part of a PhD project.

Chief Investigator: Dr Diana Frimpong (PhD student)

Clinical Lead: Miss Claire Newton (Consultant Gynaecological Oncologist)

Sponsor: University of Exeter

We would like to invite you to take part in our research study. Joining the study is entirely up to you. We would like you to understand why the study is being done and what it would involve for you. One of our team will go through this information sheet with you and answer any questions you may have. Please ask us if there is anything that is not clear to you or if you would like more information.

What is the purpose of the study?

We hope that this study will help towards improving the care of women with ovarian cancer. We aim to use the results of this study to develop, in the future, an objective tool for assessing cancer removal during surgery.

Why have I been invited?

You have been invited to take part because you are receiving treatment for Ovarian Cancer.

What is the technique being tested?

The technique being tested for the research study is called Raman Spectroscopy. Raman Spectroscopy is a non-invasive technique that allows us to use light to determine what makes up the sample being tested. This technique has been successful in identifying cancer in breast, prostate and head and neck cancer cases. It has not been used to look for signs of ovarian cancer at surgery in this way before.

What would taking part involve?

It is your decision whether or not to take part in the study. If you choose to take part, you will be given this information sheet to keep and asked to sign a consent form. You are still free to withdraw consent at any time without giving a reason. Your decision whether or not to take part will not influence the care you receive or affect your legal rights.

If after reading the information you agree to take part in the study and provide your consent, the team will then need to collect some health information about you such as medication you take regularly and pre-existing health problems.

At the time of your operation, we would like to collect 2 to 3 very small samples of tissue (less than the size of your smallest fingernail) from the surgical site where the cancer is to be removed, plus some small amounts of tissue from other areas next to where the cancer is to be removed. No extra tissue will be removed beyond that which the surgeon was planning to remove anyway.

What are the possible benefits of taking part?

Your participation in this study may not have any direct benefit to you or your care, although it is hoped that the results of this study could make a difference in the early diagnosis and care of women in the future and we thank you for your interest.

What are the possible disadvantages of taking part?

We do not expect any disadvantages to you for taking part in this study. The samples we take will not affect your care.

Will my taking part in this study be kept confidential?

For the purposes of this study we will also use consent to protect your confidentiality and provide you with choice in your participation. All information collected in this study will be kept strictly confidential and stored either on an encrypted password protected computer, or in a locked cabinet at NHS sites which can only be accessed by the PhD researcher and research supervisors.

You will be allocated a unique participant number, which will ensure the information collected about you and from your tissue samples will be protected and cannot be identified by anyone else.

Any personally identifiable information will be stored separately and securely from information obtained from the research will be securely destroyed after 5 years. We keep your information for 5 years to allow the research team to check your health records to follow up any changes that have occurred since you finished treatment, such as recurrence of the cancer.

Your rights to access, change or move your information are limited, as we need to manage your information in specific ways in order for the research to be reliable and accurate. If you withdraw from the study, we will keep the samples and information about you that we have already obtained. To safeguard your rights, we will use the minimum personally-identifiable information possible.

Due to regulatory changes in the way that data is processed (General Data Protection Regulation 2018 and the Data Protection Act 2018) the University of Exeter's lawful basis to process personal data for the purposes of carrying out research is termed as a 'task in the public interest'. The University will endeavour to be transparent about its processing of your personal data and this information sheet should provide a clear explanation of this.

If you do have any queries about the University's processing of your personal data that cannot be resolved by the research team, further information may be obtained from the University's Data Protection Officer by emailing dataprotection@exeter.ac.uk or at www.exeter.ac.uk/dataprotection.

If you have any concerns about how the data is controlled and managed for this study then you can also contact the Sponsor Representative, Pam Baxter, Senior Research Governance Officer, whose details are at the end of the information sheet.

What will happen to my samples at the end of the study?

If you agree to participate in the study, you will have an opportunity to choose what happens at the end of the study to the anonymised samples and information collected from you. With your permission, samples and data may be transferred to the Peninsula Research Bank at the University of Exeter. They will be stored securely and used in future research if you provide consent. Alternatively, samples can be destroyed at the end of the study.

You will be able to indicate your choice on the consent form.

Will I be informed of the outcome of the study?

Any shared results from the study will be anonymised to protect your confidentiality.

Anonymised research data and supporting information may also be published openly on the University of Exeter's repository, Open Research Exeter ([ORE Home \(exeter.ac.uk\)](http://ore.exeter.ac.uk))

A plain language summary of the results will also be available on Open Research Exeter should you wish to access a copy of the study results, which can be found at <https://ore.exeter.ac.uk/repository/>

The results of the study will be submitted for publication in scientific journals and may be presented at scientific meetings.

The results will also be shared with cancer charities that have supported the study and social media might also be used to share outcomes from this study in an anonymised format.

Who has reviewed this study?

The study has been reviewed by the Preston Research Ethics Committee and the Health Research Authority (HRA) Assessment process to obtain HRA Approval.

Will the study be monitored?

The study will be monitored in accordance with the University standard audit and monitoring procedures as well as participating NHS Trust's Research and Innovation departments standard procedures.

What if something goes wrong?

If you have any concerns about how you have been approached, or treated during the research study, or experienced any harm as a result of taking part, please contact to the lead researcher as below.

If you wish to make a formal complaint, please contact the hospital's Patient Advice and Liaison Service (PALS), or the Sponsor Representative from the **University of Exeter** (as below).

University Hospitals Bristol NHS Foundation Trust
Patient Support and Complaints Team
A201, Welcome Centre
Bristol Royal Infirmary
Upper Maudlin Street
Bristol. BS2 8HW
Tel: 01173421050
Email: PSCT@uhbw.nhs.uk

Head of PALS
RUH Bath NHS Trust
Coombe Park
Bath
BA1 3NG
Tel: 01225825656
Email: ruh-tr.PALS@nhs.net

Sponsor Representative contact details:

Ms Pam Baxter
Senior Research Governance Officer
University of Exeter
Research Ethics and Governance Office
Lafrowda House
St Germans Road
Exeter
EX4 6TL
Tel: 01392 723588
Email: p.r.baxter2@exeter.ac.uk

Thank you for taking the time to read this information sheet and for considering participation in this research study.

Appendix E: Participant Consent Form



Placeholder for local NHS logo
(e.g Bristol or Bath)

Consent Form

Study Title: Molecular Spectroscopy in Assessment and Detection of Ovarian Cancer

Chief Investigator: Dr Diana Frimpong

Please initial box

1. I confirm that I have read the information sheet 26th April 2021 (version 1.1) for the above study. I have had the opportunity to consider the information, ask questions and have had these answered satisfactorily.
2. I understand that my participation is voluntary and that I am free to withdraw at any time without giving any reason, without my medical care or legal rights being affected.
3. I understand that relevant sections of my medical notes and data collected during the study, may be looked at by individuals from the University of Exeter research team, NHS Trusts or from regulatory authorities, where it is relevant to my taking part in this research. I give permission for these individuals to have access to my records for 5 years.
4. I understand that the information collected about me will be used to support other research in the future and may be shared anonymously with other researchers.
5. I agree that anonymised samples of my blood may be used as described in the participant information sheet. I understand that anonymised samples may need to be transported securely between the NHS Trust and University of Exeter. If I decide to withdraw from the study, no further samples or information will be collected however samples and data already gathered will remain in the study.
6. I agree that anonymised samples of my tissue may be used as described in the participant information sheet. I understand that anonymised samples may need to be transported securely between NHS Trust and University of Exeter. If I decide to withdraw from the study, no further samples or information will be collected however samples and data already gathered will remain in the study.
7. I agree to take part in the above study

Optional Section: I would like to gift any remaining anonymised tissue, blood samples and data at the end of the study, to the ethically approved Peninsula Research Bank at the University of Exeter for use in future research.

Agree Do Not Agree

_____	_____	_____
Name of Participant	Date	Signature
_____	_____	_____
Name of person taking consent	Date	Signature

Once completed: one copy for the participant/one for the site file/one for the patient notes.

Appendix F: Participant Background Information Collection Tool



Placeholder for local NHS logo
(e.g Bristol or Bath)

Participant Background Information Data Collection Tool for Study Title: Molecular Spectroscopy in Assessment and Detection of Ovarian Cancer

Chief Investigator: Dr Diana Frimpong

Sponsor: University of Exeter

Participant Identification No.:

Age: _____ Menopausal status: Pre / Peri/ Post (please delete)
Parity: _____ Personal Cancer History? Yes / No (please delete)
Ethnicity: _____ History of blood disorders? Yes / No (please delete)

Smoking Status: Smoker Ex – Smoker Never Smoked

Symptoms:	None	<input type="checkbox"/>
Heartburn		<input type="checkbox"/>
Early Satiety		<input type="checkbox"/>
Bloating		<input type="checkbox"/>
Distension		<input type="checkbox"/>
Difficulty or frequency passing urine		<input type="checkbox"/>
Change in bowel habit		<input type="checkbox"/>
Pelvic pressure		<input type="checkbox"/>
Painful sex		<input type="checkbox"/>
Abdominal or Pelvic Pain		<input type="checkbox"/>
Back pain		<input type="checkbox"/>
Unexplained weight loss		<input type="checkbox"/>
Unexplained fatigue		<input type="checkbox"/>

Significant past gynaecology history:
.....
.....
.....
.....
.....
.....
.....
Past medical and surgical history (if not already mentioned above):
.....
.....
.....
.....
.....
.....

Appendix G: Participant Diagnostic Information Collection Tool



Placeholder for local NHS logo
(e.g Bristol or Bath)

Diagnostic Information Data Collection Tool for Study Title: Molecular Spectroscopy in Assessment and Detection of Ovarian Cancer

Chief Investigator: Dr Diana Frimpong

Participant Identification Number:

US finding:

Ca125: CEA: AFP: HCG: LDH: Ca19-9:

Diagnosis:

Type of OC:

Stage of OC:

Grade of OC:

Date of Surgery:

Procedure:

Surgeon (code):

Residual disease: R0 R1 >R1

Sites of residual disease

Genetic Tests? Yes No Results

ImmunoHistoChemistry? Yes No Results

Recurrence? Yes No Time to recurrence ___ months

Site of recurrence

Appendix H: Tentative peak assignment reference table - Tissue

Wavenumber	Tentative assignment
496-7	Glycogen
520-2	Glucose
500-50	S-S Disulphide stretch in proteins
545	Cholesterol
563	Unassigned
591	Calcium hydroxyapatite
621	C-C twisting mode of phenylalanine
642	C-C twisting mode of tyrosine
647	Tyrosine
665-5	Thymine
711	Adenine
722-4	Adenine
748	Thymine
755	Tryptophan
777-9	Nucleotides – cytosine and uracil ring breathing
806-13	ν_s O-P-O (DNA)
812	C-C stretch backbone in collagen
818-20	C-C stretch for protein
825-42	O-P-O (DNA)
851	Ring breathing of tyrosine and C-C stretch of proline ring
856	Proline
860-1	Collagen
875	C-C stretch of hydroxyproline
892	CH ₂ rocking, collagen, hydroxyproline
912	Ribose
919-922	C-C stretch of proline ring
933-5	C-C proline ring, collagen
936	Hydroxyproline
958	Hydroxyapatite
972	C-C proline ring
978	Phosphate ion stretching, phosphorylated rings and nucleic acids
1000-1	Phenylalanine
1003	Breathing mode phenylalanine
1005	Phenylalanine
1026	Phenylalanine
1032	Bending mode phenylalanine
1034-5	Ribose, phenylalanine
1040	Phenylalanine
1069	Symmetric phosphate ion stretching
1074	Triglycerides
1095-6	Phosphate stretch (DNA)
1118-9	Lipids
1127	Lipids
1137	Unassigned

1150	Carotenoids
1156	Carotenoids, C-C and C-N stretch of proteins
1158-9	Carotenoids
1173	C-H bending of tyrosine
1176	Tyrosine and phenylalanine
1205	Tyrosine and phenylalanine
1218-20	Unassigned
1227-40	Amide III (beta-sheet protein secondary structures)
1247	Amide III
1256	Cytosine
1264-95	Amide III (alpha helix protein secondary structures)
1302	Lipids
1309	CH ₃ deformation - lipids
1327	Nucleic Acid ring vibrations
1332	Guanine
1336	Wagging mode of collagen and nucleic acids (purine bases)
1360	Tryptophan
1386	CH ₃ bend
1398	Uracil, adenine
1400	Symmetric CH ₃ bending in proteins
1415	Antisymmetric CH ₃ deformation
1438-42	Lipids
1448	Bending mode of proteins
1464-5	Deoxyribose
1485	Nucleic acid purine bases
1519	Carotenoids
1524	Carotenoids
1554	Tryptophan
1573	Guanine, Adenine
1583	Nucleic acids (pyrimidine ring)
1597	Phenylalanine and tyrosine
1603	C=C bending mode of phenylalanine and tyrosine
1617	Tyrosine and Tryptophan
1622	Tryptophan
1633	Amide I
1652	Amide I
1656-7	Amide I (C=O stretch)
1658	Amide I (C=O and lipids C=C)
1667	Amide I (beta sheet)
1690	Amide I

Appendix I: Tentative peak assignments reference table - Plasma

Wavenumber	Tentative assignment
625	Phenylalanine
655	Unassigned
669	C-S stretch mode
689	Unassigned
699	Unassigned
755-8	Tryptophan symmetric breathing
825-42	O-P-O (DNA)
876	$\nu(\text{C-C})$ stretch of hydroxyproline
944	? C-C stretch of protein
961	Symmetric stretch of phosphate
999	Phenylalanine
1001-3	Breathing mode phenylalanine
1010-12	Tryptophan breathing ring
1025	Glycogen/carbohydrates
1073	Triglycerides (fatty acids)
1156	Carotenoids
1232	Amide III, C-N stretch and N-H bond
1329	CH ₃ CH ₂ wagging mode on purine bases of nucleic acids
1332	Guanine
1359-60	Tryptophan
1379-82	Lipids (CH ₃)
1392	C-H rocking
1435	Lipids (CH ₂ deformation)
1458	Nucleic acid modes
1517	Carotenoids (C-C stretch of beta carotene)
1548-50	Tryptophan $\nu(\text{C=C})$
1672-3	Amide I

Appendix J: Copyright for image from other source

Chapter 1

ELSEVIER LICENSE

TERMS AND CONDITIONS

Nov 27, 2023

This Agreement between Dr. Diana Frimpong ("You") and Elsevier ("Elsevier") consists of your license details and the terms and conditions provided by Elsevier and Copyright Clearance Center.

License Number 5676750859745

License date Nov 26, 2023

Licensed Content Publisher Elsevier

Licensed Content Publication Elsevier Books

Licensed Content Title Guyton and Hall Textbook of Medical Physiology

Licensed Content Author John E. Hall, Michael E. Hall

Licensed Content Date Jan 1, 2021

Licensed Content Pages 1

Start Page iv

End Page 0

Type of Use reuse in a thesis/dissertation

Portion figures/tables/illustrations

Number of figures/tables/illustrations 1

Format both print and electronic

Are you the author of this Elsevier chapter? No

Will you be translating? No

Title of new work Thesis - Raman spectroscopy in identification and assessment of ovarian cancer

Institution name University of Exeter

Expected presentation date Jan 2024

Portions Figure 82-2 Internal structures of the uterus, ovary, and a uterine tube.

Requestor Location

Dr. Diana Frimpong

United Kingdom Attn: Dr. Diana Frimpong

Publisher Tax ID GB 494 6272 12

Bibliography

- ALESSANDRI, F., LIJOI, D., MISTRANGELO, E., FERRERO, S. & RAGNI, N. 2006. Randomized study of laparoscopic versus minilaparotomic myomectomy for uterine myomas. *J Minim Invasive Gynecol*, 13, 92-7.
- ALMOND, L. M., HUTCHINGS, J., LLOYD, G., BARR, H., SHEPHERD, N., DAY, J., STEVENS, O., SANDERS, S., WADLEY, M., STONE, N. & KENDALL, C. 2014. Endoscopic Raman spectroscopy enables objective diagnosis of dysplasia in Barrett's esophagus. *Gastrointest Endosc*, 79, 37-45.
- ASARE-WEREHENE, M., HUNTER, R. A., GERBER, E., REUNOV, A., BRINE, I., CHANG, C. Y., CHANG, C. C., SHIEH, D. B., BURGER, D., ANIS, H. & TSANG, B. K. 2023. The Application of an Extracellular Vesicle-Based Biosensor in Early Diagnosis and Prediction of Chemoresponsiveness in Ovarian Cancer. *Cancers (Basel)*, 15.
- BAGADE, P., EDMONDSON, R. & NAYAR, A. 2012. Management of borderline ovarian tumours. *The Obstetrician & Gynaecologist*, 14, 115-120.
- BAILEY, J. & CHURCH, D. 2005. Management of Germ Cell Tumours of the Ovary. *Reviews in Gynaecological Practice*, 5, 201-206.
- BANFI, G., SALVAGNO, G. L. & LIPPI, G. 2007. The role of ethylenediamine tetraacetic acid (EDTA) as in vitro anticoagulant for diagnostic purposes. 45, 565-576.
- BARR, C. E., FUNSTON, G., JEEVAN, D., SUNDAR, S., MOUNCE, L. T. A. & CROSBIE, E. J. 2022. The Performance of HE4 Alone and in Combination with CA125 for the Detection of Ovarian Cancer in an Enriched Primary Care Population. *Cancers*, 14, 2124.
- BARTON, S. J. & HENNELLY, B. M. 2019. An Algorithm for the Removal of Cosmic Ray Artifacts in Spectral Data Sets. *Applied Spectroscopy*, 73, 893-901.
- BEFFARA, F., PERUMAL, J., PUTERI MAHYUDDIN, A., CHOOLANI, M., KHAN, S. A., AUGUSTE, J. L., VEDRAINE, S., HUMBERT, G., DINISH, U. S. & OLIVO, M. 2020. Development of highly reliable SERS-active photonic crystal fiber probe and its application in the detection of ovarian cancer biomarker in cyst fluid. *J Biophotonics*, 13, e201960120.
- BEREK, J. S., KEHOE, S. T., KUMAR, L. & FRIEDLANDER, M. 2018. Cancer of the ovary, fallopian tube, and peritoneum. *International Journal of Gynecology & Obstetrics*, 143, 59-78.
- BERGHOLT, M. S., ZHENG, W., LIN, K., HO, K. Y., TEH, M., YEOH, K. G., SO, J. B. Y. & HUANG, Z. 2011. In Vivo Diagnosis of Esophageal Cancer Using Image-Guided Raman Endoscopy and Biomolecular Modeling. *Technology in Cancer Research & Treatment*, 10, 103-112.
- BGCS. 2017. *BGCS Guidelines Ovarian Cancer: Recommendations for Practice* [Online]. Available: <https://www.bgcs.org.uk/wp-content/uploads/2019/05/BGCS-Guidelines-Ovarian-Guidelines-2017.pdf> [Accessed].
- BOLSTAD, N., ØIJORDSBAKKEN, M., NUSTAD, K. & BJERNER, J. 2012. Human epididymis protein 4 reference limits and natural variation in a Nordic reference population. *Tumour Biol*, 33, 141-8.

- BUNACIU, A. A., HOANG, V. D. & ABOUL-ENEIN, H. Y. 2017. Vibrational Micro-Spectroscopy of Human Tissues Analysis: Review. *Crit Rev Anal Chem*, 47, 194-203.
- BURGER, R. A., BRADY, M. F., BOOKMAN, M. A., FLEMING, G. F., MONK, B. J., HUANG, H., MANNEL, R. S., HOMESLEY, H. D., FOWLER, J., GREER, B. E., BOENTE, M., BIRRER, M. J. & LIANG, S. X. 2011. Incorporation of Bevacizumab in the Primary Treatment of Ovarian Cancer. *New England Journal of Medicine*, 365, 2473-2483.
- BUTLER, H. J., ASHTON, L., BIRD, B., CINQUE, G., CURTIS, K., DORNEY, J., ESMONDE-WHITE, K., FULLWOOD, N. J., GARDNER, B., MARTIN-HIRSCH, P. L., WALSH, M. J., MCAINSH, M. R., STONE, N. & MARTIN, F. L. 2016. Using Raman spectroscopy to characterize biological materials. *Nat Protoc*, 11, 664-87.
- BUYS, S. S., PARTRIDGE, E., BLACK, A., JOHNSON, C. C., LAMERATO, L., ISAACS, C., REDING, D. J., GREENLEE, R. T., YOKOCHI, L. A., KESSEL, B., CRAWFORD, E. D., CHURCH, T. R., ANDRIOLE, G. L., WEISSFELD, J. L., FOUAD, M. N., CHIA, D., O'BRIEN, B., RAGARD, L. R., CLAPP, J. D., RATHMELL, J. M., RILEY, T. L., HARTGE, P., PINSKY, P. F., ZHU, C. S., IZMIRLIAN, G., KRAMER, B. S., MILLER, A. B., XU, J.-L., PROROK, P. C., GOHAGAN, J. K., BERG, C. D. & PLCO PROJECT TEAM, F. T. 2011. Effect of Screening on Ovarian Cancer Mortality: The Prostate, Lung, Colorectal and Ovarian (PLCO) Cancer Screening Randomized Controlled Trial. *JAMA*, 305, 2295-2303.
- CANCER INTELLIGENCE TEAM. *Proportion and number of ovarian cancers diagnosed at stage 3&4* [Online]. Cancer Research UK. Available: <https://crukcanerintelligence.shinyapps.io/EarlyDiagnosis/> [Accessed October 2023].
- CANCER INTELLIGENCE TEAM. *Survival and Incidence by stage of diagnosis* [Online]. Cancer Research UK. Available: <https://crukcanerintelligence.shinyapps.io/EarlyDiagnosis/> [Accessed October 2023].
- CANCER RESEARCH UK. *Early Detection and Diagnosis of Cancer - A Roadmap to the future* [Online]. Cancer Research UK. Available: https://www.cancerresearchuk.org/sites/default/files/early_detection_diagnosis_of_cancer_roadmap.pdf [Accessed 2024].
- CANCER RESEARCH UK. *Fallopian Tube Cancers* [Online]. Available: <https://about-cancer.cancerresearchuk.org/about-cancer/ovarian-cancer/types/epithelial-ovarian-cancers/fallopian-tube> [Accessed October 2023].
- CANCER RESEARCH UK. *Ovarian Cancer Incidence* [Online]. Available: <https://www.cancerresearchuk.org/health-professional/cancer-statistics/statistics-by-cancer-type/ovarian-cancer#heading-Zero> [Accessed May 2020].
- CANCER RESEARCH UK. *Ovarian Cancer Mortality Statistics* [Online]. Available: <https://www.cancerresearchuk.org/health-professional/cancer-statistics/statistics-by-cancer-type/ovarian-cancer/mortality> [Accessed May 2020].
- CANCER RESEARCH UK. *Ovarian Cancer Statistics* [Online]. Available: <https://www.cancerresearchuk.org/health-professional/cancer-statistics/statistics-by-cancer-type/ovarian-cancer#heading-Two> [Accessed May 2020].

- CARRIERE, J. & HAVERMEYER, F. 2012. *Ultra-low frequency Stokes and anti-Stokes Raman spectroscopy at 785nm with volume holographic grating filters*, SPIE.
- CASS, G. K. & NEWTON, C. 2020. The pelvic mass: assessment and evaluation. *Obstetrics, Gynaecology & Reproductive Medicine*, 30, 139-145.
- CHARKHCHI, P., CYBULSKI, C., GRONWALD, J., WONG, F. O., NAROD, S. A. & AKBARI, M. R. 2020. CA125 and Ovarian Cancer: A Comprehensive Review. *Cancers*, 12, 3730.
- CHEN, F., SUN, C., YUE, Z., ZHANG, Y., XU, W., SHABBIR, S., ZOU, L., LU, W., WANG, W., XIE, Z., ZHOU, L., LU, Y. & YU, J. 2022a. Screening ovarian cancers with Raman spectroscopy of blood plasma coupled with machine learning data processing. *Spectrochimica Acta Part A: Molecular and Biomolecular Spectroscopy*, 265, 120355.
- CHEN, F., SUN, C., YUE, Z., ZHANG, Y., XU, W., SHABBIR, S., ZOU, L., LU, W., WANG, W., XIE, Z., ZHOU, L., LU, Y. & YU, J. 2022b. Screening ovarian cancers with Raman spectroscopy of blood plasma coupled with machine learning data processing. *Spectrochim Acta A Mol Biomol Spectrosc*, 265, 120355.
- COLLABORATORS, I. C. O. N. 2003. International Collaborative Ovarian Neoplasm Trial 1: A Randomized Trial of Adjuvant Chemotherapy in Women With Early-Stage Ovarian Cancer. *JNCI: Journal of the National Cancer Institute*, 95, 125-132.
- CRAMER, D. W., KUPER, H., HARLOW, B. L. & TITUS-ERNSTOFF, L. 2001. Carotenoids, antioxidants and ovarian cancer risk in pre- and postmenopausal women. *Int J Cancer*, 94, 128-34.
- CRANDON, S. 2019. Sensitivity and Specificity explained: A Cochrane UK Trainees blog. Available from: <https://uk.cochrane.org/news/sensitivity-and-specificity-explained-cochrane-uk-trainees-blog> [2023].
- CROSBIE, E. J., RYAN, N. A. J., MCVHEY, R. J., LALLOO, F., BOWERS, N., GREEN, K., WOODWARD, E. R., CLANCY, T., BOLTON, J., WALLACE, A. J., MCMAHON, R. F. & EVANS, D. G. 2021. Assessment of mismatch repair deficiency in ovarian cancer. *J Med Genet*, 58, 687-691.
- CROW, P., BARRASS, B., KENDALL, C., HART-PRIETO, M., WRIGHT, M., PERSAD, R. & STONE, N. 2005. The use of Raman spectroscopy to differentiate between different prostatic adenocarcinoma cell lines. *Br J Cancer*, 92, 2166-70.
- CUNNINGHAM, M. *Freezing Biological Samples* [Online]. Leica Biosystems. Available: <https://www.leicabiosystems.com/knowledge-pathway/freezing-biological-samples/> [Accessed 2023].
- CYBERPHYSICS. 2009. *Electromagnetic Spectrum* [Online]. Available: <https://www.cyberphysics.co.uk/topics/radioact/Radio/EMSpectrumcolor.jpg> [Accessed October 2023].
- D'ANIELLO, C., PATRIARCA, E. J., PHANG, J. M. & MINCHIOTTI, G. 2020. Proline Metabolism in Tumor Growth and Metastatic Progression. *Front Oncol*, 10, 776.
- DAS, K., STONE, N., KENDALL, C., FOWLER, C. & CHRISTIE-BROWN, J. 2006. Raman spectroscopy of parathyroid tissue pathology. *Lasers Med Sci*, 21, 192-7.
- DAVID, S., PLANTE, A., DALLAIRE, F., TREMBLAY, J. P., SHEEHY, G., MACDONALD, E., FORREST, L., DANESHMAND, M., TRUDEL, D., WILSON, B. C., HOPKINS, L., MURUGKAR, S., VANDERHYDEN, B. &

- LEBLOND, F. 2022. Multispectral label-free Raman spectroscopy can detect ovarian and endometrial cancer with high accuracy. *J Biophotonics*, 15, e202100198.
- DAY, J. C., BENNETT, R., SMITH, B., KENDALL, C., HUTCHINGS, J., MEADEN, G. M., BORN, C., YU, S. & STONE, N. 2009. A miniature confocal Raman probe for endoscopic use. *Phys Med Biol*, 54, 7077-87.
- DENG, K., ZHU, C., MA, X., JIA, H., WEI, Z., XIAO, Y. & XU, J. 2016. Rapid Discrimination of Malignant Breast Lesions from Normal Tissues Utilizing Raman Spectroscopy System: A Systematic Review and Meta-Analysis of In Vitro Studies. *PLoS One*, 11, e0159860.
- DEY, P. 2022. *Basic and Advanced Laboratory Techniques in Histopathology and Cytology*, Singapore, Springer Nature Singapore.
- DODGE, J. E., COVENS, A. L., LACCHETTI, C., ELIT, L. M., LE, T., DEVRIES-ABOUD, M. & FUNG-KEE-FUNG, M. 2012. Preoperative identification of a suspicious adnexal mass: a systematic review and meta-analysis. *Gynecol Oncol*, 126, 157-66.
- DU BOIS, A., KRISTENSEN, G., RAY-COQUARD, I., REUSS, A., PIGNATA, S., COLOMBO, N., DENISON, U., VERGOTE, I., DEL CAMPO, J. M., OTTEVANGER, P., HEUBNER, M., MINARIK, T., SEVIN, E., DE GREGORIO, N., BIDZIŃSKI, M., PFISTERER, J., MALANDER, S., HILPERT, F., MIRZA, M. R., SCAMBIA, G., MEIER, W., NICOLETTO, M. O., BJØRGE, L., LORTHOLARY, A., SAILER, M. O., MERGER, M. & HARTER, P. 2016. Standard first-line chemotherapy with or without nintedanib for advanced ovarian cancer (AGO-OVAR 12): a randomised, double-blind, placebo-controlled phase 3 trial. *Lancet Oncol*, 17, 78-89.
- ELATTAR, A., BRYANT, A., WINTER-ROACH, B. A., HATEM, M. & NAIK, R. 2011. Optimal primary surgical treatment for advanced epithelial ovarian cancer. *Cochrane Database Syst Rev*, 2011, Cd007565.
- FERGUSON, D., HENDERSON, A., MCINNES, E. F., LIND, R., WILDENHAIN, J. & GARDNER, P. 2022. Infrared micro-spectroscopy coupled with multivariate and machine learning techniques for cancer classification in tissue: a comparison of classification method, performance, and pre-processing technique. *Analyst*, 147, 3709-3722.
- FIELDS, M. M. & CHEVLEN, E. 2006. Screening for disease: making evidence-based choices. *Clin J Oncol Nurs*, 10, 73-6.
- FILIK, J. & STONE, N. 2007. Drop coating deposition Raman spectroscopy of protein mixtures. *Analyst*, 132, 544-550.
- FISHER SCIENTIFIC. *Scigen Tissue-Plus O.C.T Compound* [Online]. Available: <https://www.fishersci.com/shop/products/tissue-plus-o-c-t-compound/23730571> [Accessed].
- FORGO, E. & LONGACRE, T. *Low grade serous carcinoma* [Online]. PathologyOutlines.com. Available: <https://www.pathologyoutlines.com/topic/ovarytumorserouscarcinoma1g.html> [Accessed 2023].
- FROST, J. 2019. *Vibrational spectroscopy for the assessment of vulval disease*. PhD in Medical Sciences, University of Exeter.
- FROST, J., LUDEMAN, L., HILLABY, K., GORNALL, R., LLOYD, G., KENDALL, C., SHORE, A. C. & STONE, N. 2017. Raman spectroscopy and multivariate analysis for the non invasive diagnosis of clinically inconclusive vulval lichen sclerosus. *Analyst*, 142, 1200-1206.

- FULLWOOD, L. M. 2017. *Raman spectroscopy for rapid diagnosis of lymphomas and metastatic lesions found in lymph nodes*. PhD in Physics Thesis or Dissertation, University of Exeter.
- FUNSTON, G., HAMILTON, W., ABEL, G., CROSBIE, E. J., ROUS, B. & WALTER, F. M. 2020. The diagnostic performance of CA125 for the detection of ovarian and non-ovarian cancer in primary care: A population-based cohort study. *PLoS Med*, 17, e1003295.
- GANDHI, T., ZUBAIR, M. & BHATT, H. *Cancer Antigen 125* [Online]. Florida: StatPearls Publishing. Available: https://www.ncbi.nlm.nih.gov/books/NBK562245/?report=reader#_NBK562245_pubdet [Accessed November 2023].
- GARDNER, B. 2021. InVia Usage Guide. University of Exeter.
- GENTRY-MAHARAJ, A., BURNELL, M., DILLEY, J., RYAN, A., KARPINSKYJ, C., GUNU, R., MALLETT, S., DEEKS, J., CAMPBELL, S., JACOBS, I., SUNDAR, S. & MENON, U. 2020. Serum HE4 and diagnosis of ovarian cancer in postmenopausal women with adnexal masses. *Am J Obstet Gynecol*, 222, 56.e1-56.e17.
- GIAMOUGIANNIS, P., MORAIS, C. L. M., GRABOWSKA, R., ASHTON, K. M., WOOD, N. J., MARTIN-HIRSCH, P. L. & MARTIN, F. L. 2021a. A comparative analysis of different biofluids towards ovarian cancer diagnosis using Raman microspectroscopy. *Analytical and Bioanalytical Chemistry*, 413, 911-922.
- GIAMOUGIANNIS, P., SILVA, R. V. O., FREITAS, D. L. D., LIMA, K. M. G., ANAGNOSTOPOULOS, A., ANGELOPOULOS, G., NAIK, R., WOOD, N. J., MARTIN-HIRSCH, P. L. & MARTIN, F. L. 2021b. Raman spectroscopy of blood and urine liquid biopsies for ovarian cancer diagnosis: identification of chemotherapy effects. *Journal of Biophotonics*, 14, e202100195.
- GONZÁLEZ-MARTÍN, A., POTHURI, B., VERGOTE, I., DEPONT CHRISTENSEN, R., GRAYBILL, W., MIRZA, M. R., MCCORMICK, C., LORUSSO, D., HOSKINS, P., FREYER, G., BAUMANN, K., JARDON, K., REDONDO, A., MOORE, R. G., VULSTEKE, C., O'CEARBHAILL, R. E., LUND, B., BACKES, F., BARRETINA-GINESTA, P., HAGGERTY, A. F., RUBIO-PÉREZ, M. J., SHAHIN, M. S., MANGILI, G., BRADLEY, W. H., BRUCHIM, I., SUN, K., MALINOWSKA, I. A., LI, Y., GUPTA, D. & MONK, B. J. 2019. Niraparib in Patients with Newly Diagnosed Advanced Ovarian Cancer. *N Engl J Med*, 381, 2391-2402.
- GRABOWSKI, J. P., HARTER, P., HEITZ, F., PUJADE-LAURINE, E., REUSS, A., KRISTENSEN, G., RAY-COQUARD, I., HEITZ, J., TRAUT, A., PFISTERER, J. & DU BOIS, A. 2016. Operability and chemotherapy responsiveness in advanced low-grade serous ovarian cancer. An analysis of the AGO Study Group metadatabase. *Gynecol Oncol*, 140, 457-62.
- GRIMBERGEN, M. C. M., VAN SWOL, C. F. P., DRAGA, R. O. P., VAN DIEST, P., VERDAASDONK, R. M., STONE, N. & BOSCH, J. H. L. R. 2009. *Bladder cancer diagnosis during cystoscopy using Raman spectroscopy*, SPIE.
- HAKA, A. S., SHAFER-PELTIER, K. E., FITZMAURICE, M., CROWE, J., DASARI, R. R. & FELD, M. S. 2005. Diagnosing breast cancer by using Raman spectroscopy. *Proceedings of the National Academy of Sciences of the United States of America*, 102, 12371-12376.

- HAKA, A. S., VOLYNSKAYA, Z., GARDECKI, J. A., NAZEMI, J., LYONS, J., HICKS, D., FITZMAURICE, M., DASARI, R. R., CROWE, J. P. & FELD, M. S. 2006. In vivo Margin Assessment during Partial Mastectomy Breast Surgery Using Raman Spectroscopy. *Cancer Research*, 66, 3317-3322.
- HALL, J. E. G. A. C. H. M. E. 2021. Female Physiology Before Pregnancy and Female Hormones. *Guyton and Hall textbook of medical physiology*. 14 ed.: Elsevier Saunders.
- HAO, J., CHEN, C., JIN, H., CHEN, N., ZHOU, J., ZHU, Y., CHUNG, K. & PU, Q. 2020. The efficacy of Raman spectroscopy in the diagnosis of esophageal cancer: a systematic review and meta-analysis. *Transl Cancer Res*, 9, 4750-4761.
- HARBI, R. A., MCNEISH, I. A. & EL-BAHRAWY, M. 2021. Ovarian sex cord-stromal tumors: an update on clinical features, molecular changes, and management. *International Journal of Gynecologic Cancer*, 31, 161-168.
- HASKELL, J., HUBBARD, T., MURRAY, C., GARDNER, B., IVES, C. L., FERGUSON, D. & STONE, N. 2023. High wavenumber Raman spectroscopy for intraoperative assessment of breast tumour margins. *The Analyst*.
- HAUPTMANN, S., FRIEDRICH, K., REDLINE, R. & AVRIL, S. 2017. Ovarian borderline tumors in the 2014 WHO classification: evolving concepts and diagnostic criteria. *Virchows Arch*, 470, 125-142.
- HONDA, K., HISHIKI, T., YAMAMOTO, S., YAMAMOTO, T., MIURA, N., KUBO, A., ITOH, M., CHEN, W. Y., TAKANO, M., YOSHIKAWA, T., KASAMATSU, T., SONODA, S., YOSHIZAWA, H., NAKAMURA, S., ITAI, Y., SHIOTA, M., KOIKE, D., NAYA, M., HAYAKAWA, N., NAITO, Y., MATSUURA, T., IWAISAKO, K., MASUI, T., UEMOTO, S., NAGASHIMA, K., HASHIMOTO, Y., SAKUMA, T., MATSUBARA, O., HUANG, W., IDA, T., AKAIKE, T., MASUGI, Y., SAKAMOTO, M., KATO, T., INO, Y., YOSHIDA, H., TSUDA, H., HIRAOKA, N., KABE, Y. & SUEMATSU, M. 2021. Corrigendum to "On-tissue polysulfide visualization by surface-enhanced Raman spectroscopy benefits patients with ovarian cancer to predict post-operative chemosensitivity" [Redox Biol. 41 (2021) 101926]. *Redox Biol*, 44, 102028.
- HORSNELL, J., STONELAKE, P., CHRISTIE-BROWN, J., SHETTY, G., HUTCHINGS, J., KENDALL, C. & STONE, N. 2010. Raman spectroscopy--a new method for the intra-operative assessment of axillary lymph nodes. *Analyst*, 135, 3042-7.
- HUBBARD, T. J. E., SHORE, A. & STONE, N. 2019. Raman spectroscopy for rapid intra-operative margin analysis of surgically excised tumour specimens. *Analyst*, 144, 6479-6496.
- JAAFAR, H. 2006. Intra-operative frozen section consultation: concepts, applications and limitations. *The Malaysian journal of medical sciences : MJMS*, 13, 4-12.
- JEONG, D. W., LEE, S. & CHUN, Y. S. 2021. How cancer cells remodel lipid metabolism: strategies targeting transcription factors. *Lipids Health Dis*, 20, 163.
- JEONG, N. H., SONG, E. S., LEE, J. M., LEE, K. B., KIM, M. K., CHEON, J. E., LEE, J. K., SON, S. K., LEE, J. P., KIM, J. H., HUR, S. Y. & KWON, Y. I. 2009. Plasma carotenoids, retinol and tocopherol levels and the risk of ovarian cancer. *Acta Obstet Gynecol Scand*, 88, 457-62.
- KALLAWAY, C., ALMOND, L. M., BARR, H., WOOD, J., HUTCHINGS, J., KENDALL, C. & STONE, N. 2013. Advances in the clinical application of

- Raman spectroscopy for cancer diagnostics. *Photodiagnosis and Photodynamic Therapy*, 10, 207-219.
- KALOO PD., LOUDEN KA., KHAZALI S., HOY D. & SADOON S. 2011. *Green-top Guideline No. 62. Management of Suspected Ovarian Masses in Premenopausal Women* [Online]. London: Royal College of Obstetricians and Gynaecologists. Available: https://www.rcog.org.uk/media/yhujmdvr/gtg_62-1.pdf [Accessed 2020].
- KEHOE, S., HOOK, J., NANKIVELL, M., JAYSON, G. C., KITCHENER, H., LOPES, T., LUESLEY, D., PERREN, T., BANNOO, S., MASCARENHAS, M., DOBBS, S., ESSAPEN, S., TWIGG, J., HEROD, J., MCCLUGGAGE, G., PARMAR, M. & SWART, A.-M. 2015. Primary chemotherapy versus primary surgery for newly diagnosed advanced ovarian cancer (CHORUS): an open-label, randomised, controlled, non-inferiority trial. *The Lancet*, 386, 249-257.
- KENDALL, C., STONE, N., SHEPHERD, N., GEBOES, K., WARREN, B., BENNETT, R. & BARR, H. 2003. Raman spectroscopy, a potential tool for the objective identification and classification of neoplasia in Barrett's oesophagus. *The Journal of Pathology*, 200, 602-609.
- KENDALL, C. A. 2002. *A study of Raman spectroscopy for the early detection and classification of malignancy in oesophageal tissue*. PhD, Cranfield University.
- KENNEDY, S., BERGQVIST, A., CHAPRON, C., D'HOOGHE, T., DUNSELMAN, G., GREB, R., HUMMELSHOJ, L., PRENTICE, A. & SARIDOGAN, E. 2005. ESHRE guideline for the diagnosis and treatment of endometriosis. *Hum Reprod*, 20, 2698-704.
- KOHN, E. C. & IVY, S. P. 2017. Whence High-Grade Serous Ovarian Cancer. *American Society of Clinical Oncology Educational Book*, 443-448.
- KOLJENOVIC, S., CHOO-SMITH, L. P., BAKKER SCHUT, T. C., KROS, J. M., VAN DEN BERGE, H. J. & PUPPELS, G. J. 2002. Discriminating vital tumor from necrotic tissue in human glioblastoma tissue samples by Raman spectroscopy. *Lab Invest*, 82, 1265-77.
- KONG, K., ZAABAR, F., RAKHA, E., ELLIS, I., KOLOYDENKO, A. & NOTINGHER, I. 2014. Towards intra-operative diagnosis of tumours during breast conserving surgery by selective-sampling Raman micro-spectroscopy. *Phys Med Biol*, 59, 6141-52.
- KRISHNA, C. M., SOCKALINGUM, G. D., BHAT, R. A., VENDEO, L., KUSHTAGI, P., PLUOT, M. & MANFAIT, M. 2007. FTIR and Raman microspectroscopy of normal, benign, and malignant formalin-fixed ovarian tissues. *Anal Bioanal Chem*, 387, 1649-56.
- KUMAR, V., ABBAS, A. K. & ASTER, J. C. 2017. *Robbins basic pathology*, Elsevier.
- KURMAN, R. J. 2013. Origin and molecular pathogenesis of ovarian high-grade serous carcinoma. *Ann Oncol*, 24 Suppl 10, x16-21.
- KVASKOFF, M., HORNE, A. W. & MISSMER, S. A. 2017. Informing women with endometriosis about ovarian cancer risk. *Lancet*, 390, 2433-2434.
- LALKHEN, A. G. & MCCLUSKEY, A. 2008. Clinical tests: sensitivity and specificity. *Continuing Education in Anaesthesia Critical Care & Pain*, 8, 221-223.
- LAWRIE, T. A., WINTER-ROACH, B. A., HEUS, P. & KITCHENER, H. C. 2015. Adjuvant (post-surgery) chemotherapy for early stage epithelial ovarian cancer. *Cochrane Database Syst Rev*, 2015, Cd004706.

- LEVINE, D. A., KARLAN, B. Y., BRISTOW, R. E. & LI, A. J. 2015. Genetics and Biology of Gynaecologic Cancers. *Gynecologic Oncology: Clinical Practice and Surgical Atlas*. New York: McGraw-Hill Medical.
- LI, P., CHEN, C., DENG, X., MAO, H. & JIN, S. 2015. Drop coating deposition Raman spectroscopy of blood plasma for the detection of colorectal cancer. *Journal of Biomedical Optics*, 20, 037004.
- LI, X., YANG, T. & LI, S. 2012. Discrimination of serum Raman spectroscopy between normal and colorectal cancer using selected parameters and regression-discriminant analysis. *Appl Opt*, 51, 5038-43.
- LI, Z. & ZHANG, H. 2016. Reprogramming of glucose, fatty acid and amino acid metabolism for cancer progression. *Cell Mol Life Sci*, 73, 377-92.
- LLOYD, G. R., ORR, L. E., CHRISTIE-BROWN, J., MCCARTHY, K., ROSE, S., THOMAS, M. & STONE, N. 2013. Discrimination between benign, primary and secondary malignancies in lymph nodes from the head and neck utilising Raman spectroscopy and multivariate analysis. *Analyst*, 138, 3900-8.
- LYNG, F. M., TRAYNOR, D., RAMOS, I. R., BONNIER, F. & BYRNE, H. J. 2015. Raman spectroscopy for screening and diagnosis of cervical cancer. *Anal Bioanal Chem*, 407, 8279-89.
- MAHEEDHAR, K., BHAT, R. A., MALINI, R., PRATHIMA, N. B., KEERTHI, K., KUSHTAGI, P. & KRISHNA, C. M. 2008. Diagnosis of Ovarian Cancer by Raman Spectroscopy: A Pilot Study.
- MANFAIT, M., LAMAZE, P., LAMFARRAJ, H., PLUOT, M. & SOCKALINGUM, G. 2000. *Diagnosis and prognosis of tissue pathologies by Raman microspectroscopy: an application to human thyroid tumors*, SPIE.
- MCCREERY, R. L. 2000. Signal-to-Noise in Raman Spectroscopy. *Raman Spectroscopy for Chemical Analysis*.
- MEHASSEB, M., SIDDIQUI, N. & BRYDEN, F. 2016. *Green-top Guideline No. 34. Management of Ovarian Cysts in Postmenopausal Women* [Online]. London: Royal College of Obstetricians and Gynaecologists. Available: https://www.rcog.org.uk/media/4v3ncfib/gtg_34.pdf [Accessed 2020].
- MEHTA, K., ATAK, A., SAHU, A., SRIVASTAVA, S. & C, M. K. 2018. An early investigative serum Raman spectroscopy study of meningioma. *Analyst*, 143, 1916-1923.
- MENON, U., GENTRY-MAHARAJ, A., BURNELL, M., SINGH, N., RYAN, A., KARPINSKYJ, C., CARLINO, G., TAYLOR, J., MASSINGHAM, S. K., RAIKOU, M., KALSI, J. K., WOOLAS, R., MANCHANDA, R., ARORA, R., CASEY, L., DAWNAY, A., DOBBS, S., LEESON, S., MOULD, T., SEIF, M. W., SHARMA, A., WILLIAMSON, K., LIU, Y., FALLOWFIELD, L., MCGUIRE, A. J., CAMPBELL, S., SKATES, S. J., JACOBS, I. J. & PARMAR, M. 2021. Ovarian cancer population screening and mortality after long-term follow-up in the UK Collaborative Trial of Ovarian Cancer Screening (UKCTOCS): a randomised controlled trial. *The Lancet*, 397, 2182-2193.
- MEYN, A. & LIM, B. 2017. A paradigm shift in the origin of ovarian cancer: the ovary is no longer to blame. *BJOG: An International Journal of Obstetrics & Gynaecology*, 124, 859-859.
- MILLER, J. N. & MILLER, J. C. 2010. *Statistics and Chemometrics for Analytical Chemistry*, Harlow, England, Pearson education Limited.
- MITCHELL, B. S. R. 2009. *Embryology : an illustrated colour text*, London, Elsevier Saunders.

- MOLCKOVSKY, A., SONG, L. M., SHIM, M. G., MARCON, N. E. & WILSON, B. C. 2003. Diagnostic potential of near-infrared Raman spectroscopy in the colon: differentiating adenomatous from hyperplastic polyps. *Gastrointest Endosc*, 57, 396-402.
- MOOTHANCHERY, M., PERUMAL, J., MAHYUDDIN, A. P., SINGH, G., CHOOLANI, M. A. & OLIVO, M. 2022. Rapid and sensitive detection of ovarian cancer biomarker using a portable single peak Raman detection method. *Scientific Reports*, 12.
- MURUGAESU, N., SCHMID, P., DANCEY, G., AGARWAL, R., HOLDEN, L., MCNEISH, I., SAVAGE, P. M., NEULANDS, E. S., RUSTIN, G. J. & SECKL, M. J. 2006. Malignant ovarian germ cell tumors: identification of novel prognostic markers and long-term outcome after multimodality treatment. *J Clin Oncol*, 24, 4862-6.
- NEFF, R. T., SENTER, L. & SALANI, R. 2017. BRCA mutation in ovarian cancer: testing, implications and treatment considerations. *Ther Adv Med Oncol*, 9, 519-531.
- NICE GUIDELINE. 2011. *Ovarian cancer: recognition and initial management (CG122)* [Online]. National Institute for Health and Care Excellence. Available: <https://www.nice.org.uk/guidance/cg122/resources/ovarian-cancer-recognition-and-initial-management-pdf-35109446543557> [Accessed 2020].
- NICE GUIDELINE. 2017. *Endometriosis: diagnosis and management (NG73)* [Online]. National Institute for Health and Care Excellence. Available: <https://www.nice.org.uk/guidance/ng73/resources/endometriosis-diagnosis-and-management-pdf-1837632548293> [Accessed 2020].
- NICHOLSON, B. D., OKE, J., VIRDEE, P. S., HARRIS, D. A., O'DOHERTY, C., PARK, J. E., HAMADY, Z., SEHGAL, V., MILLAR, A., MEDLEY, L., TONNER, S., VARGOVA, M., ENGONIDOU, L., RIAHI, K., LUAN, Y., HIOM, S., KUMAR, H., NANDANI, H., KURTZMAN, K. N., YU, L. M., FREESTONE, C., PEARSON, S., HOBBS, F. R., PERERA, R. & MIDDLETON, M. R. 2023. Multi-cancer early detection test in symptomatic patients referred for cancer investigation in England and Wales (SYMPLIFY): a large-scale, observational cohort study. *Lancet Oncol*, 24, 733-743.
- OWENS, G. L., GAJJAR, K., TREVISAN, J., FOGARTY, S. W., TAYLOR, S. E., DA GAMA-ROSE, B., MARTIN-HIRSCH, P. L. & MARTIN, F. L. 2014. Vibrational biospectroscopy coupled with multivariate analysis extracts potentially diagnostic features in blood plasma/serum of ovarian cancer patients. *Journal of Biophotonics*, 7, 200-209.
- PARASKEVAIDI, M., ASHTON, K. M., STRINGFELLOW, H. F., WOOD, N. J., KEATING, P. J., ROWBOTTOM, A. W., MARTIN-HIRSCH, P. L. & MARTIN, F. L. 2018. Raman spectroscopic techniques to detect ovarian cancer biomarkers in blood plasma. *Talanta*, 189, 281-288.
- PARASKEVAIDI, M., MORAIS, C. L. M., ASHTON, K. M., STRINGFELLOW, H. F., MCVEY, R. J., RYAN, N. A. J., O'FLYNN, H., SIVALINGAM, V. N., KITSON, S. J., MACKINTOSH, M. L., DERBYSHIRE, A. E., POW, C., RAGLAN, O., LIMA, K. M. G., KYRGIU, M., MARTIN-HIRSCH, P. L., MARTIN, F. L. & CROSBIE, E. J. 2020. Detecting Endometrial Cancer by Blood Spectroscopy: A Diagnostic Cross-Sectional Study. *Cancers*, 12, 1256.

- PARLATAN, U., INANC, M. T., OZGOR, B. Y., ORAL, E., BAŞTU, E., UNLU, M. B. & BAŞAR, G. 2019. Raman spectroscopy as a non-invasive diagnostic technique for endometriosis. *Scientific Reports*, 9.
- PEREZ, B. H. & GIPSON, I. K. 2008. Focus on Molecules: human mucin MUC16. *Exp Eye Res*, 87, 400-1.
- PERREN, T. J., SWART, A. M., PFISTERER, J., LEDERMANN, J. A., PUJADE-LAURINE, E., KRISTENSEN, G., CAREY, M. S., BEALE, P., CERVANTES, A., KURZEDER, C., BOIS, A. D., SEHOULI, J., KIMMIG, R., STÄHLE, A., COLLINSON, F., ESSAPEN, S., GOURLEY, C., LORTHOLARY, A., SELLE, F., MIRZA, M. R., LEMINEN, A., PLANTE, M., STARK, D., QIAN, W., PARMAR, M. K. B. & OZA, A. M. 2011. A Phase 3 Trial of Bevacizumab in Ovarian Cancer. *New England Journal of Medicine*, 365, 2484-2496.
- PERUMAL, J., MAHYUDDIN, A. P., BALASUNDARAM, G., GOH, D., FU, C. Y., KAZAKEVICIUTE, A., DINISH, U. S., CHOOLANI, M. & OLIVO, M. 2019. SERS-based detection of haptoglobin in ovarian cyst fluid as a point-of-care diagnostic assay for epithelial ovarian cancer. *Cancer Manag Res*, 11, 1115-1124.
- PHELPS, D. L., BALOG, J., GILDEA, L. F., BODAI, Z., SAVAGE, A., EL-BAHRAWY, M. A., SPELLER, A. V., ROSINI, F., KUDO, H., MCKENZIE, J. S., BROWN, R., TAKÁTS, Z. & GHAEM-MAGHAMI, S. 2018. The surgical intelligent knife distinguishes normal, borderline and malignant gynaecological tissues using rapid evaporative ionisation mass spectrometry (REIMS). *Br J Cancer*, 118, 1349-1358.
- PINSKY, P. F., YU, K., KRAMER, B. S., BLACK, A., BUYS, S. S., PARTRIDGE, E., GOHAGAN, J., BERG, C. D. & PROROK, P. C. 2016. Extended mortality results for ovarian cancer screening in the PLCO trial with median 15years follow-up. *Gynecol Oncol*, 143, 270-275.
- PRAT, J. 2015. FIGO's staging classification for cancer of the ovary, fallopian tube, and peritoneum: abridged republication. *J Gynecol Oncol*, 26, 87-9.
- REHMAN, S., MOVASAGHI, Z., TUCKER, A. T., JOEL, S. P., DARR, J. A., RUBAN, A. V. & REHMAN, I. U. 2007. Raman spectroscopic analysis of breast cancer tissues: identifying differences between normal, invasive ductal carcinoma and ductal carcinoma in situ of the breast tissue. *Journal of Raman Spectroscopy*, 38, 1345-1351.
- RENISHAW. 2021. *InVia confocal Raman microscope* [Online]. Renishaw plc. Available: <https://www.renishaw.com/resourcecentre/download?data=125236&lang=en&userLanguage=en> [Accessed December 2023].
- SCHOLLER, N. & URBAN, N. 2007. CA125 in ovarian cancer. *Biomarkers in medicine*, 1, 513-523.
- SCIENTIFIC, T. F. 2007. *Plasma and Serum Preparation Protocols* [Online]. Thermofisher.com. Available: <https://www.thermofisher.com/uk/en/home/references/protocols/cell-and-tissue-analysis/elisa-protocol/elisa-sample-preparation-protocols/plasma-and-serum-preparation.html> [Accessed 2020].
- SMITH, E. & DENT, G. 2004a. Introduction, Basic Theory and Principles. *Modern Raman Spectroscopy – A Practical Approach*.
- SMITH, E. & DENT, G. 2004b. The Raman Experiment – Raman Instrumentation, Sample Presentation, Data Handling and Practical Aspects of Interpretation. *Modern Raman Spectroscopy – A Practical Approach*.

- SMITH, E. & DENT, G. 2004c. The Theory of Raman Spectroscopy. *Modern Raman Spectroscopy – A Practical Approach*.
- STANDRING 2021. Female Reproductive System. *Gray's Anatomy*. 42 ed.: Elsevier Saunders.
- STONE, N. 2001. *Raman spectroscopy of biological tissue for application in optical diagnosis of malignancy*. PhD, Cranfield University.
- STONE, N., HART PRIETO, M. C., CROW, P., UFF, J. & RITCHIE, A. W. 2007. The use of Raman spectroscopy to provide an estimation of the gross biochemistry associated with urological pathologies. *Anal Bioanal Chem*, 387, 1657-68.
- STONE, N., KENDALL, C. & BARR, H. 2001. Raman Spectroscopy as a Potential Tool for Early Diagnosis of Malignancies in Esophageal and Bladder Tissues. *Handbook of Vibrational Spectroscopy*.
- STONE, N., KENDALL, C., SMITH, J., CROW, P. & BARR, H. 2004. Raman spectroscopy for identification of epithelial cancers. *Faraday Discussions*, 126, 141-157.
- STONE, N., STAVROULAKI, P., KENDALL, C., BIRCHALL, M. & BARR, H. 2000. Raman spectroscopy for early detection of laryngeal malignancy: preliminary results. *Laryngoscope*, 110, 1756-63.
- STREPPEL, M. M., VINCENT, A., MUKHERJEE, R., CAMPBELL, N. R., CHEN, S. H., KONSTANTOPOULOS, K., GOGGINS, M. G., VAN SEUNINGEN, I., MAITRA, A. & MONTGOMERY, E. A. 2012. Mucin 16 (cancer antigen 125) expression in human tissues and cell lines and correlation with clinical outcome in adenocarcinomas of the pancreas, esophagus, stomach, and colon. *Hum Pathol*, 43, 1755-63.
- SUNDAR, S., NEAL, R. D. & KEHOE, S. 2015. Diagnosis of ovarian cancer. *BMJ : British Medical Journal*, 351, h4443.
- SURI, A., PERUMAL, V., AMMALI, P., SURYAN, V. & BANSAL, S. K. 2021. Diagnostic measures comparison for ovarian malignancy risk in Epithelial ovarian cancer patients: a meta-analysis. *Sci Rep*, 11, 17308.
- TALARI, A. C. S., MOVASAGHI, Z., REHMAN, S. & REHMAN, I. U. 2015. Raman Spectroscopy of Biological Tissues. *Applied Spectroscopy Reviews*, 50, 46-111.
- TAN, Y., LI, J., ZHAO, G., HUANG, K. C., CARDENAS, H., WANG, Y., MATEI, D. & CHENG, J. X. 2022. Metabolic reprogramming from glycolysis to fatty acid uptake and beta-oxidation in platinum-resistant cancer cells. *Nat Commun*, 13, 4554.
- TIDY, J., COLEMAN, R., HARVEY, R., HILLS, A. & MJ, S. 2016. *Scientific Impact Paper No. 52*.
- Management of Female Malignant Ovarian Germ Cell Tumours* [Online]. London: Royal College of Obstetricians and Gynaecologists. Available: https://www.rcog.org.uk/media/spph3iqq/sip_52.pdf [Accessed 2020].
- TIMMERMAN, D., TESTA, A. C., BOURNE, T., AMEYE, L., JURKOVIC, D., VAN HOLSBEKE, C., PALADINI, D., VAN CALSTER, B., VERGOTE, I., VAN HUFFEL, S. & VALENTIN, L. 2008. Simple ultrasound-based rules for the diagnosis of ovarian cancer. *Ultrasound in Obstetrics & Gynecology*, 31, 681-690.
- TOGASHI, Y., ARAO, T., KATO, H., MATSUMOTO, K., TERASHIMA, M., HAYASHI, H., DE VELASCO, M. A., FUJITA, Y., KIMURA, H., YASUDA, T., SHIOZAKI, H. & NISHIO, K. 2014. Frequent amplification of OROAV1 gene in esophageal squamous cell cancer promotes an aggressive

- phenotype via proline metabolism and ROS production. *Oncotarget*, 5, 2962-73.
- TRIMBOS, J. B., VERGOTE, I., BOLIS, G., VERMORKEN, J. B., MANGIONI, C., MADRONAL, C., FRANCHI, M., TATEO, S., ZANETTA, G., SCARFONE, G., GIURGEA, L., TIMMERS, P., COENS, C. & PECORELLI, S. 2003. Impact of adjuvant chemotherapy and surgical staging in early-stage ovarian carcinoma: European Organisation for Research and Treatment of Cancer-Adjuvant ChemoTherapy in Ovarian Neoplasm trial. *J Natl Cancer Inst*, 95, 113-25.
- TU, A. T. Raman spectroscopy in biology: Principles and applications. 1982. UAB RESEARCH. *Freezing tissues for cryosectioning* [Online]. The University of Alabama at Birmingham. Available: <https://www.uab.edu/research/home/cpl-freezing-tissues-for-cryosectioning> [Accessed 2023].
- UDENSI, J., LOUGHMAN, J., LOSKUTOVA, E. & BYRNE, H. J. 2022. Raman Spectroscopy of Carotenoid Compounds for Clinical Applications-A Review. *Molecules*, 27.
- URBAN, N., THORPE, J., KARLAN, B. Y., MCINTOSH, M. W., PALOMARES, M. R., DALY, M. B., PALEY, P. & DRESCHER, C. W. 2012. Interpretation of Single and Serial Measures of HE4 and CA125 in Asymptomatic Women at High Risk for Ovarian Cancer. *Cancer Epidemiology, Biomarkers & Prevention*, 21, 2087-2094.
- VAN DOORN, H. C., BARROSO, E. M., KOLJENOVIC, S., EWING-GRAHAM, P. C., SOARES, M. R. N., VAN DE BERG, N. J., SCHUT, T. C. B. & PUPPELS, G. J. 2021. Raman spectroscopy for guidance of vulvar cancer surgery: a pilot study. *Biomed Opt Express*, 12, 3008-3020.
- VAUGHT JB, H. M. 2011. Biological Sample Collection, processing, storage and information management. In: ROTHMAN, N. E. A. (ed.) *Molecular Epidemiology: Principles and Practices*. France: International Agency for Research on Cancer Scientific Publications.
- VERGOTE, I., TROPÉ, C. G., AMANT, F., KRISTENSEN, G. B., EHLEN, T., JOHNSON, N., VERHEIJEN, R. H., VAN DER BURG, M. E., LACAVE, A. J., PANICI, P. B., KENTER, G. G., CASADO, A., MENDIOLA, C., COENS, C., VERLEYE, L., STUART, G. C., PECORELLI, S. & REED, N. S. 2010a. Neoadjuvant chemotherapy or primary surgery in stage IIIC or IV ovarian cancer. *N Engl J Med*, 363, 943-53.
- VERGOTE, I., TROPÉ, C. G., AMANT, F., KRISTENSEN, G. B., EHLEN, T., JOHNSON, N., VERHEIJEN, R. H. M., VAN DER BURG, M. E. L., LACAVE, A. J., PANICI, P. B., KENTER, G. G., CASADO, A., MENDIOLA, C., COENS, C., VERLEYE, L., STUART, G. C. E., PECORELLI, S. & REED, N. S. 2010b. Neoadjuvant Chemotherapy or Primary Surgery in Stage IIIC or IV Ovarian Cancer. *New England Journal of Medicine*, 363, 943-953.
- WAGNER-GOLBS, A., NEUBER, S., KAMLAGE, B., CHRISTIANSEN, N., BETHAN, B., RENNEFAHRT, U., SCHATZ, P. & LIND, L. 2019. Effects of Long-Term Storage at -80 °C on the Human Plasma Metabolome. *Metabolites*, 9.
- WANG, J., GAO, J., YAO, H., WU, Z., WANG, M. & QI, J. 2014. Diagnostic accuracy of serum HE4, CA125 and ROMA in patients with ovarian cancer: a meta-analysis. *Tumour Biol*, 35, 6127-38.
- WANG, J., ZHENG, C. X., MA, C. L., ZHENG, X. X., LV, X. Y., LV, G. D., TANG, J. & WU, G. H. 2021. Raman spectroscopic study of cervical

- precancerous lesions and cervical cancer. *Lasers Med Sci*, 36, 1855-1864.
- WELTER SM. & KHALIFA MA. *Teratoma-mature* [Online]. Pathology Outlines.com. Available: <https://www.pathologyoutlines.com/topic/ovarytumorteratomamature.html> [Accessed 2023].
- WILKINSON, N., VROOBEL, K. & MCCLUGGAGE, G. 2019. *G079: Dataset for histopathological reporting of carcinomas and borderline tumours of the ovaries, fallopian tubes and peritoneum* [Online]. London: The Royal College of Pathologists. Available: <https://www.rcpath.org/static/63d413b3-ee69-43df-aa7f495e062a4d47/G079-Dataset-for-histopathological-reporting-of-carcinomas-of-the-ovaries-fallopian-tubes-and-peritoneum-For-Publication.pdf> [Accessed 2023].
- ZACH. 2021. *F1 Accuracy vs Accuracy: Which should you use?* [Online]. Statology. Available: <https://www.statology.org/f1-score-vs-accuracy/> [Accessed 2023].
- ZHANG, D., XIE, Y., MROZEK, M. F., ORTIZ, C., DAVISSON, V. J. & BEN-AMOTZ, D. 2003. Raman detection of proteomic analytes. *Anal Chem*, 75, 5703-9.
- ZHENG, Q., KANG, W., CHEN, C., SHI, X., YANG, Y. & YU, C. 2019. Diagnosis accuracy of Raman spectroscopy in colorectal cancer: A PRISMA-compliant systematic review and meta-analysis. *Medicine (Baltimore)*, 98, e16940.